Variation in endogenous SHH signalling activity accounts for differential responses of IPSC lines to neural sub-type specification in directed differentiation protocols

This dissertation is submitted for the degree of Doctor of Philosophy at Cardiff University

Kimberley Marie Jones, BSc.

PhD Thesis 2022

Abstract

Available protocols aimed at differentiating human induced pluripotent stem cells (iPSCs) from both control and Huntington's disease (HD) patients have yielded varying populations of Medium Spiny Neurons (MSNs). This is hugely problematic when trying to identify whether molecular and functional differences are disease attributes independent of individual cell line differences. Furthermore, this limits the ability to screen compounds for drug discovery which selectively target MSNs as well as their potential use in cell replacement therapies. The aim of this thesis was to investigate the inherited inter-line variability in the generation of MSNs following identical patterning cues during iPSC differentiation. Here, endogenous SHH expression and signalling at the neural progenitor stage was identified as the main contributor to the variation in differentiation outcomes. Endogenous SHH signalling resulted in the expression of NKX2.1, a master transcription factor for medial ganglionic eminence (MGE) fate specification and interneuron development. Blockade of canonical SHH signalling during neural patterning stages of *in vitro* differentiation resulted in a medial- to lateral GE-like switch and consequently an increase in LGE-derived MSNs (~70% DARPP-32/CTIP2). SHH blockade also reduced the variability in differentiation seen between cell lines. Bulk RNA sequencing confirmed SHH signalling as the main contributor to variation. In addition, a novel signalling pathway, namely non-canonical WNT, that may influence inter-line variability was identified. MSN differentiation was further investigated in SHH and NKX2.1 knockout cell lines generated by CRISPR gene editing. Using our standard protocol of BMP and WNT pathway inhibition in the presence of Activin-A, knockout of both SHH and NKX2.1 caused a reduction in MSN differentiations. However, under a 'default' cortical differentiation protocol where BMP and WNT signalling was not inhibited, we observed an increase in DARPP-32 protein expression in the NKX2.1 KO lines, however the morphology of the neurons derived appeared to be distinct from that of MSNs.

This is the first in-depth investigation into endogenous differentiation bias affecting MSN subtype specification and highlights the need to optimize protocols for individual cell lines, taking into account inherent biases that are determined by gene expression differences present in the pluripotent state and those that arise upon differentiation that influence developmental signalling, neural patterning and fate specification.

Acknowledgements

*"I love deadlines**.** I love the whooshing noise they make as they go by.". — **Douglas Adams***

I am sincerely grateful to my supervisor, Prof. Nick Allen for risking his mental sanity over the past 4 years in order to supervise this thesis. While I have significantly depleted his life force, he has shown the utmost care and patience in dealing with me for so long. Nick, I truly appreciate all the time, effort and support you have given me more than I can express. To Bridget Allen thank you for adopting me, I don't think Nick really wanted another child, but you are the best lab mother one could ask for. Thank you to everyone past and present at the NDA lab, specifically Dr. Emma Cope and Brendan Kelly.

Special thanks to Angela Marchbank, the Queen of the Genomics hub for all her support and training with RNA sequencing. Thank you to Prof. Pete Kille for his invaluable input and support with data analysis.

My appreciation to Dr Seva Telezhkin for his incredible knowledge and expertise in whole cell patch clamp. I would also like to thank Emyr Lloyd Evans for his insight and support at every stage of this project.

To all members of the 4th floor lab, thank you for being such a helpful group and making the lab a home away from home. I would also like to officially acknowledge the efforts of the staff and volunteers at CU data clinic, thank you so much for your help, I don't think you get enough credit for the work you do.

To Tony and Matt thank you for accepting me as an honorary member of stores, for keeping me grounded and listening to me talk rubbish about cells all the time. All my smoke breaks are in honour of you both.

Thank you to Rachel for putting up with me and looking after me while writing this thesis. I truly don't think I would have gotten through this without you! Thank you to Kasope Wolffs who has been with me through the ups and downs of both undergraduate and postgraduate degrees.

To my family, thank you all for believing in me and supporting me. Last but not least, big shout out to the one and only Miss Nia Gray…. We are one!!!

Abbreviations

ACHE	Acetylcholinesterase
AAO	Average age of onset
AD	Alzheimer's disease
AEP	Anterior entopeduncular area
ASO	Anti-sense oligonuecletide
ATP	Adenosine triphosphate
BAC	Bacterial artificial chromosome
BDNF	Brain-derived neurotrophic factor
BHC	Benign hereditary chorea
BMP	Bone morphogenic protein
Cas9	Caspase 9
CGE	Caudal ganglionic eminence
CHAT	Choline O-acetyltransferase
CREB	cAMP response element-binding protein
CRISPR	Clustered regularly interspaced short palindromic repeats
CRL	Crown-rump length
CTIP2	COUP-TF-interacting protein (Bcl11b)
CTX	Cortex
DARPP-32	Dopamine- and cyclic-AMP-regulated phosphoprotein of MW- 32,000
DEG	Differentially expressed gene
D-Gal	D-Galactose
DKK1	Dickkopf-related protein 1
DLX2	Distal-Less Homeobox 2
DRD1	Dopamine receptor D1
DRD2	Dopamine receptor D2
EGF	Epidermal growth factor
ESC	Embryonic stem cell
FGF	Fibroblast growth factor
FISH	Flourescent in situ hybridisation

FOXG1	Forkhead Box G1
GABA	γ-aminobutyric acid
GFAP	Glial fibrillary acidic protein
GFP	Green fluorescent protein
GLI1	GLI Family Zinc Finger 1
GLi3	GLI Family Zinc Finger 3
GP	Globus pallidus
Gpe	-external segment
Gpi	-internal segment
gRNA	guideRNA
GSE	Gene set enrichment
GO	Gene ontology
GSX2	GS Homeobox 2
HD	Huntington's disease
HGPS	Hutchinson-Gilford Progeria Syndrome
HH	Hedgehog
HHIP	Hedgehog Interacting Protein
HO	Hoesht
HTT	Huntingtin
ICC	Immunocytochemistry
iPSC	Induced pluripotent stem cell
KO	Knockout
KEGG	Kyoto Encyclopedia of Genes and Genomes
LGE	Lateral ganglionic eminence
MEIS2	Meis Homeobox 2
MGE	Medial ganglionic eminence
mHTT	Mutant huntingtin
MSN	Medium spiny neuron
MZ	Mantle Zone

NKX2.1	NK2 Homeobox 1
NPC	Neural Progenitor Cell
NPY	Neuropeptide Y
OB	Olfactory bulb
OLIG2	Oligodendrocyte Transcription Factor 2
OXPHOS	Oxidative phosphorylation
PBS	Phosphate-buffer saline
PD	Parkinson's disease
PKA	Protein kinase A
POA	Pre-optic area
PV	Parvalbumin
RARB	Retinoic acid receptor beta
RMS	Rostral migratory stream
RNP	Ribonucleoprotein particle
SHH	Sonic hedgehog
SMO	Smoothened
SNpc	Substantia nigra pars compacta
SNr	Substantia nigra reticulata
SST	Somatostatin
STN	Sub thalamic nucleus
SVZ	Sub ventricular zone
TH	Tyrosine hydroxylase
UTF1	Undifferentiated Embryonic Cell Transcription Factor 1
VIP	Vasoactive intestinal peptide
VZ	Ventricular zone
WGE	Whole ganglionic eminence
WNT	Wingless Int-1 signalling pathway
WT	Wildtype

Table of contents

Chapter 1: General introduction

In the course of this introduction, I want to give brief overviews of the basal ganglia, its main component – the striatum and the role medium spiny neurones (MSNs) play in neurodegenerative diseases, with a specific focus on Huntington's disease (HD). Furthermore, I will highlight the importance and current limitations of induced pluripotent stem cells (iPSCs) as an *in vitro* model of HD, thereby explaining the rationale behind this thesis and set the stage for the investigations undertaken in the course of my thesis.

Basal ganglia

The basal ganglia are a set of neurochemically complex subcortical nuclei including the caudate nucleus, putamen, globus pallidus (GPe and GPi), subthalamic nucleus (STN) and substantia nigra pars compacta (SNpc) and substantia nigra reticulata (SNr), in which the topographical organisation of their projections is a critical feature of the cortico-basal ganglia-thalamo-cortical circuits. The main role of the basal ganglia is the integration of cognitive and motor networks to effectively execute tasks in a coordinated manner. Subsets of basal ganglia neurons express distinct neuroactive peptides that modulate these circuits, including enkephalins, dynorphins, tachykinins, somatostatin and neuropeptide Y, and utilise a variety of neuromodulators including GABA, acetylcholine, glutamate, dopamine and serotonin. Although the basal ganglia are anatomically and functionally complex, the simplified structural/functional circuit models are characterised by the direct excitatory (glutamatergic) and indirect inhibitory (GABAergic) pathways, depicted in Figure 1.1. Here, enkephalin-containing neurons project indirectly to the GP_i via the external segment of the GP_e, STN and SNr (SN_{pr}), and constitute the indirect inhibitory striatal output pathway (Reviewed in DeLong and Wichmann, 2007). In contrast, substance P-containing neurons project directly to the GP_i, and constitute the direct stimulatory output pathway of the striatum.

The role of the basal ganglia is to fine tune and adjust motor inputs to allow smooth initiation of movement and sequence of movements appropriately. This coordinated input

into skeletal muscles should result in smooth motor initiation and function that is appropriate and responsive to events in our environment, mood or thought processes. The integration of motor outputs from this system is modulated through activation of two concurrent neural pathways, the direct and the indirect pathways. The balancing of both direct and indirect inputs into the GP allows the circuit to function as a dial rather than an on/off switch allowing the smooth motor initiation seen in normal functioning by modulating the tonic inhibition of the GPi (Reviewed in DeLong and Wichmann, 2007). GPi outputs are fed back to the cerebral cortex via the ventral thalamus. Many diseases and disorders associated with the basal ganglia circuitry are principally characterised by the motor dysfunction seen in patients, however the basal ganglia are also linked to many circuits; processing attention, emotion, memory or visual inputs, and dysfunction in many of these processes may be seen in disease states too (Reviewed in DeLong and Wichmann, 2007).

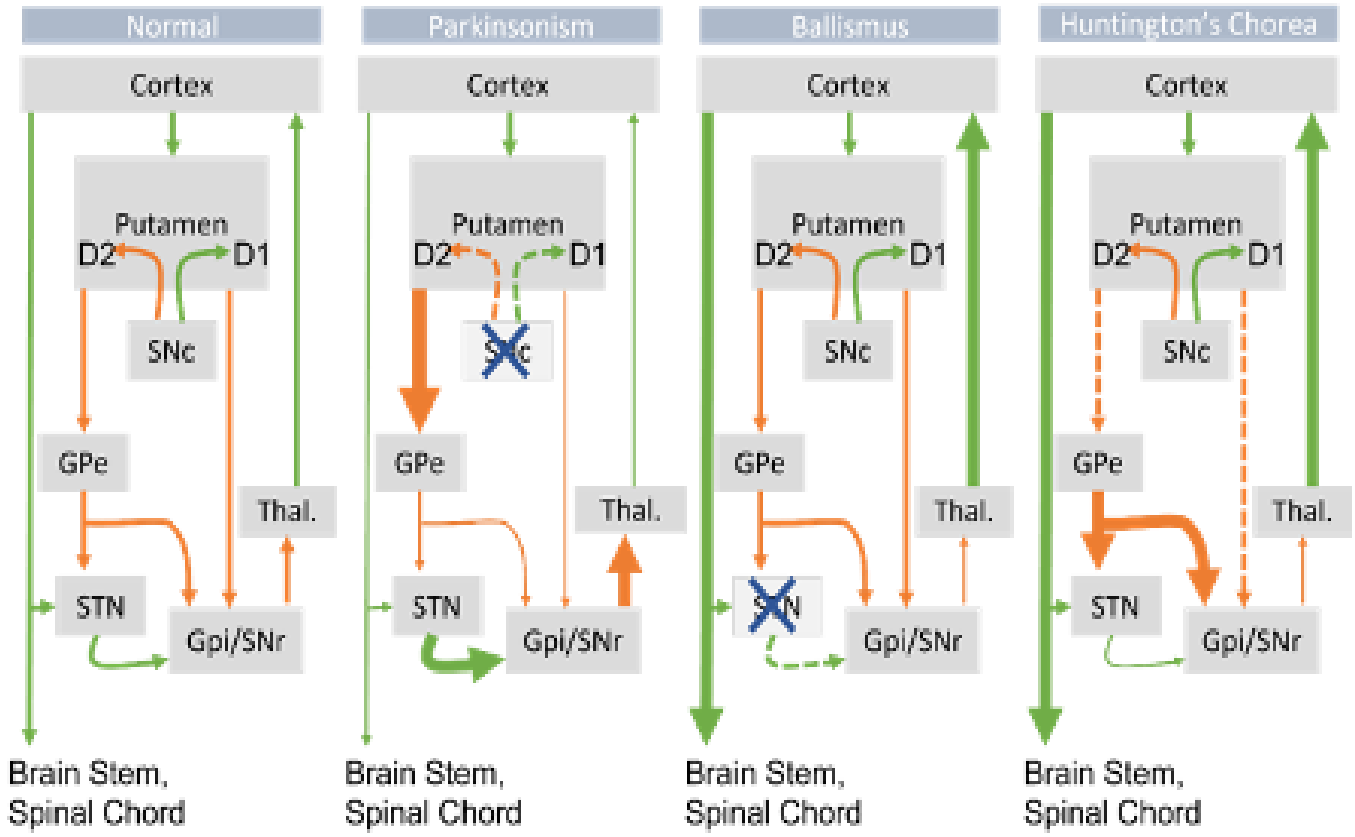

Figure 1.1. A simplified model of the basal ganglia circuitry in health and disease. Hypoknetic movement disorders such as Parkinson's (PD), Ballismus and Huntington's disease (HD) results from abnormal activity of the basal ganglia circuitry. PD lesions to the substantia nigra (SNc) results in increased excitatory input to the GPe, loss of excitatory drive from the subthalamic nucleus (STN) to the GPi and subsequently sensitisation of cortical areas. Ballismus lesions to the STN results in decreased excitatory input to the GPi resulting in decreased inhibitory output to the thalamus (Thal) and increased excitatory input to the cortex. HD lesions to the striatum causes results in increase inhibition of the STN and GPi/SNr. As a result, there is less inhibitory input to the Thal and consequently increased excitatory input to the cortex (Young, Reddy, Sonne, 2022).

Striatum

The striatum comprises the largest output nuclei of the basal ganglia, and includes the caudate, putamen and nucleus accumbens, in which the predominant (75-95%, depending on species) cell types are the medium spiny neurons (MSNs, Graveland and Difiglia, 1985). MSNs utilise GABA as their principal neurotransmitter and project directly or indirectly to output nuclei in the basal ganglia to provide inhibitory function and feedback. The dorsal striatum in humans, non-human primates and higher order mammals is formed by the caudate and putamen, which are separated anatomically by the internal capsule. In contrast, the rodent striatum is homogeneous with no delineation between the caudate and putamen, referred to as the caudate-putamen complex (Alloway *et al.,* 2006; Hooks *et al.,* 2018; Hoover *et al.,* 2003; Graybiel, 2008). Whilst the ventral and dorsal striatum both contain MSNs, the dorsal striatum is part of the basal ganglia circuit whereas the ventral part is part of the mesolimbic system.

The dorsal striatum can be further segregated neurochemically by compartments, striosomes (patch, ~10-15% of striatal volume) and matrix which participate in limbic and sensorimotor functions, respectively (Graybiel *et al.,* 1978; Gerfent *et al.,* 1984; Hong *et al.,* 2019; Brimblecombe and Cragg, 2017; Critten and Graybiel, 2011). These compartments are defined by several biochemical markers as well as their afferent and efferent connections. For example, patches are enriched in μ-opiate receptors, whereas the matrix contains Calbindin D_{28D} and somatostatin (SST) fibres (Olson *et al.,* 1976; Goldman and Nauta*.,* 1977; Herkenham and Pert*,* 1981; Gerfen, 1984; Gerfen, Baimbride, Miller, 1985). In addition, patches preferentially contain MSNs of the direct pathway where they innervate mainly the SNpc whereas the efferents from MSNs in the matrix have been found to project to the GPe, GPi and SNr in rats (Gerfen, 1984; Levesque + Parent, 2005; Chuhma *et al.,* 2011; Fujiyama *et al.,* 2011). Direct and indirect MSNs can be distinguished by their differential expression of neurotransmitter receptors and transcription factors. The indirect striato-pallidal MSNs express DRD2, GPR6, ADORA2a, PENK, GPR52 whereas direct striato-nigral MSNs express DRD1, Sub-p (Tac1), dynorphin (Pdyn) and Isl1 (Lobo *et al.*, 2006; Heiman *et al.*, 2008; Ehrman *et al.*, 2013). Furthermore, DRD1- and DRD2- MSNs can be identified by their differential regulation of the cAMP pathway through the activation and inhibition of

adenylate cyclase, respectively (Garau et al., 1978; Kebabian and Calne, 1979). Dopaminergic innervation from mesencephalic dopaminergic neurons located in the SNpc results in G_{olf} – mediated (Herve *et al.,* 1995) activation of PKA in MSNs and subsequently phosphorylation of DARPP-32 (Svenningsson *et al.,* 2004) altering neuronal function. Whereas DRD2 striato-pallidal MSNs are coupled to $G_{i/o}$ proteins and inhibit adenylyl cyclase through $G\alpha_i$ subunits (Stoof and Kebabian, 1984). The striatum also receives glutamatergic input from the cortex and thalamus (Bolam *et al.,* 2000).

Mechanisms of striatal development

During embryological development, the brain is regionalised following the closure of the neural tube, with the most caudal portion forming the spinal cord and the most rostral portion forming the prosencephalon, from which the telencephalon develops. This rostral-caudal patterning is heavily dependent on differential expression of forkhead transcription factor and orthodenticle homeobox 2 (Wichterle *et al.,* 2001; Wonders and Anderson, 2006; Tau and Lai, 1992; Shimamura and Rubenstein, 1997). Once the telencephalic primordium has been specified, typically 5 weeks post conception (PC) in humans (E8.5 in the mouse), it is further subdivided along the rostral-caudal axis. This division creates a dorsal region, which becomes the developing pallium and a ventral region designating the lateral, medial and caudal eminence (LGE, MGE and CGE respectively). The progenitor zone of the LGE is the source for striatal neurons, whilst progenitors found in the MGE make cortical and striatal interneurons. Specification of these separate neuronal populations reflects the exposure to distinct transcription factors whose expression is dependent on the molecular gradients signifying a caudal (WNTs, FGF, retinoids), rostral (αBMPs, αWNTs) or dorsal-ventral (GLI3, BMP, FGF, SHH) position within the developing brain (Figure 1.2, Wichterle *et al.,* 2001; Wonders and Anderson, 2006; Tau and Lai, 1992; Shimamura and Rubenstein, 1997).

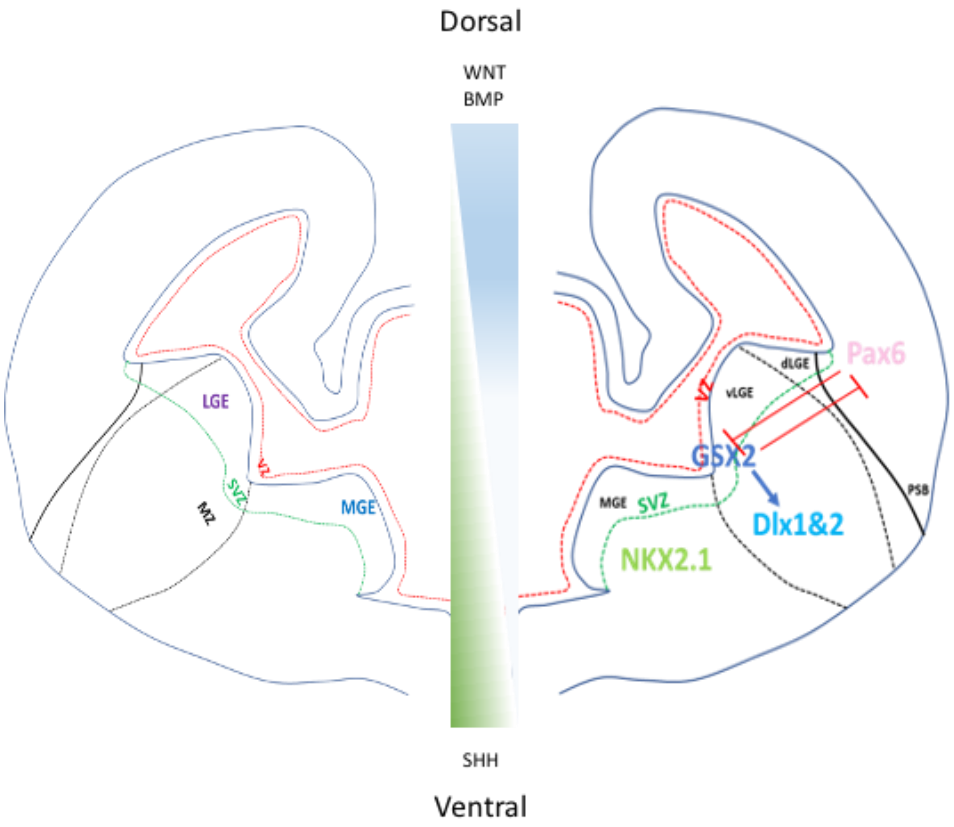

Figure 1.2. Simplified schematic representation of gene expression coundaries and dorso-ventral gradients of signalling morphogens in the developing telencephalon. The telencephalon is subdivided into the pallium (dorsally) and subpallium (ventrally)with the pallial-subpallial boundary (PSB) defined by opposing gradients of PAX6 and GSX2 expression. Further subdivisions, ventrally, are discerned by high expression of DLX1/2 and GSX2 in the LGE and NKX2.1 within the MGE.

After establishment of the neural tube, SHH is secreted from the notochord and the floor plate while BMPs and WNTs are secreted from the roof-plate and dorsal midline (Furuta *et al.,* 1997). Highly expressed SHH designates a ventral positioning within the developing telencephalon, whilst high levels of WNT and BMPs are found in dorsal areas. Through this dorsal-ventral gradient of signalling morphogens the developing cells will have relevant transcription factors expressed or inhibited depending on their sensitivity to varying levels of WNT/SHH. In this way, the developing brain differentiates between those cells that will become cortical or striatal. The WNT/SHH chemo-gradient allows patterning of the LGE, MGE and cortical areas as anatomically distinct areas (Sussel *et al.,* 1999; Gunhaga *et al.,* 2000, 2003).

While the transcription factors, Gsx2, Dlx2 and Mash1 are expressed in both MGE and LGE precursors; the homeobox transcription factor, *Nkx2.1*, is essential for MGE specification. Fate mapping in rodent models has shown that, upon exit of the cell cycle, NKX2.1 progenitors express the LIM homeodomain transcription factor Lhx6 and Lhx7. These precursors can differentiate and mature into either GABAergic (*Nkx2.1/Lhx6* +ve) or Cholinergic (*Nkx2.1/Isl1* +ve) interneurons (Sussel *et al.*, 1999; Marin, Anderson and Rubenstein, 2000; Nóbrega-Pereira *et al.*, 2008; Fragkouli *et al.*, 2009). These neurons migrate either radially to populate the striatum and GP or tangentially to the cortex (Xu *et al.,* 2008).

In the MGE, initial patterning is dependent on secreted morphogens FGF8 and SHH to induce the expression of NKX2.1. Continued expression of SHH in development allows NKx2.1 level to be maintained and its downstream target LHX6 in the MGE. These factors are required for the specification of SST and PV interneurons (Anderson et al., 2001; Xu et al., 2004; Xu et al., 2005; Butt et al., 2008; Du et al., 2008; Liodis et al., 2007). While both SST and PV interneurons originate from the same developing structure, the dorsal MGE (dMGE) predominantly generates precursors that will become SST interneurons. PV interneurons, however, originate from the ventral MGE (vMGE), Flames et al., 2007; Wonders et al., 2008; Hu et al., 2017). The distinction between these populations of cells is created by differential expression of SHH between the dMGE and vMGE, where it is enriched dorsally, shown by higher expression of GLI1, Ptch1/2, HHIP1 and NKX6.2 transcripts (Xu et al.,2005; Chuang et al., 2003; Xu et al., 2010; Wonders et al., 2008; Yu et al., 2009). The effect of other chemical signals present in the MGE and surrounding area is yet to be fully investigated. Recent findings have indicated a further role of WNT, being expressed in a non-canonical fashion from dorso-caudal structures creating a rostral-caudal gradient. High caudal concentrations of WNT promote a SST interneuron outcome, while lower concentrations at a rostral position cause PV interneuron to develop (Mckenzie *et al.,* 2019).

Within the sub ventricular zone (SVZ) of the LGE, transcription factors DLX1/2, ER81, PAX6 and SP8 are enriched in the dorsal portion (Stenman *et al.,* 2003; Kohwi *et al.,* 2005; Hack *et al.,* 2005; Waclaw *et al.,* 2006, 2009). Here, olfactory bulb interneurons are predominantly generated (E14) and migrate tangentially via the rostral migratory stream (RMS).

During early stages (E9-13) of neurogenesis striatal projection neurons are generated from the ventral LGE, where they will migrate radially to the mantle zone and ultimately reside in the stiatosome compartment. Later in neurogenesis (>E14) MSNs that will reside in the matrix are generated (Gerfen *et al.,* 1992; Mason *et al.,* 2005). In addition, transcription factors such as Nolz1, BCL11B, Ebf1 and FoxP1/2 are expressed in LGE precursors, and are essential for MSN cell fate (Takahashi *et al.*, 2003; Chang *et al.*, 2004; Arlotta *et al.*, 2008)

Considering the complexity of the basal ganglia, it is not surprising that there are several diseases associated with basal ganglia dysfunction including, Wilson's disease, progressive supranuclear palsy, multiple system atrophy, Parkinson's disease (PD) and Huntington's disease (HD), which can present with a combination of sensory, motor and psychiatric symptoms. Different symptoms manifest depending on the nature of lesions involved. For example, Parkinson's disease is characterised by a loss of 50-80% of the dopaminergic neurons projecting from the substantia nigra. The lack of dopamine release into the striatum results in a loss in inhibitory input and an increase in excitatory inputs into the GPi, from the direct and the indirect pathways, respectively. The clinical hallmarks of PD include motor symptoms (bradykinesia, shuffling gait rigidity), and significant cognitive and psychiatric symptoms. Of relevance here, damage to the subthalamic nucleus in the basal ganglia circuit results in the loss of excitatory drive from the STN to the GPi and subsequent sensitisation of the cortical areas. This is known as Ballismus, a hyperkinetic movement disorder characterised by violent, involuntary limb movements either on one side of the body (hemiballismus) or bilaterally (Young, Reddy and Sonne, 2022).

Whilst PD affects the dopamine input neurons to the striatum, HD primarily affects the MSN output neurons of the striatum, and the latter is the neurodegenerative disorder focussed on in this thesis. HD is an autosomal dominant, progressive neurodegenerative disorder, affecting 12.3 persons per 100,000 in the UK (Wexler et.al, 2016), with a growing prevalence rate worldwide, most significantly in predominantly Caucasian populations (Rawlins M.D. et.al, 2016). This may be due to more accurate diagnosis and greater willingness to register a diagnosis of HD in patients' electronic medical records (Evans *et al.,* 2013).

HD results in the loss of MSNs in the dorsal striatum which leads to the disinhibition of striatal outputs through the direct and indirect pathways culminating in multiple poorly synchronised movements (chorea), a major motor symptom of disease. Thus, highlights the

importance of MSNs in HD pathology. If we are to generate MSNs from ES or iPSC sources, either for disease modelling or cell replacement therapies it is crucial to verify that these exhibit a "true" MSN-type phenotype. Therefore, fully understanding the *in utero* development of the striatum allows better adaptation of differentiation protocols to improve MSN yield and efficacy.

Huntington's Disease

HD is characterised by selective degeneration and loss of striatal MSNs resulting in progressive deterioration of striatal function and consequent loss of motor and cognitive functions, as these are dependent on striatal integration of basal ganglia circuitry. Post-mortem examinations predominantly show striatal atrophy, which has been classified into five pathological grades, 0-4 (Vonsattel *et al.*, 1987; Halliday *et al.*, 1998; Thu *et al.*, 2010). This grading system correlates with disease progression, with greatest neuronal loss (95%) seen in the caudate nucleus, which forms part of the dorsal striatum, in grade 4 (Vonsattel *et al.*, 1987). In addition, posterior and anterior thinning of the cortical ribbon has been found in HD patients (Rosas *et al.,* 2002).

In early- to middle stages of the disease the greatest neuronal loss is seen in the indirect pathway enkephalin/DRD2-expressing MSN population (Reiner *et al.*, 1988). Preferential loss of indirect pathway MSNs reduces inhibitory output, leading to overexcitement of thalamic regions and results in the choreic movement which is characteristic of HD (Graveland, Williams and DiFiglia, 1985; Huerta-Ocampo, Mena-Segovia and Bolam, 2014).

An extensive 10-year natural observation study in premanifest HD (NS040068), has shown that HD patients develop motor, cognitive and psychiatric deficits decades before clinical diagnosis (Paulsen *et al.,* 2014). This is coupled with early changes in brain morphology and connectivity (Ciarochi *et al.,* 2016; Epping *et al.,* 2016; Harrington *et al.,* 2015; Kim J-I *et al.,* 2015; Paulsen *et al.,* 2008; Williams *et al.,* 2015). Furthermore, studies in Q111 *HdH* knock-in mice have shown gene expression changes in the striatum, prior to onset of pathology (Fossale *et al.,* 2011), alongside abnormal striatal intermediate progenitor cell cycle regulation and neuronal specification (Molero *et al.,* 2009).

The genetic mutation responsible for HD (Huntingtin; HTT) was among the first to be cloned by genetic linkage analysis using patient kindreds and the molecular tools of positional cloning (The HD iPSC Consortium, 1993). HTT is located on chromosome 4p16.3 and the mutation was identified as an unstable expansion of the CAG repeat (>35) in exon 1 of the gene, encoding an expanded polyglutamine tract in the N-terminal domain of the Huntingtin protein (MacDonald *et al.*, 1993). HD was therefore identified as a member of a new class of genetic disorders – the so-called triplet repeat disorders. A key feature of these disorders is the genetic instability of the affected CAG repeat, such that, beyond a threshold length of 35 CAGs the repeat can undergo germline expansion. This results in increased disease severity in subsequent generations. Importantly, the average age of onset (AAO) of the first clinical symptoms (defined as first motor symptoms) of HD is inversely correlated with inherited CAG repeat length (Trottier, Biancalana and Mandel, 1994; Furtado *et al.*, 1996; Penney *et al.*, 1997; Rosenblatt *et al.*, 2006; Vassos *et al.*, 2008). Although CAG repeats >40 are fully penetrant, approximately 30% of the variance in the AAO cannot be accounted for the length of the polyQ stretch (Trottier, Biancalana and Mandel, 1994; Furtado *et al.*, 1996; Penney *et al.*, 1997; Rosenblatt *et al.*, 2006; Vassos *et al.*, 2008) Instead, genome-wide association studies have now identified a number of modifier genes (including DNA mis-match repair genes) that act directly to regulate the extent of repeat expansion.

In addition, repeat expansion in somatic cells can accelerate AAO and the severity of disease progression in individual patients. Repeat instability is thought to be one of the molecular mechanisms that drive disease pathology – generating more severely mutated protein in affected cells. This appears to be relevant for the striatum as it could account for some of the selective vulnerability of MSNs as they show higher levels of somatic repeat expansion than neurons from other brain regions (Kennedy *et al.,* 2003).

HTT function and pathogenic mechanisms in HD

HTT is an ancient and highly evolutionary conserved gene (Iennaco et al 2022), expressed ubiquitously in humans with the highest levels of expression in the brain (Ferrante *et al.*, 1997; Fusco *et al.*, 1999). Consistent with its high evolutionary conservation, knockout models of mouse *Htt* result in early embryonic lethality , with embryos unviable at E7.5

following neurodevelopmental deficits and failed completion of gastrulation (Nasir et al. 1995; Zeitlin et al. 1995).

The function of HTT is hard to succinctly define as it interacts with >300 binding partners in the cell (Kaltenbach *et al.,* 2007). It is also subject to ~50 known post-translational modifications. Accordingly, HTT has been directly implicated in a wide range of intracellular functions, suggesting a broad and essential homeostatic function for the protein in all cells. Ascribed functions include transcriptional regulation, cell division, cell organisation, intracellular transport and signalling, proteostasis and energy metabolism (Velier *et al.*, 1998; Labbadia and Morimoto, 2013; Ferrante *et al.*, 1997; Fusco *et al.*, 1999). An example of this is brain-derived neurotrophic factor (BDNF) which has been shown to have distinct trophic effects on a variety of neurons, including cortical neurons the main site of BDNF synthesis (Huang & Reichardt, 2001). It is anterogradely transported in vesicles via cortio-striatal afferents to the striatum where it plays a key role in neuronal survival (Conner *et al.* 1997; Altar *et al.* 1997). BDNF exerts its effects via activation of the TrkB receptor in MSNs (Marty *et al.* 1996) and ligand-induced dimerization activates a number of targeted proteins, including PLC-γ1 and Shc. Subsequently, this can lead to stimulation of various signalling cascades including the Ras-MAPK pathway and phosphorylation of CREB (Patapoutian & Reichardt, 2001; Segal 2003). The interaction between BDNF and mHtt was hypothesised following an observed reduction in BDNF expression in the post-mortem striatal tissue and serum samples from HD patients. The decrease in BDNF was seen to correlate with CAG length and disease progression (Bachoud-Levi *et al.* 1975; Ferrer *et al.* 2000; Ciammola *et al.* 2007). The link between BDNF and mHtt was demonstrated by Zuccato *et al.* in 2001. CNS cells obtained from heterozygous *Hdh 109* KI mice, revealed that *mHtt* decreases BDNF levels in a dose-dependent manner. Additionally, *mHtt* was also found to supress BDNF protein in the cerebral cortex of 9-month-old YAC72 mice, thus resulting in a 48% reduction in cortical derived BDNF in the striatum. In this model, overexpression of WT *Htt* resulted in increased BDNF production in the cerebral cortex and striatum. Thereby showing that WT *Htt* enhances BDNF transcription, while mHtt inhibits BDNF transcription.

In 2003, Zuccato *et al.* further went on to elucidate the underlying mechanism of BDNF gene regulation. They showed that REST, a zinc finger transcription factor, interacts with WT *Htt*. Normally REST targets *Htt* to a promoter region of BDNF and *Htt* inhibits the silencing

activity of REST by cytoplasmic sequestering, resulting in an increase in BDNF transcription. However, in HD, accumulation of REST in the nucleus is observed, this is believed to be, in part, responsible for the reduction in BDNF mRNA levels in HD models. Furthermore, REST accumulation and concomitant BDNF reduction was shown in neural cell lines derived from knock-in mice, in which a CAG expansion (109 CAG repeat) is inserted into the endogenous mouse Huntington gene (Zuccato *et al.,* 2003).

Htt has also been shown to act as a selective scaffold protein that regulates selective macroautophagy (Rui *et al.*, 2015), the process by which cytoplasmic proteins and dysfunctional organelles tagged with ubiquitin for degradation interact with the C-terminal UBA domain on p62 (a cargo recognition receptor) (Pankiv *et al.*, 2007). This p62-cargo complex is then incorporated into the autophagosome through direct binding to LC3 via its LIR motif; the autophagosome then fuses with the lysosome for hydrolytic cargo degradation (Pankiv *et al.*, 2007). However, in HD, these autophagosomes are often devoid of any contents. The cellular consequence of this has been shown to be a marked increase in lipid droplets and increased mitochondria to cell ratio (Martinez-Vicente *et al.*, 2010). In addition, there was also an abnormal association between p62 and *mHtt,* thus raising the question whether this abnormal interaction is the cause of defective cargo recognition. This group went on to further investigate the normal role of WT *Htt* in autophagy and found that *Htt* contains two binding regions: a ULK1 and p62 protein binding domain. *Htt* was found to facilitate the binding of p62 to protein aggregates. In addition, *Htt* also binds ULK1, releasing it from mTORC1. Following this ULK1 undergoes an activating phosphorylation event that induces the formation of autophagosomes (Rui *et al.*, 2015).

In addition to cargo recognition proteins, *mHtt* has been shown to interact with proteins on mitochondria such as Pink1, a modulator of parkin-mediated mitophagy (Khalil *et al.*, 2015). Valosin-containing protein (VCP, AKA p97), a protein able to translocate to mitochondria that is required for both turnover of mitochondrial outer membrane proteins and parkin-dependent mitophagy has also been shown to interact with mHtt (Guo *et al.*, 2016). BNIP3 a pro-apoptotic member of the Bcl-2 family members is another example mitochondrial associated proteins that interact with mHtt. In this case *mHtt* enhances its activity resulting in depolarisation and fragmentation of mitochondria (Sassone *et al.*, 2010, 2015). These mitochondrial targets provide a source for disease treatment or modulation. A study by Guo

et. al., 2016 showed that inhibition of the abnormal association between *mHtt* and VCP with a third hypervariable region peptide (HV-3; located in the control region of the mitochondrial genome) produced favourable outcomes such as increased cell viability as well as the restoration of normal mitochondrial biogenesis and morphology in mouse and patient derived cells.

It has also been shown that *mHtt* can directly bind to mitochondria, affecting their morphology and bioenergetic status by interacting with associated proteins (Sassone *et al.* 2010). For example, *mHtt* has been shown to lower mitochondrial membrane potential and reduce ATP production, resulting in ROS production and cell death (Quintanilla and Johnson 2009; Yang et al. 2014). As a result, mitochondria are extensively depolarised leading to prolonged calcium increase which increases the vulnerability of neurons to excitotoxic insult (Orrenius *et al.* 2003; Bano *et al.* 2007; Ankorciona *et al* 1995). In addition, *mHtt* inhibits the expression of PGC-1α, a key regulator of energy metabolism and transcriptional co-activator, in turn compromising mitochondrial biogenesis and respiration (Cui *et al.* 2006).

Disease modifying therapies of HD

To date, there are no curative therapies or treatments which attenuate HD disease progression. There is only one FDA approved drug, Tetrabenazine, a reversible antagonist of the vesicular dopamine transporter VMAT2 Tommaso. This drug is used to treat only the hyperkinetic movements seen in HD and has no effect on disease aetiology or other symptoms (Tommaso, Serpino and Sciruicchio, 2011). Thus, considerable investment has gone into developing drugs that target the expression of mHTT directly. Of recent approaches, anti-sense oligonuecletide (ASO) mediated lowering of HTT has received the most attention. ASOs are small (~30 nucleotides) synthetic, single-stranded oligo-deoxynucleotides designed to target specific proteins. Once taken up by cells, ASOs form DNA/RNA heteroduplex structures that are then substrates for RNaseH1 endonuclease degradation (Bennett and Swayze, 2010). By targeting the HTT mRNA degradation mechanisms it is hoped that mHTT levels will decrease significantly and restore normal cell function. In addition to overall lowering of HTT mRNA, allele specific ASOs can be designed to target mutant HTT mRNA only based on single nucleotide sequence polymorphisms in the

gene (Bennett and Swayze, 2010; Kordasiewicz *et al.,* 2012; Tabrizi *et al.,* 2018; Butler *et al.,* 2015; Hersch *et al.,* 2017). In pre-clinical models, the use of ASOs resulted in significant reduction of mHTT protein and rescued of some phenotypes associated with HD in both animal and stem cells. As a result, there has been much hope in the HD community of the ASO lead compound, Tominersen, developed by Ionis Pharmaceuticals, and licenced to Roche in 2017. Roche's phase I/II trial showed that Tominersen's significant lowering of total Htt (wtHTT and mHTT) in cerebral spinal fluid without serious side effects (https://clinicaltrials.gov/ct2/show/results/NCT03342053). However, in the Phase III trial, a route mid-study analysis by the independent Data Monitoring committee revealed that that the higher dose (120mg administered every two months) had led to more adverse events than the lower dose (120 mg administered every 4 months) or placebo, and that there was a trend for individuals on the higher dose to performing less well clinically than placebo. Consequently, dosing in the trial was discontinued (Nature reviews drug discover, 2021). The apparent toxicity in the higher dose cohort could be a consequence of the non-allele specific nature of Tominserin (it lowers both WT and mutant huntingtin) or due to ASO class toxicity. Data from the Tominersen trial has been re-evaluated, in collaboration with Ionis Pharmaceuticals, and post-hoc analysis revealed a potential benefit for younger patients with lower disease burden. Roche is proceeding with a new dosing study for Tominsersin, although concerns over the lack of allele specificity of this drug remain (Ionis, News release, 2022; Roche, News release, 2021; Tabrizi *et al.,* 2019). Attempts are underway to identify an allele specific ASO. Wave Life Sciences is attempting to achieve this through development of an ASO which selectively targets SNPs in the mHtt allele. Their first attempts with products designed to target two independent alleles failed to show a significant reduction of mHTT in early phase I/II trials (ie lack of target engagement) (https://clinicaltrials.gov/ct2/show/NCT03225846). However, another product designed to target a third SNP (WVE-003) has recently been shown to successfully lower mutant huntingtin (https://practicalneurology.com/news/allele-specific-antisense-oligonucleotide-lowers-mutant-huntingtin-protein-selectively-in-huntington-disease).

An alternative approach to drug therapy is cell replacement therapy, that aims, through neural stem cell transplantation, to restore functional striatal neuronal circuits lost by

neuronal degeneration. Decades of preclinical studies in rodents have provided proof-of-concept and addressed the feasibility of this approach for clinical translation (Dunnett and Rosser, 2007). Collectively, data have shown that the developmental properties of donor cells are critical to transplantation success. For grafted cells to grow, differentiate, express functional properties of MSNs and to innervate and integrate into host neuronal circuit they must have authentic developmental specificity of MSN progenitor cells, acquired through a process of developmental patterning in the lateral ganglionic eminence (LGE)- the foetal primordium to the striatum. However, the correct staging of MSN progenitors for transplantation is an important area of study. As the transplantation process is noxious to the cells often a low yield of transplanted cells is seen post-recovery. In order to survive the transplantation process, more plastic cells which are at an earlier developmental stage are preferable as more mature populations have poor survival and integration into the host brain. However, choosing very early progenitors may mean that the fate of these cells is not specified and while the resulting grafts may be full of cells, these may not be of the required phenotype. Furthermore, using early progenitor cells also introduces the risk of too much proliferation within the graft causing tumour-like growth in the transplanted region. Authentic donor LGE cells have been sourced from first-trimester aborted foetuses, with an optimal age of 8-10 weeks post conception and evaluated in a series of clinical trials. Although the safety and feasibility of intrastriatal foetal transplantation for HD has been demonstrated (Kopyov *et al.,* 1997a, 1997b; Philpott *et al.,* 1997) graft survival and integration and thus clinical motor and cognitive improvement has been variable both between centres and within trials (Philpott *et al.,* 1997; Kopyov *et al.,* 1997b; Keene *et al.,* 2009; Ross *et al.,* 1999; Bachoud-Lévi *et al.,* 2002; Gaura *et al.,* 2004; Bachoud-Lévi *et al.,* 2000; Barker *et al.,* 2013; Reuter *et al.,* 2008; Gallina *et al.,* 2010; Paganini *et al.,* 2014; Bachoud-Lévi *et al.,* 2006). While several years of improvement and stability in patient outcomes have been shown (Bachoud-Lévi *et al.,* 2000; Bachoud-Lévi *et al.,* 2002) benefit from grafts were seen to fade 4-6 years following surgery and is therefore not a permanent cure (Bachoud-Lévi *et al.,* 2006).

Whilst many variables can be optimised to improve graft outcomes, such as patient selection, pre- and post- operative evaluation, tissue processing, surgical procedures, instrument design, etc (NCT01898390; Barker and TRANSEURO consortium 2019),

difficulties in collection of clinical grade donor cells suitable for intrastriatal grafting will continue to account for a large source of variability seen between trials. Dependency on foetal tissues as donor cells also limits the possibility of histocompatibility matching, resulting in a greater need for immunosuppression and greater risk of allograft rejection. With significant ethical, as well as logistical concerns over foetal tissue collections, it is therefore a priority for renewable sources of donor MSN progenitor cells to be developed. Current research suggests that this need could be met by directing the differentiation of pluripotent stem cells (ESCs or iPSCS) to generate authentic MSN progenitors as a pharmaceutical grade cell therapy product (Reviewed in Li and Rosser, 2017; Bachoud-Levi *et al.,* 2021).

Taken together, future therapeutic developments for HD, for disease modelling, drug discovery and cell therapy, will be greatly enhanced by the application of iPSC/ESC technologies and the efficient and reproducible in vitro derivation of authentic MSNs.

Human induced pluripotent stem cell models of disease

Despite the significant impact of animal studies on our understanding and research into treatments for HD there is a growing need to study disease mechanisms, and to translate findings to drug discovery, in human cell models. The discovery that four transcription factors (Oct3/4, Sox2, cMyc and Klf4) can induce pluripotency in both mouse and human somatic cells (Takahashi and Yamanaka, 2006; Takahashi *et al.*, 2007) to derive induced pluripotent stem cells (iPSCs) has reshaped the way in which the mechanisms underlying neurodegeneration can be studied.

iPSCs are somatic cells that have been reprogrammed into a state of pluripotency. Thus, pluripotent cells have the ability to differentiate into a vast range of cells. Prior to iPSCs, pluripotent proliferative embryonic stem cells (ESCs) were taken from blastocysts. The reprogramming of adult somatic cells by-passes any ethical or logistical issues with ESC usage and confers many other potential benefits to the scientific and medical fields. Once generated these iPSCs can be differentiated into required cell types and used to look at

reparative treatments or disease modelling. Reparative therapies with patient derived IPSC lines could negate the requirements of immune suppression post-transplantation, indeed, preliminary results show successful dopamine cell transplantation into the CNS of a Parkinson's patient using this autologous approach (Schweitzer et.al., 2020). Cell lines for disease modelling can also use this angle of personalised medicine and drug discovery. By using a variety of iPSCs from a range of sources researchers are able to look at the genetic, patient-specific angle of disease treatment.

iPSC technology, together with advances in controlling cell differentiation have opened the possibilities of renewable sources of many cell types. Numerous studies have been published that claim to generate multiple neuronal subtypes of biomedical interest using human iPSCs by manipulation of the rostral-caudal and dorsal-ventral signalling pathways and transcription. It is important to understand the proper developmental stages involved in brain development in order to generate the correct cell type from iPSCs. This understanding is crucial since differentiation protocols aim to mimic *in vivo* expression patterns in the developing brain. Protocols which were originally developed using ESCs have been adapted to differentiate iPSCs to the desired cell fate. Notably, several differentiation protocols have been utilised to differentiate iPSC from both control and HD patients with varying success and generating sometimes conflicting phenotypic observations. Therefore, highlighting a need for the standardisation of iPSC differentiation protocols. Pertinently, differentiation to the MSN fate typically follows 3 stages: Neural induction, Patterning and Terminal differentiation.

Neural induction

Experiments utilising the xenopus animal cap have found that genes, such as, Noggin (Zimmerman et al., 1996), Chordin (Piccolo et l., 1996) Follistatin (Fainsod et al., 1997), Cerberus (Bouwmeester et al., 1996) and XNr (Smith et al., 1995) emanating from the organiser in animal cap ectoderm explants influence neural fate. By binding tightly to BMP, activation of its receptor and subsequent downstream SMAD1/5/8 signalling that promote epidermal fate, is inhibited (Meinhardt, 2001; Vonica and Gumbiner, 2007). Additionaly it

was shown that FGF/MAPK signalling is involved in anterior-posterior patterning of neural tissue (Ribisi et al., 2000).

With this in mind, several methods to generate neuroectoderm-like cells from ESCs and iPSCs have been developed including, serum free culture of embryoid bodies (EBs) and the more widely currently used Dual SMAD inhibition.

Although the EB method recapitulates the lineage specific (ectoderm, mesoderm and endoderm) differentiation processes that occurs *in vivo*, high concentrations of recombinant growth factor proteins such as FGF2 are required to form a concentration gradient within the embryoid (Itskovitz-Eldor *et al.,* 2000). In addition, the degree of heterogeneity in EB size affects viability, for example EBs that are too large can result in core necrosis due to restricted access to nutrients and hypoxia affecting downstream differentiation and application (McKee and Chaudhry, 2017).

More recently, the use of small molecules to inhibit Activin/Nodal/TGF-b and BMP signalling pathways (dual SMAD inhibition) (Chambers *et al.,* 2009; Kim et al., 2010) enhance neural induction. This eliminates the need for EB formation or co-culturing with stromal feeders, allowing for fully adherent (monolayer) techniques resulting in a more uniform and more consistent yield of anterior neuroectoderm cells with >80% $PAX6^+$ cells (chambers et al., 2009; Zhang et al., 2001 and Pankratz et al., 2007; Kirby et al 2012).

Deriving and culturing human iPSC-derived neurons *in vitro* relies primarily on either, EB formation followed by dissociation of rosettes and plating onto POL/laminin coated surfaces in N2/B27 medium, supplemented with exogenous patterning factors (Zhang et al., 2001; Pankratz et al., 2007) or fully adherent monolayer culture (Chambers *et al.,* 2009).

Cell Line(s)	Neural induction	Regionalisation	Terminal differentiation	Neuronal population(s)	Days *in vitro* (DIV)	Reference
iPSC - WT (15/17, Camnasio *et al.*, 2011) **ESC- HS401 (Inzunza *et al.*, 2004)** **H9**	Monolayer, induction as described by Chamber *et al.,* 2009. 5uM dorsomorphin or 500ng/ml noggin and 10uM SB431542 (12 days)	At D5, 200ng/ml SHHC-25II and 100ng/ml DKK1 (3 weeks)	N2 medium supplemented with B27 and 30ng/ml BDNF	D45 80% B-III D80: MAP2/GABA ~40% MAP2/CTIP2 ~30% MAP2/DARPP-32 ~10%	>80	Carri *et al.,* 2013
hESC: H9 and H1	1) EB suspension for 3 days KSR medium 2) N2 medium supplemented 2ug/ml heparin 3) D7 attachment and maintained	1) D12-25 addition SHH (200ng/ml) or 0.65uM purmorphamine was added 2) neural rosette detachment and cultured in suspension overnight	1) Neurobasal medium supplemented with VPA (10mM) For 1 week 2) plating at D32 laminin and addition of BDNF (20ng/ml), GDNF (10ng/ml), IGF-1 (10ng/ml) and cAMP (1mM)	B-III/GABA ~84.1% GABA/DARPP ~89.7%	>45	Ma *et al.,* 2012
hESCs: SA-01 and H9	1) Monolayer Stromal feeder based (MS5) in KSR medium 12 days	N2 medium supplemented with 200ng/ml SHH, 100ng/ml DKK1, and 20ng/ml BDNF	N2 medium supplemented with BDNF, 0.5mM dbcAMP and 0.5mM VPA	8% MAP2/GABA 12% MAP2/DARPP-32	>60	Aubry *et al.,* 2008

	2) Changed to N2 medium (D21) and rosette selection	Passaged after 8-10 days for up to 3 passages in the same conditions				
hESCs: H9 and H1	1) EB suspension for 4 days KSR medium 2) N2 medium supplemented 2ug/ml heparin 3) D7 attachment and maintained 4) rosette formation (D14-17)	SHH (100ng/ml) and DKK1 (100ng/ml) (D10-20)	N2/B27 Neurobasal medium supplemented with 10ng/ml BDNF, GDNF, IGF1 (6 weeks)	~40% ISLET1 ~10% Tbr1/Tub ~14% CTIP2 WB: DARPP-32, GAD65/67	>40	Li *et al.,* 2009
hESC: H9 and RC9 **iPSC - 190c17**	EB aggerates plated POL in N2/B27 medium supplemented with 0.1uM LDN193189 or 500ng/ml Noggin, 20uM SB431542 and 1uM XAV939 or 100ng/ml DKK1 (10days) rosette formation	1uM XAV939 or 100ng/ml DKK1 and 50ng/ml SHHC25II (D10-20)	N2/B27 medium supplemented with 20ng/ml BDNF, 0.5mM dbcAMP and 0.5mM VPA (D17-45)	~18% MAP2/DARPP-32	>60	Nicoleau *et al.,* 2013
hESCs: H9 and H1 **Q-CTS-hESC-2**	EB/Monolayer protocol Kirkeby *et al.,* 2012	SAG (100 nM) or purmorphamine (1 uM) (D0-D5)	NDM supplemented with BDNF (20ng/ml), GDNF(10ng/ml), AA	80-95% of MAP2 express DARPP-32	>20	Wu *et al.,* 2018

	1) EB suspension in NIM supplemented with XAV939 (1uM), LDN-193189 (100 nM), SB431542 (10 uM) and SAG (100nM) 2) Plate EBs D4 in NPM supplemented with LDN-193189 (100 nM), SB431542 (10 mM) (5-11days)		(0.2mM), and DAPT (1mM).	>89% TUJ1 express GABA		
hESC: H1, H7) hiPSC: 2F8, 4FH	Monolayer, induction as described by Chamber *et al.,* 2009. 200nM dorsomorphin or 500ng/ml LDN-193189 and 100nM SB431542 (12 days)	N2/B27 medium supplemented with 200ng/ml C24II-N (SHH), or cyclopamine (2uM) or Activin-A (25ng/ml) (D0-D9)	N2/B27 supplemented with BDNF (10ng/ml), and GDNF (10ng/ml)	20-50% DARPP-32 10-80% CTIP2	>40	Arber *et al.,* 2015
iPSC: 34D6 and 33Qn1	SLI medium: containing Advanced DMEM: F-12, supplemented with 1% Glutamax, 2% Neurobrew-21 (without Vit A), 1uM LDN-193189 and	LI medium: containing Advanced DMEM: F-12, supplemented with, 2% Neurobrew-21 (without Vit A), 2nM L-gluamine	SCM1 medium: containing Advanced DMEM:F-12 supplemented with, 1% Glutamax, 2% NeuroBrew21 (with Vit A), 2 uM PD0332991, 10 uM DAPT, 0.6 mM	~94% Map2 ~30% GABA ~6% DARPP-32 ~55% CTIP2	37	Telezhkin et al., 2015

	10uM SB431542, IWR-1 1.5uM (D0-D8)	(D8-D16)	$CaCl_2$, 200 mM ascorbic acid, 10 ng/ml BDNF, 1 uM LM22A4, 10 uM forskolin, 3 uM CHIR 99021 and 300 uM GABA (7 days) SCM2 medium: containing 1:1 Advanced DMEM/F-12: Neurobasal A supplemented with, 1% Glutamax, 2% NeuroBrew21 (with Vit A), 2 uM PD0332991, 0.3 mM $CaCl_2$, 200 mM ascorbic acid, 10 ng/ml BDNF, 1 uM LM22A4 and 3 uM CHIR 99021 (14 days)			

Table 1.1. Original differentiation protocols developed aimed at differentiating hESC to an MSN-fate.

Patterning

Taking advantage of the dorsal ventral gradient in the telencephalon, where SHH levels are highest ventrally and there is a high BMP concentration dorsally, protocols have been generated using small molecules and/or recombinant proteins to manipulate these pathways (Table 1). These molecules such as WNT and SHH pattern neural cells to a ventral LGE-fate.

Directed differentiation of iPSCs to MSNs

Aubry *et al.,* (2008) published the first protocol for MSN differentiation using the human ES cell line H9. This protocol was based on using an established neural induction step of co-culture with MS5 stromal cells to derive forebrain (anterior)-like neural progenitors. These could then be patterned using a combination of SHH and DKK treatment to ventralise naïve anterior neuroectoderm cells, with the aim of imparting an LGE-like fate on the cultures. Upon terminal differentiation some neurons expressed the mature striatal marker DARPP-32. Whilst this provides a good proof-of-concept that MSNs could be derived *in vitro* from pluripotent stem cells the efficiency of MSN generation was low with just ~22% cells expressing the post-mitotic neuronal marker MAP2, of which 36% expressed GABA. Of this small percentage of GABAergic neurons, 53% expressed the striatal marker DARPP-32.

A subsequent protocol that used dual SMAD inhibition (Chamber *et al.,* 2009) for the neural induction step, and then the same patterning cues, as above, to ventralise neuroectoderm cells, Carri *et al.,* generated a similar striatal yield. Here, after 80 days of terminal differentiation ~10% of MAP2 neurons co-expressed DARPP-32, whereas ~40% expressed GABA and ~30% expressed CTIP2, a marker commonly used in combination with DARPP-32 to identify MSN fate and discriminate between DARPP-32+ve/CTIP2-ve cortical neurons. Efficient neuronal induction was observed at D45 with ~80% Beta tubulin III (Tuj-1) neuronal cells. However, unlike Aubry *et al.,* Dibutyryl-cAMP was not used in their terminal differentiation medium which promotes the differentiation of pre-mitotic neural progenitor cells to post-mitotic neurons. Therefore, it is possible that some of these cells were too immature to be expressing the mature DARPP-32 MSN marker.

Utilising the small molecule purmorphomine to activate the hedgehog pathway, Ma *et al.,* (2012) showed that ~84% B-III tubulin neurons co-expressed GABA, and ~89% GABA neurons co-expressed DARPP-32 following terminal differentiation.

Although Ma *et al.,* and Carri *et al.,* differ in the neural induction methods and monolayer versus embryoid body protocols, this is unlikely to be the main source of variation as both protocols efficiently and consistently generate neuronal marker B-III tubulin. A more likely source could be the use of recombinant proteins which are known to show variation in bioactivity between lots and manufacturers versus small molecules. In addition, these protocols differ slightly in their terminal differentiation, in which during the first week, Ma *et al.,* treated cultures with Valproic acid (VPA), a HDAC inhibitor, in the absence of BDNF. Following this, VPA was removed and BDNF was added in addition to other neurotrophic support, whereas Carri *et al.,* used VPA in combination with BDNF. This is particularly interesting as a subsequent study showed that HDAC inhibitors in combination with BDNF can decrease the level of DARPP-32 expression by almost 50% relative to BDNF alone (Chandwani *et al.,* 2013). Therefore, this could also be the likely source of variation between protocols.

However, the use of SHH and/or purmorphamine in LGE specification and MSN generation has come into question. Arber *et al.,* 2015 suggested that SHH acts indirectly in culture rather than directly promoting an LGE fate. This study found that Activin-A treatment during patterning, increased LGE transcripts such as NOLZ1, FOXP2 and CTIP2, and upon terminal differentiation generated 20-50% of DARPP-32 neurons that co-expressed CTIP2, as opposed to fewer than 1% under basal culture conditions. More importantly, applying SHH upregulated more ventral MGE markers such as NKX2.1 in a dose dependent manner whilst it had no effect on LGE-enriched transcripts. Recently this has not been supported using iPSCs in both monolayer and EB-like neurospheres (Amimoto *et al.,* 2021). By directing iPSCs to a neuronal linage utilising dual SMAD inhibition and WNT inhibition, a study using different windows of purmorphamine treatment to identify the most appropriate for LGE specification was conducted. Here they found that addition of purmorphamine from D13 to D17 was the most appropriate window for LGE specification as assessed by an increase in LGE enriched transcript GSX2 and minimal expression of NKX2.1 protein (~6% NKX2.1^{+}).

Following terminal differentiation (64DIV), the majority of these cultures expressed DARPP-32 and GABA (~60%) and all DARPP-32 cells expressed CTIP2.

Terminal Differentiation

Astrocytes are essential for neuronal survival throughout *in vivo* development, by regulating metabolic properties (Attwell et al., 2010; Pellerin et al., 2007). For example, they physically form synapses with developing neurons and promote synaptogenesis via PKC activation (Hana et al., 2004; Risher and Eroglu 2012, Kucukdereli et al 2011). Therefore, in order to generate functionally mature neurons, studies have utilised rodent astrocyte co-cultures, which have been shown to promote a more physiological resting membrane potential (RMP) enabling neurons to fire spontaneous action potentials (Johnson *et al.,* 2007; Tang *et al.,* 2013; Kaczor et al 2015; Hu et al., 2016; Odawara et al., 2014). However, the use of rodent and human cocultures limits their capacity for drug screening. In addition, culturing 'healthy' cells with HD-iPSC derived neurons may mask functional deficits to paracrine and contact-mediated alterations in synaptic development.

Therefore, in order to obtain functionally mature MSNs, the above protocols have relied on extended terminal differentiation, requiring months in culture and manipulation of the CREB pathway with small molecule dbcAMP (Arber *et al.,* 2015; Carri *et al.,* 2012). Although neurons are able to elicit an action potential following a depolarising current, no spontaneous activity was observed even after prolonged culture (>80D). In addition, passive properties such as a hyperpolarised RMP, large membrane capacitance and input resistance were reminiscent of an immature neuron. More recently, Telezhkin *et al. 2016,* developed a two-step terminal differentiation medium, SCM1/2, to specifically accelerate maturation which included a combination of small molecules targeting NOTCH, WNT and CREB pathways. This maturation protocol only required 21 days of terminal differentiation and compared with standard neuronal differentiation protocols enhanced spontaneous action potential activity. However, compared to *in vivo,* the observed RMP was still relatively hyperpolarised (~-46mV). Immature electrophysiological properties are particularly problematic when studying neurogenerative disease such as HD, as it limits their utility for both disease modelling and the development of drugs in vitro.

Nevertheless, the neural induction, patterning and terminal differentiation protocols highlighted here have been implemented within the HD field to specifically generate MSNs and seek further understanding on the mechanisms underlying disease pathology.

HD-iPSC-disease models

First generated by Park *et al.* (2008), stable patient-specific HD-iPSCs have, to date, been shown to have the ability to self-renew, and differentiate into neuronal populations (Takahashi *et al.*, 2007; Yu *et al.*, 2007; Park *et al.*, 2008). In addition, HD-specific iPSC-derived neurons are like those generated from HD-embryonic stem cells (ESCs) (Zhang *et al.*, 2010; Camnasio *et al.*, 2012; The HD iPSC Consortium., 1993, The HD Ipsc and Phenotypes, 2012),thus, making HD-iPSCs a favourable model and eliminating any controversy surrounding ESC procurement. Furthermore, iPSCs will also bear all genetic or sporadic mutations from the donor. This makes iPSCs the most genetically precise model of HD, enabling investigations into modifiers of the AAO as well as high-throughput drug screening and testing. A collaborative effort involving multiple groups with the main goal of generating lines from patients with varying CAG repeat range (from 17-180 repeats) has been undertaken (The HD iPSC Consortium, 2012, 2017).

To date the best described HD iPSC line was generated by Park containing 72 CAG repeats (An *et al.,* 2012; Chae *et al.,* 2012; Chae *et al.,* 2012; Ring *et al.,* 2015; Charbord *et al.,* 2013; Jeon *et al.,* 2012,2014; Cheng *et al.,* 2013; Naphade *et al.,* 2018; Zhang *et al.,* 2010; Lopes *et al.,* 2020; Cann *et.,* 2021). However, in 2012 the HD iPSC consortium generated and extensively characterised 14 iPSC lines from HD and control patients using lentiviral transfection, with the longer juvenile CAG repeats (>60 CAGs) widely used (The HD iPSC Consortium 2012; Lu et al., 2014; Mattis et al., 2015). Subsequently, these iPSC lines have been generated using retroviral or the non-integrating episomal transfection methods (The HD iPSC Consortium 2012, 2017).

Many of these groups have differentiated these lines to MSN fates by adapting the protocol originally developed by Aubry *et al.,* 2015 and Carri *et al.,* 2013, and have shown a wide range of cellular phenotypes such as neurodevelopmental and maturation deficits, excitotoxicity, mitochondrial and autophagic dysfunctions.

There are currently >40 studies that have generated human iPSC lines from both HD and control patients, ranging from 18-180 CAG repeats. While a comprehensive review can be found elsewhere (Monk and Connor, 2021), this thesis will focus on the neuronal phenotypes across the studies listed below (Table 1.2).

HD Cell Lines	Control Cell Lines	Regionalisation	Terminal Differentiation	Neuronal Population(s)	Days in Vitro	HD Phenotype	Reference
HD60i.x, and HD180i.x	HD33i.x HD28i.2	Modified protocol based on Aubry *et al.,* BDNF (20 ng/ml) (2 days) Medium supplemented with rhShh (200 ng/ml), and Dkk1 (100 ng/ml). (21 days)	BDNF, dibutyryl cyclic AMP (dbcAMP, 0.5 mM) and valproic acid (VPA, 0.5 mM). If cells were differentiated as aggregates, they were plated on day 42.	<10% βIII-Tubulin- or Map2a/b < 5% DARPP-32/Bcl11B Variation between cultures	42	Altered gene expression: expression cell growth, proliferation, cell function, cell-cell signalling, and embryonic development Increase Ca^{2+} dyshomeostatsis with glutamate pulse Increase death upon BDNF withdrawal Increase caspase 3/7 with BDNF withdrawal CAG instability 110-118	The HD iPSC Consortium 2012

HD Cell Lines	Control Cell Lines	Regionalisation	Terminal Differentiation	Neuronal Population(s)	Days in Vitro	HD Phenotype	Reference
GM09197 (180/18 CAG repeats) *ND39258 (109/19 CAG repeats)*	GM05400 (21/18CAG repeats)	Neurospheres in medium supplemented with EGF and FGF (100mg/ml)	HD iPSC Consortium 2012 method	~5% DARPP32 ~10% Tuj1 ~20% GFAP	42	Increased cell death upon BDNF withdrawral	Lu et al., 2014
CS97iHD-180nXX *CS109iHD-109nXX*	CS00iCTR-21nXX CS14iCTR-nXX CS83iCTR-33nXX	Modified protocol based on Aubry *et al., Medium supplemented with* 20 ng/ml BDNF, rhShh (200 ng/ml) and Dkk1 (100 ng/ml) (21 days)	BDNF (20ng/ml), dibutyryl cyclic AMP (dbcAMP, 0.5 mM) and valproic acid (VPA, 0.5 mM).	1-5% DARPP-32, TUJ 15-35%, GFAP 10-40%	42	Increase expression of RIN2B NMDA R subunit mRNA. Increase persistance nestin + cells BDNF withdrawal increases cell death	Mattis et al., 2015
CS13iHD-43nXX, CS03iHD53nXX, and CS109iHD-109nXX	CS00iCTR-21nXX, CS14iCTR-nXX, CS25iCTR-18nXX, CS83iCTR-33nXX	Same protocol as The HD iPSC Consortium, 2012	Same protocol as The HD iPSC Consortium, 2012	~16% GFAP 27% TUJ1 14.8% MAP2ab 14.3% DARPP-32	56	Decrease in calcium signalling pathway genes Decrease in striatal and neurodevelopmental genes	The HD iPSC Consortium

HD Cell Lines	Control Cell Lines	Regionalisation	Terminal Differentiation	Neuronal Population(s)	Days in Vitro	HD Phenotype	Reference
CAG180 (ND36999)	CAG33 (ND36997) Isogenic control	Following the same protocol as Li *et al.,* N2/B27 medium supplemented SHH (100ng/ml) and DKK1 (100ng/ml)	N2B27 medium supplemented with BDNF (20 ng/mL), GDNF (20 ng/mL), cAMP (0.5 mM), and ascorbic acid (0.2 mM).	ICC images for MAP2/GABA MAP2/SYP No quantitate data presented	48	Mitochondrial dysfunction, rescued with Isogenic	Xu et al., 2017
iPSC lines were obtained from Mattis et al Q60, Q109, and Q180	Q21, Q28, Q33	N2/B27 medium supplemented with SHHC-25II (200 ng/mL) and DKK1 (100 ng/mL) (3 weeks)	Addition of 30 ng/mL BDNF	ICC staining MAP2/TUBB3 CTIP2/DARPP-32 No quantitate data presented	50	Abnormal striatal progenitor differentiation and maturation Decresed neuronal yeilds Altered expression relating to function	Conforti et al 2018
CS97iHD180, CS09iHD109, CS77iHD77, CS81iHD71 CS21iHD60	CS83iCTR33 CS14iCTR28 CS00iCTR21 CS25iCTR18	Modified protocol based on Aubry *et al.,* Medium supplemented *with* 20 ng/ml	N2B27 medium supplemented with BDNF (20 ng/mL), cAMP (0.5 mM), and VPA (0.5 mM).	5-25% TuJ1 1-15% GFAP	42	Persistent nestin cells	Mathkar et al., 2019

		BDNF, rhShh (200 ng/ml) and rhDkk1 (100 ng/ml) (21 days)	Up to day 42 and 56) Medium changed 3 time a week with 1:1 new medium and conditioned medium				
HD Cell Lines	Control Cell Lines	Regionalisation	Terminal Differentiation	Neuronal Population(s)	Days in Vitro	HD Phenotype	Reference
GM09197 *GM04212*	GM04204	Medium supplemented with SAG (50 nM) and XAV-939 (1 µM) (D10 to 20)	Medium supplemented with BDNF (20 ng/ml), dbcAMP (0.5 mM), and Valpromide (0.5 mM).	>95% MAP2 >80% DARPP32	45	Differentially expressed genes enriched in neurogenesis following progerin treatment	Cohen-carmon et al 2020
HD iPSC consortium cell lines *CS04iHD46n10* *CS03iHD53n3* *CS02iHD66n4* *CS81iHD71n3* *CS09iHD109n1*	CS25iCTR18n2 CS25iCTR18Qn6 CS14iCTR28n6 CS83iCTR33n1	Combination of protocols addated from both Telezhkin et al., 2015 and Arber *et al.,* 2015	Following the protocol developed by Telezhkin et al., 2015	79%–98% $MAP2^{+}$ 5-25% DARPP-32/CTIP2	37	Persistant cyclin D1 + NSC like population in adult HD Upreg of cell cycle related genes in HD	2020 Smith-Geater et al., 2020

Table 1.2. Neurodevelopmental and degenerative phenotypes observed in iPSC-derived neurons.

Neurodevelopmental phenotypes

Following neural induction, a number of studies have reported early developmental phenotypes correlating with CAG repeat length (≥60 CAG) such as inefficiency or inability to adopt a neural fate (Jeon *et al.,* 2012; The HD iPSC Consortium, 2012; Conforti *et al.,* 2018; Xu *et al.,* 2017). For example, following dual SMAD inhibition Conforti *et al., reported* that all HD lines (HD60, HD109 and HD180) were unable to switch off OCT4 expression following 15 days *in vitro* and observed abnormal rossette formation. Analysis of the population of OCT4 cells at D8 revealed a clear correlation between CAG repeats. In addition, neuronal rosette formation has also been observed in HD180 (Xu *et al.,* 2017); this phenotype was corrected for use in the isogenic control containing 33CAG repeat.

Following terminal differentiation (>40 DIV), The HD iPSC Consortium showed HD positive, striatal-like cells increased expression of genes involved in cellular growth, proliferation, function and maintenance compared to control lines (The HD iPSC Consortium, 2012). At a functional level, HD neurons with longer CAG repeats (HD180) showed no spontaneous or induced action potentials, in contrast to both controls and HD lines with lower CAG repeat lengths (HD109 and HD60). However, this was shown to be due to the viability of this line, with cell death occurring by three weeks of differentiation as assessed by caspase 3 quantification. Utilising episomal reprogramming of donor HD and control lines, the HD iPSC consortium further identified alterations in genes and pathways associated with neurodevelopment using RNA sequencing comparing the differential gene expression profiles in HD iPSC-derived neurons to controls. Here, out of 1,869 of DEGs, 29% centred on development, including, cellular, nervous system and function/tissue development. In addition, there was a significant decrease in genes involved in neuronal development and maturation, as well as genes encoding proteins involved in synaptic development.

A neurodevelopmental phenotype has also been illustrated by, Mattis *et al.,* in which a significantly higher proportion of nestin^{+} cells following 42 days of differentiation in HD lines (HD60, HD109, HD180) compared to controls. Following on from this, Mathkar *et al.,* examined at which stage during differentiation this phenotype appears. Here they found

that following 14 days of striatal differentiation, HD neural progenitor cells expressed a significantly higher percentage of nestin$^+$ cells (34-54%) than controls (19-37%). This difference remained significant by 28 DIV with nestin$^+$ cells accounting for ~ 27-44% of HD and 3-16% of control cells. The results from their previous study were also confirmed this at 42DIV in a following study (Mattis *et al.,* 2015). However, extending culture beyond 56 DIV resulted in no significant difference.

Perhaps the most compelling argument for a neurodevelopmental and or maturation phenotype has come from the work of Conforti *et al.,* 2018, in which HD and control lines were differentiated into both striatal and cortical neurons. Following 30 DIV, control and HD striatal neurons were assessed for their electrophysiological properties by whole cell patch clamp. Applying current injection resulted in only 8% of HD109 neurons generating 1 action potential, whereas 58% of controls did. Furthermore, at a gene expression level, HD lines were shown to have significantly less sodium channel transcripts such as SCN1B, SCN2B, SCN3B, and SCN4B which play essential roles in regulating excitability *in vivo* (reviewed in Brackenbury and Isom, 2011). Gene expression changes were also observed following 45 days of cortical organoid differentiation, resulting in 1,452 DEGs between control and HD (HD109) in which downregulated genes were significantly associated with nervous stem cell development, morphology of the cerebral cortex, differentiation, and maturation.

These studies support the hypothesis that mHTT causes a neurodevelopmental delay, however it would appear this phenotype is not specific to striatal linage and or neurons at the gene expression level. Although the above studies aimed to generate MSNs, neuronal yield was low, as assessed by b-III-Tubulin (<10%, 27%, 5-20%, 10-20%, ICC quantification not presented) and DARPP-32 alone or co-localised with CTIP2 was also low (<5% DARPP-32/CTIP2, 14% DARPP-32, 1-4% DARPP-32, ICC quantification not presented).

Neuron function and neurodegenerative phenotypes

Following neural induction and patterning a number of calcium signalling gene have been reported to be altered in the HD60 line (The HD iPSC Consortium). In addition, An *et al.,* found that isogenic controls of the HD180 line corrected the altered BDNF levels found in

NPCs. In HD iPSC-derived neurons multiple chronic glutamate pulses resulted in calcium dyshomeostasis and cell death upon BDNF withdrawal (The HD iPSC Consortium, 2012). Following this Mattis *et al.,* investigated the NMDAR subunits expression, GRIN2A and GRIN2B, and found under basal conditions there were no significant differences in expression between HD and control. However, upon BDNF withdrawal, GRIN2B subunit was upregulated, and blocking NMDAR with memantine during BDNF withdrawal prevented cell death in HD NPCs. This glutamate excitotoxicity following BDNF withdrawal was not specific to NMDARs as blocking AMPA/Kainate receptors with CNQX also prevented cell death (Mattis *et al.,* 2015). In addition, at a gene expression level, differentially expressed genes between differing CAG lengths, were enriched in the calcium signalling pathway (The HD iPSC Consortium, 2017), surprisingly GRIN2B was not shown to be differentially expressed. This may be explained by the maturity and/or differing populations of neurons within the cultures. These studies provide evidence for the glutamate excitotoxicity hypothesis of HD and which is likely mediated through calcium signalling.

Considerations for the use of iPSC-derived to model HD

Although there are currently >40 studies that have generated human iPSC lines from both HD and control patients ranging from 18-180 CAG repeats, they differ considerably in reprograming methods, culture conditions, donor genetic background, HTT genotype, age and sex, and differentiation protocols. Thereby making comparisons between studies difficult as variation in phenotype may be attributed to any one of these factors. It is important to note that some of the studies show some consistency in the phenotypes observed. However, one fundamental problem is that these protocols generate low neuronal populations, specifically the MSN population. Gene expression data are from bulk RNA sequencing with little to no evidence of MSN-specificity. To counter this limitation, advances in CRISPR-Cas9 technology has allowed for the assessment of inter-line variability by producing isogenic lines but it still does not address the cell population heterogeneity.

Recently, the challenge in generating MSNs from both control and HD-derived iPSCs was investigated (Le Cann et al. 2021). Following two MSN-differentiation protocols (Arber et al. 2015; Stanslowsky et al. 2016), Cann *et al.,* found that both protocols not only generated low to no DARPP-

32 expressing neurons (0-60%), but the efficiency of generating neurons at all was poor and variable (9-42% Tuj1$^+$ cells). This contrasts to the efficiencies previously reported by Stanslowsky *et al.,* (2016) and by Arber *et al.,* (2015) who generated ~80% TUBB3$^+$ neurons of which ~80% expressed GABA and ~40% expressed DARPP-32; or 20-50% DARPP-32/CTIP2 positive neurons respectively. Interestingly, differing populations of interneuron subtypes have also been reported using MSN differentiation protocols. Cann *et al*., found that both the Stanslowsky and Arber protocols generated TH, calretinin and somatostatin interneurons, however neither protocol produced Parvalbumin, NPY or VIP-expressing interneurons. The presence of TH$^+$ neurons is consistent with many MSN-differentiation protocols (Comella-Bolla et al. 2020). Whilst Cann *et al.,* highlighted the lack of reproducibility of generating the desired populations of cells across labs, they failed to address the cause of clone-to-clone variability under the same patterning and maturation cues and offered no resolution to the problem.

For iPSC-derived neurons to be useful for drug screening it is imperative they acquire mature functional characteristics both passive and active membrane properties similar to neurons *in vivo.*

Aims of this thesis

It is evident from the research outlined in this introduction that there is a lack of an efficient and reproducible differentiation protocol to generate MSNs from iPSC lines. In order to expand our knowledge on the earlier molecular and functional consequences that HD has, it is imperative to generate an appropriate model to study the disease. Whilst phenotypes are observed, these are not specific to MSN, which are selectively vulnerable to mHtt. If iPSC-derived neurons are to be used for drug screening and/or regenerative medicine, there is a desperate need for optimised protocols.

In my PhD I aim to investigate the inherited inter-line variability in generating MSNs from iPSCs following identical cues. I aim to identify signalling pathways that may be biasing cell lines to an alternative fate, such as those influencing the dorso-ventral axis *in vitro.* By doing so, I also aim to optimise our protocols in order to generate an efficient, reproducible and enrich population of MSN differentiation protocol.

Main objectives

- To further investigate the variation seen in MSN populations differentiated from iPSC lines and how this is influenced by changes in differentiation protocol and donor cell variance.

- To explore the HH pathway as a source of iPSC differentiated MSN variation. By inhibiting its action and using RNA sequencing analysis to identify downstream signalling pathways as potential targets for intervention.

- To generate a CRISPR KO line ablating both upstream and downstream targets of the HH pathway and to investigate the effects this has on MSN differentiation.

Chapter 2: Methods

Ethics and tissue collection.

Products of conception were donated through medical terminations of pregnancy using South Wales Initiative for Foetal Tissue (SWIFT). All procedures were approved by ethics committee (project # RTB45). Relevant tissues: cortex (CTX), lateral- or medial- ganglionic eminence (LGE and MGE, respectively) were dissected by tissue bank staff at Brain Repair Group, Cardiff University. All tissues were stored in physiological medium (Hibernate-E) at 4 degrees until collection and processing.

Key Resources

Cell Lines							
Name	**Donor**	**Disease Status**	**CAG repeat length**	**Source Material**	**Sex**	**Company**	**Other Notes**
Kolf2	HPSI0114i-Kolf2	Normal	~20/19	Fibroblast	Male	HipSci	Bill Skarnes collaborators at the Jackson Labs have identified a 19bp deletion in the ARID2 gene (c.590-608del CTAAAATCATCACTTTACT, p.(Prol197Hisfs*12), het)). This mutation was overrepresented in the read data in early passages suggesting a growth advantage. This line was used throughout this thesis. Although this SNP was not confirmed by genotyping it is likely.
18n6	CS25iCTR18Qxx	Clinically Normal	~18/21	Fibroblast	Male	Cedars Sinai	
33n1	CS83iCTR-33nxx	Clinically Normal; At risk (50%) for Huntington's Disease, 33 CAG repeats	~33/22	Fibroblast	Female	Cedars Sinai	
60n4	CS21iHD-60xx	Onset at age 18 years; similarly affected	~60/20	Fibroblast	Female	Cedars Sinai	

		grandmother and father					
60n5	CS21iHD-60xx	Onset at age 18 years; similarly affected grandmother and father	~60/20	Fibroblast	Female	Cedars Sinai	
109n1	CS09iHD-109xx	Clinically Affected	~120/21	Fibroblast	Female	Cedars Sinai	CAG repeat expansion. Also prone to Trisomy of chromosome 1
109n5	CS09iHD-109xx	Clinically Affected	~120/21	Fibroblast	Female	Cedars Sinai	CAG repeat expansion. Also prone to Trisomy of chromosome 2

Table 2.1. Cell line information

Edited Cell Lines from the Allen lab and those generated in this thesis					
Name	Parent Line	Disease status of Parent Line	CRISPR Edited	CAG repeat length	Other notes
A6 **33n1$^{+/+\ A6}$**	33n1	Clinically Normal; At risk (50%) for Huntington's Disease, 33 CAG repeats	non-edited control	33/21	Collectively with clones F1, C1 and parent 33n1 as Control in Chapter 5.
F1 **33n1$^{+/+\ F1}$**	33n1	Clinically Normal; At risk (50%) for Huntington's Disease, 33 CAG repeats	non-edited control	33/21	Collectively with clones A6, C1 and parent 33n1 as Control in Chapter 5.
C1 **33n1$^{+/+\ C1}$**	33n1	Clinically Normal; At risk (50%) for Huntington's Disease, 33 CAG repeats	non-edited control	33/21	Collectively with clones A6, F1 and parent 33n1 as Control in Chapter 5.

G5 **33n1$^{+/+\ G5}$**	33n1	Clinically Normal; At risk (50%) for Huntington's Disease, 33 CAG repeats	non-edited control	33/21	Although sequencing of Exon1 showed no targeting. At D16 NKX2.1 protein was not expressed and therefore was excluded from further analysis
C3 **33n1$^{NKX2.1-/-\ C3}$**	33n1	Clinically Normal; At risk (50%) for Huntington's Disease, 33 CAG repeats	NKX2.1 knockout, Homozygous	33/21	Collectively with clones E6 and H3 as NKX2.1 $^{-/-}$ or NKX2.1 KO in Chapter 5.
E6 **33n1$^{NKX2.1-/-\ E6}$**	33n1	Clinically Normal; At risk (50%) for Huntington's Disease, 33 CAG repeats	NKX2.1 knockout, Homozygous	33/21	Collectively with clones C3 and H3 as NKX2.1 $^{-/-}$ or NKX2.1 KO in Chapter 5.
H3 **33n1$^{NKX2.1-/-\ H3}$**	33n1	Clinically Normal; At risk (50%) for Huntington's Disease, 33 CAG repeats	NKX2.1 knockout, Homozygous	33/21	Collectively with clones C3 and E6 as NKX2.1 $^{-/-}$ or NKX2.1 KO in Chapter 5.
4E6 **33n1$^{SHH-/-\ 4E6}$**	33n1	Clinically Normal; At risk (50%) for Huntington's Disease, 33 CAG repeats	SHH knockout, Homozygous	33/21	Both WT alleles were targeted in this line, however one of predicted deletion and another which contained insertions/deletion which ultimately resulted in loss of protein. See Chapter 5 for more details. Referred to as SHH $^{-/-}$ or SHH KO in Chapter 5.
4E6_SC11A **33n1$^{SHH-/-\ SC11A}$**	33n1	Clinically Normal; At risk (50%) for Huntington's Disease, 33 CAG repeats	SHH knockout, Homozygous	33/21	Low SHH efficiency, therefore Clone 4E6 was plated as single cells and subcloned generating this line. Referred to as SHH $^{-/-}$ or SHH KO in Chapter 5.
4E6_SC11F **33n1$^{SHH-/-\ SC11F}$**	33n1	Clinically Normal; At risk (50%) for Huntington's Disease, 33 CAG repeats	SHH knockout, Homozygous	33/21	Low SHH efficiency, therefore Clone 4E6 was plated as single cells and subcloned generating this line. Referred to as SHH $^{-/-}$ or SHH KO in Chapter 5.

2H1 CTRL$^{ISO\text{-}HD109\text{-}2H1}$	109n1	Clinically Affected	Corrected Htt gene. Expanded CAG length replaced with 22CAG	22/21	Prone to Trisomy Chromosome 1 Created by Dr Jasmine Donaldson Collectively with 3H2 and 5H9 referred to as Isogenic in Chapter 3.
3H2 CTRL$^{ISO\text{-}HD109\text{-}3H2}$	109n1	Clinically Affected	Corrected Htt gene. Expanded CAG length replaced with 22CAG	22/21	Prone to Trisomy Chromosome 1 Created by Dr Jasmine Donaldson Collectively with 2H1 and 5H9 referred to as Isogenic in Chapter 3
5H9 CTRL$^{ISO\text{-}HD109\text{-}5H9}$	109n1	Clinically Affected	Corrected Htt gene. Expanded CAG length replaced with 22CAG	22/21	Prone to Trisomy Chromosome 1 Created by Dr Jasmine Donaldson Collectively with 2H1 and 3H2 referred to as Isogenic in Chapter 3

Table 2.2. CRISPR Cas9 gene edited lines

Foetal SWIFT Samples				
Name	Brain Region	Age (post conception day; pcd)	Crown-to-Rump-Length (CRL)	Other notes
SWIFT #2449	CTX, LGE, MGE	71	~70	Used in BioMark qPCR assay
SWIFT #2452	CTX, LGE, MGE	63	~59.6	Used in BioMark qPCR assay
SWIFT #2457	CTX, LGE, MGE	76	~71.5	Used in BioMark qPCR assay
SWIFT #2458	CTX, LGE, MGE	82	~87	Used in BioMark qPCR assay
SWIFT #2459	CTX, LGE, MGE	62	~46	Used in BioMark qPCR assay
SWIFT #2462	CTX, LGE, MGE	73	~52	Used in BioMark qPCR assay
SWIFT #2544	CTX, LGE, MGE		116	Used in BioMark and LightCycer qPCR assay
SWIFT #2513	CTX, LGE, MGE	92	113	Used in BioMark and LightCycer qPCR assay
SWIFT #2535	CTX, LGE, MGE	86	95	Used in BioMark and LightCycer qPCR assay

Table 2.3. – SWIFT Foetal sample information. Each sample was weighed out ~20mg taken for RNA (X2/region). Remaining tissue was processed for protein

Cell culture reagents		
Item	**Company**	**Product code**
Culture Media		
E8 Flex medium	Thermofisher	A2858501
Advanced DMEM/F-12	Thermofisher	12634028
KnockOut™ DMEM	Thermofisher	10829018
Neurobasal-A Medium	Thermofisher	10888022
Glutamax	Thermofisher	35050061
MACS® NeuroBrew®-21	Miltenyibiotech	130-093-566
MACS® NeuroBrew®-21 w/o Vitamin A	Miltenyibiotech	130-097-263
Cell Dissociation		
Accutase	Sigma	A6964
ReLeasR	Stem cells	100-0484
Trypsin	Thermofisher	25300054
Neural Induction Small Molecules		
SB431542	Tocris	1614
LDN193189	Tocris	TB6053-RMU
endo-IWR1	Tocris	3532
Patterning		
Activin-A	Peprotech	12014
Cyclopamine - KAAD	Milipore	239804
Purmorphamine	Tocris	4551
PluriSln-1 10mg	Stem cells	72822
BMP6	Miltenyibiotech	130-112-948
Terminal Differentiation		
PD0332991	Tocris	4786
DAPT	Tocris	2634

CHIR99021 Trihydrochloride	Tocris	4953
Human BDNF	Miltenyibiotech	130-093-811
LM22A4	Tocris	4607
Forskolin	Tocris	1099
GABA	Tocris	344
$CaCl_2$ (1M)	Sigma	21115
Ascorbic acid	Sigma	A4544
Coating Matrix		
Vitronectin	Thermofisher	A14700
Matrigel GFR LDEV-free 10ml	SLS	354230
PDL	Sigma	P6407
Cell culture ware		
T25	Thermofisher	136196
12 well plates	Thermofisher	150628
6 well plates	Thermofisher	140685
4 well plates	Thermofisher	176740
13mm Coverslips	VWR	631-0149
Cell culture microplate 96 well PS F-bottom Black u-clear	Greiner	655090
13mm coverslips	VWR	631-0149
Other		
Cryostor CS10	Stem cells	CS10
ROCK inhibitor Y-27632	HelloBio	HB2297
PBS, pH 7.2	Thermofisher	20012027
DPBS, calcium, magnesium	Thermofisher	14040133
Hibernate™-E Medium	Thermofisher	A1247601
d H_2O	Thermofisher	15230089
Demecolcine	Sigma	D1925
Penicilin/Streptomycin 100x	Thermofisher	15140122

Table 2.4. Cell culture reagents

PCR reagents		
Item	**Company**	**Product code**
Demecolcine solution	Sigma	D1925
LA Taq DNA polymerase with GC buffers	Takara	RR02AG
LightCycler 480 SYBR Green I Master	Roche	4707516001
PowerUp SYBR Green Master Mix	Thermofisher	A25777
qScript cDNA Synthesis Kit	VWR	733-1177
QuickExtract™ DNA Extraction Solution	Cambio	QE0901L
GoTaq® G2 Flexi DNA Polymerase	Promega	M7801
RNeasy Kit	Qiagen	74104
RNase-free Dnase set	Qiagen	79254
2-Mercaptoethanol	Sigma	M3143
DNeasy Blood & Tissue Kit	Qiagen	69504
Exonuclease I (E.coli)	New England labs	M0293S
SsoFast EvaGreen Supermix with Low ROX (200 x 20ul)	Biorad	1725210
Preamp master mix	Fluidigm	100-5580
96.96 Dynamic array	Fluidigm	BMK-M-96.96
GE 48.48 Dynamic Array	Fluidigm	100-3400
Control Line Fluid Kit- 192.24	Fluidigm	100-4058
TE Buffer	Thermofisher	12090015
100bp DNA Ladder	Promega	G2101
1kb DNA Ladder	Promega	G5711
96 well PCR plate, non-skirted, Low-Profile, White	StarLab	E1403-0209-C
TAE Buffer (Tris-acetate-EDTA) (50X)	Thermofisher	B49
Agarose	Sigma	1012360500
SafeView Nucleic Acid Stain	NSB Biologicals	NBS-SP1

2.5. PCR reagents

CRISPR reagents		
Item	**Company**	**Product code**
Alt-R® CRISPR-Cas9 tracrRNA, ATTO™ 550, 20 nmol	IDT	1075928
Alt-R® S.p. HiFi Cas9 Nuclease V3, 500 µg	IDT	1081061
P3 Primary Cell 4D-NucleofectorTM	Lonza	V4XP-3024
Nuclease Free Duplex Buffer	IDT	11-01-03-01

2.6. CRISPR reagents

Immunocytochemistry reagents		
Item	**Company**	**Product code**
Paraformaldehyde	Sigma	8187150100
Probumin® Bovine Serum Albumin Microbiological Grade, Powder	Sigma	810651
Normal Goat Serum	Abcam	ab7481
Foetal Bovine Serum	Sigma	F7524
Triton™ X-100	Sigma	T8787
Glycine	Sigma	50046
Recombinant Anti-TTF1 antibody [SP141]	Abcam	ab227652
Anti-Ctip2 antibody [25B6]	Abcam	ab18465
Recombinant Anti-DARPP32 antibody [EP721Y]	Abcam	ab40802
Anti-Tyrosine Hydroxylase Antibody	Milipore	AB152

Anti-CHAT	Milipore	AB144P
Anti-GABA	Sigma	A2052
Anti-VGluT1 (discontinued)	Abcam	ab72311
Goat anti-Rabbit IgG (H+L) Cross-Adsorbed Secondary Antibody, Alexa Fluor 488	ThermoFisher Scientific	A-11008
Goat anti-Rabbit IgG (H+L) Cross-Adsorbed Secondary Antibody, Alexa Fluor 594	ThermoFisher Scientific	A-11012
Goat anti-Rat IgG (H+L) Cross-Adsorbed Secondary Antibody, Alexa Fluor 555	ThermoFisher Scientific	A-21434
Goat anti-Rat IgG (H+L) Cross-Adsorbed Secondary Antibody, Alexa Fluor 594	ThermoFisher Scientific	A-11007
Goat anti-Mouse IgG (H+L) Cross-Adsorbed Secondary Antibody, Alexa Fluor 594	ThermoFisher Scientific	A-11005
Goat anti-Mouse IgG (H+L) Cross-Adsorbed Secondary Antibody, Alexa Fluor 488	ThermoFisher Scientific	A-11001
Hoechst 33258, Pentahydrate (bis-Benzimide)	ThermoFisher Scientific	H3569

2.7. Immunohistochemistry reagents

Western blot		
Item	**Company**	**Product code**
RIPA buffer	ThermoFisher Scientific	89900
PhosSTOP™	Sigma	4906845001
cOmplete™, Mini, EDTA-free Protease Inhibitor Cocktail	Sigma	11836170001
Pierce™ BCA Protein Assay Kit	ThermoFisher Scientific	23225
NuPAGE™ 4 to 12%, Bis-Tris, 1.0 mm	ThermoFisher Scientific	NP0322PK2
NuPAGE™ MOPS SDS Running Buffer (20X)	ThermoFisher Scientific	NP0001
NuPAGE™ Transfer Buffer (20X)	ThermoFisher Scientific	NP0006
NuPAGE™ LDS Sample Buffer (4X)	ThermoFisher Scientific	NP0008
10X Bolt™ Sample Reducing Agent	ThermoFisher Scientific	B0009
Nitrocellulose Membranes, 0.45 µm	ThermoFisher Scientific	88025
Western Blotting Filter Paper, 0.83 mm thick	ThermoFisher Scientific	84784
Recombinant Anti-TTF1 antibody [EP1584Y][1]	Abcam	ab76013
Sonic Hedgehog[2]	DSHB	5E1
Anti-alpha Tubulin antibody [DM1A]	Abcam	ab7291

IRDye® 680RD Goat anti-Mouse IgG Secondary Antibody	LI-COR	926-68070
IRDye® 800CW Goat anti-Rabbit IgG Secondary Antibody	LI-COR	926-32211
Precision Plus Protein™ Unstained Protein Standards, Strep -tagged recombinant	Bio-Rad	1610363
TWEEN® 20	Sigma	P9416

[1] non-specific bank at ~32kDa

[2] 3 SHH banks at ~30kDa, 20kDa and 16kDa

2.8. Western Blot reagents

Electrophysiology		
Item	**Company**	**Product code**
Potassium chloride	Sigma	P9541
Sodium chloride	Sigma	S3014
HEPES	Sigma	54457
Adenosine 5'-triphosphate disodium salt hydrate	Sigma	A26209
Guanosine 5'-triphosphate sodium salt hydrate	Sigma	51120
Phosphocreatine disodium salt hydrate	Sigma	P7936
Magnesium chloride	Sigma	M8266
$CaCl_2$ (1M)	Sigma	21115-100ml
EGTA	Sigma	324626

D-Glucose	Sigma	G7528

2.9. Electrophysiology reagents

RNA Sequencing		
Item	**Company**	**Product code**
Qubit RNA BR assay kit	ThermoFisher Scientific	Q10210
High Sensitivity RNA ScreenTape	Agilent	5067-5579
High Sensitivity RNA ScreenTape Ladder	Agilent	5067-5581
High Sensitivity RNA ScreenTape Sample Buffer	Agilent	5067-5580
TruSeq® Stranded mRNA Library Prep	Illumina	20020594

2.10. RNA sequencing reagents

Software and Algorithms		
Name	**Reference**	**URL/doi/CRAN**
R version 4.1.1	R Core Team (2021). R: A language and environment for statistical computing. R Foundation for Statistical Computing, Vienna, Austria Statistical Computing, 2017	https://www.R-project.org/.
R Package: 'edgeR'	Robinson MD, McCarthy DJ and Smyth GK (2010). edgeR: a Bioconductor package for differential analysis of digital gene expression data. Bioinformatics 26, 139-140 expression	10.1093/bioinformatics/btp616
R Package: 'EnhancedVolcano'	Kevin Blighe, Sharmila Rana and Myles Lewis (2021). EnhancedVolcano: Publication-ready volcano plots with enhanced colouring and labelling.	https://github.com/kevinblighe/EnhancedVolcano
R Package: 'tidyverse'	Wickham et al., (2019). Welcome to the tidyverse. Journal of Open-Source Software, 4(43), 1686	https://doi.org/10.21105/joss.01686
R Package: 'gplots'	Gregory R. Warnes, Ben Bolker, Lodewijk Bonebakker, Robert Gentleman, Wolfgang Huber, Andy Liaw, Thomas Lumley, Martin Maechler, Arni Magnusson, Steffen Moeller, Marc Schwartz and Bill Venables (2020).	https://CRAN.R-project.org/package=gplots
R Package: 'RColorBrewer'	Erich Neuwirth (2014). RColorBrewer: ColorBrewer Palettes. R package version 1.1-2.	https://CRAN.R-project.org/package=RColorBrewer

R Package: 'devtools'	Hadley Wickham, Jim Hester and Winston Chang (2021). devtools: Tools to Make Developing R Packages Easier	https://CRAN.R-project.org/package=devtools
R Package: 'ggrepel'	Kamil Slowikowski (2021). ggrepel: Automatically Position Non Overlapping Text Labels with 'ggplot2'.	https://CRAN.R-project.org/package=ggrepel
R Package: 'ComplexHeatmap'	Gu, Z. Complex heatmaps reveal patterns and correlations in multidimensional genomic data. Bioinformatics 2016. https://github.com/jokergoo/ComplexHeatmap	
R Package: 'circlize'	Gu, Z. circlize implements and enhances circular visualization in R. Bioinformatics 2014.	10.1093/bioinformatics/btu393
R Package: 'SARTools'	Hugo Varet, Loraine Brillet-GuÃ©guen, Jean-Yves CoppÃ©e and Marie-AgnÃ¨s Dillies (2016): SARTools: A DESeq2- and EdgeR-Based R Pipeline for Comprehensive Differential Analysis of RNA-Seq Data. PLoS One, 2016	http://dx.doi.org/10.1371/journal.pone.0157022
R Package: 'clusterProfiler'	T Wu, E Hu, S Xu, M Chen, P Guo, Z Dai, T Feng, L Zhou, W Tang, L Zhan, X Fu, S Liu, X Bo, and G Yu. clusterProfiler 4.0: A universal enrichment tool for interpreting omics data. The Innovation. 2021, 2(3):100141, Guangchuang Yu, Li-Gen Wang, Yanyan Han and Qing-Yu He. clusterProfiler: an R package for comparing biological themes among gene clusters. OMICS: A Journal of Integrative Biology 2012, 16(5):284-287	10.1016/j.xinn.2021.100141, 10.1089/omi.2011.0118
R Package: 'enrichplot'	Guangchuang Yu (2021). enrichplot: Visualization of Functional Enrichment Result. R package version 1.12.3	https://yulab-smu.top/biomedical-knowledge-mining-book/

R Package: 'altair'	Ian Lyttle, Haley Jeppson and Altair Developers (2021). altair: Interface to 'Altair'. R package version 4.1.1	https://CRAN.R-project.org/package=altair
R Package: 'pathview'	Luo, W. and Brouwer C., Pathview: an R/Bioconductor package for pathway-based data integration and visualization. Bioinformatics, 2013, 29(14): 1830-1831	10.1093/bioinformatics/btt285
R Package: 'DESeq2'	Love, M.I., Huber, W., Anders, S. Moderated estimation of fold change and dispersion for RNA-seq data with DESeq2 Genome Biology 15(12):550 (2014)	10.1186/s13059-014-0550-8
BIC: Bayesian Information Criterion	Schwarz, G. (1978) "Estimating the Dimension of a Model", *Annals of Statistics*, 6, 461-464.	
ClampFit 11.1.0.23	Molecular Devices, LLC, pCLAMP™ Software Suite Version 11	https://www.moleculardevices.com/products/axon-patch-clamp-system/acquisition-and-analysis-software/pclamp-software-suite
Harmony High-Content Imaging and Analysis Software	Perkin Elmer	https://www.perkinelmer.com
GraphpadPrism	GraphPad Software, Inc	https://cdn.graphpad.com/downloads/prism/9/InstallPrism9.dmg

2.11. Software packages and Algorithms

Resources availability

Bulk RNA sequencing data from Foetal samples used in chapter 5 were generated by Onorati *et al.,* 2014 and accessed through ArrayExpress (E-MTAB-1918). Samples were chosen based on the first trimester from CTX, MGE and LGE and for paired end samples we chose to exclude the second reads to make datasets comparable to our datasets.

Method Details

Experimental model and subject details

Details of all cell lines and foetal samples used are provided in Table 2.1.

IPSC culture

All iPSCs used were cultured in feeder-free conditions and maintain in E8 Flex medium (Chen *et al.*, 2011) on Vitronectin coated plates (1:100 in PBS, 0.5µg/cm^2). Medium was changed daily (100%) and passaged using ReLeasR every 3-5 days. Cells were incubated in a humidified incubator at 37°C and 5% CO_2. Please note, depending on cell confluence and morphology, occasionally weekend medium changes were not necessary.

The three main cell lines chosen to be assessed throughout this thesis were termed 18n6, 33n1 and Kolf2. The 18n6 and 33n1 cell lines were chosen due to their extensive use as control lines within the HD consortium. The Kolf2 cell line was chosen as it has been extensively characterised within dementia institutes.

Master and working banks of these lines were generated and one vile from differing passages were thawed to generate 3 separate differentiation per line per treatment. The starting passage numbers for these cell lines are as follows: 18n6, p22, p24, p26; 33n1, p28, p30, p32, p34 and Kolf2, p21, p24, p26.

Quality Control of iPSC

Chromosomal spread. iPSCs were grown in a 6cm dish until 100% confluency and split at a ratio of 1:5 using Accutase. The following day, Demecolcine (10µg/ml) was added to the media and cells were incubated for 2 hours at 37°C. Cells were harvested by Trypsin (2 minutes) and its activity was stopped by adding media (1:1) and centrifuged at 1300rpm for 3 minutes. The supernatant was aspirated, leaving approximately 300µl and cells were re-suspended in the remaining media plus 6ml of PBS. Cells were centrifuged for 3 minutes at 1300rpm and the previous step was repeated. Cells were then re-suspended in 2ml PBS plus 6ml of hypertonic KCL (0.0375M) and incubated for 12 minutes at 37°C. Following this, 4ml of KCL (0.0375M) was added and cells were re-suspended and precipitated by centrifugation for 5 minute at 1100rpm. The supernatant was aspirated leaving approximately 300µl and re-suspended by flicking and simultaneously adding 3ml of pre-chilled (-20°C) methanol/acetic acid (3:1) by a dropwise action. This suspension was then left at room temperature for >20 minutes followed by centrifuging for 5 minutes at 1100 rmp. The supernatant was aspirated leaving approximately 300µl and the previous step was repeated leaving approximately 500µl after aspirating. The remaining suspension was then dropped onto a pre-chilled slide placed at ~45° angle from at least 60cm height. Slides were then air dried and 100µl of Hoechst (1:10,000 in PBS) was added to each slide and chromosome spreads were viewed under x100 magnification florescent microscope. 50 images were collected per cell line and those containing >70% 46 chromosomes per cell were deemed good cell lines.

CNV genotype arrays. DNA was isolated from cells using DNeasy Blood & Tissue Kit following manufacturer's instructions. 200ng of DNA was given to Core facility for genotyped on the Infinium PsychArray-24 Kit (Illumina) or the Infinium Global Screening Array-24 (Illumina) and scanned using the iScan System (Illumina)

qPCR Trisomy Chromosome 1. This method was originally designed by D'Hulst *et al.,* 2013 to detect aneuploidy in mouse ES cells, and can detect as low as 10% aneuploidy rate. This was implemented in our lab and required validation as below:

Primer design. qPCR primers were designed by Nina Stoberl (Cardiff University) that amplified 94bp of exon 7 in the C1orf43 gene (Chromosome 1) and 73bp of exon 1 in the ZGRF1 gene (Chromosome 4, reference). Amplification efficiencies of C1orf43 and ZGRF1 were calculated based upon standard curves using serial dilutions of gDNA (Figure 2.1).

Symbol	Forward (5'-3')	Reverse (5'-3')	Tm (F)	Tm (R)	GC (F)	GC (R)	Length	Slop (m)	E (%)	R^2	Linear Dynamic range (ng)
C1orf43	CGGCATCCCCGTTCCTT AAT	GTGCTTTGCGTACACCC TTG	60.18	60.04	55	55	94	-3.1789	108	0.9185	45-2.8
ZGRF1	CGGTTTTTGGCTTAGGC GGA	GTCATTAACGCGGGACC TCA	61.24	60.11	55	55	73	-3.5866	91	0.984	180-2.8

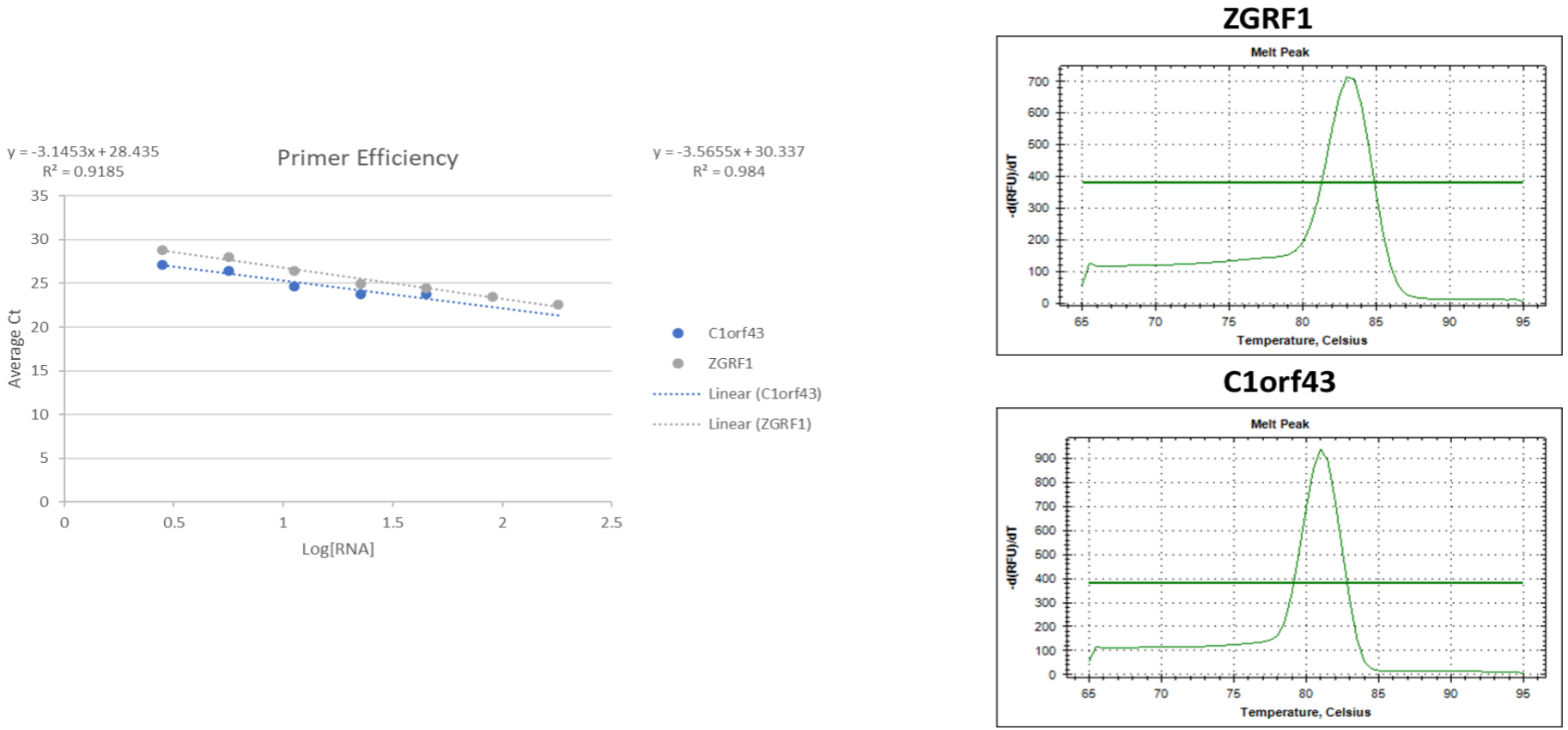

Figure 2.1: Primer efficiencies and melt curves showing primers fall within the 90-110% range for δδCT algorithm and generate one major peak.

A

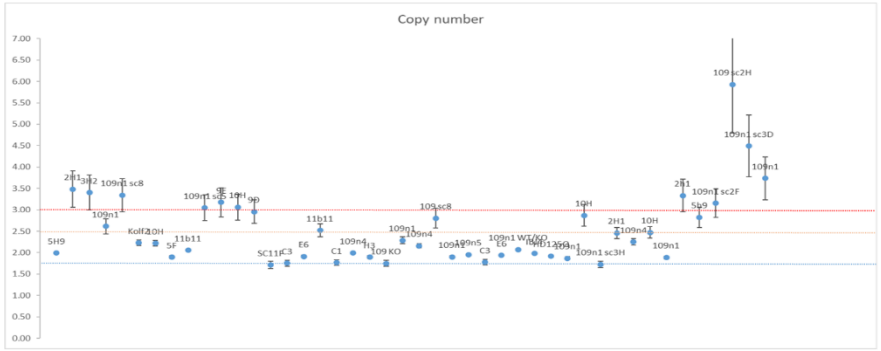

B

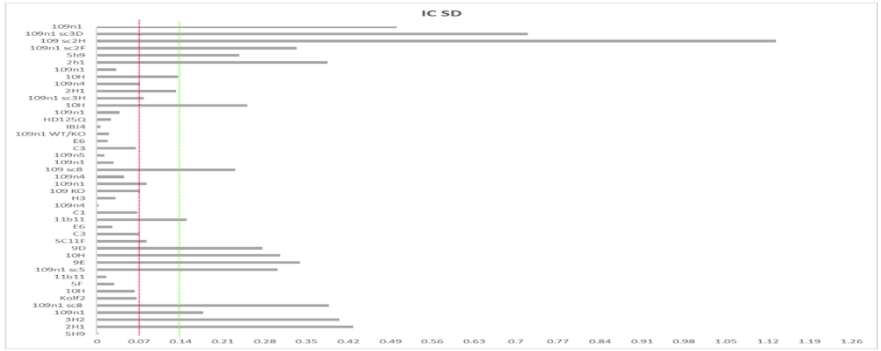

C

Sample ID	Cell line	Cell Type	Clone ID	Passage number	chr1:1-249250621
					Whole Chr 1
S1	CRISPR Cas9 KO Fan1 109n1	iPSC	10H	5	Normal
S2	CRISPR Cas9 KO Fan1 109n1	iPSC	10H	12	Normal
S3	CRISPR Cas9 KO Fan1 109n1	iPSC	9D	6	Normal
S4	CRISPR Cas9 KO Fan1 109n1	iPSC	9D	13	Normal
S5	CRISPR Cas9 KO Fan1 109n1	iPSC	9D	20	Poss Dup
S6	Isogenic 109n1 + CRISPR Cas9 KO Fan1	iPSC	9E	9	Normal
S7	Isogenic 109n1 + CRISPR Cas9 KO Fan1	iPSC	9E	11	Duplication
S8	109n1	iPSC	11B11	28	Poss Dup
S9	CRISPR Cas9 KO Fan1 109n1	iPSC	5F	4	Normal
S10	CRISPR Cas9 KO Fan1 109n1	iPSC	5F	40	Normal
S11	109n4	iPSC	109N4 SC1	27	Likely dup
S13	Isogenic 109n1	iPSC	3H2	19	Duplication
S19	109n5	iPSC	109n5	18	Normal
Unknown S1	CRISPR Cas9 KO Fan1 109n1	NPC	5F	6	Normal
Unknown S2	Isogenic 109n1	NPC	2H1	8	Normal
Unknown S3	CRISPR Cas9 KO Fan1 109n1	NPC	9D	31	Duplication
Unknown S4	Isogenic 109n1 + CRISPR Cas9 KO Fan1	NPC	9E	13	Duplication
Unknown S5	109n1	NPC	11B11	12	Normal

Figure 2: Single- and double – blind cross-validation qPCR for Chromosome 1 trisomy. A) Copy number generated based on δδCT algorithm. B) IC SD, red line with a cut-off of 0.07 indicates 67% CL, green line with a cut-off of 0.1 indicates 95% CL. C) Cell line information and GSA results.

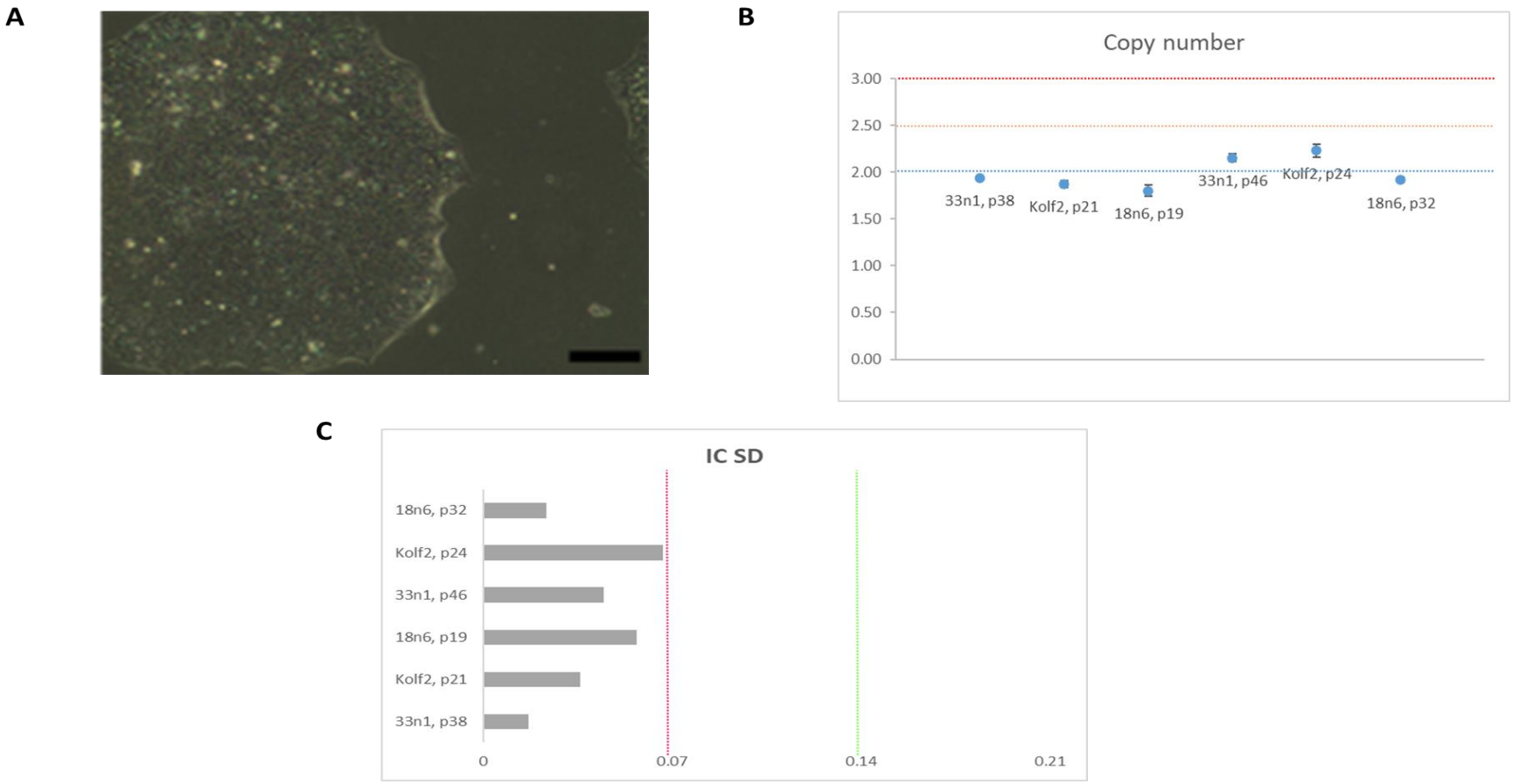

Figure 2.3 *A) exemplar brightfield image of iPSCs under phase contrast microscope (Magnification x20 Bar =500µm) B) qPCR analysis of chromosome 1 copy number relative to chromosome 4 (reference gene) from low and high passaged cells. C) Interchromosomal standard deviation (IC SD), over the green dotted line illustrates 95% confidence level that cells contain a trisomy of chromosome 1, red dotted line illustrate 67% confidence level (more stringent). Copy number determination was based on the* 2^{-ddCt} *method and qPCR method and IC SD calculations were adapted from D'Hulst et al., 2013.*

DNA extraction: Cells were washed three times with DPBS and manually counted to obtain 5 X 105. Cells were centrifuged at 300 x g for five minutes and the pellet was resuspended in 200µl of PBS and 20µl of proteinase K. DNA was extracted using a DNeasy Blood & Tissue Kit following manufacturer's instructions.

qPCR settings. A total of 5.625 ng of gDNA was used including 500nM primer pairs and Powerup SYBR green master mix (following manufacturers protocol). The following thermal profile was used: 1) 50°C, 2 minutes, 2) 95°C, 2minutes, 3) 95°C, 15 seconds, 4) 60°C, 15 seconds, 5) 72°C, 1 minute, 6) X 39 cycles Steps 2-5, 7) 65°C, 5 seconds.

Copy number and interchromosomal SD. Calculation for generating copy number and intrachromosomal standard deviation (IC SD) can be found in the supplementary material D'Hulst *et al.,* 2013. In order to identify an acceptable IC SD in this study, 8 'Normal' hiPSC lines were used to calculate 95% confidence interval (95% CL) generating a cut-off of 0.1 as well as the more stringent cut-off of 0.07 (67% CL). 18 samples were used in the validation experiment in which samples labelled S1-S19 had been previously assessed for trisomy using Infinium PsychArray-24 chip by Dr Jasmine Donaldson and 5 unknown samples for cross-validation. Analysis of these samples by qPCR are consistent with GSA when using 95% CL for IC SD (Figure 2.1). Therefore, this CL was used for further screening.

Mycoplasma testing. Mycoplasma contamination can be detected by PCR (originally designed by Uphoff and Drexler, 2002), which is easy, sensitive, fast and cost effective. It is based on 16S rRNA molecules of the most common species of mycoplasma contaminating cell cultures. iPSC's were allowed to grow to 80% confluency, and 100µl of cell culture medium was collected. Supernatant was denatured at 95°C for 5 minutes and centrifuged at maximum speed for 2 minutes. Positive and negative controls were included with every reaction, and 2µl of denatured samples were used for PCR reactions. PCR reaction was carried out using GoTaq® G2 Flexi DNA Polymerase following manufacturer's instructions. The following thermal profile was used:1) initial denaturation at 95°C for 2 minutes, 5 x cycles of: 2) 94°C for 30 seconds, 3) 50°C for 30 seconds, and 4) 72°C for 35 seconds, followed by 30 cycles of 5) 94°C for 15 seconds, 6) 56°C for 15 seconds, and 7) 72°C for 30 seconds with an infinite hold at 4°C. PCR products were analysed using 1.5% agarose gel electrophoresis run at 80V for 40minutes and visualised utilising SafeView. Positive contamination resulted in a 500bp PCR product.

CAG Sizing. PCR primers were designed by Dr Jasmine Donaldson to amplify 143bp of the exon 1 HTT gene (Table 2.2). PCR performed using LA TAQ (Takara) and 10ng of DNA according to the manufacturer's instructions using following protocol: 1) initial denaturation 94°C (1.30 minute), and 35 cycles of 2) 94°C (30 seconds), 3) 65°C (30 seconds), 4) extension 72°C (10 minutes) followed by a final extension at 72°C for 10 minutes. Resulting PCR products were analysed using capillary electrophoresis (GA3130XL Genescan, Heath Hospital) by Dr Jasmine Donaldson. Peak scanner v2.0 was used to view CAG repeat size distribution traces.

Name	Primer Sequence (5'-3')	Tm	GC (%)
FAM hu HTT exon 1F	ATGAAGGCCTTCGAGTCCCTCAAGTCCTTC	69.09	53.33
Hu HTT 1R-4	GGCGGCTGAGGAAGCTGAGGA	66.53	66.67

Table 2.12: HHT primer sequences amplifying 143bp of exon 1.

Neuronal Differentiation

Neural induction. iPSC colonies grown to ~60% confluency were treated with rock inhibitor (10µM) for one hour prior to single cell dissociation with Accutase (5-10 minutes). Cells were plated onto Matrigel-coated plates (1:100 in KO-DMEM) in E8 Flex medium plus Rock inhibitor (10µM) and allowed to settle overnight. The next day cells were washed, three times with DPBS and medium was changed to SLI medium which contained; Advanced DMEM/F-12 supplemented with 1% penicillin/streptomycin and Glutamax (ADF/PSG), and Neurobrew 21 (without Vit A), SB431542 (10µM), LDN193189 (200nM) and endo-IWR1 (1.5µM). This was defined as day 0 (D0) and medium was changed daily until D8. Note, neuronal rosette formation appears from D5-D8 of differentiation.

Neural patterning. At D8 cells were treated with Rock Inhibitor (10µM) for one hour and passaged using Accutase at a ratio of 1:3 into fresh Matrigel-coated plates. Medium was changed to media listed in Table 2.13, which was replenished daily until neuronal progenitor cell (NPC) stage. At D16 NPCs were manually counted and 6 x 10^6 were frozen in 500µl of Cryostor (CS10). Frozen cells were stored in the -80 for a maximum of 2 months or transferred to liquid nitrogen for longer storage.

Recovery. Following thawing, NPCs were allowed to recover in the neural patterning media they were grown in a T25 for four days before plating for terminal differentiation. Please note, optimised protocol for recovery is now NA media which consisted of ADF/PSG supplemented with 2% Neurobrew (with Vit A) and 25ng/ml Activin-A. This however was not used in this thesis.

Media Name	NeuroBrew-21 (without Vit A)	LDN193189 (200nM)	IWR1 (1.5µM)	Activin-A (50ng/ml)	Puromorphamine (0.1 µM or 0.3µM)	Cyclopoamine (0.5µM or 1 µM)
NB (without Vit A)	**X**					
L	**X**	**X**				
LI	**X**	**X**	**X**			
LIA	**X**	**X**	**X**	**X**		
LIC	**X**	**X**	**X**			**X**
LIAP	**X**	**X**	**X**	**X**	**X**	
LIAC	**X**	**X**	**X**	**X**		**X**

Table 2.13: Commonly used media composition for neural patterning

Terminal Differentiation.

Prior to plating, coverslips (Nitric acid treated) and plates were coated with PDL (100µg/ml in Borate buffer) for >1 hour and washed three times with cell culture grade water. These were aired dried overnight in the hood and coated with Matrigel (1:50 in KO-DMEM) and incubated at 37 5% humidified incubator overnight. NPCs were dissociated using Accutase and plated at a density of 0.8 x 10^5 cells/13-mm glass coverslips, 5 x 10^5 cells/well of a 12 well plate, or 1 x 10^5/well of a 96 well plate. Cells were plated in SJA which contained; Advanced DMEM/F-12 supplemented with Neurobrew 21 (2%, with Vit A), PD0332991 (2µM), DAPT (10µM), BDNF (10ng/ml), LM22A4 (12.5µM), Forskolin (10µM), CHIR TRI 99021 (3µM), GABA (300µM), $CaCl_2$ (1.8mM) and Ascorbic acid (200µM). Please note, cells were plated in RI, following 24h plating there was a full medium change and media was replenished (50%) every other day for seven days. Following this media was changed to SJB which contained; Advanced DMEM/F-12 and NeuroBasalA (1:1) supplemented with Neurobrew 21 (2%, with Vit A), PD0332991 (2µM), BDNF (10ng/ml), LM22A4 (12.5µM), CHIR TRI 99021 (3µM), $CaCl_2$ (1.8mM) and Ascorbic acid (200µM). Media was replenished (50%) every other day for 14 days.

Quantitative PCR (qPCR).

RNA extraction.

Cells cultured on 12-well plates were washed three times in DPBS and 250µl of ice cold RLT buffer (b-ME, conc) was added to each well. Cells were allowed to lyse for 10 minutes on ice and collected into an ice cold RNAse free Eppendorf's. Total RNA was extracted using an RNeasy Kit, according to the manufactures instructions. RNA (ng/µl) was measured with a NanoDrop200 and A_{260}/A_{280} ratios ≥1.8, with a RNA concentration ranging from 20ng/µl - 1µg/µl from each sample were used for cDNA preparation.

cDNA synthesis.

cDNA was generated using qScript™ cDNA Synthesis Kit following manufacturer's instructions using the following thermal cycler program; 1 cycle: 22ºC (5 minutes), 1 cycle: 42ºC (30 minutes), 1 cycle: 85ºC (5 minutes) and a 4ºC hold.

Primers.

All primers were assessed for amplification efficiencies. Only those falling within the recommended efficiency, 90-110%, were used. All data were subjected to δδCT algorithm (Livak and Schmittgen, 2001) to calculate the expression of the genes of interest and relative to the reference genes.

LightCycler.

qPCR was carried out using LightCycler® 480 SYBR Green I Master for a small panel of genes following manufactures protocol.

Fluidigm.

A total of 25ng of RNA per sample were used for cDNA preparations. Following cDNA synthesis, samples were preamplified using Preamplification master mix with the following thermal cycler program: Hold 95ºC (2 minutes), 14 cycles: 95ºC (15 seconds) and 60ºC (4 minutes) and a 4ºC hold. Preamplifed Reactions were cleaned using Exonuclease I, digested at 37ºC for 30 minutes and inactivated at 80ºC for 15 minutes. Gene expression on diluted preamplified samples (1:5 diluted in DNA suspension buffer) was carried out using SsoFast EvaGreen supermix and binding dye. For Quick reference guides refer to Fluidigm: PN 1000-7070 and PN 100-9792.

SYMBOL	FORWARD (5'-3')	REVERSE (5'-3')	TM (F)	TM (R)	GC % (F)	GC % (R)	LENGTH	SLOPE (M)	E (%)
UBC	GGGATTTGGGTCGCAGTTCT	GTCAAGTGACGATCACAGCG	60.32	59.29	55	55	51	-3.0977	110
EIF4A2	TAGGCGATCACAACGTGCAT	CACGACTAACGTCGCTTTGC	60.11	60.18	50	55	113	-3.0778	111
ATP5F1B	TCTGCTAGCTCCCTATGCCA	CTCCAGCACCACCAAAAAGC	60.11	59.97	55	55	56	-3.2522	103
YWHAZ	CGTCATCGTGCGTGTGGTGC	TGGATCTCGCTGCTCACAGGCT	64.83	65.98	65	59.09	96	-3.0946	110
GAPDH	CAATGACCCCTTCATTGACC	GAC AAG CTT CCC GTT CTC AG	56.38	58.57	50	55	52	-3.1732	107
NPY	GGAAAACGATCCAGCCCAGA	CAGGGTCTTCAAGCCGAGTT	60.04	59.96	55	55	91	-3.0595	112

SIX3	GTCCATGGTATTCCGCTCCC	ATGGAGCGGTGGTGAGAATC	60.25	59.82	60	55	84	-3.1273	109
SP9	CCACGTCTATACTCGGGGAAG	GTTGCCGATCTTGTTGCAGG	59.39	60.11	57.14	55	83	-	-
SP8	ACT TTT GTG TGA TGG CAA CTTC	GAA GAA GAG CTG TCC GAG AG	57.95	57.44	40.91	55	139	-	-
DLX6	CGGAAGCCTCGGACCATTTA	ACTGTGTCTGCTGAAAGCGA	59.82	59.9	55	50	70	-3.194	106
DLX5	GTC TCC AGC TAC CGA TTC TGA C	CTT TGC CAT AGG AAG CCG AG	60.22	58.7	54.55	55	89	-3.478	94
DLX1	TGGAGGACCCAGGTCAAGAT	ATATAGGAGCCCGCGTTTCC	59.88	59.68	55	55	200	-3.3136	100
DLX2	GCC TCA ACA ACG TCC CTT ACT	TCA CTA TCC GAA TTT CAG GCT CA	60.27	59.55	52.38	43.48	150	-3.2289	104
ISL1	ATA TCC AGG GGA TGA CAG GA	TTT CCA AGG TGG CTG GTA AC	56.87	58.01	50	50	110	-	-
EBF1	GTG GAG ATC GAG AGG ACA GC	AAG CTG AAG CCG GTA GTG AA	59.62	59.31	60	50	99	-3.2455	103

FOXP1	TGC AAG AAT CTG GGA CTG AG	AGA CCG CCG CAC TCT AGT	57.22	60.36	50	61.11	91	-3.4349	95
FOXP2	GGGGCCTCTCACACTCTCTA	CACCACCTGCATTTGCACTC	60.03	60.04	60	55	156	-3.4482	95
GAD2	ATT GGG AAT TGG CAG ACC AAC	TTG AAG TAT CTA GGA TGC CCT GT	59.1	58.7	47.62	43.48	103	-3.2173	105
CTIP2	CCA TCC TCG AAG AAG ACG AG	ATT TGA CAC TGG CCA CAG GT	57.52	59.81	55	50	106	-3.1375	108
ASCL1/MASH1	CCAAGCAAGTCAAGCGACAG	AGATGCAGGTTGTGCGATCA	59.76	60.04	55	50	533	-3.2201	104
GSX1	AGTTCCACTGCATCTCTGTG	GGCGGGACAGGTACATATTAG	57.53	57.69	50	52.38	132	-	-
GSX2	TCA CTA GCA CGC AAC TCC TG	TTT TCA CCT GCT TCT CCG AC	60.04	58.12	55	50	117	-3.0973	110

NKX2.1	AGG ACA CCA TGA GGA ACA GC	CCC ATG AAG CGG GAG ATG	59.67	57.53	55	61.11	88	-3.1891	106
LHX6 (V1)	GGCAAGAACATCTGCTCCAG	ACGTGCCAGATGAGGTTGTT	58.91	59.89	55	55	80		
MEIS2	AAA AGG TCC ACG AAC TGT GC	GAG CTG CCG TCT CTT TCA TC	58.98	58.71	50	55	103	-	-
CALB2	CCTGCCTGTCCAGGAAAACTT	AGCCGCTTCTATCCTTGTCG	60.48	59.9	52.38	55	104	-3.0877	110
LHX1	TACGACTTCTTCCCGCAAGG	AAGGGTAGGTCCACTGGTGT	59.75	60.1	55	55	62	-3.4477	95
SST	ACCCCAGACTCCGTCAGTT	CCAGGGCATCATTCTCCGTC	60.15	60.53	57.89	60	123	-3.2887	101
CALB1	AAC TTT TGT GGA TCA GTA TGG GC	GGT AAT ACG TGA GCC AAC TCT AC	59.24	58.64	43.48	47.83	72	-	-
GLI1	CTA CAT CAA CTC CGG CCA AT	CGG CGT TCA AGA GAG ACT G	57.67	58.27	50	57.89	110	-3.551	91
NKX6.2	CTTCCGTTTTCCCGCTTTGG	CTGATGCGCAGAGGGACTTT	60.04	60.39	55	55	100	-3.483	94

EMX1	TGA CGG TTC CAG TCC GAA GT	CCA AGG ACA GGT GAG CAT CC	61.11	60.39	55	60	53	-	-
PAX6	AGG CCA GCA ACA CAC CTA GT	AGC CAG ATG TGA AGG AGG AA	61.42	58.34	55	50	108	-3.4393	95
TBR1	CGTCTGCAGCGAATAAGTGC	AATGTGGAGGCCGAGACTTG	59.97	60.04	55	55	280	-	-
FOXG1	AGA AGA ACG GCA AGT ACG AGA	TGT TGA GGG ACA GAT TGT GGC	59.12	60.55	47.62	52.38	189	-	-
SLC17A6 (VGLUT2)	TTGAGGGTGTGACCTACCCA	GGAGGTGGTTGCCAGTCTAC	60.1	60.04	55	60	86	-3.3884	97
LIMCH1	TAAGTTCTGGGCATGGGACC	TCTCCTGGAGCAAACGTTCC	59.38	59.97	55	55	83	-3.2356	104
ETV1	TGCATATGACTCAGGCTGTATG TT	GTGATCCTCGCCGTTGGTAT	60.14	59.9	41.67	55	146	-3.5221	92
SHH	CTC GCT GCT GGT ATG CTC G	ATC GCT CGG AGT TTC TGG AGA	60.95	60.96	63.16	52.38	176	-	-

GLI2	CCA CGC TCT CCA TGA TCT CT	CCA AAC AGT CCC CTC TCC TT	58.96	58.93	55	55	85	-3.2522	103
GLI3	CCA TCG CTC TCC ATG ATC TC	TAT TCT GCT GGG CTG ACT CC	57.63	59.17	55	55	80	-3.2107	105
HHIP	AAGCACACAGTCTCGAATGGA	TCAACTGACAACCGCAGCTTA	59.66	60.2	47.62	47.62	142	-3.2405	104
LHX9	CAGTGCAACCACCATTACGG	TTGGATCTGCGCTCCATCTC	59.48	59.89	55	55	144	-3.1874	106
ACHE	ATGAGTGGTCGGACCGTG	TCTCGGTTTGAGGAGGAAGG	59.03	58.73	61.11	55	76	-	-
TGFB1	GGACCAGTGGGGAACACTAC	GCACTTCAACAGTGCCCAAG	59.68	59.97	60	55	66	-3.116	109
BMP7	CCGACTTCAGCCTGGACAACGA	TGGGGCAAGCCCAAAATGGAG	64.72	63.53	59	57.14	112	-3.125	109
ID4	AGCTCCGAAGGGAGTGACTA	TCGCTCTGGGTTTTACGAGG	59.67	59.75	55	55	130	-3.1302	109

BCL2	ACACACACAGAGCGGAGTC	TTTCTTGTGCTCCTCGGCAA	59.64	60.18	57.89	50	92	-3.3452	99
GPR161	CTCCCTGGCCTTTTGGTTCC	CCACAGTGAATTCGTCCCGA	60.9	60.04	60	55	105	-3.1734	107
FGF19	CACATGCCTCCCCATGGATT	GCTGGGGAAAGGGTTCTAGG	60.11	59.74	55	60	163	-3.2439	103
EDNRB	AGACTGTGAACTGCCTGGTG	AACCACAGCATGGGTGAGAG	59.89	59.96	55	55	75	-3.2413	103
GNAI2	GCTGTCCATTGCTCTTCATCTG	GCACCTCTCATTTCCTGCAAC	59.64	59.8	50	52.38	109	-3.2173	105
GABBR1	TGGGAAGGTTTTCCTGACGG	TGTGGCGTTCGATTCACAGA	59.89	59.97	55	50	101	-3.1176	109

ZIC1	ACAAGTCCTACACGCATCCC	GCTTGTGGTCGGGTTGTCT	59.75	60.23	55	57.89	158	-3.3737	98
ZIC2	TCCCTTCCGGAGTCTTTGAA	ACGTGGGCATGGAGATTAGC	58.28	60.18	50	55	109	-3.4301	96
ZIC3	TGCATGTGCATACCTCGGAC	GAGACTGTCCCGGATACCAAG	60.46	59.59	55	57.14	120	-3.3585	98
SIX6	ATTGGCAACATGTGAGCGTC	ATTACCTGTGCTGGGGATGC	59.48	60.11	50	55	59	-3.4415	95
MEIS1	TCTGCACTCGCATCAGTACC	ATTGACAGAGGAGCCCATGC	59.83	60.11	55	55	73	-3.3048	101
GPR153	GGCGCTCGAATGCAGGAT	ATCACTCATGGTGCAGACCG	60.59	60.11	61.11	55	134	-3.1454	108

DRD1	TGCCATAGAGACGGTGAGTA	CAGCATGTGGGATCAGGTAAA	57.57	59.81	55	50	116	-3.4779	94
DRD2	CTCTTCGGACTCAATAACGCAG	GACGATGGAGGAGTAGACCAC	59.15	59.32	50	57.14	78	-3.5522	91
ZNF503	CAAACTCTCCTCGGTTGCCT	AACTCGACTTGTCCTCCACG	59.96	59.69	55	55	128	-3.1592	107
PBX3	CTCTGCACAGGAGCGGAC	AACAAGGCGGACCCATCTG	60.13	60	66.67	57.89	154	-3.1857	106
GPR6	CGCGCTCACCTATTACTCGC	CTAGGGACACGGTCCAAGTG	61.27	59.75	60	60	77	-3.5256	92
GPR88	ATC CCG GTG TCA CTC CTG TAT	CAC GAG ATA GAT GAC CAT GCC	60.34	58.32	52.38	52.38	75	-3.4421	95

ONECUT2	ACCTCTGCAACTCCGAATGG	GGTGGCTTGGCTAATGTCCT	60.04	60.03	55	55	93	-3.1582	107
DACH1	GAGACCCACACAACAACAGC	GCAAGTCGAAATGCGAGTCC	59.34	59.9	55	55	98	-	-
ZNF521	CATCCTGATGGCTTTGGGGG	TCGCTCCGGTAGTCCACATA	60.76	60.11	60	55	62	-3.2455	103
NEUROD2	CGTTGTGCGTCATGCTGTTT	GTGGTGTGCGTGTGTCTTTC	60.32	59.97	50	55	115	-3.2152	105
NEUROD6	CTACAAACTTGGTGGCAGGC	CAGGAAACTCCTGGCGTTGA	59.4	60.25	55	55	50	-3.2256	104
NEUROG2	GTGCAGCGCATCAAGAAGAC	GAGGTTGTGCATGCGGTTTC	60.18	60.39	55	55	69	-3.1274	109
FEZF2	CCCTGTATGATCCCCCTCCA	GTCTTTGACGGCACCTCGTA	60.1	60.04	60	55	50	-3.2189	104
POU3F4	GGTGCGTGTCTGGTTCTGTA	CCCTGGCGGAGTCATTCTTT	59.97	60.04	55	55	58	-3.245	103

PPP1R1B	CTG AGG ACC AAG TGG AAG AC	GAT GTC CCC TCC ACT TCC TC	57.54	59.17	55	60	125	-3.4191	96
PTCH1	CACACACACAGAGCGGAGT	CTTTCTTGTGCTCCTCGGCA	59.93	60.6	57.89	55	97	-	-
ADORA2A	CTGGCTGCCCCTACACATC	TCACAACCGAATTGGTGTGGG	60.15	61.09	63.16	52.38	116	-	-
NOTCH2	GAT CAC CCG AAT GGC TAT GAAT	CAA TGC AGC GAC CAT CGT TC	58.32	60.25	45.45	55	226	-3.5132	93
P53	GCC CAA CAA CAC CAG CTC CT	CCT GGG CAT CCTTGA GTT CC	62.98	60.39	60	60	140	-3.2662	102
MOP	ATC ACG ATC ATG GCC CTC TAC TCC	TGG TGG CAG TCT TCA TCT TGG TG	63.65	62.94	54.17	52.17	106	-3.2339	104
OLIG2	TGA AAA GGT ACC GCT GTG TG	CAC GCT CTC AGG GAA AGA AG	58.41	58.28	50	55	100	-	-
SOX2	TAC AGC ATG TCC TAC TCG CAG	GAG GAA GAG GTA ACC ACA GGG	59.59	59.44	52.38	57.14	110	-	-

GBX1	TGA CGG TTT CCT GGA CAG TTC	GCT CGC TGG TAA ATG CTG TG	60.2	59.9	52.38	55	170	-	-
IHH	CTG GCC AAT GTG ACC GTA GT	GTG GGG ATC ATG GTT CAG CA	60.04	60.03	55	55	102	-	-
PENK	ATC CTC GCC AAG CGG TAT G	GGT TGT CCC CTC TTT CCA GA	59.93	58.94	57.89	55	109	-3.3867	97
TAC1	GGT ACG ACA GCG ACC AGA TCA	CCC GTT TGC CCA TTA ATC CA	61.88	58.52	57.14	50	114	-3.17	107
RALDH2	TGG AAC TTG GAG GCA AAA GT	GAC CTT GAT TGA AGA ACA CAC C	57.55	57.51	45	45.45	99	-	-
VGLUT1	GGA CGA CAG CCT TTT GTG GT	GCC GTA GAC GTA GAA AAC AGA G	60.82	58.83	55	50	107	-	-
TBR2	CGG CCT CTG TGG CTC AAA	AAG GAA ACA TGC GCC TGC	59.97	59.04	61.11	55.56	76	-	-
CHAT	AGT CCG ACC TCT GGA AAT GT	TCC TCA CTG CTG GGA GTT TT	58.35	58.86	50	50	115	-	-
ARPP21	CTC CAG AGA ACG GCA TTG TT	TCC TGC TCC TGA CTT GGA TT	58.19	58.34	50	50	116	-	-

HELIOS	TCA CCC GAA AGG GAG CAC T	CAT GGC CCC TGA TCT CAT CTT	60.84	59.58	57.89	52.38	175	-3.1828	106
PTCH2	CCC AGA AGA GCA CCA AAG AG	GAG GAG GAG ACA AGG CAG AA	58.18	58.73	55	55	149	-	-
SMO	TGC CCA AGT GTG AGA ATG AC	AAG CGG TCA GGA GTG CAG	58.1	59.65	50	61.11	130	-	-
HES1	CTG AGC ACA GAC CCA AGT GT	GAG TGC GCA CCT CGG TAT TA	59.89	59.9	55	55	115	-	-
RARB	GCA CCA GGT ATA CCC CAG AA	GGC AAA GGT GAA CAC AAG GT	58.79	58.89	55	50	119	-3.1093	110
OCT-4 (POU5F1)	GAC AGG GGG AGG GGA GGA GCT AGG	CTT CCC TCC AAC CAG TTG CCC CAA AC	68.88	67.87	70.83	57.69	114	-	-
NANOG	ACG CAG AAG GCC TCA GCA CCT	CCC AGT CGG GTT CAC CAG GCA	66.45	66.72	61.9	66.67	78	-	-

Table 2.14: Primers used for qPCR via Lightcyler or Fluidigm dynamic array. Forward and Reverse primer sequences were designed using Primer-BLAST NCBI. Those with missing values of Primer efficiencies have previously been optimised in house. By Dr Sona Joy

Electrophysiology.

Whole cell recordings were carried out using standard techniques (Hamil *et al.,* 1984). Thin-wall capillary glass recording pipettes (World presion instruments, TW100F-6) were pulled resulting in a tip resistance of 5-6 MΩ and loaded with intracellular solution containing; KCl (117mM), NaCl (10mM), HEPES (11mM), Na2-ATP (2mM), Na-GTP (2mM), Na2-phosphocreatine (1.2mM), $MgCl_2$ (2mM), $CaCl_2$ (1mM), EGTA (2mM) and pH to 7.2 with KOH. Cell capacitance was measured and compensated for manually before recording commenced. All experiments were conducted at room temperature and data analysis was carried out using Clampfit 11.1 software. Glass coverslips with a monolayer of neurons were assessed periodically by transferring to a bath with constant flow through of extracellular solution which contained; NaCl (135mM), KCl (5mM), $MgCl_2$ (1.2mM), $CaCl_2$ (1.25mM), D-Glucose (10mM), HEPES (5mM) and pH to 7.4 with NaOH.

Maturation of neurons was assessed using 4 protocols; 1) Gapfree, current clamp (I=0), to measure the resting membrane potential (Vm) and to record any spontaneously activity; 2) Gapfree, current clamp (I= that required to generate a Vm of approximately -70mV); 3) Current step from a holding of -70 mV in increments of 10pA from -20 to +180 pA, to assess input resistance (Ri) and induced action potential activity; 4) Activation/Inactivation in voltage clamp from a holding potential of -90mV, the first 200 ms steps increased in +5mV increments to 0mV (to elicit Na^+, the K^+, current activation) and these were followed by a 100ms step to 0mV (to asses Na^+ current inactivation). Please note that data from protocol 4 is not presented in this thesis but is available.

Immunocytochemistry (ICC).

Cells were washed three times with DPBS and fixed with 4% paraformaldehyde (PFA) in PBS for 15 minutes at room temperature, quenched and permeabilised followed by incubation at 4°C overnight in primary antibodies (Table 2.3). Cells were washed three times with PBS and incubated at room temperature for 2 hours on a rocker with secondary antibodies. All secondary antibodies conjugated to Alexa – 488 – 594 or -555 were diluted 1:400 in blocking buffer. Cells were counter-stained with Hoechst at 1:10,000 in PBS, imaged and analysed using an Opera Phoenix.

Primary antibody	*Species raised in*	*Dilution*	*Permeabilization*	*Unmasking*	*Blocking buffer*
CTIP2	Rat monoclonal IgG	1:500	0.1% Triton-X, 20 minutes, RT	1M Glycine, 20 minutes or ice cold 100% ethanol 2 minutes at RT	3% NGS 3% BSA 0.1% Triton-X
NKX2.1	Rabbit monoclonal IgG	1:500	0.1% Triton-X, 20 minutes, RT	N/A	3% NGS 3% BSA 0.1% Triton-X
DARPP-32	Rabbit monoclonal IgG	1:500	0.1% Triton-X, 20 minutes, RT	1M Glycine, 20 minutes or ice cold 100% ethanol 2 minutes at RT	3% NGS 3% BSA 0.1% Triton-X
GABA	Rabbit polyclonal	1:500	N/A	N/A	3% NGS 3% BSA
VGLUT1	Rabbit polyclonal	1:500	N/A	N/A	3% NGS 3% BSA
CHAT	Goat	1:500	0.1% Triton-X, 20 minutes, RT		3% NGS 3% BSA 0.1% Triton-X
TH	Rabbit, polyclonal	1:500	N/A	N/A	3% NGS 3% BSA

Table 2.15: Antibodies used for immunocytochemistry.

Western Blot.

Cells grown in 12 well plate were washed three times with DPBS and lysed in ice cold RIPA buffer containing protease inhibitor cocktail and phosphatase inhibitor for 10 minutes at 600rpm shaker at 4°C. Lysed cells were centrifuged at 13,000 x g at 4°C for 15 minutes and the supernatant containing the protein was used. Protein concentration was determined using Pierce BCA Protein Assay Kit following manufactures protocol. Samples (20µg) were run on a 4-12% Tris-Bis NuPAGE protein gel using 1X MOPS SDS buffer (pH = 7.7) at 165V for 45 minutes and transferred onto a 0.45 µm nitrocellulose membrane using 1 X Bis-Tris transfer buffer (pH = 7.2) for 1 hour at 10V. Membranes were blocked for 1 hour in 5% milk followed by primary antibodies at 4°C on a rocker overnight (Table 2.4). Membranes were then washed 3 times in PBS containing 0.1% Tween and incubated with LI-COR secondary antibodies conjugated to IRDye® -800 and -680.

PRIMARY ANTIBODY	SPECIES RAISED	EPITOPE	ANTIGEN MOLECULAR WEIGHT	SPECIFICITY	DILUTION
NKX2.1	rabbit monoclonal IgG	Information proprietary to Abcam	Predicted 38-42kDa	As Predicted and a non-specific ~ 32kDa band	1:1000
SHH	mouse monoclonal MIgG1	SHH N-terminal fragment 157-178 amino acids	20kDa SHH-N	30kDa, 16 and 20kDa bands	0.5µg/ml
A-TUBULIN	Abcam, AB7291, mouse monoclonal IgG1	DM1A clone to alpha tubulin, full length native protein	50kDa	As predicted Kolf2 cell line: doublet	1:5,000

Table 2.16: Primary Antibodies used for western blot

CRISPR

DNA extraction.

Genomic DNA was isolated from iPSCs lines for analysis, using QickExtractTM DNA extraction solution. QuickExtract was added for 3-5 minutes at room temperature to allow the cells to lysed. Cell solutions were then processed using a thermocycler using the following protocol: 68°C for 6 minutes and 95°C for 15 minutes.

Design.

Guide RNAs were designed using the Wellcome Sanger institute and Deskgen CRISPR design tools to target SHH and NKX2.1 genes (Tables 2.17-2.18) and resuspended in IDT buffer to 200 µM.

RNP complex.

A fluorescent tracer (ATTO550, 20nmol) was mixed in equimolar concentrations using IDT duplex buffer with each sgRNA and annealed for 2 minutes at 95°C and allowed to cool at RT. Following this, Cas9 protein (6.2µg/µl) was added to each tracer/sgRNA complex and incubated at RT for 20minutes.

Transfection.

A total of 1 million cells were transfected using 78µl of Lonza P3 buffer, 22µl of supplement 1 and 5µl each RNP complex using the Lonza 4D-neucleofector unit, program CA-137. Cells were allowed to recover for 10 minutes at RT before plating onto a VTN-coated plate. 24h post-transfection cells were FACS sorted, and the top 10% fluorescent cells were collected and replated onto a 10cm VTN-coated dish. Colony formation was monitored, and single colonies were picked for screening and expansion. Please note, this protocol was optimised by Dr Emma Cope.

NKX2.1 sgRNA

sgRNA	sgRNA Sequence (5'-3')	sgRNA Context Sequence (5'-3')	PAM	Exon	Target cut length	Targets	Mutation
Guide 1	TGACATCTTGAGTCCCCTGG	TGTCTGACATCTTGAGTCCCCTGGAGGAAA	AGG	1	633	NKX2.1 + NKX2.1-AS1	Sense
Guide 2	CGGCCTCGGGGCTCCGCTGG	GCGGCGGCCTCGGGGCTCCGCTGGCGGCGT	CGG	1	687	NKX2.1	Sense

Table 2.17. NKX2.1 CRISR sgRNA sequence information

SHH sgRNA

sgRNA	sgRNA Sequence (5'-3')	sgRNA Context Sequence (5'-3')	PAM	Exon	Target cut length	Targets	Mutation
Guide 1	GTATGCTCGGGACTGGCGTG	GCTGGTATGCTCGGGACTGGCGTGCGGACC	CGG	1	1239	SHH	Sense
Guide 2	CAGAAAACTCCGAGCGATTTA	TCTCCAGAAACTCCGAGCGATTTAAGGAAC	AGG	1	1388	SHH	Sense

Table 2.18. SHH CRISPR sgRNA sequence

PCR.

PCR*s* were preformed using GoTaq® G2 Flexi DNA Polymerase according to the manufactures instructions using NKX2.1 forward (gCCGCCGCCGAATCATGT) and reverse (gCCGCCGCCGAATCATGT) and SHH forward (cctgccattccagcccctgt) and reverse (tgttcggcttctcgtaacccc) primer pairs. The following Thermocycler program was used: initial denaturation 94°C (1 minute), and 30 cycles of 94°C (30 seconds), annealing temperature 68°C (30 seconds), extension 72°C (45 seconds) followed by a final extension at 72°C for 5 minutes. Please note, PCR reactions contained 2% DMSO. 100ng of total DNA were sent for Sanger sequencing to confirm correct gene editing using the above primer sequencing.

RNA Sequencing.

Total RNA was extracted from 18n6, 33n1 and Kolf2 cell lines under LI, LIA and LIAC protocols, with an RNAeasy Kit as previously described. Optical density values of extracted RNA were measured with Nanodrop2000 to confirm A260/A280 >1.9. RNA was subjected to

further quality control using Agilent 4200 TapeStation system and RIN values >9 was used for the preparation of unstranded polyA libraries (Figure 2.4). Libraries were generated from 500ng of total RNA using TruSeq® Stranded mRNA Library Prep Kit following manufacturer's instructions. Sequencing was performed with illumine HiSeq 2500 platform by Angela Marchbank, Cardiff University, Genomic Hub, with an average depth of 30 million reads per sample. The raw sequencing reads were aligned to human hg19 genome by Prof. Pete. Keel using Star aligner and feature counts were used to quantify the gene expression at the gene level based on ENSEMBL gene model GRCh37 version 93. RNA sequencing data from foetal LGE, MGE and CTX (E-MTAB-1918) were downloaded from https://www.ebi.ac.uk/arrayexpress/experiments/E-MTAB-1918/ and aligned to the same genome. Genes with at least 1 count per million in more than three samples were considered expressed and hence retained for further analysis, otherwise removed.

Gel Image

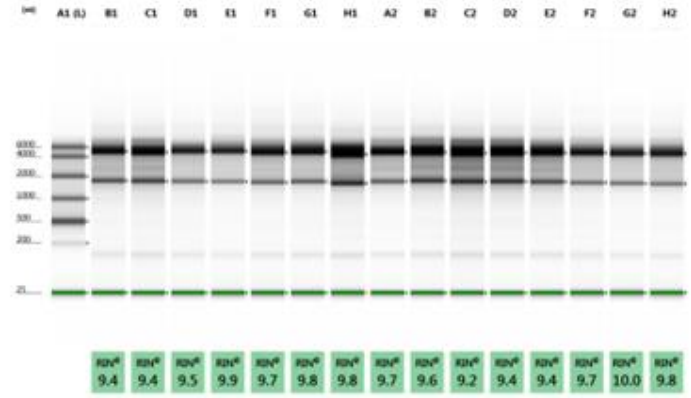

Default image (Contrast 100%), Image is Scaled to view larger Molecular Weight range

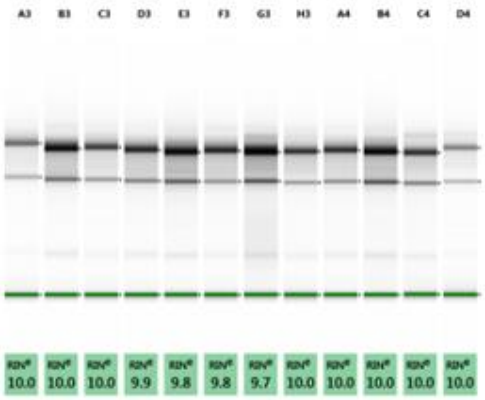

Default image (Contrast 100%), Image is Scaled to view larger Molecular Weight range

Sample Info

Well	RINe	28S/18S (Area)	Conc. [ng/µl]	Sample Description	Alert	Observations
A1	-	-	226	Ladder		Ladder
B1	9.4	3.0	248	18n6 D16 LI S1		
C1	9.4	2.6	302	18N6 D16 LI S2		
D1	9.5	2.7	179	18N6 D16 LI S3		
E1	9.9	3.6	161	KOLF2 D16 LI S1		
F1	9.7	4.1	214	KOLF2 D16 LI S2		
G1	9.8	3.4	219	KOLF2 D16 LI S3		
H1	9.8	1.6	344	33N1 D16 LI S1		
A2	9.7	3.5	251	33N1 D16 LI S2		
B2	9.6	2.8	356	33N1 D16 LI S3		
C2	9.2	2.6	409	18N6 D16 LIA S1		
D2	9.4	3.2	380	18N6 D16 LIA S2		
E2	9.4	3.2	285	18N6 D16 LIA S3		
F2	9.7	3.9	190	KOLF2 D16 LIA S1		
G2	10.0	3.3	160	KOLF2 D16 LIA S2		
H2	9.8	3.7	175	KOLF2 D16 LIA S3		
A3	10.0	3.2	78.7	33N1 D16 LIA S1		
B3	10.0	3.4	198	33N1 D16 LIA S2		
C3	10.0	3.7	114	33N1 D16 LIA S3		
D3	9.9	3.5	151	18N6 D16 LIAC S1		
E3	9.8	3.9	218	18N6 D16 LIAC S2		
F3	9.8	4.4	142	18N6 D16 LIAC S3		
G3	9.7	4.0	249	KOLF2 D16 LIAC S1		
H3	10.0	4.5	112	KOLF2 D16 LIAC S2		
A4	10.0	4.1	135	KOLF2 D16 LIAC S3		
B4	10.0	3.1	221	33N1 D16 LIAC S1		
C4	10.0	3.1	130	33N1 D16 LIAC S2		
D4	10.0	3.0	57.1	33N1 D16 LIAC S3		

Figure 2.4: Quality control of RNA samples following prior to Library prep and sequencing.

Bioinformatics and statistical analysis

For RNA sequencing a total of 27 samples were used, which included, three cell lines (33n1, Kolf2 and 18n6) three differentiation protocols (LI, LIA and LIAC) all of which was repeated three times. In order to make the RNAseq read counts comparable across samples, normalisation was carried out by DESeq2 (R software, Bioconductor packages, developed at PF2-Indtitute Pastear) computing a scaling factor for each sample, independent filtering to increase the detection power of differentially expressed features and p-adjustment (Benjamini-Hochberg, BH, $p<0.05$) to control for false positives. Multiple pairwise comparisons were preformed and differentially expressed genes (DEGs) with a Log2 fold change ≥1 or ≤ -1 with an adjusted p-value ≤0.05 were further evaluated.

Fluidigm dynamic array qPCR data (δδCt values) were analysed using the empirical Bayes statistics for differential expression in the Limma package (R software). Light cycler qPCR (Fold change) immunocytochemistry and western blot data were analysed using GraphPad Prism version 9.1.0.

In order to have sufficient power for statistical analysis for qPCR, three biological and three technical repeats were included for each condition (i.e 9 samples per line per treatment). For ICC analysis, three biological and three technical repeats were included for each condition (i.e 9 wells in total). As neurons cluster following terminal differentiation, images with no nuclei present were excluded from analysis, resulting in a total of 72-96 fields of view per line per treatment. However, unbiased cell counts were made using the opera phenix image analysis and Harmony software.

Comparisons between 3 or more groups was preformed using one-way ANOVA followed by Tukey's post hoc test while 2 groups were analysed using 2-sample T-test or Welchs test depending on normally distributed data.

Chapter 3: Endogenous SHH expression biases hiPSCs to an MGE fate during forebrain neural differentiation

Abstract

Human induced pluripotent stem cell (iPSC) models of Huntington's disease (HD) allow the study of the mechanisms underlying the disease neuropathology. However, a major challenge in studying HD is the ability to efficiently and correctly differentiate human iPSCs into the desired neuronal population, medium spiny neurons (MSNs). Available protocols aiming to mimic normal human development have yielded varying populations of MSNs from both control and HD cell lines from different donors, with the largest population reported to date being 50% and the average being just 10-15% of neurons. Considerable inter-line variability and cell heterogeneity of differentiated cultures causes huge problems, in trying to identify whether differences in gene expression and function are disease attributes independent of individual cell line differences. To begin to investigate endogenous mechanisms that account for inter-cell line variability in responses to directed programs of differentiation we first documented neural differentiation across a panel of control and HD iPSCs and focussed our analysis on 3 control cell lines that showed variable responses to established differentiation protocols.

Graphical abstract

- Dual SMAD and WNT inhibition efficiently generate naïve neuroectodermal cells.
- Patterning of neuroectoderm cells following two differentiation protocols generates varying population of LGE-like and MGE-like NPCs within treatment and between cell lines.
- Variation may be due to endogenous SHH expression
- Terminal differentiation of these cultures results in variable MSN populations between cell lines and treatment with an undetermined cell population in the presence of endogenous SHH expression.

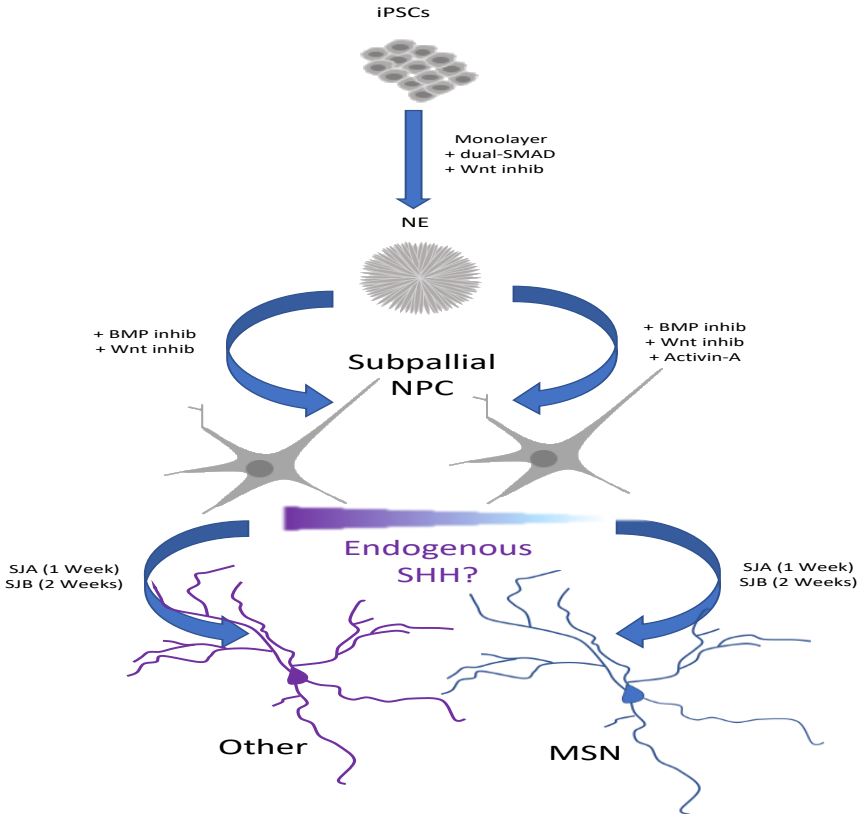

Introduction

Patient derived Induced pluripotent stem cells (iPSCs) can be differentiated into several neuronal populations for *in vitro* disease modelling, and if protocols are robust enough for large-scale drug screening. In the case of HD, several studies have independently developed differentiation protocols to generate medium spiny neurons (MSNs) which are selectively vulnerable to degeneration. However, one key issue is inter-cell line variability in responses to specific protocols, and consequently variable cell heterogeneity present in differentiated cultures. This is hugely problematic as differentially expressed cell and molecular phenotypes can relate to differences that are inherent in the cell models rather than the disease. Genetic background differences between cell lines can influence IPSC differentiation and can be addressed through the generation of isogenic cell models by gene editing (Szlachcic *et al.,* 2017; Ooi *et al.,* 2019; Malankhanova *et al.,* 2020; The HD iPSC Consortium, 2020; Oura *et al.,* 2021). However, it is also likely that differences in reprogramming and epigenetic status of cell lines will influence cell line behaviour.

Of the neural progenitor lineages, directed MSN differentiation is particularly complicated. Directed differentiation protocols specify target cell types by recapitulating, in culture, mechanisms of dorsal-ventral and rostro-caudal patterning. Specifying cell fates with dorsal and ventral identity can be readily achieved, however targeting populations that arise from intermediate domains, as in the case of the lateral ganglionic eminence (LGE) requires more precise/fine tuning of dorsal-ventral patterning. MSN differentiation requires the integrated use of various small molecules and peptides at appropriate times to modulate signalling pathways. Following forebrain neural induction by dual SMAD and canonical WNT pathway inhibition, regional identity along the dorsal-ventral axis, is achieved by further modulation of WNT/β catenin, BMP4, Activin and hedgehog (HH) pathway signalling. Culturing anterior neural ectoderm in the absence of small molecules and recombinant proteins results in a 'default' cortical phenotype attributed to activation of endogenous WNT/ β-catenin signalling, in the absence of endogenous SHH (Li *et al.,* 2009; Nicoleau *et al.,* 2013). Thus, differentiation protocols implement the use of WNT pathway antagonist DKK1, or more commonly small molecules such as, XAV939 or IWR1, to downregulate canonical WNT pathway target genes. (Aubry *et al.,* 2008; Li *et al.,* 2009; Zhang *et al.,* 2010; The HD iPSC

Consortium 2012; Carri *et al.,* 2013; Nicoleau *et al.,* 2013; Lin *et al.,* 2015). In addition to WNT/β-catenin inhibition, small molecules to inhibit BMP4 (SMAD1,5,8) signalling are also employed, such as Dorsomorphin or its derivative LDN-193189, to further restrict a dorsal phenotype (Carri *et al.,* 2013; Telezhkin *et al.,* 2015; Comella *et al.,* 2020). Recombinant protein SHH or the small molecules SAG or purmorphamine are routinely used to activate the HH pathway to ventralise neuroectodermal cells. However, in mice, ablation of SHH in the telencephalon has no effect on LGE cell proliferation or differentiation into MSNs (Rallu *et al.,* 2002; Machold *et al.,* 2003; Xu *et al.,*2010) and direct evidence that HH agonists directly promote MSN fate in differentiation cultures is still lacking. Importantly, the endogenous expression levels of HH ligands, namely SHH, has not been assessed in published MSN studies. When used, the timing, duration of exposure and concentration of SHH (50-200 ng/ml), purmorphamine (0.65-1µM) or SAG (100nM) vary significantly between protocols, for example ranging from 5 to 21 days of treatment (Aubry *et al.,* 2008; Li *et al.,* 2009; Zhang *et al.,* 2010; Ma *et al.,* 2012; Nicoleau *et al.,* 2013; Lin *et al.,*2015).

Lastly, a role of TGF-β signalling in MSN fate has been shown with the use of Actvin-A (Arber *et al.,* 2015, Smith-Geater *et al.,* 2020). Neuroectodermal (NE) cells treated with Activin-A for 10 days resulted in a significant increase in LGE specific gene expression and upon terminal differentiation these cells generated 20-50% MSNs, identified by co-expression of DARPP32/CTIP2.

We still lack a comprehensive view of the molecular events regulating neural progenitor cell (NPC) progression to post-mitotic GABAergic MSN fate. Thus, it is imperative to study individual differences between the cell lines used and optimise protocols with the aim to have a more enriched and consistent population of MSNs. In order to achieve this, we investigate the sources of variation present between three control cell lines, at discrete developmental stages during differentiation iPSC-NE-NPC-Neuron and following 2 differentiation protocols adapted from Telezhkin *et al.,* (2015) and Smith-Geater et al., (2020). In addition, we examined how variation can bias results and interpolate phenotypes not otherwise seen in HD

Results and Discussion

Independent iPSC lines show variable MSN differentiation in response to the same protocols

It has been previously shown that continued progenitor differentiation with WNT inhibition (IWR-1) and SMAD1/5/8 inhibition (LDN193189) in LI medium limits pallial differentiation and promotes subpallial specification with increased expression of GSX2 and DLX2 (Straccia *et al.*, 2015; Telezhkin *et al.*, 2016; Lim *et al.*, 2017; Comella *et al.,* 2020). However, upon terminal differentiation and maturation, only 4-6% of MAP2 positive cells expressed DARPP-32 (Telezhkin *et al.,* Comella *et al.,* 2020). In addition, treating cultures with Activin A (LIA medium) has been shown to induce a more LGE phenotypic gene expression pattern (Smith-Geater et al 2020, Arber et al., 2015). We therefore first decided to compare differentiation of 3 independent cell lines under LI and LIA culture conditions.

To analyse differentiation, we performed immunocytochemistry on terminally differentiated cultures for DARPP-32, combined with colocalization with CTIP2, markers of mature MSNs. Using LIA medium two out of the three cell lines (Kolf2 and 18n6) over three separate differentiations showed >60% MSN fate, whereas the 33n1 cell line consistently showed a low percent of MSNs (30% +/- 17%, Figure 3.1). As DARPP-32/CTIP2 positive cells are also located within the developing cortex but are glutamatergic, the percentage of GABA and vGLUT1 positive cells was also assessed. All cell lines showed variation in the population of GABAergic cells with 33n1 cell line generating the highest (70% +/- 13%) followed by Kolf2 (66% +/- 18%) and 18n6 (52% +/- 10%) with low vGlut1 expression (33n1: 7% +/- 3%, Kolf2: 10% +/- 5%, 18n6: 4% +/- 3%; Figure 3.1).

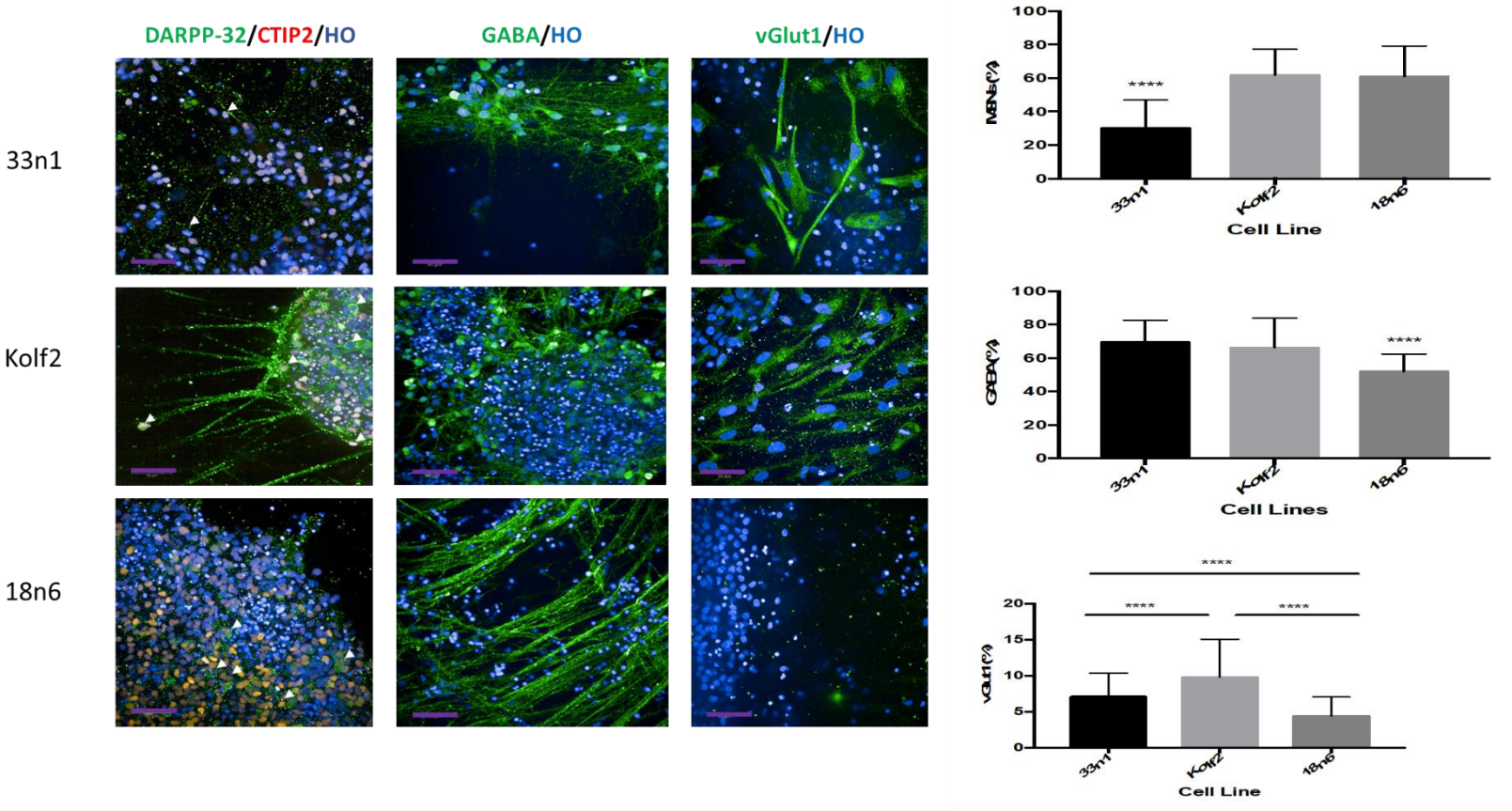

*Figure 3.1: iPSC differentiation following LIA protocol (Smith-Geater et al., 2020 and Telezhkin et al., 2015) in 3 independent cell lines. Left: Exemplar ICC images of MSNs as identified by co-expression of DARPP-32 and CTIP2 and GABA. Note: vGlut1 images are not representative of the entire population of cells but are presented to show positive identification only (scale bar 50μm). Right: Percentage of MSNs (co-localisation of CTIP2 and DARPP-32) shows variation in is predominantly within the 33n1 cell line ($F(2,261)=106.1$, $p<0.0001$) with the majority of all cell lines expressing GABA, albeit lower in the 33n1 cell line ($F(2, 261)=34.02$, $p<000.1$). Low glutamatergic (<15%) populations of cells are present within all cell lines with variation in each line ($F(2,277)=46.32$, $p<0.0001$). Data was calculated from 3 independent differentiations and are presented as the mean with SD and one-way ANOVA with Tukey's multiple comparisons test. * $p<0.05$, ** $p<0.01$, *** $p<0.001$, **** $p<0.0001$.*

Assessment of transcriptional variability in hiPSCs and neural progenitors

To investigate where variability across cell lines is first observed, changes in gene expression during differentiation from iPSCs to anterior neuroectoderm and 'LGE' neural progenitor cells were assessed. Cell lines used were first validated for genomic integrity by qPCR for trisomy of chromosome 1 and pluripotent cells assayed for expression of core pluripotency genes, OCT4, NANOG and SOX2 by qRT-PCR (Figure 3.2B) with no significant inter-line variability being observed.

In order to adopt an anterior neuroectoderm fate, dual SMAD and WNT inhibition was employed for 8 days resulting in induction of PAX6 (Figure 3.3D, 0.5-3.5-fold) and an increase in SOX2 expression (1.5-2.5-fold). Although there was a significant difference in the level of PAX6 between Kolf2 and 18n6 cell lines relative to GAPDH (Figure 3.3C, dCT), all lines presented typical columnar neuroectoderm morphology and organised rosette formation (Figure 3.3B) and expression of the pluripotency markers OCT4 and NANOG were switched off (Figure 3.3D)

This illustrates that all lines efficiently adopt an anterior neuroectoderm fate.

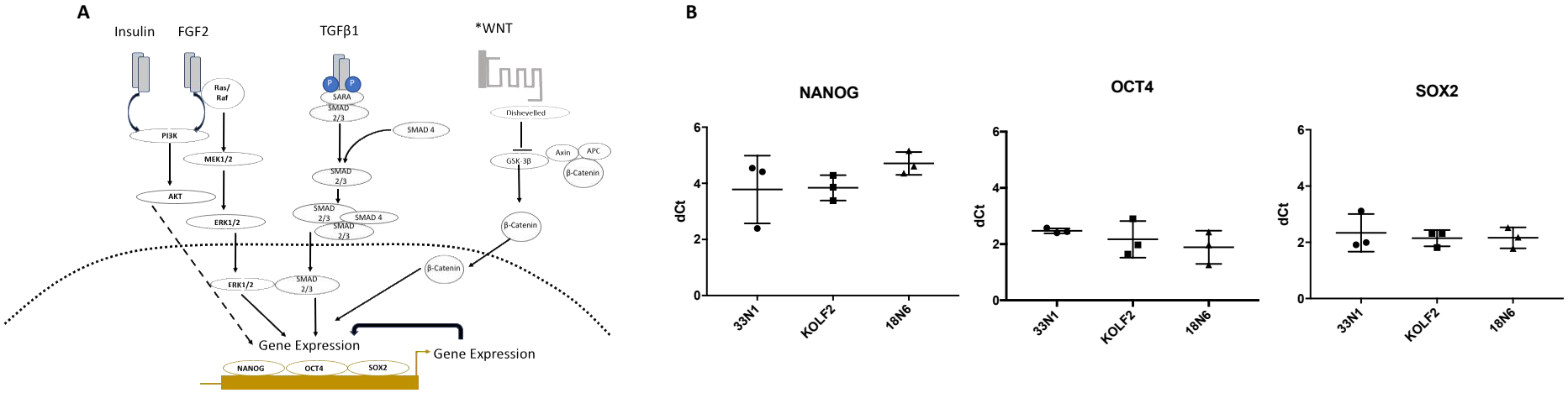

*Figure 3.2: A) Pathways promoting pluripotency in iPSCs. Insulin, FGF2 and TGFβ1 are three of the essential components contained in E8 medium that promote and maintain pluripotency in iPSCs. * WNT, is active in the naïve state of pluripotency in hPSC. B) qPCR analysis shows the core pluripotency genes expressed in 33n1, Kolf2 and 18n6 cell lines relative to GAPDH (dCT). Data represents the mean of 3 biological and 3 technical repeats with SD and ordinary one-way ANOVA with Tukeys multiple comparisons test (NANOG, F(2,6)=1.337, p=0.3310; OCT4, F(2,6)=0.9790, p=0.4286; SOX2, F(2,6)=2.107, p=0.8634). * p<0.05, ** p<0.01, *** p<0.001, **** p<0.0001.*

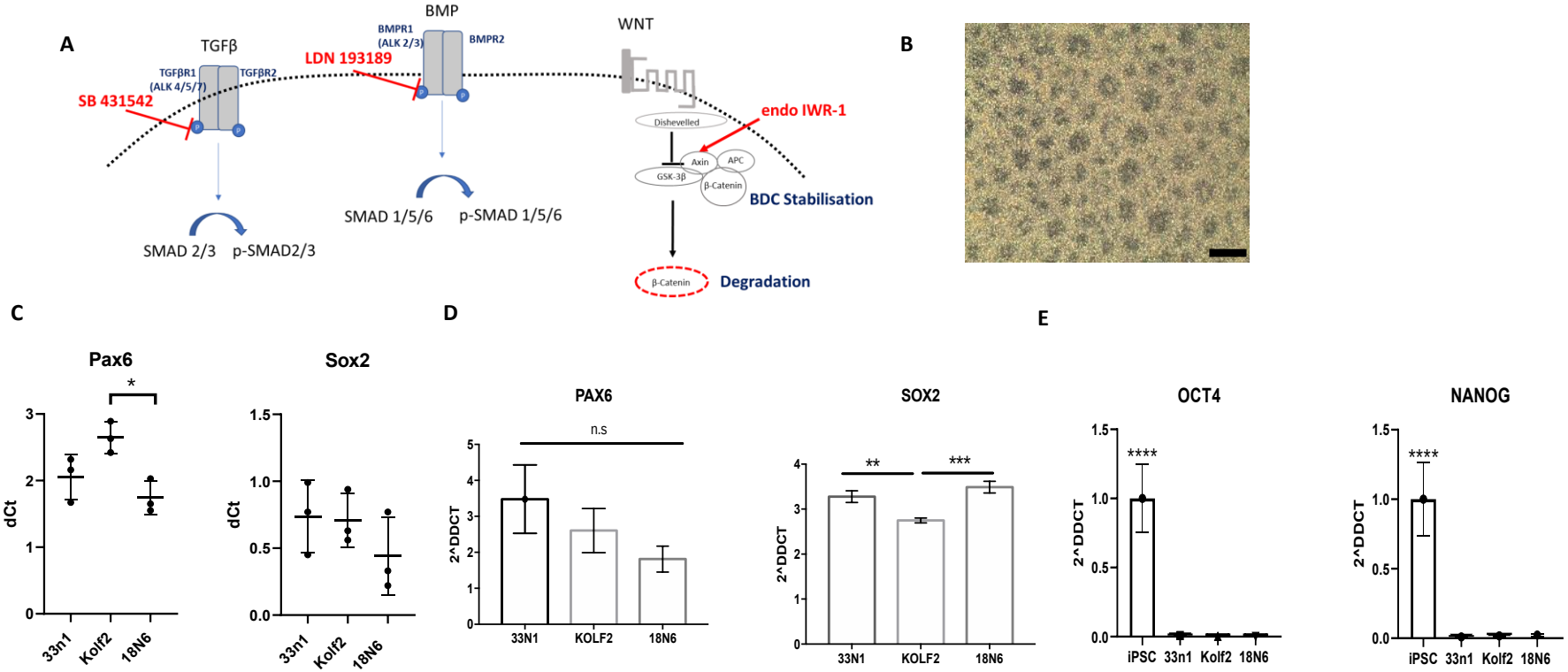

*Figure 3.3: A) Pathways targeted for neural induction in SLI medium. B) exemplar image of neuroectodermal rosettes. C) qPCR analysis shows expression of PAX6 ($F(2,6)=8.107$, $p=0.0197$) and SOX2 ($F(2,6)=1.216$, $p=0.3602$) relative to the reference gene GAPDH. D) Fold change expression of PAX6 ($F(2,24)=1.474$, $p=0.2489$) and SOX2 ($F(2,24)=11.91$, $p=0.0003$) and E) OCT4 ($F(3,32)=16.35$, $p<0.0001$) and NANOG ($F(3,32)=14.04$, $p<0.0001$) relative to GAPDH compared to its D0 expression. Data represents the mean of tree biological and 3 technical repeats with SD and ordinary one-way ANOVA with Tukeys multiple comparisons test, * $p<0.05$, ** $p<0.01$, *** $p<0.001$, **** $p<0.0001$.*

Activin-A treatment upregulates LGE transcription factor expression but is dependent on HH signalling

To examine whether independent control cell lines show variability in their responses to LGE differentiation protocols, gene expression patterns were assessed within and between cell lines using LI and LIA protocols.

Consistent with previous studies (Smith-Geater *et al.,* 2020*;* Arber *et al.,* 2015*)* expression of LGE transcription factors, GSX2 (Kolf2, $t(4)=11.69$, $p=0.0003$; 18n6, $t(4)= 3.171$, $p=0.0338$), and DLX2 (Kolf2, $t(4)=62.62$, $p<0.0001$; 18n6, $t(4)= 62.62$, $p<0.0001$), were upregulated in Activin-A treated cultures compared to LI controls in both the 18n6 and Kolf2 cell lines (Figure 3.4B-C). However, there was a slight (0.3-fold) but significant reduction in expression GSX2 ($t(4)=3.022$, $p=0.0391$) in the 33n1 cell line with an increase in DLX2 ($t(4)=17.53$, $p<0.0001$) when compared to LI control. In addition, the MGE specific transcription factor, NKX2.1, was significantly downregulated in Kolf2 ($t(4)= 37.93$, $p<0.0001$) and 18n6 ($t(4)= 1939$, $p<0.0001$) but with no effect on the 33n1 cell line ($t(4)=0.8660$, $p=0.4351$, Figure 3.4D). Furthermore, LGE specific markers of the SVZ and MZ were also increased with the addition of Activin-A, including, DLX5 (33n1, $t(4)=7.187$, $p=0.002$; Kolf2, $t(4)=23.28$, $p<0.0001$; 18n6, $t(4)= 8.853$, $p=0.0009$, Figure 3.5B), MEIS2 (33n1, $t(4)=10.38$, $p=0.0005$; Kolf2, $t(4)=11.65$, $p=0.0009$; 18n6, $t(4)= 12.73$, $p=0.0002$, Figure 3.5C), CTIP2 (33n1, $t(4)=12.9$, $p=0.0002$; Kolf2, $t(4)=16.86$, $p<0.0001$; 18n6, $t(4)= 60.27$, $p<0.0001$, Figure 3.5D) and EBF1 33n1, $t(4)=3.774$, $p=0.0195$; Kolf2, $t(4)=5.635$, $p=0.0049$; 18n6, $t(4)= 5.635$, $p=0.0049$, Figure 3.5E).

Overall, all three cell lines showed similar patterns of increasing expression of more LGE transcriptional markers, while significantly downregulating NKX2.1 within the Kolf2 and 18n6 cell lines but not the 33n1 line. To further examine for difference in the expression between all three cell lines, under LI and LIA treatment, data was re-analysed and compared to average foetal LGE expression (PCW 8-12;). All foetal samples were isolated from first trimester conceptuses, however as age varied and could potentially alter gene expression, a correlation between age and genes of interest was assessed. This showed that no correlation between age the genes tested (Figure 3.6D), therefore for further analysis foetal samples were grouped based on developmental area (LGE, MGE or CTX).

Under the LI protocol significant differences in expression of pan-GE and MGE markers were seen, predominantly within the 33n1 cell line with a 0.5-fold decrease in GSX2 (Figure 3.7B), and >40-fold increase in NKX2.1 (Figure 3.7D) expression compared to Kolf2 and 18n6, with no differences in DLX2 expression (Figure 3.7C).

With the addition of Activin-A this caused variation in expression again predominantly with the 33n1 cell line showing a 0.5-1-fold decrease in GSX2 and DLX2 expression and > 40-fold increase in NKX2.1 compared to Kolf2 and 18n6 cell lines. In addition, variation was seen in GSX2 expression between Kolf2 and 18n6 cell lines.

Initial data suggests that the 33n1 cell line generates MGE-like progenitor cells while Kolf2 and 18n6 do not. To further validate an MGE identity, immunocytochemistry was employed for NKX2.1 following LI and LIA protocols in all cell lines. Here, low NKX2.1^{+} cells were observed under both conditions for cell lines 18n6 and Kolf2 (LI; 18n6 11.7% $\pm$13.4, Kolf2 13.3 $\pm$11.6; LIA; 18n6 9.3%$\pm$3, Kolf2 10.6% $\pm$ 7.8). However, in the 33n1 cell line high numbers of NKX2.1^{+} cells were present in both LI (59.5% $\pm$15.3) and LIA (64.4% $\pm$14.3) cultures. Further illustrating the variability primarily with the 33n1 cell line compared to 18n6 and Kolf2 (Figure 3.7E-F).

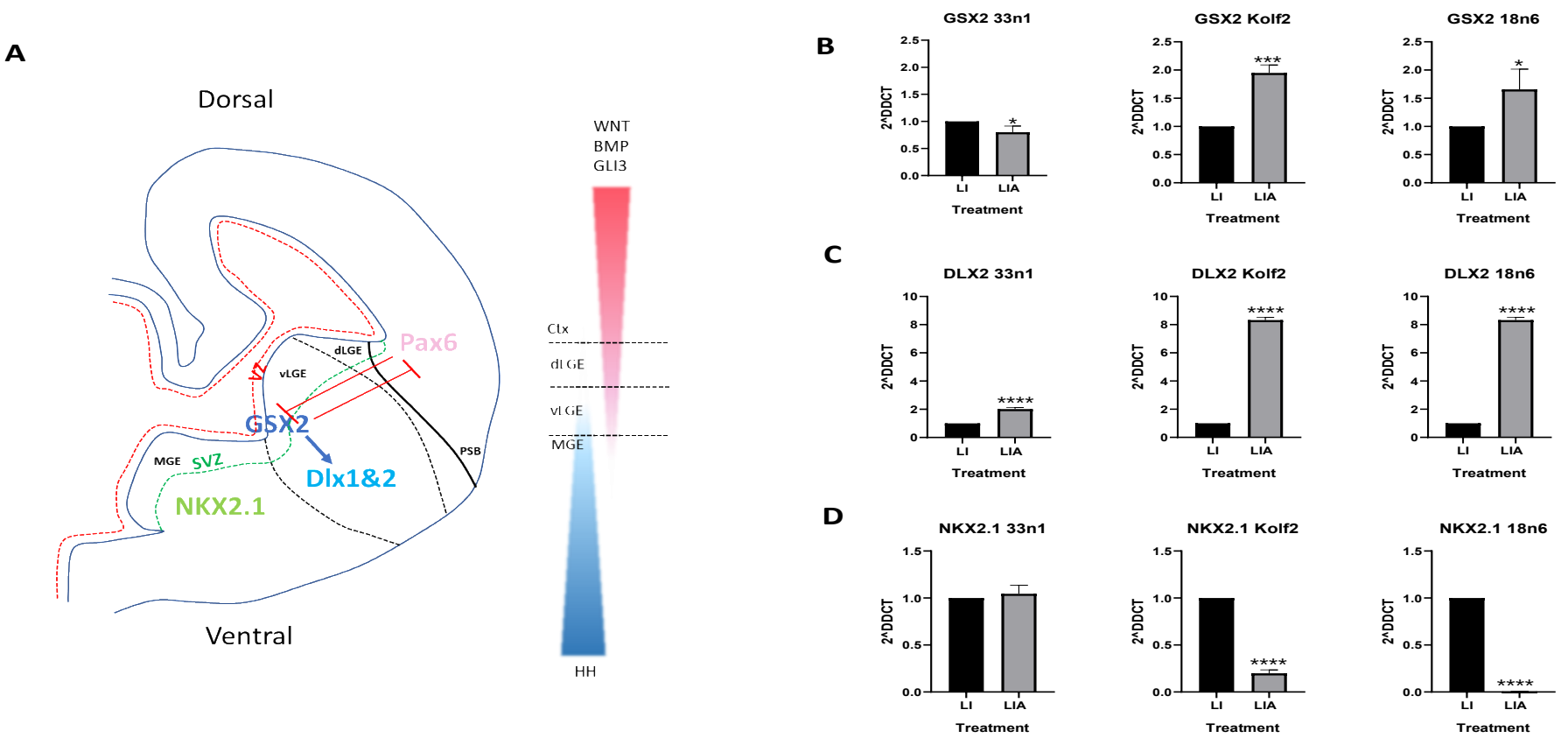

*Figure 3.4: Left: schematic showing dorso-ventral gradient of HH, WNT and BMP families of signalling proteins which in turn regulate transcription factor expression in the developing telencephalon. The antagonistic role of PAX6 (high pallial) and GSX2 (high subpallial) within the ventricular zone compartments forms the Pallial-Subpallial boundary (PBS). GSX2⁺ progenitor cells within the VZ later express DLX genes in the SVZ of the LGE while cells expressing NKX2.1 are found in the MGE only. B-D) qPCR analysis of LGE and MGE markers, GSX2, DLX2 and NKX2.1, of D16 cultures following LI and LIA treatment from D8 to D16, fold change was generated for each line compared to expression under LI protocol. Data shown are the average of 3 independent differentiations in triplicate in 3 cell lines 18n6, Kolf2 and 33n1. * P≤0.05, ** P≤0.01, ***P≤0.005, ****P≤0.001, two-tailed t-test.*

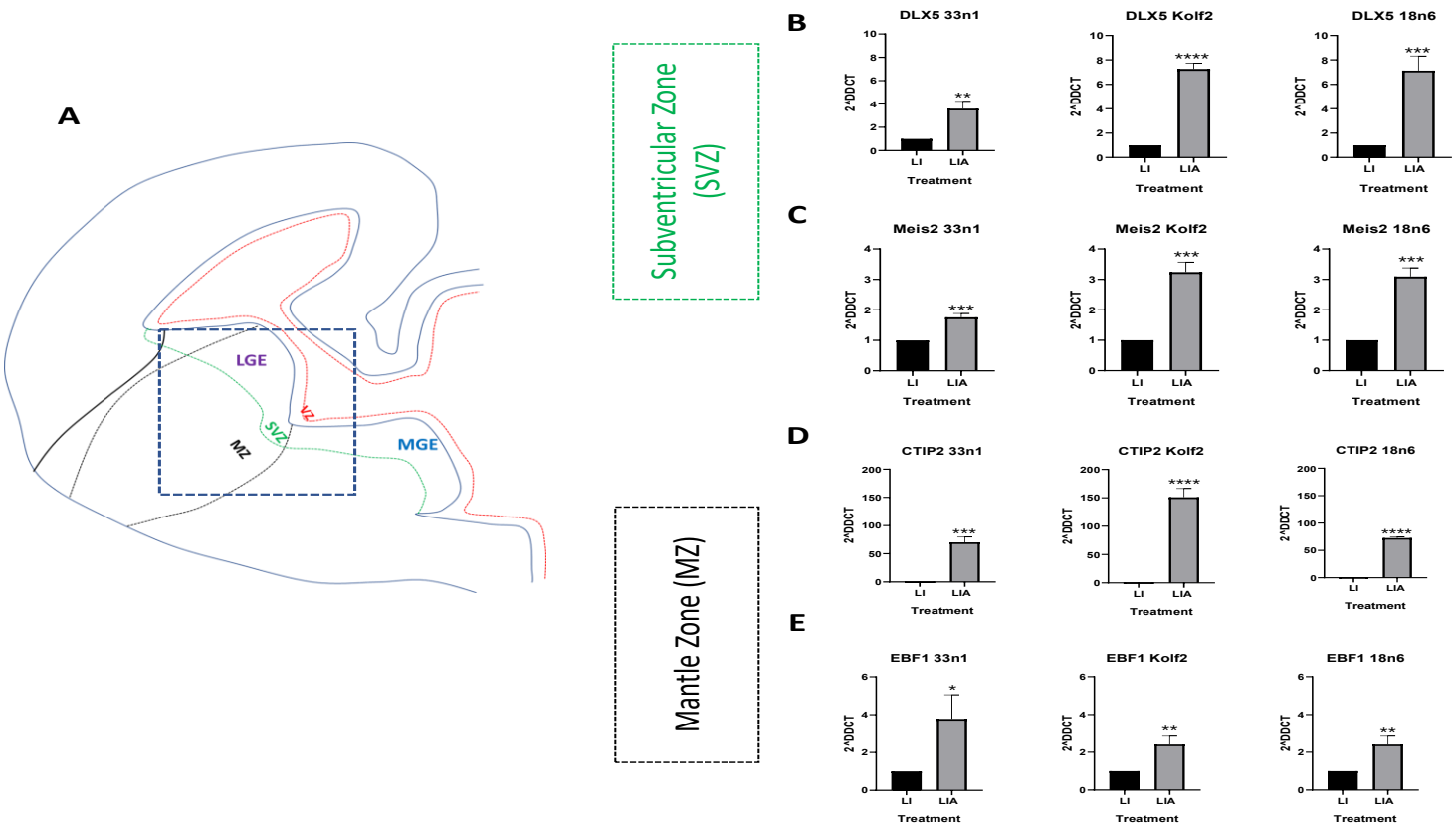

*Figure 3.5: Left: schematic showing proliferating zones of the ventral telencephalon, the ventricular and subventricular zones (VZ and SVZ, respectively), where progenitors are generated. Postmitotic cells from these regions migrate basally into the mantle zone (MZ) and to their final location and can be identified by the enrichment of specific transcription factors. B-E) qPCR analysis of LGE genes enriched in pre- and post- mitotic neurons following LI and LIA treatment from D8 to D16, fold change was generated for each line compared to expression under LI protocol. Data shown are the average of 3 independent differentiations in triplicate in 3 cell lines 18n6, Kolf2 and 33n1. * P≤0.05, ** P≤0.01, ***P≤0.005, ****P≤0.001, two-tailed t-test.*

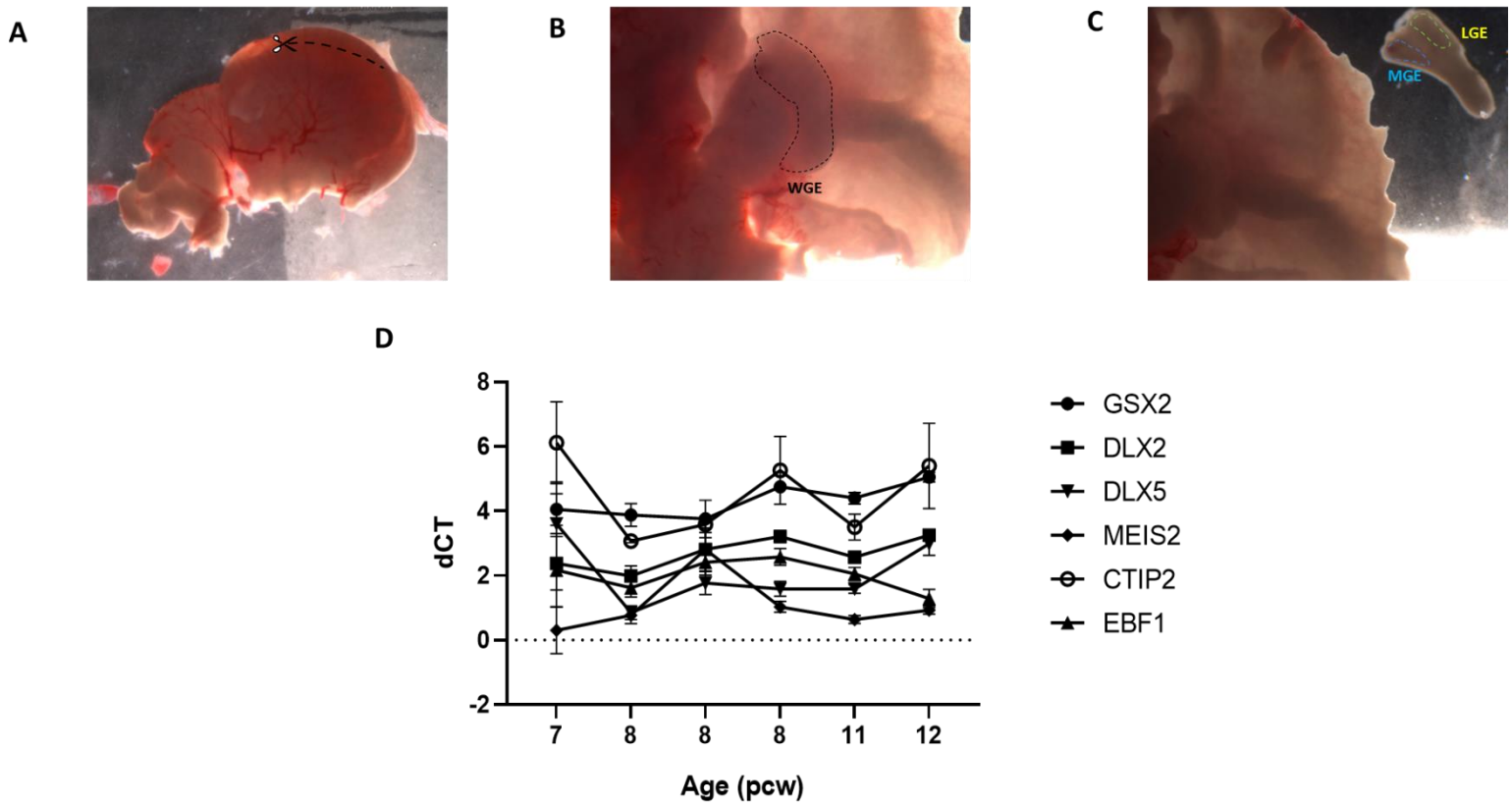

*Figure 3.6: Human foetal dissection to obtain the lateral and medial ganglionic eminences (LGE and MGE, respectively). A) Whole brain was removed from the head and the cortex was opened B) The choroid plexus was removed revealing the whole ganglionic eminence (WGE), c) The WGE was dissected out and the MGE and LGE was taken for RNA extraction. D) qPCR analysis of pan-GE/LGE enriched genes in pre- and post-mitotic neurons show no correlation between gene expression and Age (GSX2: R^2=0.8036, Dlx2: R^2=0.5731, Dlx5: R^2=0.02661, Meis2: R^2= 0.003836, CTIP2: R^2=0.08314, EBF1: R^2=0.6244). Data shown are the average of 3 independent dissections grouped based on age and ran in triplicate * P≤0.05, ** P≤0.01, ***P≤0.005, ****P≤0.001, Pearson's correlation*

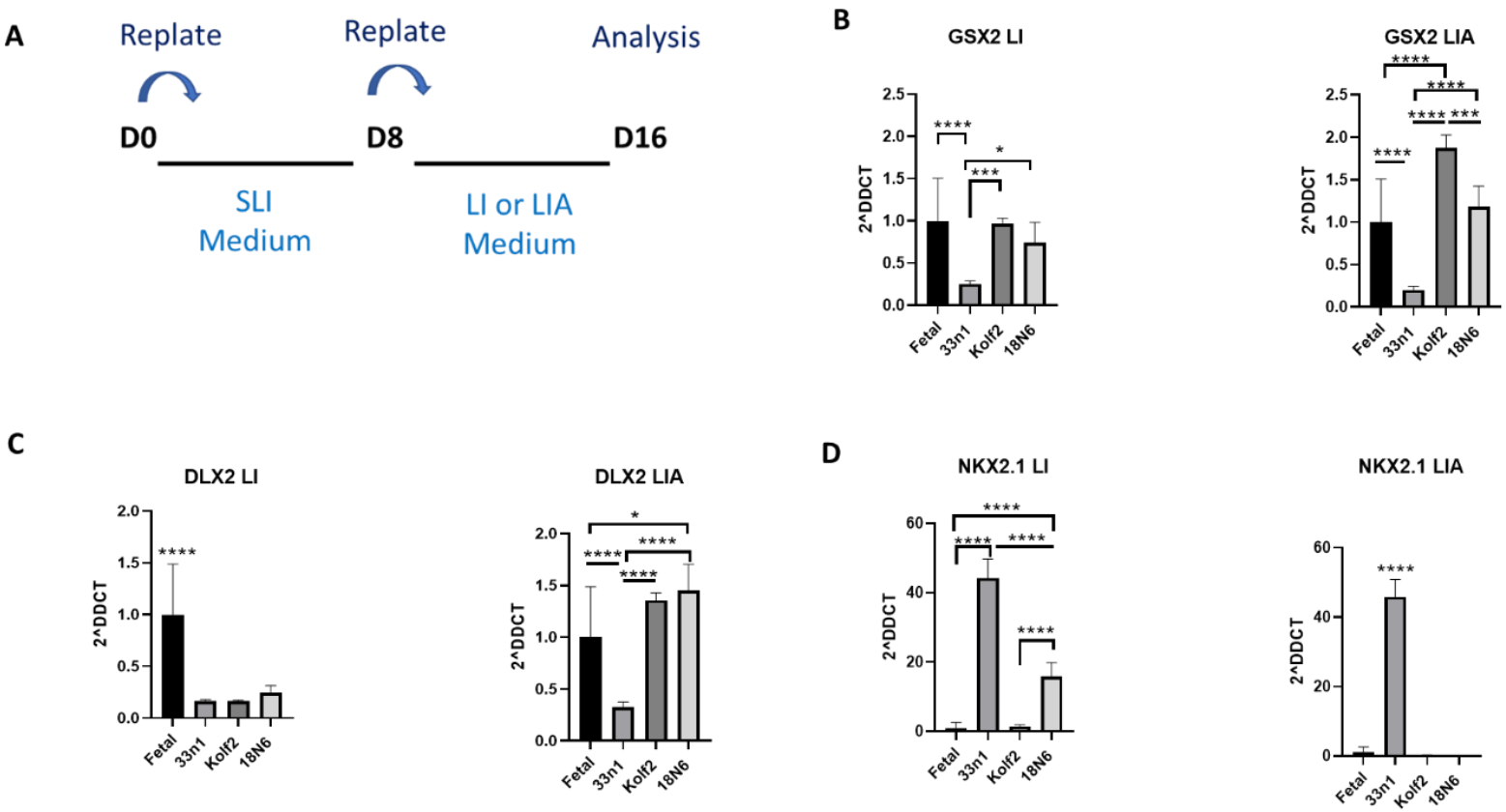

Figure 3.7. A) Schematic showing differentiation protocols used to pattern cell lines 33n1, Kolf2 and 18n6 in comparison to fetal tissue. B-C) qPCR analysis of LGE and MGE markers, GSX2 (LI, $F(3,41)=10.25$, $p<0.0001$; LIA, $F(3,41)=34.80$, $p<0.0001$), DLX2(LI, $F(3,41)=23.76$, $p<0.0001$; LIA, $F(2,41)=20.91$, $p<0.0001$) and NKX2.1(LI, $F(3,35)=341.3$, $p<0.0001$; LIA, $F(3,35)=742.9$, $p<0.0001$) of D16 cultures following LI and LIA treatment from D8 to D16 compared to average SWIFT foetal LGE or MGE gene expression.

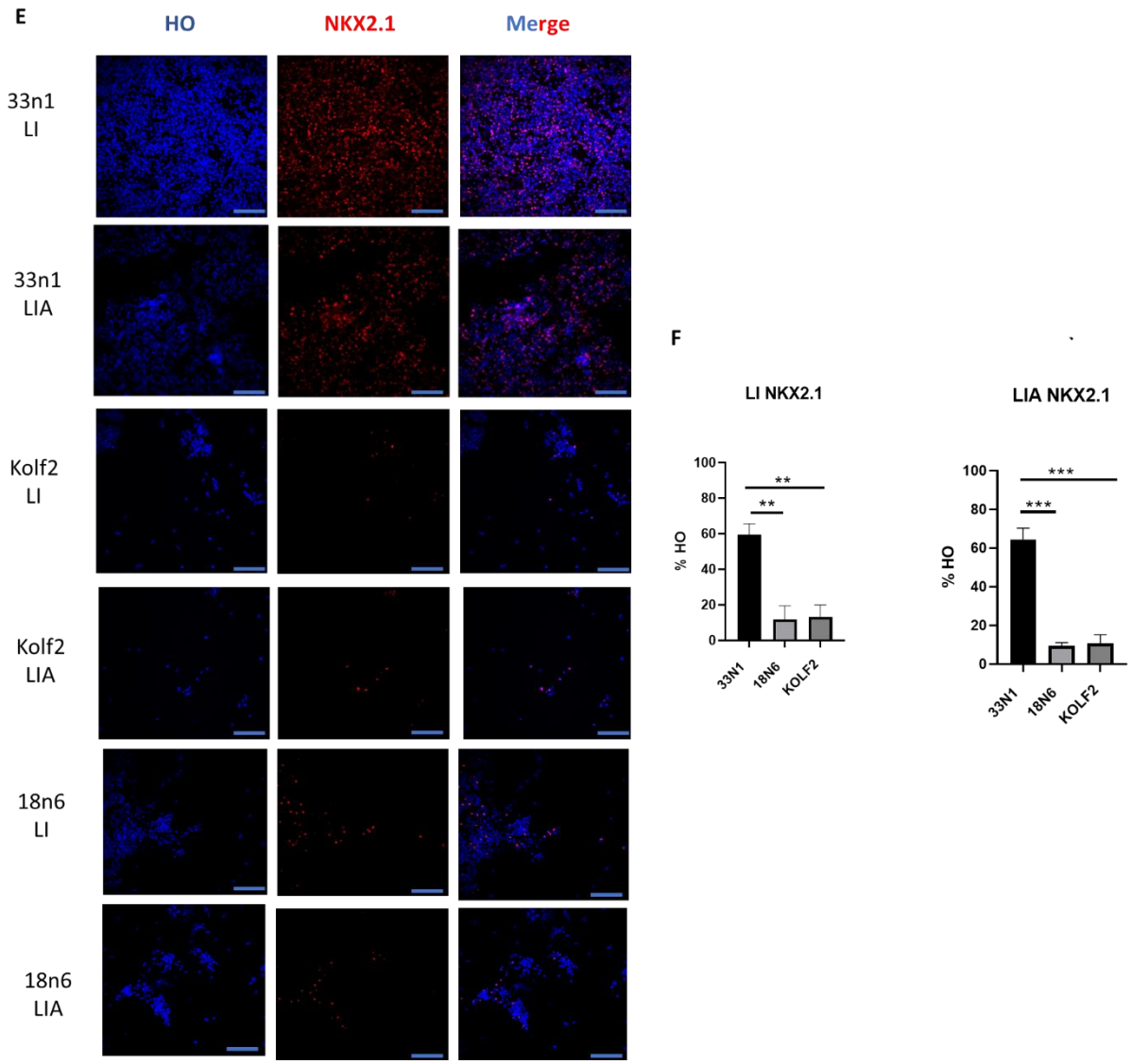

*Figure 3.7. continued. E) Exemplar ICC images of NKX2.1 positive cells (scalebar 100µm) F) Percentage of NKX2.1 shows variation in is predominantly within the 33n1 cell line under both LI ($F(2,9)=16.53$, $p=0.001$) and LIA ($F(2,9)=34.38$, $p<0.0001$) protocols. F). Data shown are the average of 3 independent differentiations in triplicate in 3 cell lines 18n6, Kolf2 and 33n1. * $P\leq0.05$, ** $P\leq0.01$, ***$P\leq0.005$, ****$P\leq0.001$, one-way ANOVA followed by Tukey's post-hoc test.*More mature LGE enriched genes (DLX5, MEIS2, CTIP2 and EBF1), albeit lowly expressed compared to foetal expression (2^DDCT=1), showed no significant difference in expression between all cell lines under LI protocol (Figure 3.8A-D).

With the addition of Activin-A, no variation was observed between cell lines 18n6 and Kolf2 in expression levels of DLX5, MEIS2 and CTIP2 and were comparable to that of foetal

expression, whereas expression of these genes within the 33n1 cell line were significantly lower. Although an increase in EBF1 expression is observed in all lines with the addition of Activin-A, expression levels are lower than that observed in foetal and do not differ between all cell lines (Figure 3.8A-D). To examine the effect of Activin-A at a protein level, immunocytochemistry was employed for CTIP2. Here, an increase was seen in the number of $CTIP2^+$ cells by the addition of Activin-A in 18n6 ($t(2)=2.558$, $p=0.0628$) and Kolf2 ($t(2)=0.8609$, $p=0.0495$) cell lines (18n6, 70.9% $\pm$23.3; Kolf2, 74.6 $\pm$14.1) compared to LI (18n6, 28.8% $\pm$27.7; Kolf2, 41.3% $\pm$7.8). However, in the 33n1 cell line there was no difference in $CTIP2^+$ cells between LI (43.4% $\pm$7.8) and LIA (48.7% $\pm$12.9), further illustrating the variability primarily within the 33n1 cell line compared to 18n6 and Kolf2 (Figure 3.8E-F). Data shows that under LI conditions both MGE- and LGE- specific transcription patterns are present in all cell lines. With the addition of Activin-A a more LGE-like transcription pattern is induced which significantly downregulated MGE fate in the 18n6 and Kolf2 cell line. However, pronounced expression of NKX2.1 is still present in the 33n1 cell line, suggesting a more MGE phenotype in the cell line.

In vivo, Sonic Hedgehog (SHH) maintains NKX2.1 expression in the MGE, therefore we next examined expression of the SHH target gene GLI1 and SHH itself using qRTPCR. During differentiation SHH or its downstream effector, GLI1, were not expressed at D0 to D8 in all cell lines with amplification within the negative control (data not shown). However, at D16 there was a >10-fold increase in SHH expression in the 33n1 cell line only in LI medium and >40-fold increase in LIA compared to D8 expression (Figure 3.9, $F(2,24)=36.02$, $p<0.0001$). Furthermore, there was a 55-fold increase in GLI1 in LI medium and a 45-fold increase in LIA ($F(2,24)=151.1$, $p<0.0001$. Based on the above results we propose that the hedgehog signalling, in part, is biasing the 33n1 cell line to a more MGE cell fate, resulting in the outcome variations seen between the cell line.

In LI conditions both MGE- and LGE- specific transcription patterns are present in all cell lines. With the addition of Activin-A a more LGE transcription pattern is induced which significantly downregulated MGE fate in the 18n6 and Kolf2 cell line. However, pronounced expression of NKX2.1 is still expressed in the 33n1 cell line, suggesting a more MGE phenotype in the cell line.

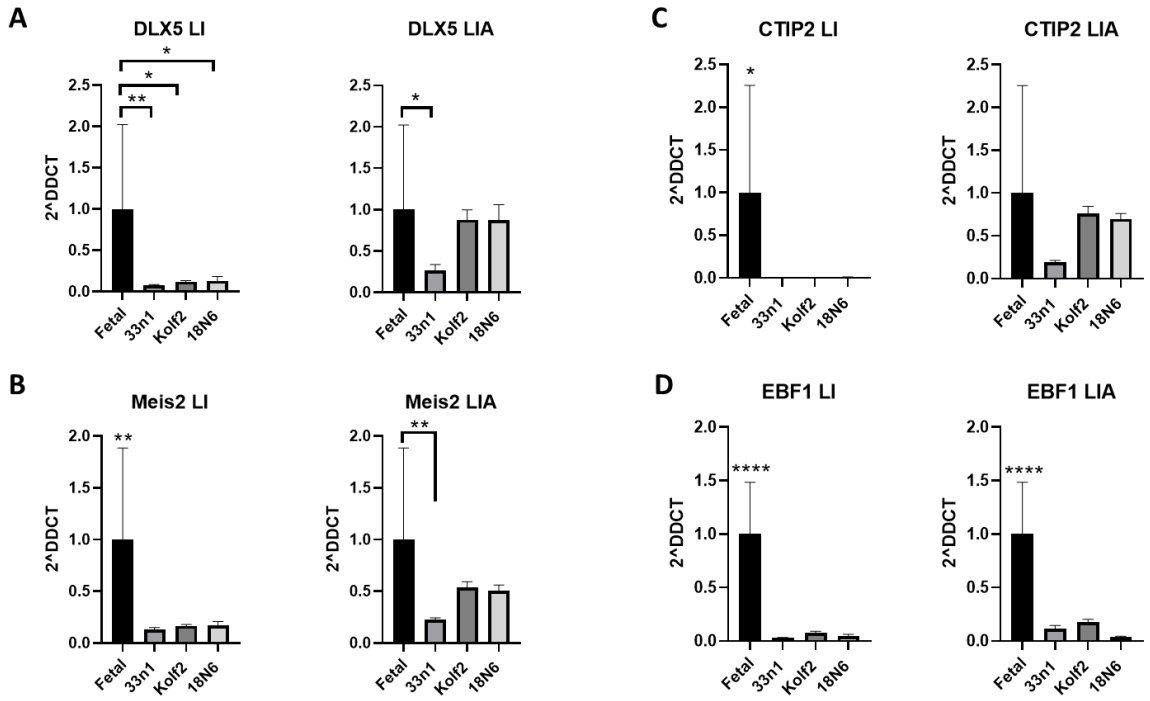

*Figure 3.8. A-D) qPCR analysis of LGE enriched transcription factors DLX5 (LI, F(3,41)=6.608, p=0.001; LIA, F(3,41)=2.553, p=0.0686), Meis2 (LI, F(3,41)=7.915, p=0.0003; LIA, F(3,41=4.226, p=0.0108), CTIP2 (LI, F(3,41)=5.436, p=0031; LIA, F(3,41)=2.016, p=0.1266) and EBF1 (LI, F(3,41)=33.33, p<0.0001; LIA, F(3,41)=29.52, p<0.0001) of D16 cultures following LI and LIA treatment from D8 to D16 compared to average SWIFT foetal LGE gene expression. Data shown are the average of 3 independent differentiations in triplicate in 3 cell lines 18n6, Kolf2 and 33n1. * P≤0.05, ** P≤0.01, ***P≤0.005, ****P≤0.001, one-way ANOVA followed by Tukey's post-hoc test*

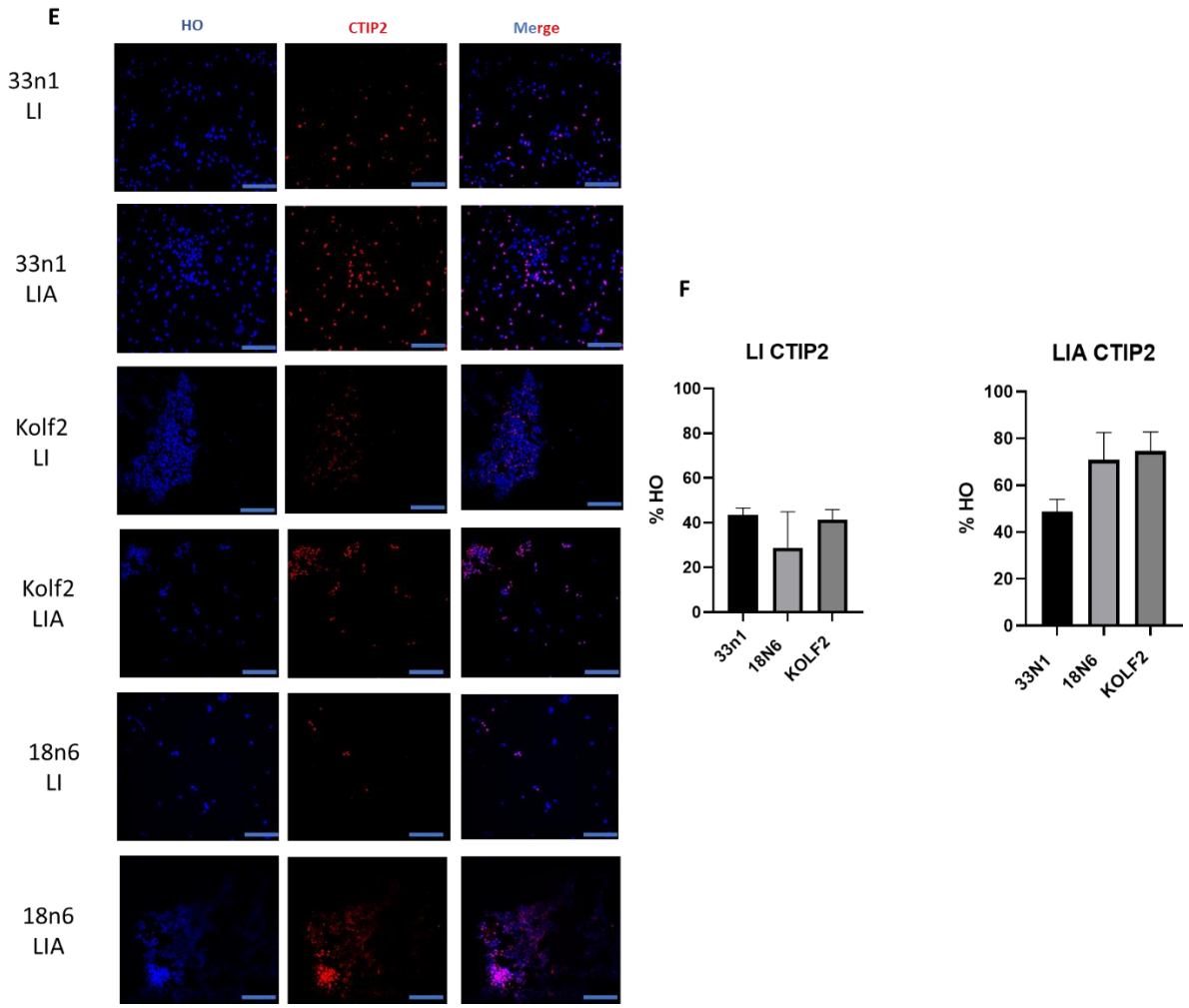

Figure 3.8. continued. E) Exemplar ICC images of CTIP2 positive cells in all cell lines under LI and LIA protocols (scalebar 100µm). F) Percentage of CTIP2 shows 25-40% positive cells under LI protocol ($F(2,9)=1.018$, $p=0.3996$) in all cell line and > 40% increase under LIA protocol in the 18n6 and Kolf2 cell line with no significant effect on the 33n1 cell line ($F(2,10)=3.229$, $p=0.0828$).

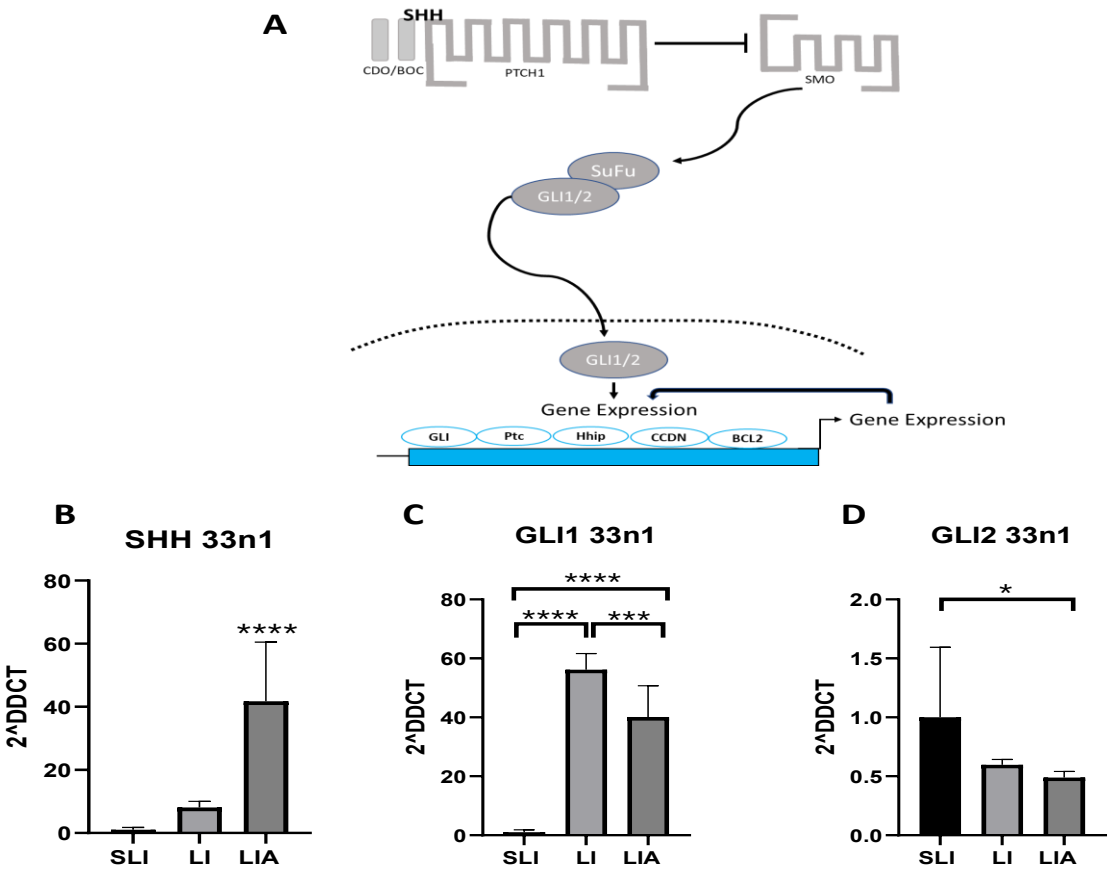

*Figure 3.9. Left: schematic showing HH signalling pathway and downstream targets. B-C) qPCR analysis shows SHH and HH targets GLI1 and GLI2 expression in 33n1 cell line only relative to GAPDH compared to D8 expression (SLI). Data represents the mean of tree biological and 3 technical repeats with SD and ordinary one-way ANOVA with Tukeys multiple comparisons test., * p<0.05, ** p<0.01, *** p<0.001, **** p<0.0001*

Variation in MSN differentiation between HD IPSC lines is partly due to differences in endogenous HH signalling seen in D16 NPCs

As under the LIA protocol we see the highest efficiency of MSN differentiation within the 18n6 and Kolf2 cell lines, we next examined whether the LIA protocol was optimal and reproducible in HD-iPSC lines and their controls. Four HD lines were used, HD109n1, HD109n4, HD60n4 and HD60n5 together with 3 control lines isogenic to HD109 lines, and the 33n1 control line that is a non-HD sibling control to the HD60 lines.

Since the HD109 lines are known to be susceptible to Chromosome 1 trisomy all lines were screened at D0, D16 and D44 of differentiation for trisomy of chromosome 1 via qPCR (see methods p49) and any cultures positive for Chr1 trisomy (with 95% CL) were excluded from analysis.

Following 16 days of differentiation under the LIA protocol gene expression of the isogenic, 33n1 and HD lines were assessed. We chose to utilise a 96:96 Dynamic for gene expression which enables 9,216 reactions using 96 samples and assays. This allowed for a wider panel of genes to be assessed and larger sample number, thus increasing the statistical power. The panel of genes were chosen based on the literature to be differentially expressed along the dorso-ventral axis (Table 2.14). The suitability and stability of housekeeping genes used for normalisation for the use in expression analysis in HD models has shown that UBC, Eif4a2 and ATP5B are the most usable reference genes for analysis of striatal tissue (Benn, Fox and Bates 2008). With this in mind, we increased our panel of genes to include these housekeeping genes as well as GAPDH (which was stable in these differentiations) and the genomic mean was derived for normalisation and further normalised to average human foetal LGE expression.

Analysis of HD109 and isogenic cultures at D16 did not reveal differential expression of any of the 80 genes tested, which serves here as a good quality control in terms of differentiation propensity under the same biological background irrespective of CAG repeat (Figure 3.10A). However, comparing the 33n1 line to the HD60 (60n4 line) revealed 10 differentially expressed genes; those that were upregulated in the 33n1 cell line were genes downstream of the HH pathways including GLI1 (Log fold change = 6.1, p.adjusted = 0.004), NKX2.1 (Log fold change = 6.8, p.adjusted = 0.0005) and its downstream target LHX6 (Log

fold change = 5, p.adjust = 0.004) and its downstream target GSX1(Log fold change = 6.3, p.adjusted = 0.0009) and SST (Log fold change = 3.5, p.adjusted = 0.04). Whereas, in the HD60, genes that are known to be enriched in the developing CTX were upregulated including, TBR2 (Log fold change = 22.6, p.adjusted = 4.96×10^{-9}), NeuroD6 (Log fold change = 3.7, p.adjusted = 0.04) and Zic1 (Log fold change = 3.3, p.adjusted = 0.04). This further illustrates the bias of the 33n1 cell line towards an MGE fate (Figure 3.10C). Although 33n1 served as a sibling control for the HD60, the data highlights the need for isogenic controls of identical biological backgrounds in order to assess whether there are any developmental differences at the gene expression level due to expanded CAG repeat only. Furthermore, when comparing HD60 and HD109 lines, expression of LGE-like, MGE-like and pan-GE genes were significantly less than in the HD109 lines (Figure 3.10D). Again, as no significant differences were observed between isogenic and HD109 cultures at this stage, the difference observed here is unlikely to be due to differences in CAG repeat length and is likely due to inter-line variability.

A

Contrast	Up	Down	N.S
Isogenic vs HD 109	0	0	83
33n1 vs HD 60n4	4	6	73
HD 60 vs HD 109	1	46	36

B

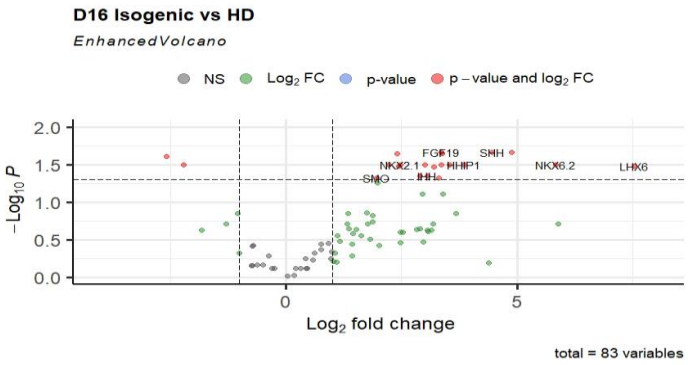

C

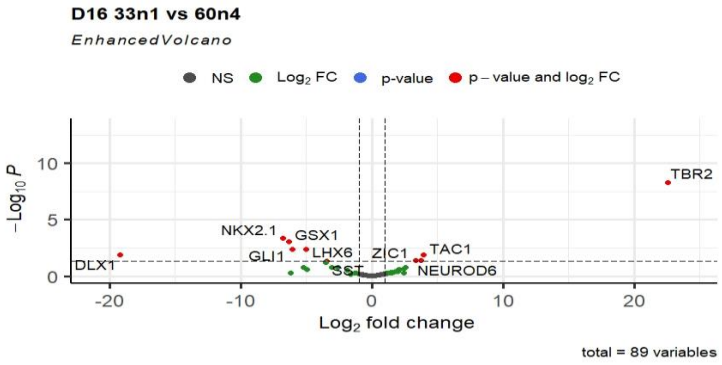

D

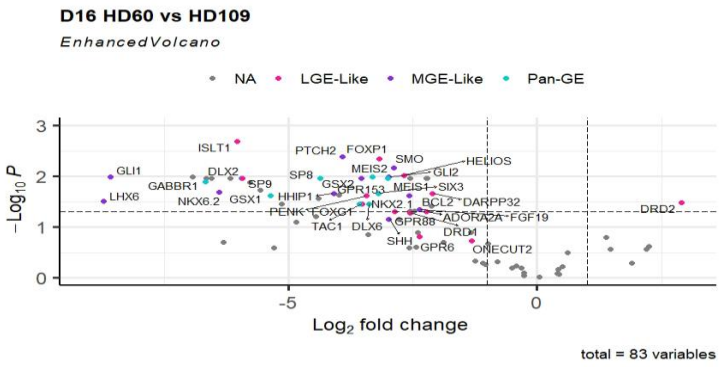

Figure 3.10. Isogenic Control and HD-derived neural progenitor cells following LIA protocol. A) Contrast matrix used to analyse Fluidigm Biomark qPCR with the number of up and down DEGs and non-significant genes (N.S). B-D) Volcanoplots of DEGs shows variation is due to HH signalling genes resulting in differential expression in MGE-like and LGE-like enriched genes.

Variation in MSN differentiation between HD IPSC lines and controls following terminal differentiation.

Following terminal differentiation of the HD and control NPCs to D37, the same gene sets were compared and a heatmap was generated of δδCt values to illustrate the technical and biological reproducibility of differentiations (Figure 3.11A). This resulted in all Isogenic controls, HD60's, HD109's (with the exception of HD109n_S1) and 33n1 lines clustering based on technical replication. Comparing the isogenic and HD109 lines revealed none of the genes to be differentially expressed (Figure 3.11B). Whereas 73 out of the 82 genes tested were differentially expressed when comparing the HD60 and 33n1 lines. Interestingly, in terminally differentiated neurons, the HD60 cultures and not the 33n1 cultures (as seen at D16) showed enrichment of HH pathway genes including SHH, HHIP1, PTCH1, BCL2, IHH, NKX6.2, GPR161 and GPR153, suggesting that a HH pathway bias can operate in different cell lines but in different temporal windows of development.

In addition, genes involved in MSN differentiation (ONECUT2, ISLT1, ZNF521, ARPP21, HELIOS, DLX6, SP9, FOXP1, MEIS2, DLX5, EBF1, MASH1 and DLX2) and genes enriched in direct and indirect MSNs (GPR88, PENK, SP8, DRD1, DARPP32, DRD2, ADORA2A, GPR6, and TAC1) were also upregulated in the HD60. Furthermore, genes enriched in the cortex were also upregulated, such as VGlut1/2, FOXP2, TBR1, FGF19, FEZF2, DACH1, LMCH1 and NEUROD6. These groups of DEGs suggest a heterogeneous population of pallial and sub-pallial neurons.

Comparing HD60 and HD109 cultures, 8 genes were upregulated in HD109 including CHAT, OLIG2, ACHE, TGFB1, RALD2 and FGF19. Cholinergic neurons originating from the MGE that express CHAT are demarcated by expression of OLIG2, thus a population of cells may be for a cholinergic interneuron fate.

To further examine terminal differentiation of HD neuron, cells were plated for immunocytochemistry for DARPP-32 and GABA in three clones of the HD109 line (109n1, 109n5 and 109n1 sc3D). At D37, an average of 51.6% ±5.8 of total cells expressed DARPP-32 ($F(2,241)=9.301$, $p=0.0001$) and 78% ±11.8 are positive for GABA ($F(2,277)=684.3$, $p<0.0001$, Figure 3.12), consistent with the numbers of MSNs observed following differentiation of control lines (Figure 3.1).

In addition, development of functional properties of the HD109 were compared to those of isogenic control neurons by patch-clamp electrophysiology, in which we measured resting membrane potential, capacitance, input resistance and the ability of neurons to fire induced and spontaneous action potentials. After culture in SCM1/2 medium, that has previously been shown to accelerate the functional maturation of control neurons by D37 (Telezhkin *et al.,* 2015), 22% of isogenic control neurons generated spontaneous action potentials compared to just 7% spontaneous activity of HD109 neurons (Figure 3.13A-B). This observation of HD was reproducible and consistent through 3 separate differentiations of the HD109 lines. Isogenic and HD neurons also differed in their passive membrane properties, including depolarised RMP values (Isogenic: -49.6 $\pm$ 1.7mV, HD109: -39.1 $\pm$ 2.4mV, $t(37)=12.19$, $p < 0.0001$; Figure 3.13C), less capacitance (Isogenic: 105 $\pm$ 25pF, HD109: 58.4 $\pm$ 7.7pF, $t(8.479)=5.623$, $p=0.0004$; Figure 3.13D) and greater input resistance (Isogenic: 113.57 $\pm$ 40.66MΩ, HD109: 174.25 $\pm$ 31.63MΩ, $t(37)=4.725$, $p<0.0001$; Figure 3.13E). Together these data suggest that the HD neurons are less mature than their controls counterparts. To confirm this, more analysis of the isogenic controls is needed as well as post-hoc analysis to identify the population of cells that have been recorded. Nevertheless, we investigated whether extending HD109 terminal differentiation for a further two weeks would result in neurons having a more hyperpolerised membrane potential and consequently able to generate spontaneous action potential activity. Following six weeks of terminal differentiation the majority of HD neurons at this stage (71%) were spontaneously active (Figure 3.13F-G). In addition, compared to the four-week cultures, extended culture resulted in a more hyperpolarised RMP (HD109 Week 6: -42.5 $\pm$ 2mV, $t(45)=4.943$, $p<0.0001$; Figure 3.13H), and increase in both capacitance (HD109 Week 6: 107.5 $\pm$ 13.5, $t(22.03)=13.78$, $p<0.0001$; Figure 3.13I) and input resistance (HD109 Week 6: 252.72 $\pm$ 87.26, $t(18.41)=3.577$, $p=0.0021$; Figure 3.13J). While at week 4 there was a difference in capacitance between isogenic and HD109 neurons, this was no longer significant at week six suggesting cells were now of a similar size ($t(10.64)=0.2841$, $p=0.7818$).

A

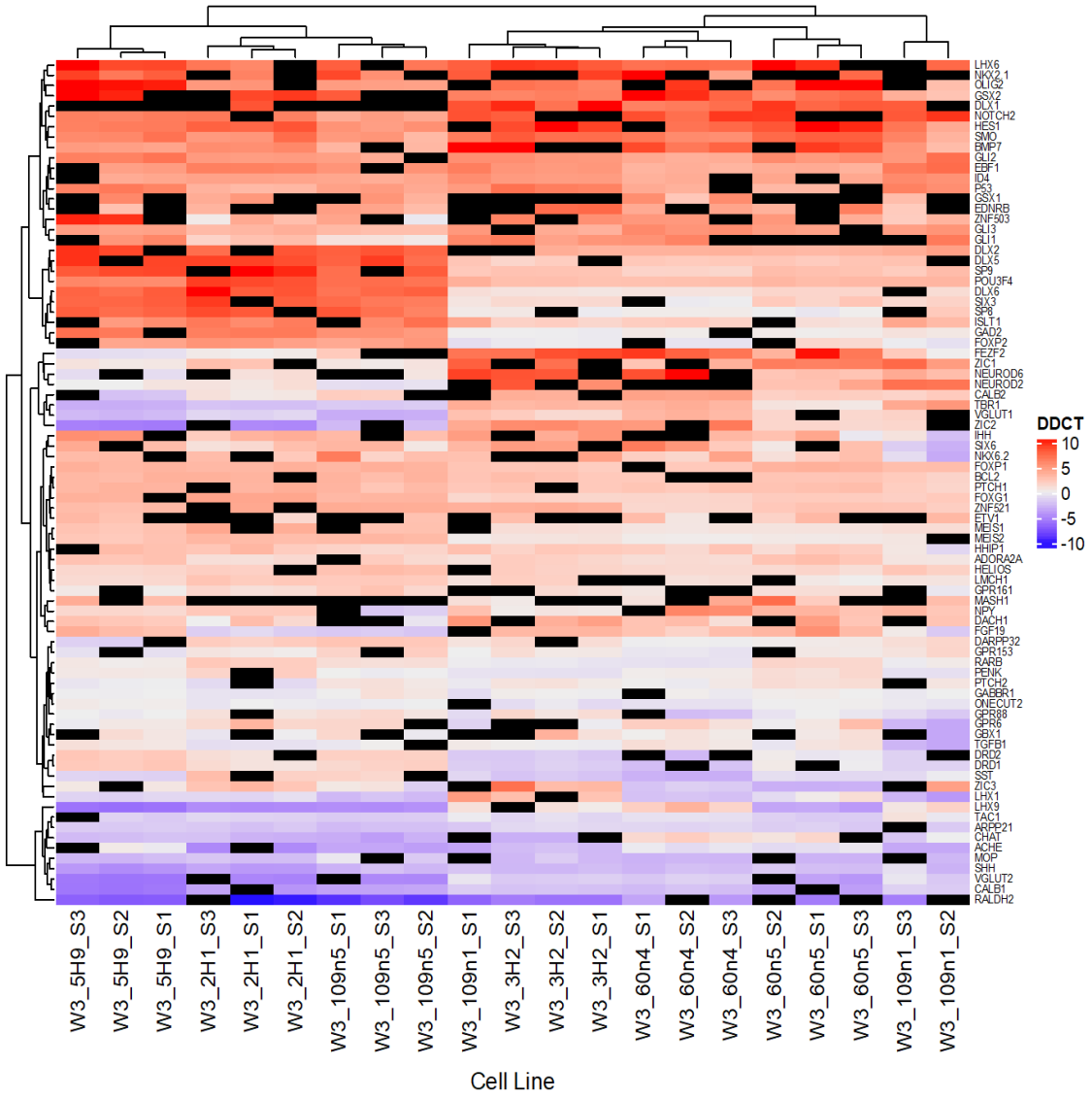

Figure 3.11. Isogenic Control and HD-derived neurons following LIA protocol to D16 followed by terminal differentiation (SJA/SJB protocol). A) Heatmap of DDCT values compared to average LGE shows clustering of triplicates, with the exception of 109n1 sample 2.

B

Contrast	Up	Down	N.S
Isogenic vs HD	0	0	82
Isogenic vs HD 109	0	0	83
Isogenic vs HD 60	18	6	58
HD 60 vs HD 109	8	6	68

C

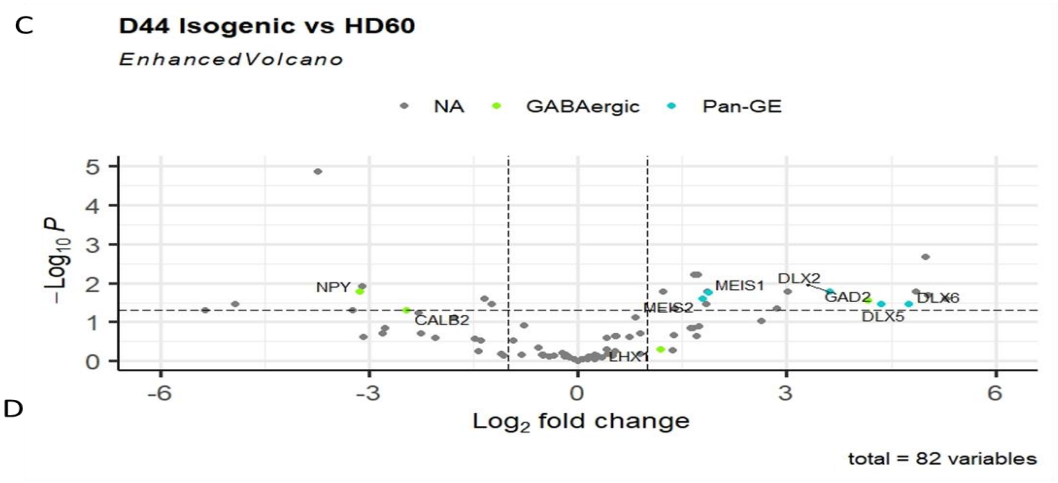

D

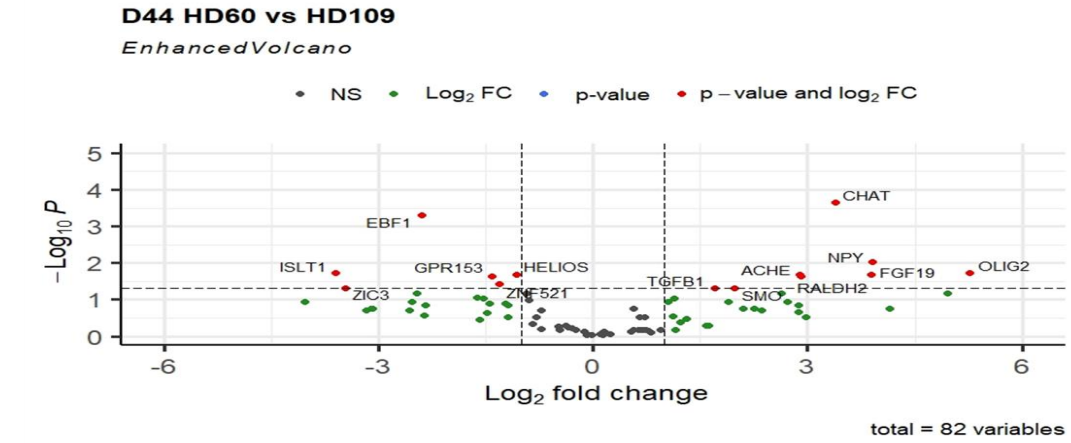

Figure 3.11. continued. B) Contrast matrix used to analyse Fluidigm Biomark qPCR with the number of up and down DEGs and non-significant genes (N.S) shows HD109 and isogenic controls do not differ and HD60'd are biasing DEGs. C) Volcanoplot of DEGs shows variation in pan-GE and GABAergic genes as well as HH signalling an interneuron genes.

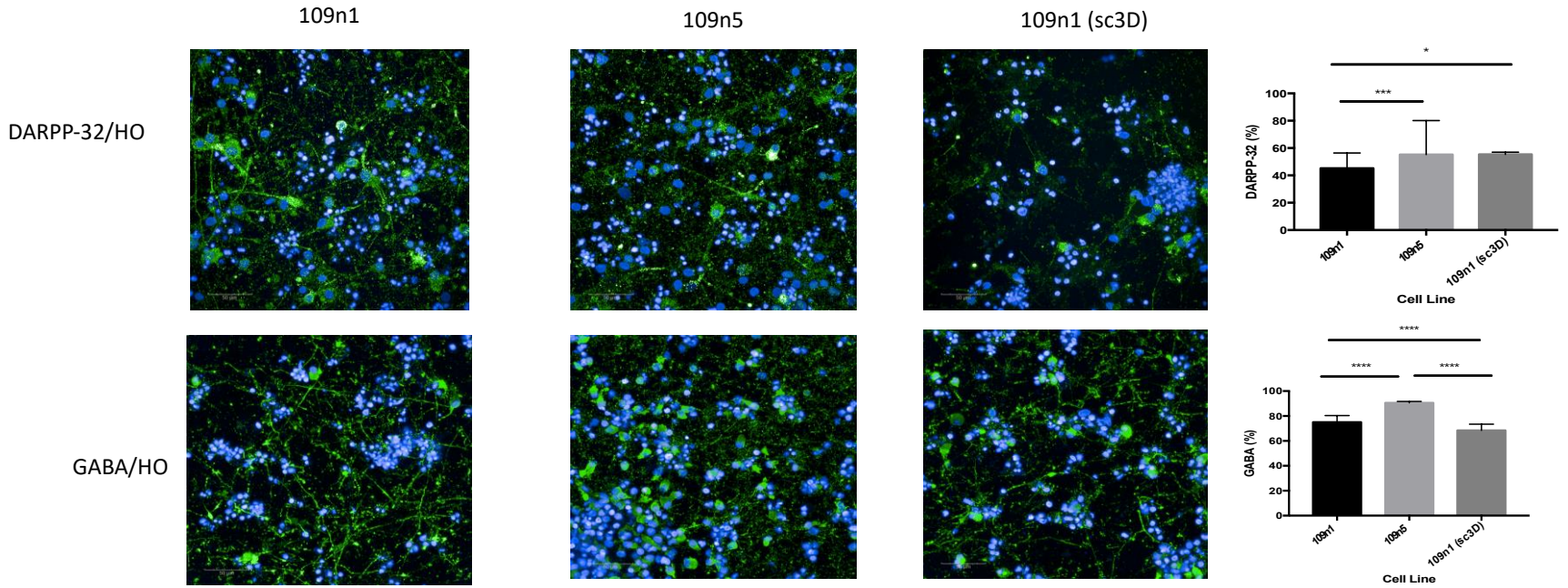

*Figure 3.12. iPSC differentiation following LIA protocol. Left: Exemplar ICC images of DARPP-32 and GABAergic positive neurons (scale bar 50μm). Right: Percentage of DARPP-32 shows variation within different clones of the HD109 lines. Note: 109n1 (sc3D) has a 130/21 CAG repeat length. The majority of all cell lines expressing GABA but vary from clone to clone. Data was calculated from 3 independent differentiation and 72-96 fields of view and are presented as the mean with SD and one-way ANOVA with Tukey's multiple comparisons test. * p<0.05, ** p<0.01, *** p<0.001, **** p<0.0001.*

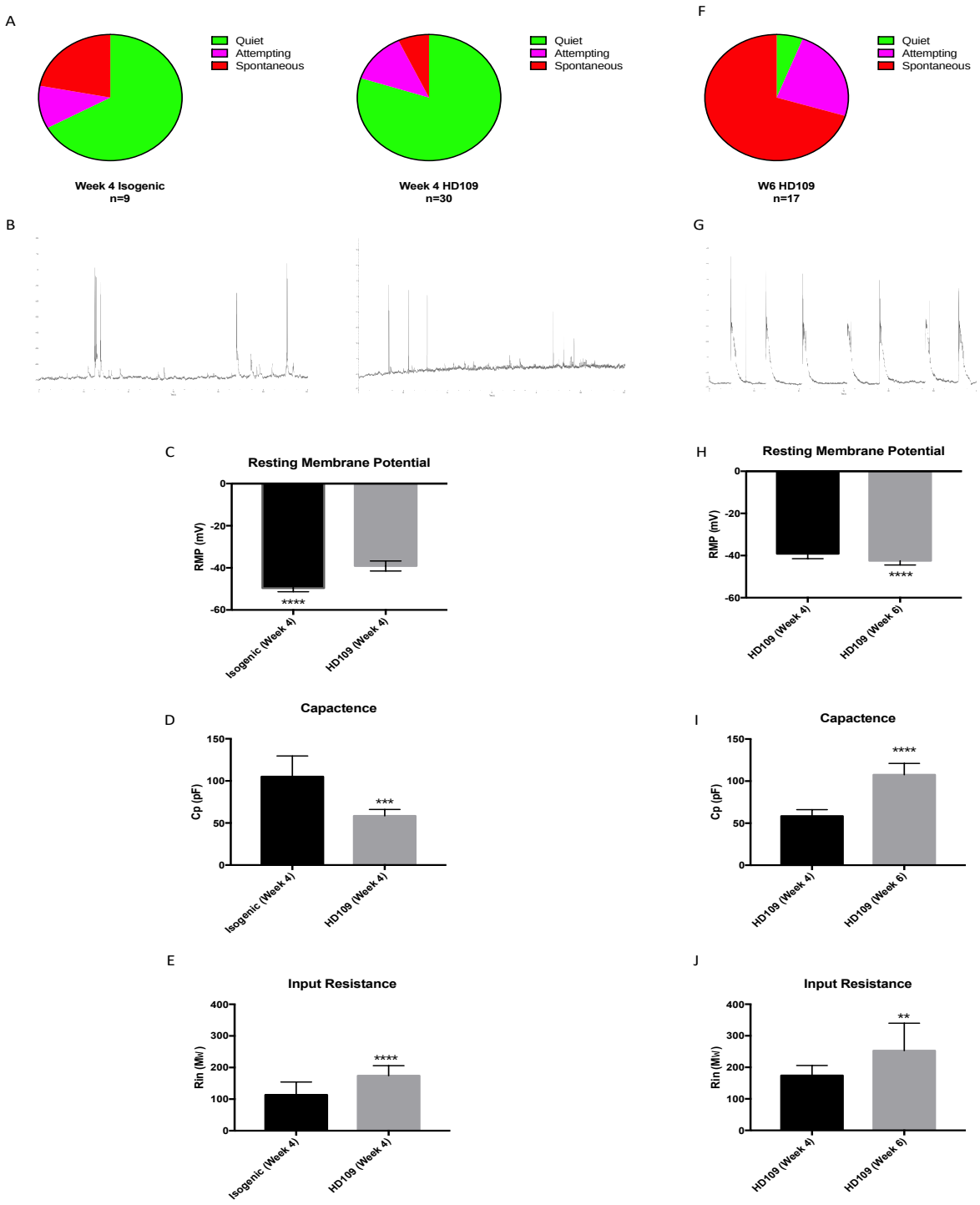

*Figure 3.13. Electrophysiological Assessment of Isogenic and HD109 Neurons following LIA patterning and three (A-E) or six (F-J) weeks of terminal differentiation. A + F) percentage of neurons that attempted or spontaneously generated an action potential or were otherwise silent. B + G) Exemplar traces of spontaneous action potentials. Passive membrane properties of Week 4 isogenic and HD109 neurons show differences in C) Resting membrane potential (RMP) D) Capacitance and E) Input Resistance. Extended culture of the HD109 show C) Hyperpolerised RMP and increase in D) Capacitance and E) Input Resistance. * p<0.05, ** p<0.01, *** p<0.001, **** p<0.0001, was determined by either parametric with Welch's correction or non-parametric t-tests depending on distribution of data.*

Summary

Using our previously published LGE differentiation protocols (LI), and a LIA protocol (Comella 2020; Smith-Geater 2020) we examined gene expression profiles of 3 independently derived IPSC lines and their responses to forebrain dorsal –ventral patterning cues. This revealed high NKX2.1 expression (higher than that present in primary foetal LGE samples) indicative of MGE fate specification within the cultures. This was also apparent in the HD60 line further supporting the need to optimise MSN differentiation protocols and quality control of differentiating cultures used for disease modelling.

It has been well documented that there is a gradient of SHH within the telencephalon with highest expression ventrally and lowest dorsally. During embryonic development SHH acts to induce and maintain expression of the MGE through regulation of the master regulatory transcription factor, NKX2.1, which in turn feeds back to promote SHH expression, as evident from NKX2.1 and SHH mutant mice (Ericson *et al.*, 1995; Dale *et al.*, 1997; Pera and Kessel, 1998; Sussel *et al.*, 1999). Since no SHH or HH pathway agonists are used in our MSN differentiation protocol this suggests that cultures possess high endogenous HH signalling activity. This was supported by RT-QPCR data showing high SHH and GLI1 expression in D16 33n1 cell line cultures.

In order to assess whether independent control cell lines showed similar patterns of response to differentiation media, three control cell lines were examined in detail after differentiation using the LI- LIA- protocols. Here, all control cell lines 18n6, kolf2 and 33n1 showed ventral MGE-like progenitor cell fate differentiation under LI differentiation protocols, as evident by NKX2.1 expression.

In addition, SHH expression was not detected in the 18n6 and kolf2 cell line, but under LI and LIA conditions, NKX2.1 is expressed in both cell lines, furthermore, GLI2 is expressed. This suggests there are other contributing factors. The canonical activation of SHH occurs via SHH binding to its receptor Patched resulting in a de-inhibition of Smoothened which initiates the downstream signalling cascade leading to the activation of GLI transcription factors; GLI1 and 2 primarily functioning as activators and GLI3 a repressor (Ingham and McMahon, 2001; Fuccillo, Joyner and Fishell, 2006). However, activation of GLI's can be

independent of SHH. This can occur via a crosstalk that exists between other signalling pathways, such as TGF-β, Notch and Wnt/β-catenin (Song *et al.*, 2015; DiRenzo *et al.*, 2016; McCubrey *et al.*, 2016; Morris and Huang, 2016). This is particularly relevant in our study as Activin A is a TGF-β pathway a ligand. Activation of the TGF-β pathway results in the phosphorylation and activation of R-SMADs (SMAD2 and SMAD3) which then trimerise with co-SMAD (SMAD4). This complex can either enter the nucleus to activate gene transcription or activate GLI's within the cytoplasm which then translocate to the nucleus resulting in an increase in GLI1/2 (Dennler *et al.,* 2007). In the telencephalon, activators can mimic SHH signalling while the repressor GLI3 supresses its function. Differential expression along the dorsal ventral axis of the telencephalon can induce different cell types as evident from knock out or overexpression of these genes in the mammalian telencephalon (Kuschel, Rüther and Theil, 2003; Fotaki *et al.*, 2006; Yu *et al.*, 2009).

In order to determine where in the differentiation protocol variation in gene expression occurs initially, we re-examined gene expression from D0 to D8. Here, there was no significant difference in the levels of expression of the pluripotent markers, OCT4, NANOG and SOX2 in the different cell lines. In addition, when differentiated to D8 using SLI-medium, these cells efficiently differentiated to neuroectoderm with no significant differences between cell lines in PAX6 expression.

In addition, SHH, a signalling morphogen responsible for ventralising the telencephalon, acts through the regulation of GLI activators and repressors. Therefore, we hypothesised that endogenous SHH could be antagonising GLI3 activity. However, SHH was not expressed at D0 or after 8 days of SLI treatment in any cell line. Thus, GLI's must be regulated in these cells independently of SHH via an alternative mechanism which is also independent of canonical WNT, TGF-β and BMP signalling that are all supressed in SLI medium. One possible regulator is protein kinase A (PKA) which is a key regulator of the HH pathway, downstream of SMO (Fan *et al.*, 1995; Tuson, He and Anderson, 2011; Niewiadomski *et al.*, 2013; Niewiadomski, Jennifer H Kong, *et al.*, 2014). Phosphorylation of GLI3 on its first four serine residues by PKA leads to its truncation into GLI repressor fragments, whereas loss of phosphorylation at all 6 residues in GLI2 results in nuclear translocation and transcriptional activation (Wang, Fallon and Beachy, 2000; Pan, Wang and Wang, 2009; Niewiadomski, Jennifer H. Kong, *et al.*, 2014). Thus, it is plausible that there may be less PKA activity in the

33n1 cell line compared to 18n6 and kolf2. Further investigation via western blot analysis will determine this.

Our results indicate that endogenous SHH and or GLI activity bias cell differentiation towards a ventral MGE-like fate. We therefore hypothesise that inhibiting HH signalling either by small molecule Cyclopamine-KAAD or genetic editing would induce a more LGE-like phenotype in the 33n1 cell line and reduce the variability within our differentiations.

Chapter 4: Variable outcomes in Medium Spiny Neuron differentiation protocols is due to intrinsic dorso-ventral and rostro-caudal differences

Abstract

Medium spiny neurons (MSNs) constitute ~95% of the population of cells in the human striatum and are selectively vulnerable to degeneration in Huntington's Disease. Yet we still lack an efficient and reproducible protocol for differentiating human induced pluripotent stem cells (iPSCs) to MSNs to study the disease. Here we compare transcriptomic profiles of three independent cell lines using three protocols using bulk RNA Sequencing. Major variability between cell lines in their responses to differentiation protocols was found to be due to endogenous expression and activation of the Hedgehog pathway. Blocking endogenous HH pathway activity by treatment with Cyclopamine-KAAD removed a differentiation bias towards the MGE and increased the efficiency of LGE and MSN differentiation. All cell lines under our optimised protocol efficiently and reproducibly generated >70% MSNs, the highest reported thus far. Transcriptomic data also identified that additional bias, although small, may be due to endogenous FGF and non-canonical WNT signalling during patterning.

Data further suggest that the differentiation protocols used biases the MSN populations towards a DRD2+ve (indirect pathway) MSN fate. To address this, preliminary data shows that manipulation of BMP signalling used in an extended NPC culture, is capable of generating both DRD1- and DRD2- expressing MSNs.

Graphical Abstract

- RNA Sequencing confirms endogenous SHH expression following patterning using LIA medium biases cells to an MGE-like gene expression pattern
- Additional bias may come from endogenous expression of non-canonical WNT ligand WNT5A which may pattern MGE-like neural progenitor cells (NPCs) to somatostatin (SST) or parvalbumin (PV) interneurons.
- In the absence of endogenous SHH following patterning using LIA medium neural progenitor cells adopt an LGE-like gene expression.
- Terminal differentiation of LGE-like NPCs generate predominantly DRD2-expressing medium spiny neurons (MSNs).
- Terminal differentiation of LGE-like NPCs, following extended culture in the presence of WNT inhibition, Activin-A and BMP-6 treatment, generate both DRD1- and DRD2-expressing MSNs.

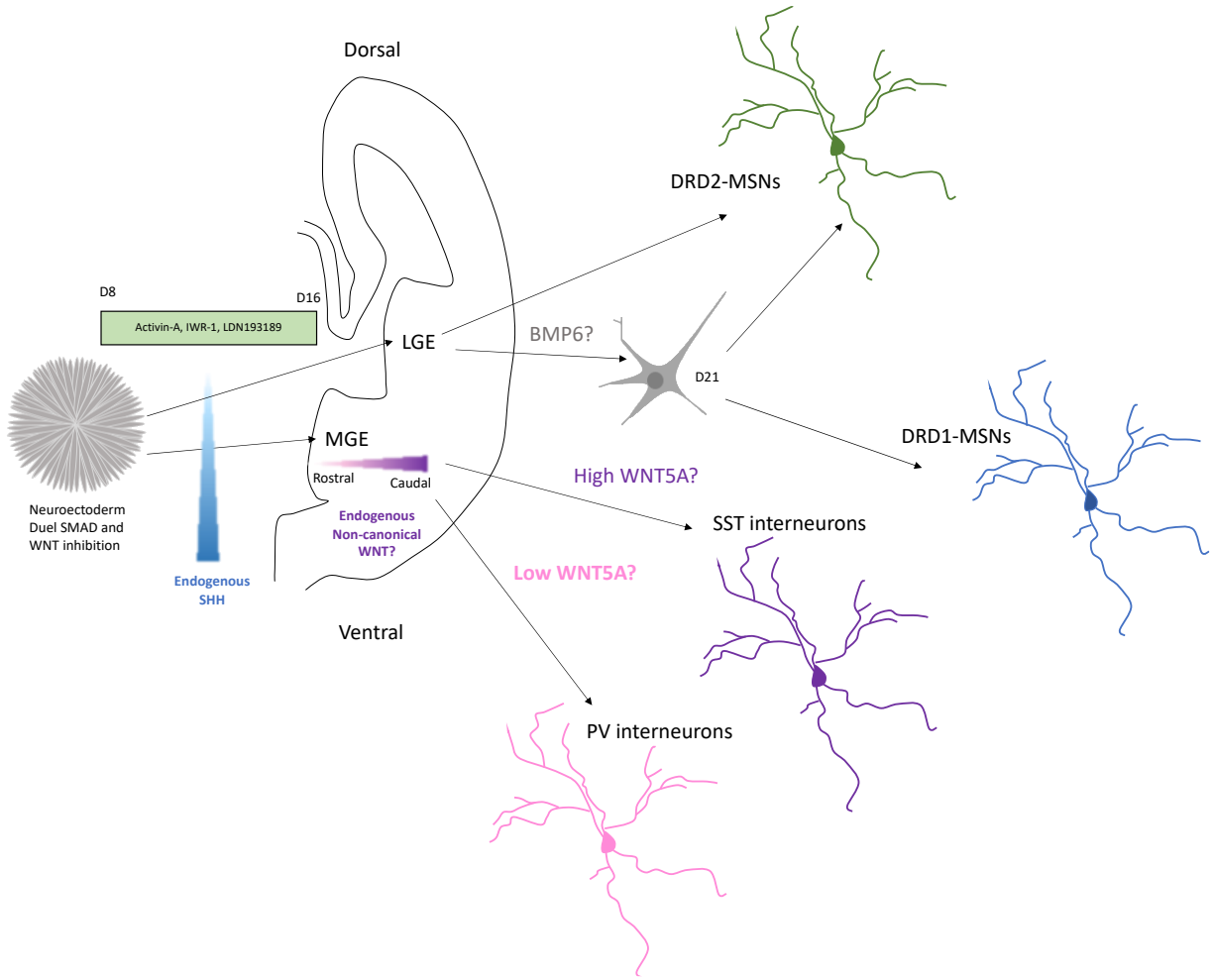

Introduction

Available protocols aimed at differentiating iPSCs to the MSN fate to study the mechanisms underlying Huntington's disease have yielded varying populations of the desired cell populations. Data presented in Chapter 3 showed that a major source of variation between cell lines could be accounted for by varying degrees of endogenous HH signal activation.

Similar variation in endogenous HH signalling during differentiation has been observed in human and mouse embryonic stem cells (ESCs) and PSC lines generated to look at cortical pyramidal projection neurons. Low density mESC cultures devoid of exogenous dorsalising or ventralising signals during neural induction has resulted in anterior neuroectoderm cells expressing predominantly ventral markers GSH2 (~10%), NKX2.1 (~25%), and NKX2.2 (~30%) following 14 days of differentiation. The source of this ventralising effect was found to be endogenous SHH expression which was apparent 4 days following differentiation (Gaspard et al., 2008). Furthermore, inhibition of HH signalling with Cyclopamine (1µM) resulted in minimal ventral expression as evident from ~20% $NKX2.1^{+}$ cells, and a largely homogenous population (~70%) of dorsal $vGlut1^{+}$ cells, of which ~80% displayed pyramidal morphology index (PMI) illustrating functional excitatory pyramidal neuron specification (Gaspard et al., 2008).

However, the requirement of Cyclopamine for cortical differentiation is controversial with others reporting that in the absence of added morphogens but prolonged inhibition of BMP signalling using Noggin (100ng/ml) human ESC and iPSC efficiently convert to a cortical identity without the need of Cyclopamine (Espuny-Camacho et al 2013). This would suggest that while the 'default' differentiation of mESC is a ventral fate resulting from endogenous HH signalling and human 'default' is a dorsal fate, probably owing to high WNT signalling. However, the same year Vazin et al., (2013) supported the use of cyclopamine in human ECS and iPSCs utilising both monolayer and embryoid body cultures. Here, cyclopamine treatment during neural induction resulted in an upregulation of the dorsal marker, EMX1 and consequent downregulation of the ventral marker DLX2 and following terminal differentiation >70% were glutamatergic. (Vazin et al 2013).Rather than a species-specific

default program during differentiation it appears that cell line variations in endogenously expressed signalling morphogens bias fate determination.

As Cyclopamine has been shown to limit NKX2.1 expression, in this chapter we employed to endo-IWR-1 and LDN193189 (LI medium) to limit dorsal phenotype, LI + Activin-A to promote LGE-specification (LIA medium) and LIA+Cyclopamine (LIAC medium) to inhibit variable endogenous HH activity and thus remove potential bias to generate MGE at the expense of LGE. To further investigate whether SHH expression is the main source of variation and to examine in more detail the responses of cultures to LI, LIA and LIAC media we used RNA seq to analyse the transcriptomes in 'patterned' D16 NPCs from the 3 independent control cell lines 18n6, Kolf2 and 33n1. We find that most variation occurs along spatial gene expression axes known from in vivo brain development with a clear cell line dependent bias. Regional drift from LGE to MGE occurs mainly due to endogenous SHH and is largely corrected for using Cyclopamine. Additional bias during patterning may also be influenced by endogenous FGF and non-canonical WNT signalling.

Results and Discussion

Cyclopamine inhibits HH signalling and downstream targets at a lower dose than the literature

Previous studies, primarily cortical differentiation, using Cyclopamine (1μM) has resulted in a significant downregulation of downstream HH signalling transcripts including NKX2.1 (Gaspard *et al*., 2008; Vazin *et al.,* 2013). To investigate if this is true in our differentiation protocol, we added Cyclopamine at 0.5μM or 1μM and assessed gene expression changes with a panel of 89 genes by microfluidic QRT-PCR. Both 1μM and 0.5μM sufficiently downregulated genes downstream of HH signalling including GLI1, NKX2.1 and LHX6 (Figure 4.1A). LGE-enriched transcripts SP8, TAC1 and FOXP2 were upregulated at the lower concentration of 0.5μM as well as GABAergic genes NPY and CALB2 whereas at 1μM, TAC1 and NPY were upregulated, as well as EBF1 (Figure 4.1A). In addition to its role in patterning SHH can exert a proliferative effect on NPCs (Ruiz, Palma & Dahmane, 2002; Wechsler-Reya & Scott, 1999; Britto, Tannahill & Keynes, 2002). Accordingly, at both concentrations of Cyclopamine there was an observed decrease in the proliferation of NPCs within the 33n1 cell line compared to LIA alone (data not shown). However, at 0.5μM the number of cells at the NPC stage was not significantly different from that obtained from 18n6 and Kolf2 cell lines. To assess whether Cyclopamine at was sufficient to abolish NKX2.1 expression at a protein level, western blot analysis was carried out and compared to protein derived from the LI and LIA protocols (Figure 4.1B). Under the LI protocol NKX2.1 is expressed, with the addition of Activin-A this significantly increased, whereas addition of 0.5μM Cyclopamine was sufficient to abolished NKX2.1 protein expression (Figure 4.1C). As a result, this concentration of 0.5μM Cyclopamine was used for further analysis.

To assess whether the effects of Cyclopamine were specific to the 33n1 cell line and no other effects in the 18n6 and Kolf2 cell line, 3 genes expressed in the pan-GE were assessed via qRT-PCR in all lines comparing LIAC to LIA. Following an 8-day exposure of LIAC medium, there was a significant upregulation of the pan-GE transcription factors GSX2 (1-fold; Figure 2A) and CTIP2 (>1-fold; Figure 4.2C) with no significant increase in DLX2 expression (Figure 4.2B) in the 33n1 cell line compared to LIA. No significant difference was observed in the

18n6 and Kolf2 cell lines (Figure 4.2A-C). To further demonstrate the shift from an MGE- to a more LGE- cell fate, we preformed immunostaining for CTIP2 in the 33n1 cell line (Figure 4.2D). Under the LIA protocol ~54% ±8% $CTIP2^+$ cells were present whereas with the addition of Cyclopamine this increased to ~77% ±5%, which resulted in reduced variability between all 3 cell lines (70-80%). Overall, all three cell lines showed similar patterns of increasing expression of LGE-selective transcripts whilst significantly downregulating or switching off the MGE specific transcription factor, NKX2.1.

Although LIA and LIAC increases the proportion of LGE/striatal transcription factors while downregulating MGE-specific transcripts, more dorsal markers were omitted. This was due to the presence of LDN193189 and IWR1 which inhibit canonical BMP and WNT signalling pathways, respectively limiting a more dorsal phenotype. However, other patterning factors secreted within differentiating cultures such as fibroblast growth factors (FGFs), retinoids and NOTCH and non-canonical activation of the WNT pathways can influence the fate of these cells. Therefore, we carried out bulk RNA sequencing to examine further variation between the cell lines and treatments on a larger set of genes and performed pathway analyses to reveal potential regulatory genes associated with pallial and subpallial development.

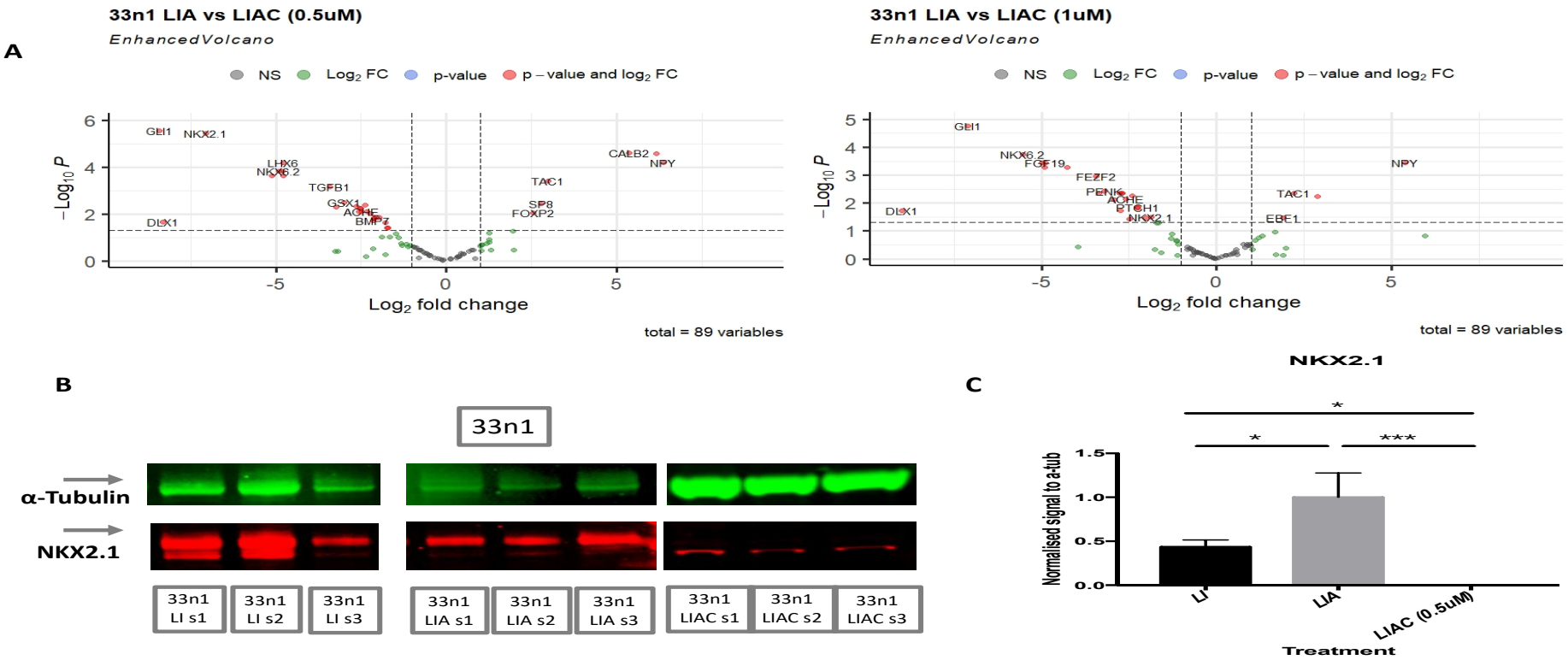

*Figure 4.1. Fluidigm BioMark qPCR analysis of a panel of 89 genes of interested known to be differentially expressed during Dorso-ventral patterning of the telencephalon and enriched in the MGE and LGE/Striatum. A) Two doses of Cyclopamine-KAAD (0.5μM and 1μM) where used based on the literature to inhibit HH signalling at the level of SMO. Both doses significantly downregulated gene downstream of HH signalling while increasing some Striatal and GABAergic genes. B) western blot image of NKX2.1 shows under LI and LIA protocol the protein is being translated whereas the addition of Cyclopamine-KAAD no protein product is expressed. C) Western blot analysis relative to α-tubulin shows highest NKX2.1 protein expression is seen in the LIA protocol with significantly less under LI treatment and no product under LIAC ($F(2,6)=27.46$, $p=0.001$). Data represents the mean of tree biological and 3 technical repeats. Volcanoplots were generated using R and Fold change and p-adjust (BH) values are presented. Western blot analysis are presented with SD and ordinary one-way ANOVA with Tukeys multiple comparisons test., * p<0.05, ** p<0.01, *** p<0.001, **** p<0.0001*

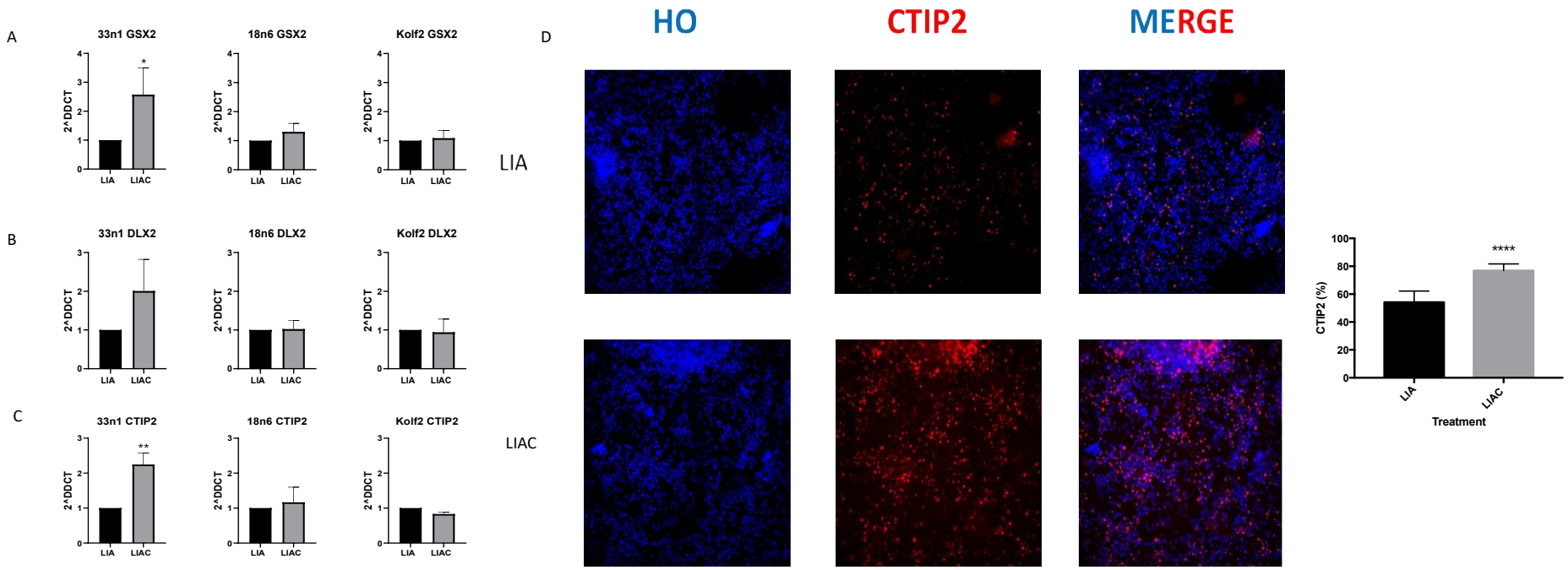

*Figure 4.2. LIAC protocol applied to 3 independent cell lines. A-C) Pan-GE transcription factor GSX2 and LGE-enrich gene CTIP2 are significantly upregulated under LIAC protocol in the 33n1 cell line with and increase DLX2, albeit not significant. No difference is observed in LIAC protocol compared to LIA in 18n6 and Kolf2 cell lines. D) Exemplar ICC image of 33n1 cell line under LIA and LIAC, right: Percentage of CTIP2 shows ~50% positive cells under LIA protocol and > 30% increase under LIAC protocol ($t(52)=12.59$, $p<0.0001$). qPCR data shown are the average of 3 independent differentiations in triplicate in 3 cell lines 18n6, Kolf2 and 33n1. * $P \leq 0.05$, ** $P \leq 0.01$, ***$P \leq 0.005$, ****$P \leq 0.001$, one-way ANOVA followed by Tukey's post-hoc test.*

Efficient differentiation to neural progenitor fates with variation in developmental stage

Following transformation of count data (Variance stabilising transformation, VST) the main variability within the experiment was explored. To determine the optimal mode and number of clusters, parameter estimations via expectation-maximisation algorithm and the Bayesian information criterion (BIC) combined model-based hierarchical clustering was implemented. Samples separated into two clusters with cell lines 18n6 and Kolf2 under LIA and LIAC treatment within cluster 1 and all LI treatment groups as well as LIA and LIAC treatment in the 33n1 cell line in cluster 2 (Figure 4.3A-B). Correct and efficient differentiation of iPSC lines to a neural progenitor fate was achieved within all cell lines and treatment with the key pluripotent genes involved in, cell maintenance, transcription, signalling, and epigenetics showing no counts illustrating that differences in early germ layer specification is not a contributor to variation at this stage (Appendix 1).

A direct comparison of LI verses LIA treatments between cell lines confirmed the robust induction of LGE/striatal enriched markers such as the DLX family members DLX-1, -5 and -6, Meis2, CTIP2, ASCL1/MASH1, SP8, SP9 and GAD1 (Figure 4.3C). In addition, within the 18n6 and Kolf2 lines, Activin-A caused a down-regulation of MGE/interneuron transcripts including NKX2.1, NKX2.2, NKX6.2 and OLIG2 (Figure 4.3C) while these transcripts were only down-regulated with the addition of Cyclopamine in the 33n1 cell line (Figure 4.3D). No. differential gene expression was observed when comparing LIA verse LIAC treatments with the 18n6 and Kolf2 cell lines further supporting the hypothesis that HH signalling is not influencing these NPCs at this stage of differentiation and that Cyclopamine appears to have no other off-target effects that influence cell differentiation.

Comparing individual cell line responses to different treatments revealed 1,762 (LI vs LIA treatment) and 2,635 (LI vs LIAC treatment) differentially expressed genes (DEGs) in common. Gene ontology (GO) analysis on genes with significance (FDR<0.05, log2FC= <-1,>1) showed strong enrichment for the biological process neurogenesis (GO:0022008, 884 DEGs) with the addition of Activin-A (LIA, adjusted-p=1.190 x 10^{-26}) and Cyclopamine (LIAC, adjusted-p=1.588 x 10^{-26}) compared to LI treatment alone. High gene counts were observed for the SOXB1 (SOX1, SOX2, SOX3) and SOXC class (SOX4 and SOX11) gene families which have important sequential roles in regulating NPC maintenance and neuronal differentiation

(Guth & Wegner 2008; Bylund *et al.,* 2003; Graham *et al.,* 2003; Favaro *et al.,* 2009; Bergsland *et al.,* 2006; Hoser *et al.,* 2008), in part, through the SHH and NOTCH pathways (Favaro *et al.,* 2009; Bergsland *et al.,* 2011). All SOXB1 proteins are expressed in NPC's of the developing telencephalon acting redundantly as pioneering factors to maintain neural cells in a progenitor state and prevent differentiation into neurons. Under LI condition, higher expression of SOXB1 genes were expressed with lower expression of immature neuronal markers MAP2 and GAP43. Transcription factors with later roles in neurogenesis (SOX4, SOX11, MAP2, DCX, and GAP43) showed highest expression under LIA and LIAC treatment with variations within each cell line. In addition to their role in neurogenesis, SOX genes bind transcription factors implicated in cell type specification and therefore variation here could also be due to specification.

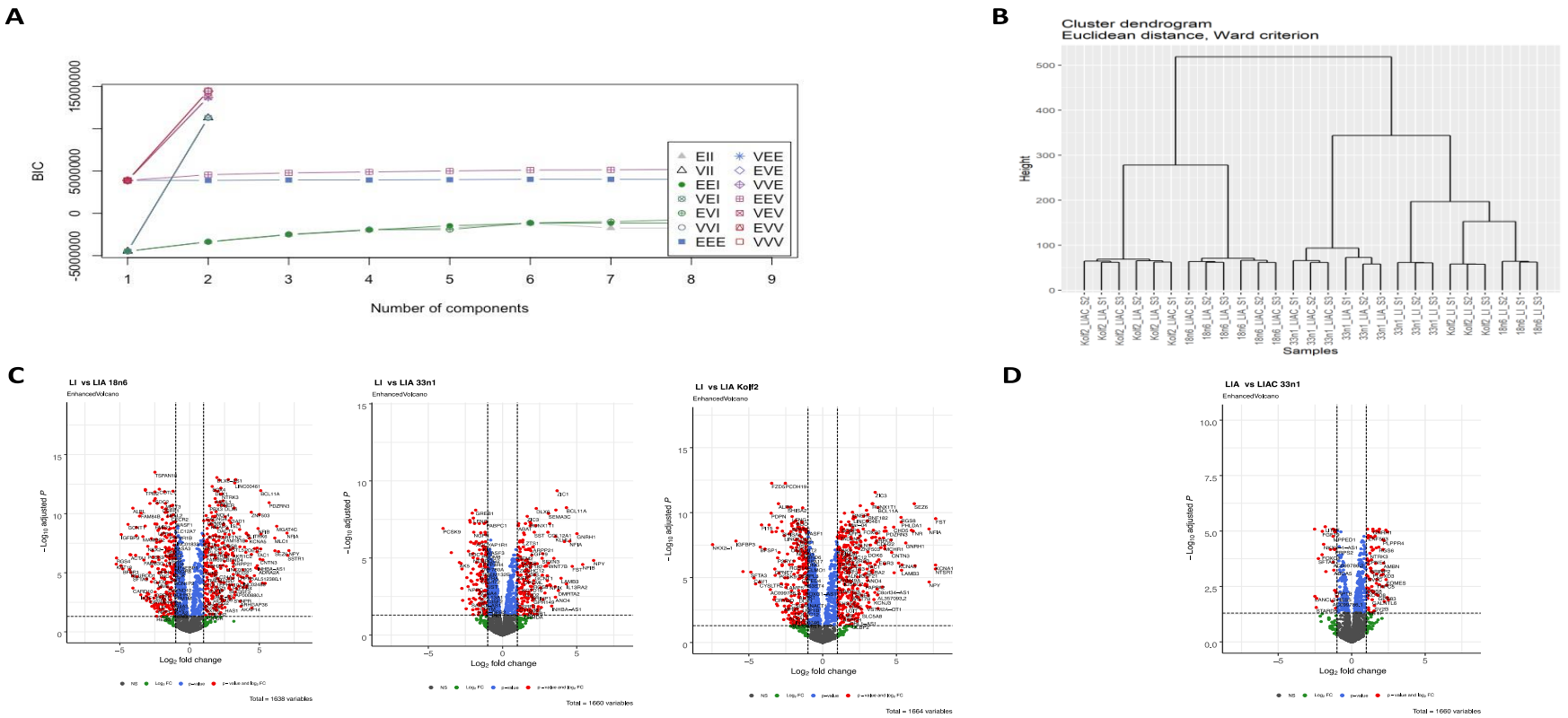

Figure 4.3: RNA Sequencing form D16 neural progenitor cells under LI, LIA and LIAC protocols in 33n1, 18n6 and Kolf2 cell lines. A) Bayesian information criterion (BIC) for all considered Gaussian mixture models with one to nine components. The highest BIC value is achieved by the VVE model with 2 components. B) Hierarchical clustering dendrogram obtained by Ward's algorithm and Euclidean distance criterion shows 2 major groupings 1) all cell lines under LI treatment with LIA and LIAC in the 33n1 cell line 2) LIA and LIAC treatment in the Kolf2 and 18n6 cell line. C) VolcanoPlots of differentially expressed genes (DEGs) up and downregulated under LIA protocol compared to LI in all cell lines. D) DEG up and downregulated in the 33n1 cell line under LIAC protocol compared to LIA.

Dorsal-Ventral signalling pathways are major contributors to patterning during the first trimester of foetal development within the telencephalon

In order to gain a better understanding of what transcriptional genes and pathways are involved in specification within the telencephalon and which cell line/treatment best resembles that of an LGE/striatal phenotype, RNA Sequencing data from early foetal (PCW 8-13) was accessed via ebi.ac.uk/biostudies (accession: E-MTAB-1918). Cortical (CTX), lateral- and medial- ganglionic eminence (LGE and MGE, respectively) were analysed and compared to our datasets.

After transformation of count data (VST) the main variation within this dataset was due to source (i.e foetal vs cell culture) this was visualised using principal component analysis (PCA). Here, samples separated into foetal and cell culture conditions (PC1) capturing >53% of the variance (Figure 4.4A). Minimal variation was captured between cell lines and treatment (PC2, 14.52%) or brain region (PC3, 9.83%) (Figure 4.4B). This is probably owing to the presence of multiple cell types within foetal tissue, such as glia. To compensate for source effect, design matrices comparing different brain regions (i.e LGE verse MGE and LGE verse CTX) were generated to produce specific gene sets and signalling pathways influencing neural progenitor cells arising from these areas. A total of 2467 DEGs were expressed between the LGE and MGE, of which 326 and 442 were upregulated in those regions, respectively (Figure 4.4C, Log2FC= -1,1, p-adjusted = 0.001). Comparing the LGE and CTX, 4352 DEGs were expressed and of these 1380 were upregulated within the CTX (Figure 4.4D, Log2FC= -1,1, p-adjusted = 0.001). It should be noted that when comparing the LGE and MGE samples, genes such as TBR1, NeuroD6 and PAX6 showed enrichment for the LGE. However, these genes are not uniquely expressed in this region and are expressed at higher levels within the CTX. An explanation for this is incomplete removal of lateral cortical tissue with regards to Tbr1 and NeuroD6 genes. Alternatively, with respect to Pax6 may reflect expression spanning the PSB and thus resulting in enrichment in the LGE verses the MGE. Therefore, DEGs that showed strong enrichment within the CTX (apart from DARPP-32) were excluded from further analysis. As interpreting genes individually is not practical, over-representation and gene set enrichment (gse) analysis for KEGG pathways using clusterProfiler package in R was employed. Currently there is no technology which can decide which functional pathways are enriched over the bias present in the samples. As a

result, the top pathways for each brain region were selected based on p-adjusted value and also for being known to the literature, whilst those that were deemed to arise from sample source bias were excluded. For example, using gseKEGG which ranks genes based on log2 fold change, gene set enrichment was found for KEGG pathway Allograft rejection (hsa05330, p-adj= 5.85×10^{-5}), which shares many similar immunopathological mechanisms with recurrent abortions (Reviewed in Wilczynski, 2006) and many of these genes are not known to the literature to be differentially expressed between the LGE and MGE. Over-representation analysis (enrichKEGG) also has its drawbacks with only requiring gene names therefore those of significance (p-adjust <0.001) were assessed and consequently corrected for some bias. As a result, top KEGG pathways used for subsequent analysis included cAMP and Dopamine (LGE), WNT (negative regulation) and HH (MGE) (Figure 4.4E). While enrichment was found for WNT and Glutamate signalling within the CTX, our samples showed bias for a GABAergic cell fate and both BMP and canonical WNT signalling is inhibited in our culture, we therefore focused our analysis on subpallial development.

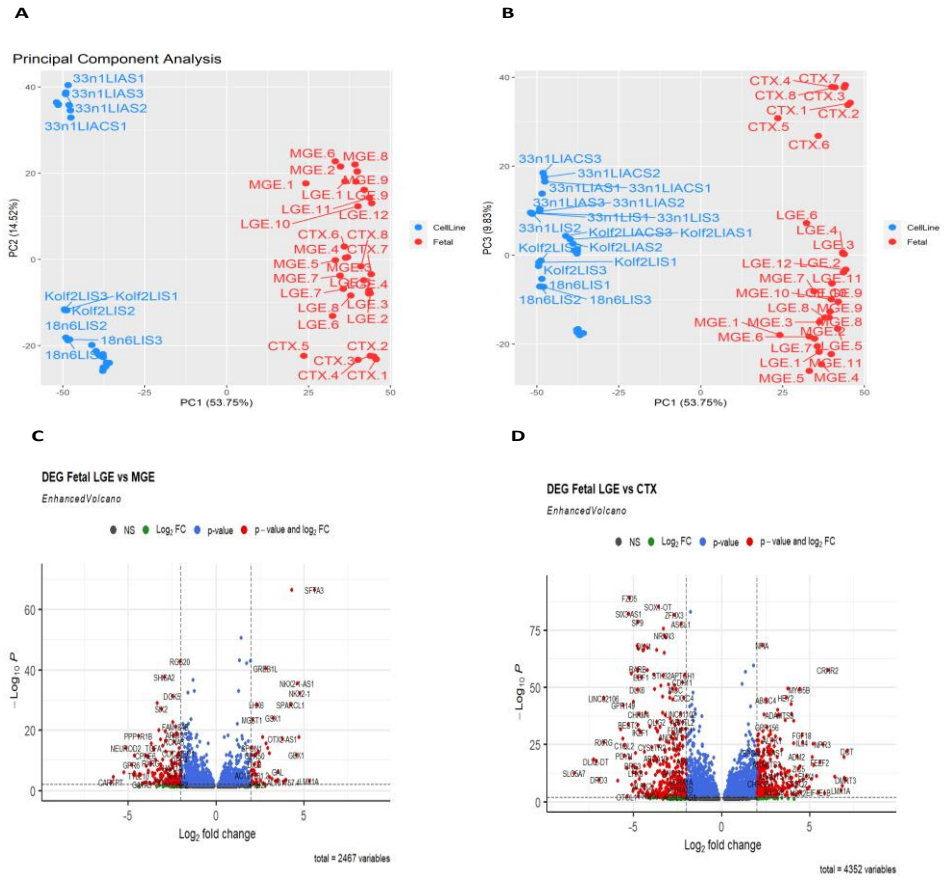

E

ID	Description	GeneRatio	BgRatio	pvalue	p.adjust	qvalue	Sample enrichment
hsa04728	Dopaminergic synapse	38/841	132/8102	2.540 E-09	2.019e-07	1.517e-07	LGE
hsa04024	cAMP signaling pathway	50/841	219/8102	4.53 E-08	1.440E-06	0.000001	LGE
hsa04310	Wnt signaling pathway	42/841	166/8102	2.52 E-08	1.003E-06	7.54E-07	MGE
hsa04340	Hedgehog signaling pathway	13/841	56/8102	0.004	0.023	0.0175	MGE
hsa04310	Wnt signaling pathway	51/1490	166/8102	0.00007	0.001	0.00079	CTX
hsa04724	Glutamatergic synapse	38/1490	114/8102	0.00008	0.001	0.00086	CTX

Figure 4.4. Human Foetal RNA Sequencing data obtained from publicly available datasets (E-MTAB-1918). A) Principal Component Analyses (PCA) with percentage of variance associated with each axis shows >50% of the variation is due to donor bias (i.e. Foetal vs cell culture). C + D) DEGs up and downregulated in the MGE (C) or CTX (D) compared to the LGE. E) Top KEGG pathways selected for further analysis based upon enrichment and the literature.

Differences in Dopaminergic receptor expression influences differential signalling through cAMP.

The neostriatum receives dopaminergic innervation from mesencephalic dopaminergic neurons where dopamine is released and modulates cAMP via activation of DRD1 and DRD2-expressing MSNs. During development altered dopamine signalling within the LGE are attributed to the changes in neural progenitor proliferation, where D1-like receptor (DRD1 and DRD5) activation promotes cell cycle exit and maturation by activating adenylyl cyclase and increasing intracellular cAMP and D2-like receptor (DRD2, DRD3, DRD4) activation promotes G_1- to S-phase entry (Ohtani *et al.,* 2003; Popolo *et al.,* 2004). As DRD1 MSNs promote intracellular cAMP levels whereas DRD2-MSNs activate $G\alpha_{i/o}$ to reduce cAMP levels.

Overrepresentation and GSE analysis on gene sets differentially expressed between the LGE and MGE showed strong enrichment for Dopaminergic synapse (hsa04728, p-adjusted= 2.019×10^{-7}, Figure 4.5A) and cAMP (hsa04024, p-adjusted= 1.44×10^{-6}, Figure 4.6A). Out of these, 16 Dopaminergic signalling genes were significantly different (log2 fold change 1,-1, p-adjusted= 0.001) and were subsequently used for further analysis.

To visualised how cell lines and/or treatment differ with these gene sets from the LGE, a heatmap was generated of normalised log2 counts. Dopaminergic genes showed similar levels of expression with the majority of cell lines and treatments grouping within cluster 2 with two cell lines under LI treatment (18n6 and Kolf2) generating another cluster (cluster 1). Both these clusters grouped away from the LGE indicating dopamine signalling here is not similar to that of the LGE (Figure 4.5B). DEG analysis confirmed this with cell lines and treatment showing significantly more DRD2 expression, with the exception of the 33n1 cell line, compared to the LGE. Furthermore, both DRD1 and DRD3 expression are significantly downregulated in all lines and treatments whereas there was no difference in DRD5 expression (Figure 4.5C). Here, the addition of Activin-A and/or Cyclopamine does not appear to influence dopamine receptor expression. However, with the addition of Activin-A a significant increase in Tyrosine Hydroxylase (TH), the rate limiting enzyme of dopaminergic and noradrenergic neurons, was observed in all cell lines compared to the LGE. In primary forebrain cultures, addition of Activin-A in concert with FGF2 has been reported to increase

both the mRNA and protein levels of TH (Daadi, and Weiss 1999; Bao etal., 2004), while Activin-A and FGF2 alone had no or minimal effect, respectively. This is particularly relevant here as FGF2 mRNA transcripts are expressed in all cell lines and could indicate a population of cells may be destined to become Dopaminergic. Furthermore, the gene responsible for producing the enzyme Dopamine β-hydroylase (DBH) and controls norepinephrine synthesis was expressed at lower levels than that seen in the LGE (<30 normalised counts) under LIA treatment in all lines and therefore a noradrenergic fate is unlikely. In the 33n1 cell line under LI treatment DBH was enriched and thus a population of cells may be destined to a noradrenergic fate.

There also appeared to be no apparent cell line or treatment bias with regards to cAMP signalling with all LI treatments including 18n6 following LIA and LIAC protocols clustering together (Cluster 1) and 33n1 and Kolf2 under LIA and LIAC clustering together (Cluster 2), both of which grouped away from the LGE (cluster 3) (Figure 4.6B). DEG analysis showed the majority of genes downstream of cAMP signalling were expressed at higher or equivalent levels in cell lines compared to the LGE, such as PPP1R1B (AKA DARPP-32), GLI3, ATP2B2, PTCH1, GRINA4 and ATP1A1 (Figure 4.6C). It should be noted that PPP1R1B gene is enriched in the CTX compared to the LGE with 2,819 normalised counts compared to 255 normalised counts, respectively. This is consistent with the literature at this developmental period (Straccia *et al.,* 2015). D1-like receptors stimulate adenylyl cyclase which is responsible for catalysing ATP to cAMP and thus regulation of this pathway. However, DRD1 is not expressed in cell culture neural progenitors (<2 normalised counts) under all conditions possibly due to their immature state, or additional patterning factors present in all cultures biasing cells towards a DRD-2 expressing MSN fate as opposed to a DRD1-MSN fate. There are multiple means of regulation of the cAMP pathway via G-protein-coupled signal activation including hormones such as noradrenaline and VIP, or modification via calcium signalling, these are likely contributors to the differential expression seen in cell culture.

In conclusion, both dopaminergic synapse and cAMP signalling genes are differentially expressed within cell line and treatments compared to the LGE. Differential expression here is not likely to be a major contributor to the variation seen with respect to MSN population generated under LIA protocol as no bias was seen towards either cell line or treatment. It is

interesting to note that DRD2 mRNA transcripts predominate within the cell cultures, whether this is an indication of the subpopulation of MSNs generated using these differentiation protocols will need to be investigated in post-mitotic neurons.

TH mRNA transcripts with the addition of Activin-A and the presence of endogenous FGF2 in all cell lines and treatment, suggests that a small population of these cells may differentiate into dopaminergic striatal and/or olfactory bulb interneurons, both of which are generated in the mouse dLGE and have been shown to be present in 'MSN'-differentiation protocols, many of which also express GABA (Comella-Bolla *et al.,* 2020; Cann *et al.,* 2021). TH immunoreactivity will need to be carried out as well as dopamine content estimate via HPLC.

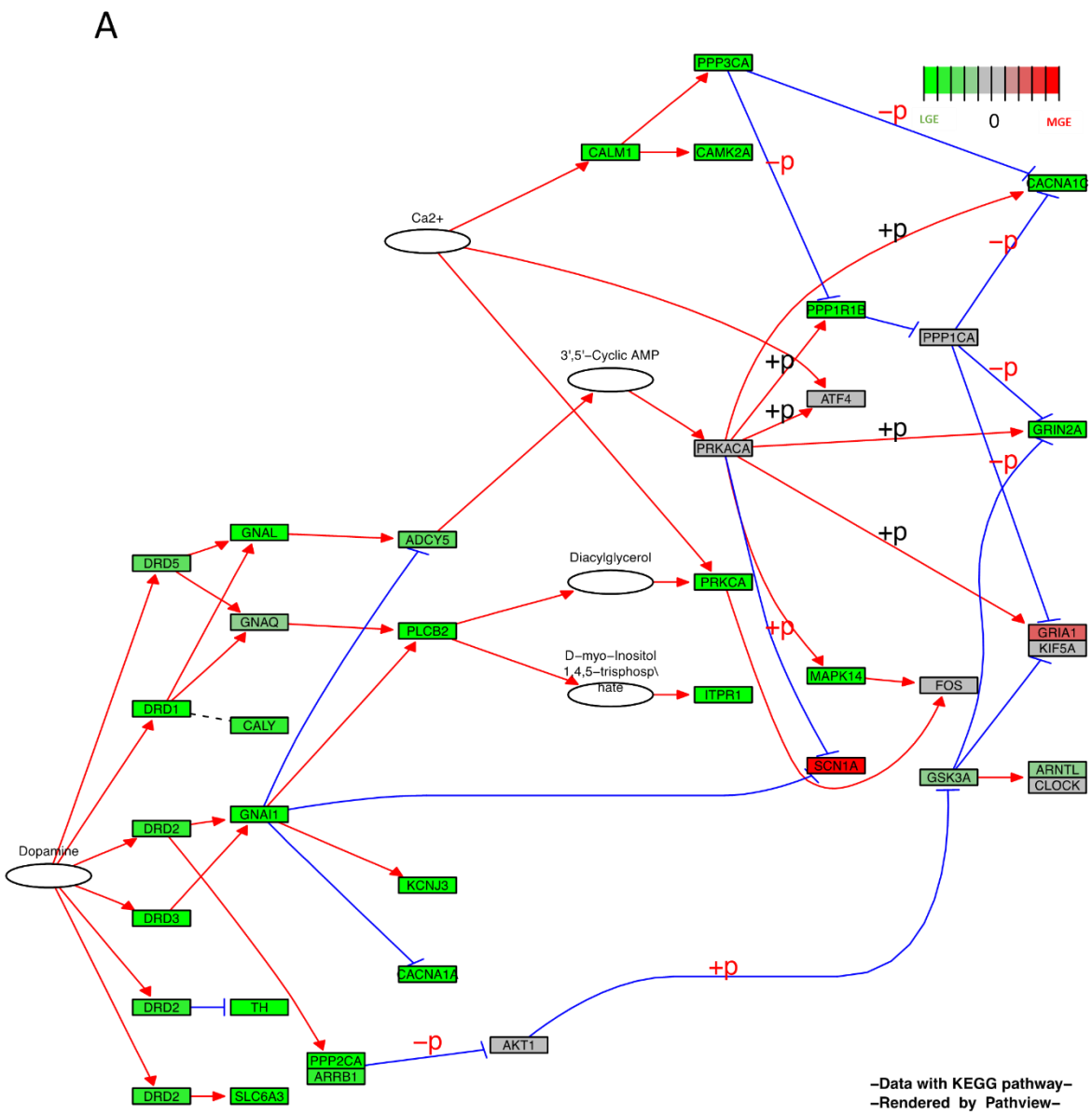

Figure 4.5. LGE gene set enrichment. A) Highlighted genes within the Dopaminergic Synapse pathway are enriched in the LGE (green) compared to the MGE (red).

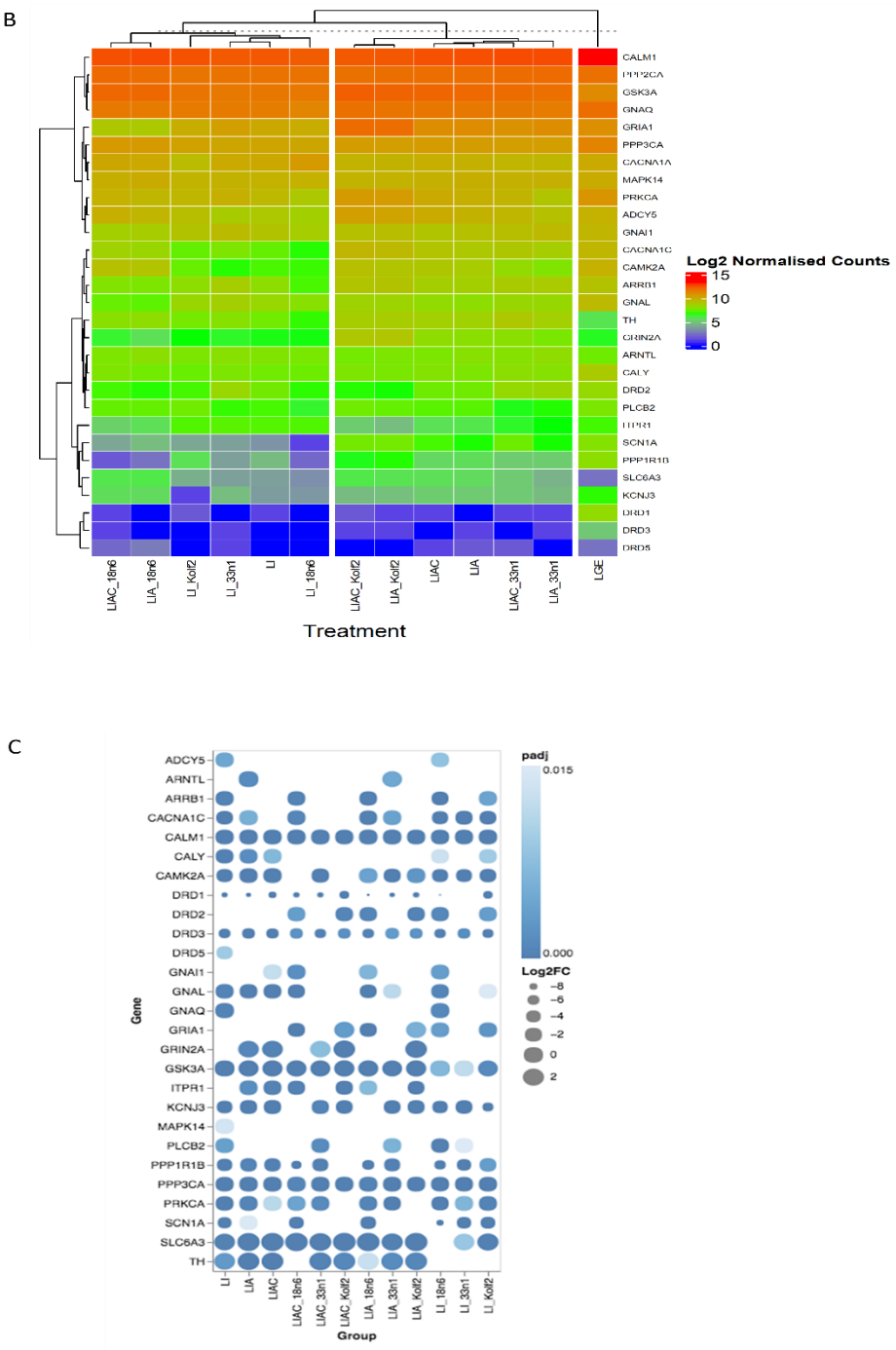

Figure 4.5. continued B) Heatmap of normalised Log2 normalised counts of DEGs within the Dopaminergic Synapse across all cell lines and treatment and average LGE expression. C) Dot plot showing Log2 Fold change (-1/1) and p-adjusted values (BH, <0.05) of all cell lines and treatment compared to average LGE samples.

A

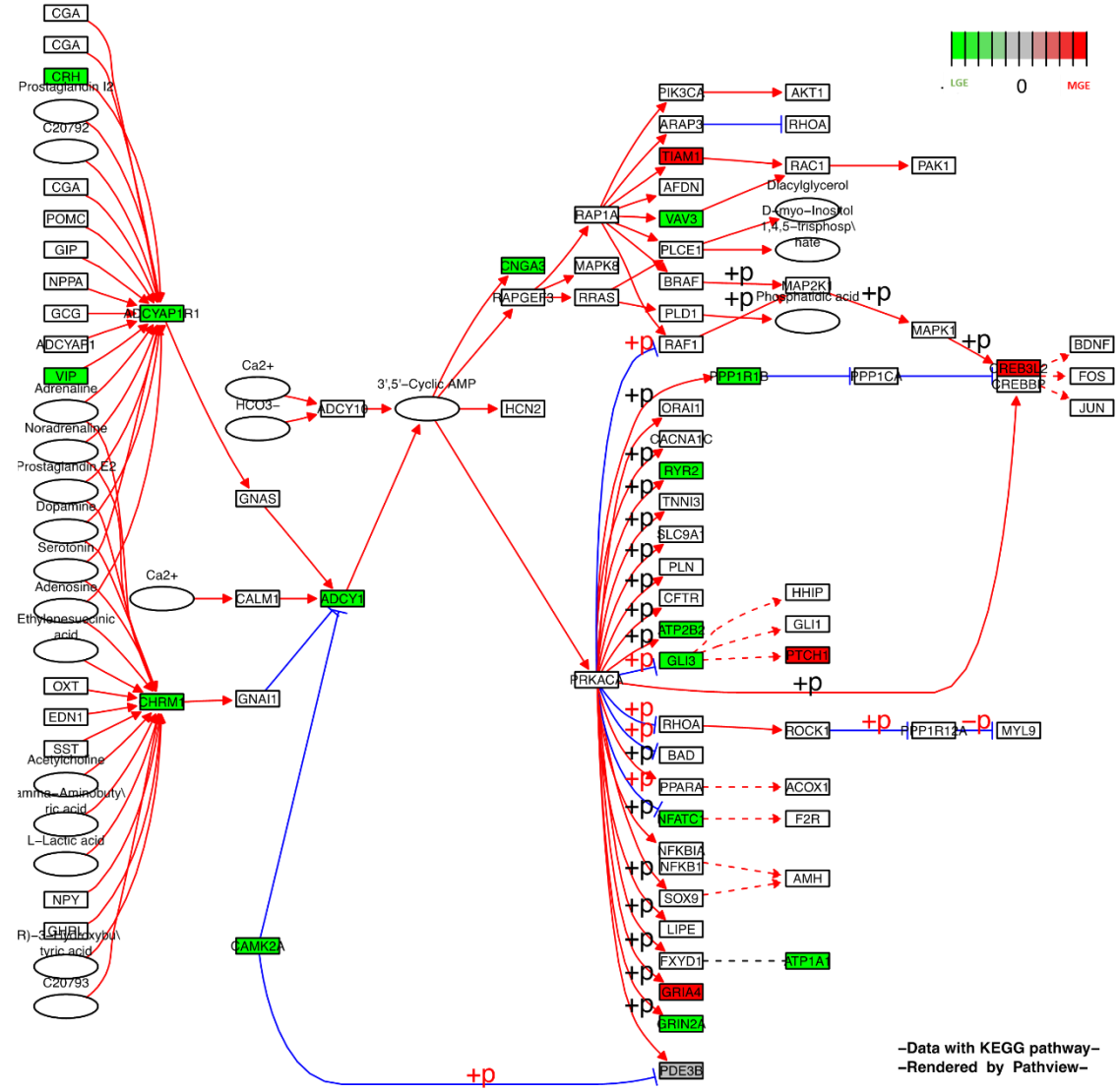

Figure 4.6. LGE gene set enrichment. A) Highlighted genes within the cAMP pathway are enriched in the LGE (green) compared to the MGE (red).

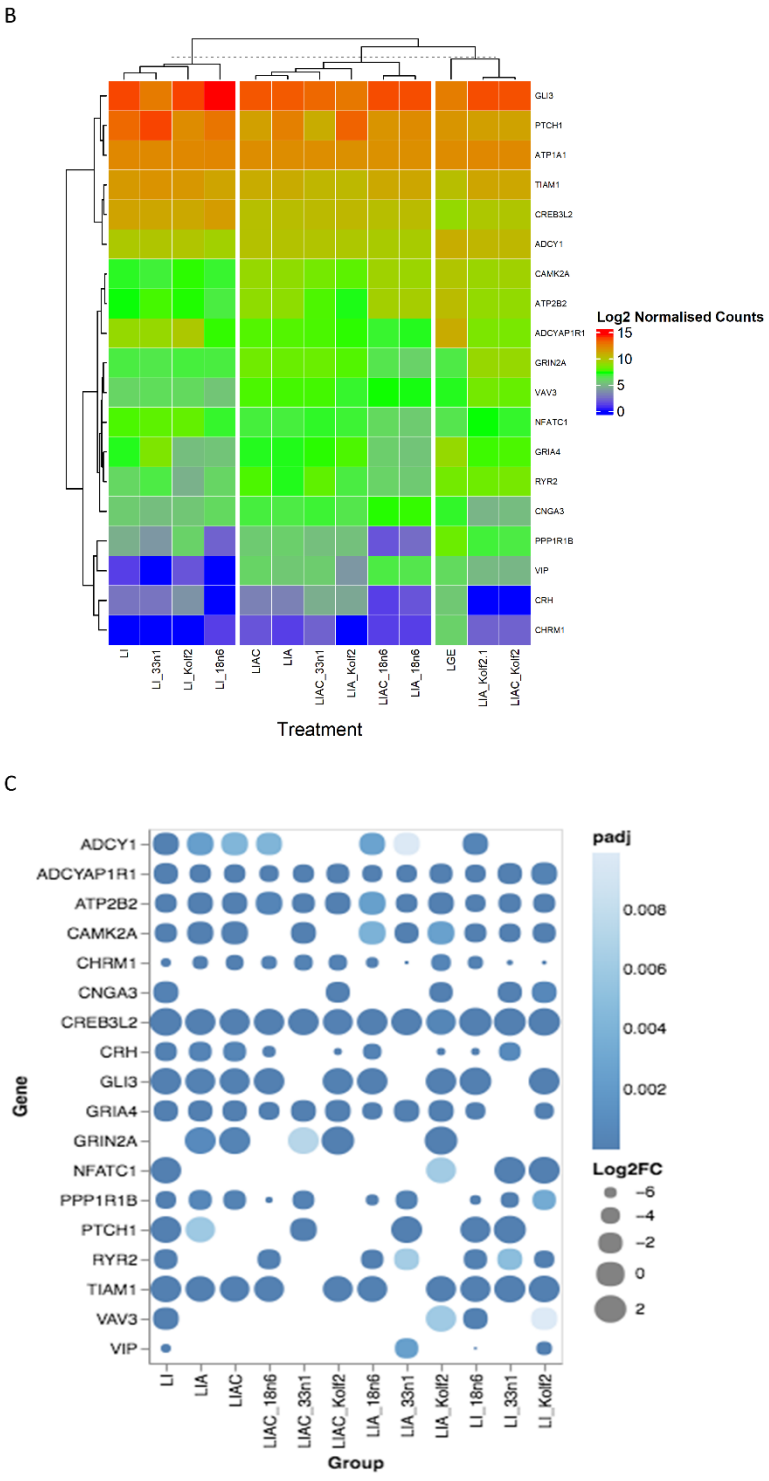

Figure 4.6. continued. B) Heatmap of normalised Log2 normalised counts of DEGs within the cAMP pathway across all cell lines and treatment and average LGE expression. C) Dot plot showing Log2 Fold change (-1/1) and p-adjusted values (BH, <0.05) of all cell lines and treatment compared to average LGE samples.

Differential signalling through HH is a major contributor to variation within cell lines and induces an MGE phenotype

In the MGE initial patterning is dependent on secreted morphogens FGF8 and SHH to induce the expression of NKX2.1. During the period of neurogenesis, continued SHH permits the continued expression of NKX2.1 and its downstream target, LHX6, in MGE progenitors, the latter two being required for the specification of SST and PV interneurons (Anderson et al., 2001; Xu et al., 2004; Xu et al., 2005; Butt et al., 2008; Du et al., 2008; Liodis et al., 2007). Although these two populations of interneurons originate from the same embryonic structure, there is a bias in the ontogeny of SST interneurons from the dorsal MGE (dMGE) whereas the ventral MGE (vMGE) is the major source of PV interneurons (Flames et al., 2007; Wonders et al., 2008; Hu et al., 2017). Expression domains of SHH mRNA are in the VZ of the POA and MZ of the MGE, however, bias of SST interneurons ontogeny has been shown to be due to enrichment of SHH signaling in the dMGE relative to the ventral as evident by higher expression of GLI1, Ptch1/2, HHIP1 and NKX6.2 transcripts (Xu et al.,2005; Chuang et al., 2003; Xu et al., 2010; Wonders et al., 2008; Yu et al., 2009). This suggests that other signaling morphogens diffusing into the MGE from adjacent regions may be influencing this. While most work has been on additional dorsal-ventral patterning cues such as that of FGF8 in ventral identity of MGE progenitors, recent work has implicated a rostral-caudal gradient of non-canonical WNT signaling (WNT/RTK). Here, WNTs emanating from dorso-caudal structures (likely the thalamus) promote SST interneuron development whereas more rostrally at lower concentrations, PV interneurons are mainly produced (McKenzie et al., 2019).

In our analysis of the foetal RNAseq data WNT signalling was shown to be negatively regulated within the MGE, which is consistent with development where highest enrichment is seen in the CTX (padj=0.001). Interestingly, WNT5A which signals via the non-canonical WNT pathway, showed highest expression in the MGE compared to the CTX (Log2 fold change = 0.7, padj=0.04) and LGE (Log2 fold change = 2, padj= 9.05×10^{-11}). Therefore, we chose to investigate this further with gene sets based on the literature as well as some canonical WNT signalling genes to confirm inhibition.

Indeed, both HH (hsa04340, p adjusted = 0.002, Figure 4.7A) and Wnt (hsa04310, p adjusted = 1.003 x 10^{-6}, Figure 4.8A) signalling pathways showed strong enrichment for the MGE compared to the LGE via over-representation and GSE analysis. In our cell cultures, highest log2 normalised counts of SHH and signalling transcripts PTCH1, PTCH2, HHIP, GLI1, NKX2.1 and NKX6.1 were seen in the 33n1 line under both LI and LIA protocols, which clustered with that of the expression of the foetal MGE (Cluster 3). While the 33n1 cell line under the LIAC protocol does not cluster with 18n6 and Kolf2 under LIA or LIAC protocols (Cluster 1), this is likely due to high mRNA transcripts for SHH, NKX2.1, Lhx6 and LHx8 that are still present (Cluster 2) (Figure 4.7B). Western blot analysis confirmed the protein expression of SHH (although apparent differences in SHH isoforms or post-translational modifications were observed, SHH 16KDa $F(2,6)=896.2$, $p<0.0001$, 20KDa $F(2,6)=4.705$, $p=0.0590$). However, NKX2.1 protein expression was absence following the addition of Cyclopamine in all cell lines, therefore it is unlikely that SHH signalling alone is biasing cell differentiation using this protocol (Figure 4.9). Differential expression analysis revealed that the majority of SHH signalling genes were at significantly lower levels than that of the MGE, with the exception of 33n1 under LI or LIA protocol (Figure 4.7C). Interestingly, under the LIAC protocol, within the 33n1 cell line, SST mRNA expression remained at a similar level to that found in the MGE. Within the developing mouse ventral telencephalon four distinct territories are present, the striatum, pallidum, the preoptic area (POA) and anterior entopeduncular area (AEP or diagonal area). The latter has been shown to generate a small population of $SST^+/Lhx6^+$ cells that migrate tangentially to the developing amygdala ($SST^+/Lhx6^-$) in NKx2.1 null embryo's (Asgarian et al., 2019). While it cannot be concluded if these populations of cells normally develop or weather an abnormal population of cells have developed in mutant embryos, this could point to a population of cells present within our cell cultures.

As genes for WNT signalling were also enriched within the MGE relative to the LGE and non-canonical WNT signalling has been shown to bias $NKX2.1^+$ cells towards an SST interneuron fate, we assessed non-canonical WNT signalling as well as signalling ligands known to activate canonical WNT. Here some bias was seen with cell lines and treatment with all cell lines under the LI protocol, in addition to 18n6 LIA and LIAC cultures showing similar log2 normalised counts (Cluster 1), whereas Kolf2 under LIA and LIAC protocol grouped together

(Cluster 3). Furthermore, both LIA and LIAC protocols within the 33n1 cell line clustered with that of the MGE (Cluster2) (Figure 4.8B).

The main differences seen within these clusters appear to be in the expression of signalling ligands, WNT7a, WNT7b and WNT3A, all of which activate the canonical WNT signalling pathway. All protocols used here employed the use of endo-IWR-1 which inhibits Tankyrase activity and therefore the canonical WNT pathway downstream of Lrp6 and Dvl2, therefore differences here can be attributed to endogenous WNT ligand expression. Furthermore, genes downstream of WNT signalling such as ATOH1, FGF20 and CD44 showed no to low expression, whereas high counts were seen for negative regulators of the WNT pathway, such as AXIN2 and ZNRF3 suggesting efficient inhibition of the canonical WNT pathway. Differential expression compared to the MGE showed that receptor expression of ROR1/ROR2/RYK were all upregulated in all cell lines and treatments whereas the majority of canonical WNT ligands were similar or significantly down-regulated (Figure 4.8C). While under LIA and LIAC protocols both 18n6 and Kolf2 cell lines showed significantly less expression of the non-canonical WNT ligand WNT5A, the expression within the 33n1 cell line did not differ between protocols or compared to the MGE.

High expression of the Ryk receptor is found in the VZ of the developing MGE and LGE where it is expressed in both proliferating neural progenitor cells and post-mitotic neurons where it is required for proper GABAergic neuronal differentiation and regulates oligodendrocyte and neuronal cell fate by regulating the expression of DLX2 and OLIG2 genes (Zhang et al., 2011). Activation of Ryk receptors in this context has been shown to be mediated by WNT3A β-catenin-independent signalling. Interestingly, in Ryk null mouse embryos there was an observed decrease in Lhx6, a transcription factor required for the normal migration of cortical interneurons (Liodis et al., 2007; Alifragis et al., 2004; Yuan et al 2020; Neves et al., 2013). While WNT5A was not investigated here, it is plausible to suggest a common mechanism for this non-canonical WNT ligand. In fact, in the differentiating anlage of the olfactory bulb where DLX2/5 are expressed, its transcriptional target, WNT5A, shows overlapping expression. Furthermore, in DLX5$^{-/-}$ mice (E14.5) there is a reduction in WNT5A expression which was associated with a 50% decrease in the phosphorylated form of JnK1-3 whereas the level of dephosphorylated β-catenin was unchanged (Paina et al., 2011). While in the mouse VZ-SVZ of the ganglionic eminence WNT5a is nearly undetectable

(Paina et al., 2011), the opposite is found in our human foetal tissue (whole tissue). Negligible counts (< 5 normalised counts) were observed for WNT3A whereas there was a significant upregulation of WNT5A in the MGE compared to the LGE (Log2 fold change = 2, padj= 9.05×10^{-11}). This expression was similar to that of the 33n1 cell line.

These results may reflex species variation and differential requirement of non-canonical WNT ligand expression and signalling within the developing telencephalon but may hint to common mechanisms. Further investigation to the requirement of WNT5A in proper human MGE derived interneuron development is warranted.

A

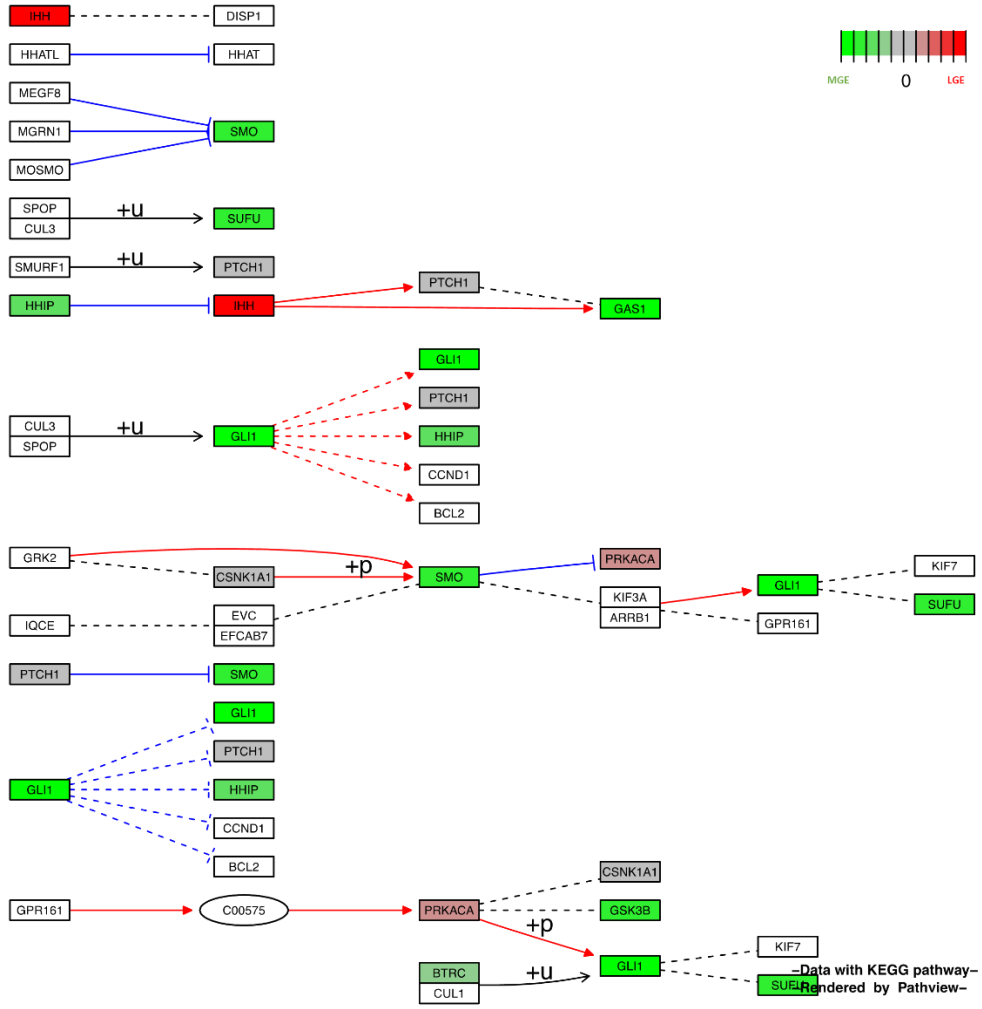

Figure 4.7. MGE gene set enrichment. A) Highlighted genes within the HH pathway are enriched in the MGE (green) compared to the LGE (red). B) Heatmap of normalised Log2 normalised counts of DEGs within the HH pathway across all cell lines and treatment and average MGE expression. C) Dot plot showing Log2 Fold change (-1/1) and p-adjusted values (BH, <0.05) of all cell lines and treatment compared to average MGE samples.

B

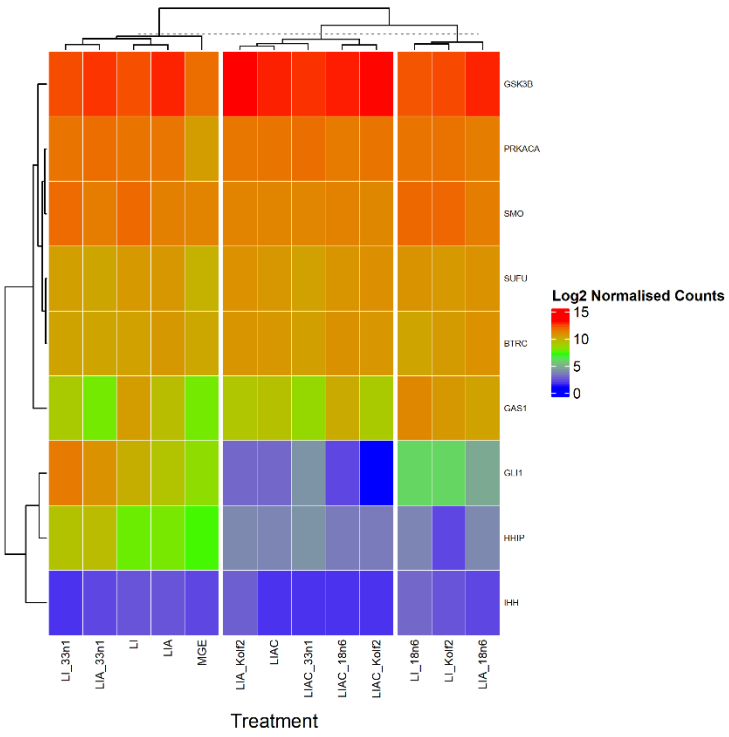

C

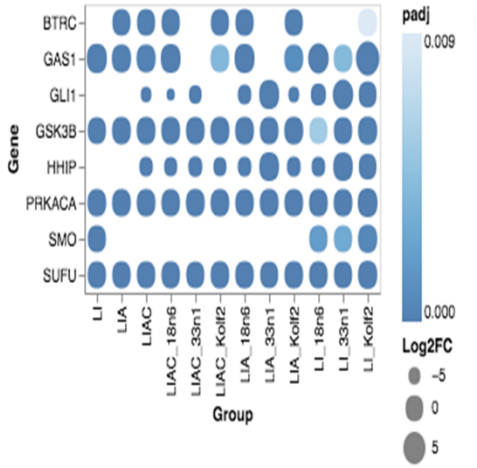

Figure 4.7. continued. B) Heatmap of normalised Log2 normalised counts of DEGs within the HH pathway across all cell lines and treatment and average MGE expression. C) Dot plot showing Log2 Fold change (-1/1) and p-adjusted values (BH, <0.05) of all cell lines and treatment compared to average MGE samples.

A

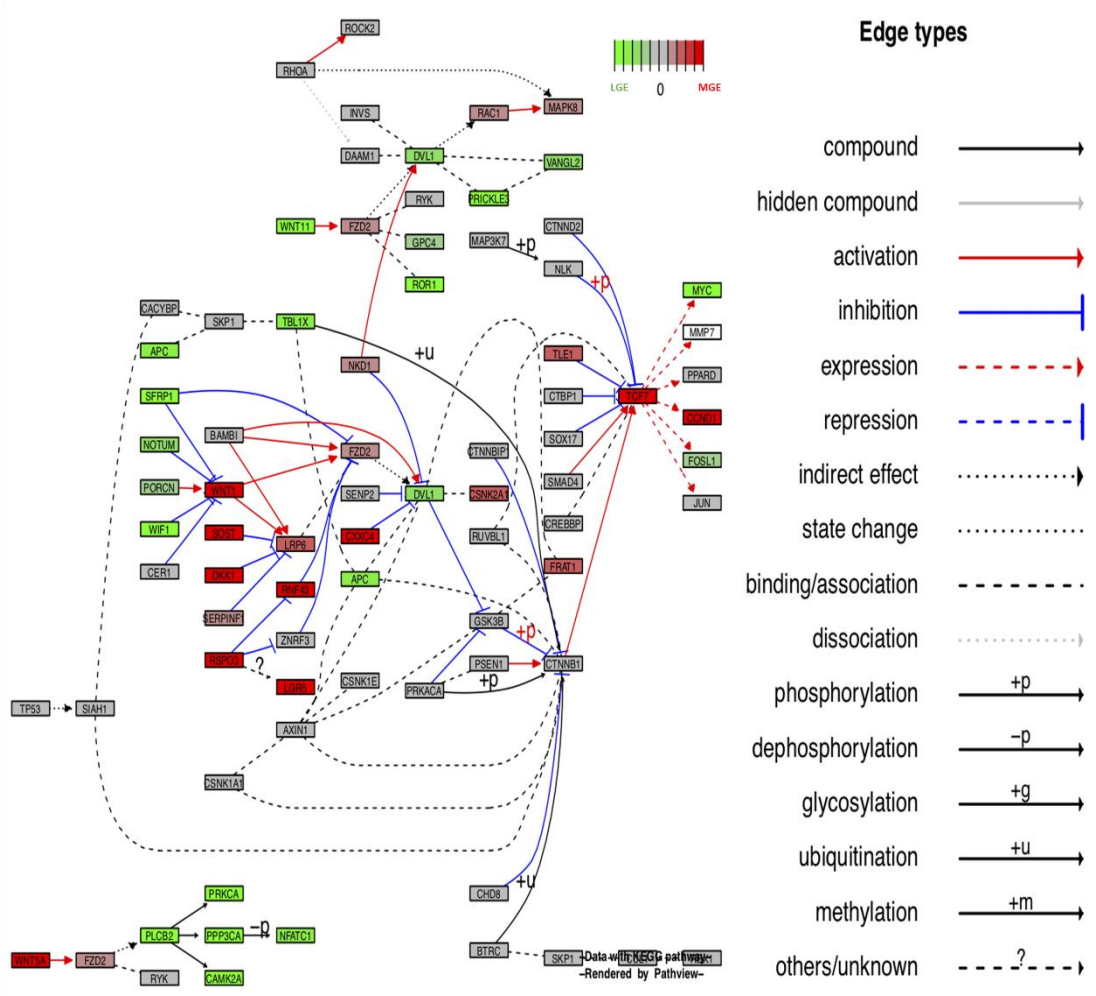

Figure 4.8. MGE gene set enrichment. A) Highlighted genes within the non-canonical Wnt pathway are enriched in the MGE (red) compared to the LGE (green).

B

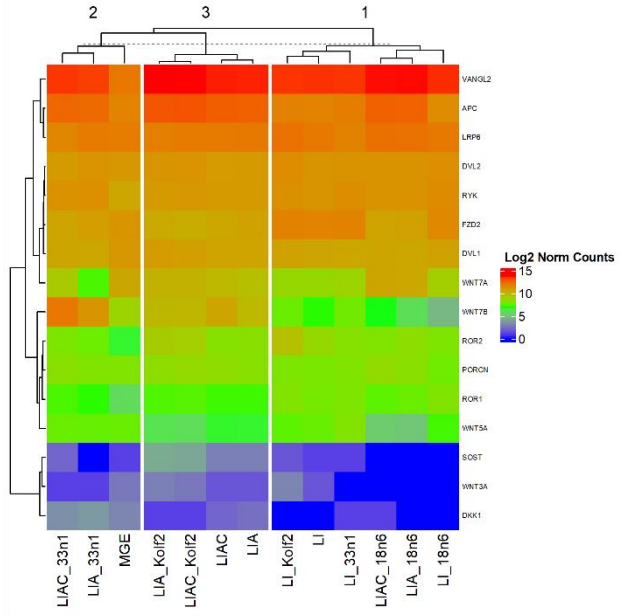

C

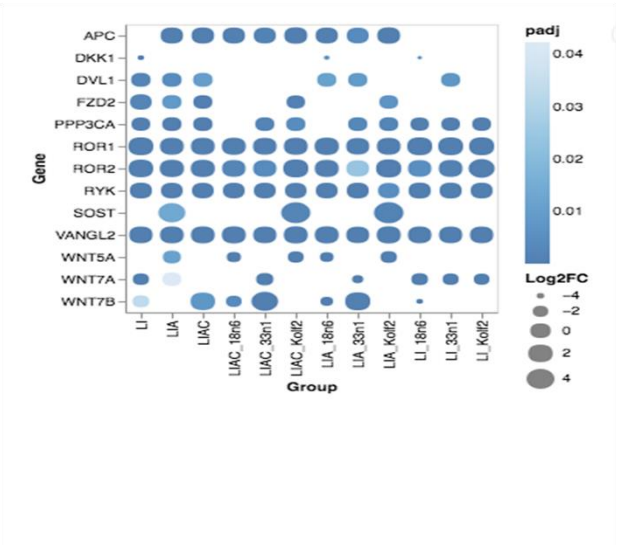

Figure 4.8. continued. B) Heatmap of normalised Log2 normalised counts of DEGs within the non-canonical Wnt pathway across all cell lines and treatment and average MGE expression. C) Dot plot showing Log2 Fold change (-1/1) and p-adjusted values (BH, <0.05) of all cell lines and treatment compared to average MGE samples.

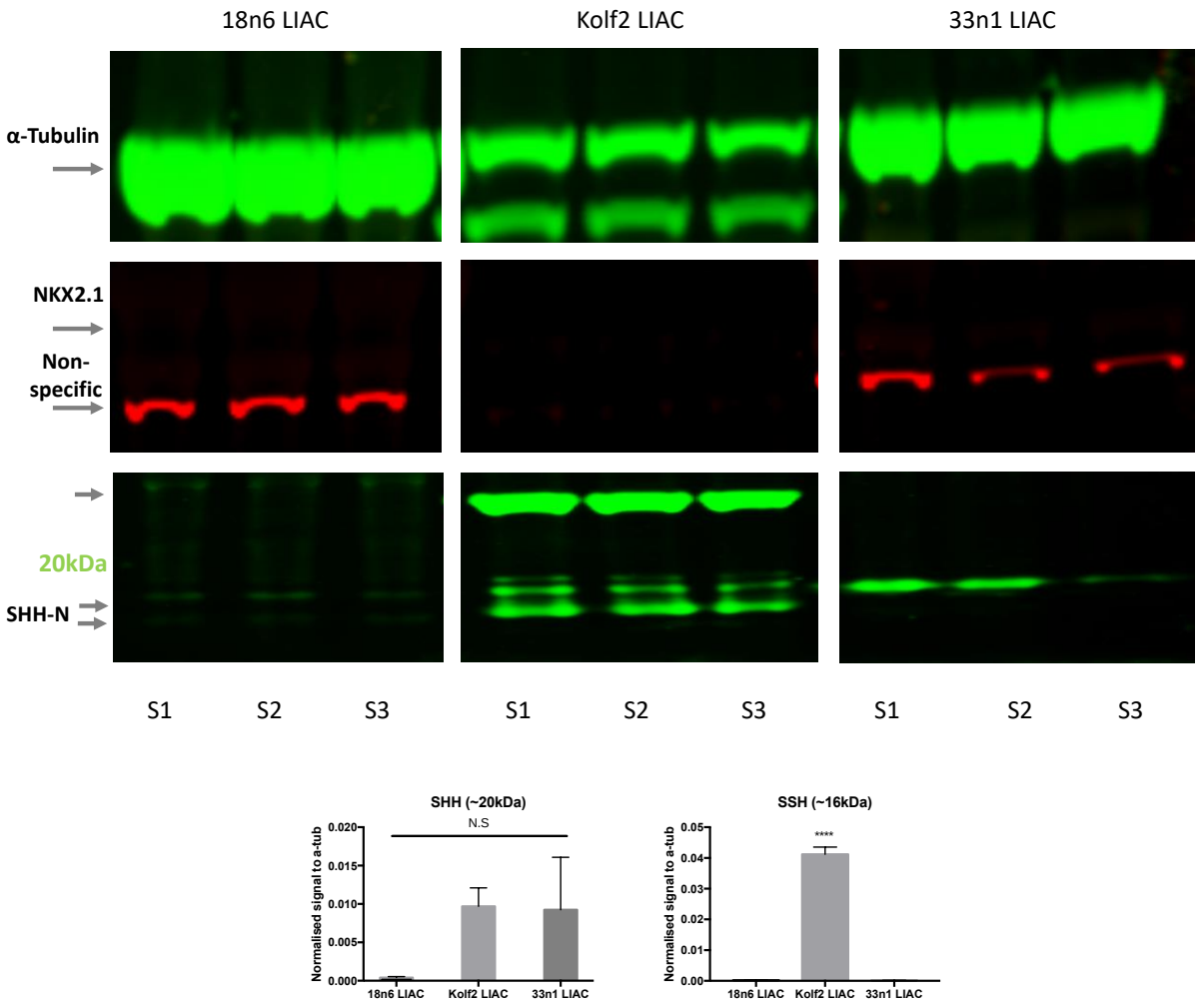

*Figure 4.9. Control lines were differentiated to D16 following LIAC protocol. Top) Western blot image of loading control (α-Tubulin), NKX2.1 and SHH. Note: non-specific band at a lower MW predicted for NKX2.1. In addition, differing MW bands for SHH across all lines, presumably due to post-transcriptional modifications. Bottom) Western blot analysis for SHH normalised to loading control. Data shown are the average of 3 independent differentiations in 3 cell lines 18n6, Kolf2 and 33n1. * P≤0.05, ** P≤0.01, ***P≤0.005, ****P≤0.001, one-way ANOVA followed by Tukey's post-hoc test.*

Inhibition of HH pathway during patterning increases terminally differentiated MSN's and corrects for some variation seen between cell lines

As independent cultures show similar patterns of increased LGE/striatal and decreased MGE specific gene expression following the addition of Activin and Cyclopamine, we terminally differentiated these NPCs using a protocol previously described (Telezhkin et al., 2015). We performed immunocytochemistry and qRT-PCR gene expression analysis on a panel of genes known to be differentially expressed during telencephalon development and compared data to that of human foetal LGE.

Using LIAC medium all cell lines over three separate differentiations showed >70% MSN fate specification and differentiation as indicated by co-expression of DARPP-32 and CTIP2 (33n1: 74.7% ± 8.8%, Kolf2: 81.3% ± 6.7%, 18n6: 76.5% ± 0.4%, $F(2,`89)=14.05$, $p<0.0001$). Although the Kolf2 cell line showed significantly more MSNs over differentiation compared to 33n1 (padj<0.0001) and 18n6 (padj=0.0029) the percentage of GABAergic neurons differed ($F(2,237)=59.07$, $p<0.0001$). Compared to the Kolf2 cell line (77.6% ± 12.1%) there was significantly more GABAergic cells present within the 33n1 cell line (87.1% ± 0.9%, padj<0.0001) as well as the 18n6 cell line (88.6% ± 1.7%, padj<0.0001). Variation in the percentage of Glutamatergic neurons, albeit low, were also apparent ($F(2,237)=21.29$, $p<0.0001$) primarily within the 33n1 cell line (5.6% ± 5.3) compared to the Kolf2 (12.6% ± 10.5%, padj<0.0001) and 18n6 cell line (10.3% ± 0.7%, padj=0.0014) (Figure 4.10).

At a gene expression level, all cell lines consistently and efficiently showed down-regulation or equivalent mRNA transcript levels of the HH signalling and effector genes LHX6, SMO, IHH, BCL2, SIX3, SHH, NKX2.1, NKX6.2, OLIG2, GLI1 and PTCH2 compared to the LGE (Figure 4.11 A-C). Furthermore, genes known to be expressed in the developing cortex such as TBR1, NeuroD6, vGlut1, and ETV1 were suppressed. While mRNA transcripts such as SST and CHAT hint to the possibility of GABAergic or cholinergic interneuron differentiation, respectively, it would appear that a strong bias is present within all cell lines for the generation of indirect pathway DRD2-expressing MSNs as opposed to direct pathway DRD1 expressing MSNs.

Direct-pathway MSN genes DRD1 and TAC1 were down-regulated compared to the foetal LGE, whereas in-direct pathway MSN genes DRD2, ARPP21 and ONECUT2 were all up-

regulated. Bias for dopamine receptor transcripts were also seen and the NPC stage with differential expression of both dopaminergic and cAMP signalling gene transcripts. A transcription factor that has been shown to promote DRD1-MSN fate is ZNF503 (previously known as NOLZ-1) which is down-regulated in all cell lines. In ZNF503 KO mice there is a significant reduction in striatal markers FOXP2 and DRD1 as well as an enrichment of DRD2, ADORA2A and PENK mRNA within the striatum (Lu et al., 2018). However, within the 18n6 cell line, some DRD1-specific mRNA transcripts are upregulated, such as FOXP2, EBF1 and SP8. While ZNF503 is required for patterning in the developing mouse striatum, its expression in postmitotic neurons within our terminally differentiated cultures may not be relevant. Therefore, normalised gene counts for this transcript were looked at in samples from the LIAC protocol at D16 from our RNA Seq data. Here, 18n6 showed higher ZNF503 expression compared to the 33n1 and Kolf2 cell lines. In the developing limb bud ZNF503 expression is regulated by BMP signalling (Posteriorly) (McGlinn et al., 2008). If a similar mechanism of regulation occurs in LGE-like neural progenitors, we might expect a higher expression of endogenous BMP ligands within the 18n6 cell line, which could potentially signal via BMPR with the removal of LDN in terminal differentiation medium. Out of all the signalling BMP ligands BMP2, BMP7 and BMP6 were expressed within all cultures at D16. As BMP2 and BMP7 have not been shown to elicit ectopic ZNF503 expression (McGlinn et al., 2008), a candidate worth further investigation is BMP6 which was expressed at higher levels in 18n6 cultures than the Kolf2 and 33n1. Furthermore, BMP6 was enriched in the foetal LGE compared to the MGE (Log2 fold change = 1.105, padj=0.0003).

Therefore, BMP6 was added to our terminal differentiation medium in combination with Activin-A following LIA and LIAC protocols. Preliminary data showed non-overlapping protein expression of both DRD1- and DRD2- neurons within clusters of neurons, previously shown to be the source of DARPP-32/CTIP2 MSNs (Figure 4.12A). At a gene expression level, mRNA transcripts were shown to be like that of foetal LGE (Figure 4.12B). As previous differentiation protocols have shown that extended NPC culture increases DRD1 transcripts, we investigated different time windows of BMP6 addition. Utilising the 18n6 cell line (chosen for its lower SHH expression), NPCs cultured in ADF/PSG supplemented with 2% Neurobrew-21 (with Vit A), IWR-1 (1.5µM), Activin-A (25ng/ml) and BMP6 (10ng/ml) from D16 to D21 following initial patterning with LIA were subsequently terminally differentiated.

This resulted in a significant increase in DRD1 mRNA compared to average foetal LGE ($F(3,23)=3.757$, $p=0.0248$), whereas inhibiting BMP signalling (LIA) or allowing endogenous BMP signalling (IA) did not. Furthermore, in these experiments there was significantly more DRD2 mRNA expression compared to foetal samples ($F(3,23)=39.51$, $p<0.0001$), with no difference between treatment and transcription factor

that has been shown to promote DRD1-MSN fate is ZNF503 (previously no difference in DARPP-32 expression ($F(3,20)=0.09799$, $p=9602$, Figure 4.12C), suggesting BMP signalling is specific to DRD1.

Summary

Here, RNA Sequencing from three independent cell lines following three protocols confirmed a robust induction of LGE/striatal enriched transcripts with the addition of Activin-A, consistent with previous reports (Arber *et al.,* 2015, Smith-Geater *et al.,* 2020). No DEGs were observed when comparing LIA and LIAC protocol within the 18n6 and Kolf2 cell lines while within the 33n1 cell line there was a significant down-regulation of MGE-specific transcripts NKX2.1, NKX2.2, NKX6.2 and OLIG2, further supporting the idea that HH signalling is biasing the 33n1 cell line differentiation, with no apparent off-target effects. In order to determine if cell line and or treatment showed bias for the LGE or MGE we utilised the publicly available RNA sequencing human foetal datasets and compared DEGs enriched within KEGG pathways specific to each brain region. Although no bias was seen for cell lines or treatments with Dopaminergic and cAMP signalling DEGs were significantly different from that of the LGE. This is likely attributed to culture maturity and or to a bias of differentiation to indirect pathway MSNs – expressing DRD2 receptor transcripts which attenuate cAMP signalling. The major source of variation was confirmed to be associated with HH signalling that induced an MGE-like transcriptomic signature within the 33n1 line under LI and LIA protocol, whereas under LIAC conditions this was not true. To investigate whether inhibiting SHH during patterning increases and or corrects inter-line variation, cell lines following LIAC protocol were terminally differentiated and assessed for DARPP-32/CTIP2 protein expression (indicative of MSNs). Here >70% of MSNs were generated which is the highest and most consistent population of MSNs in our hands to date. However, inter-line variation is still apparent and possible bias towards DRD2-expressing MSNs was observed. Through RNA sequencing in addition to HH signalling we have identified that variations in endogenous FGF and non-canonical WNT pathways may be further sources of variation within our cultures. To date no differentiation protocol has examined non-canonical WNT in human iPSC-derived MSN or interneuron differentiation.

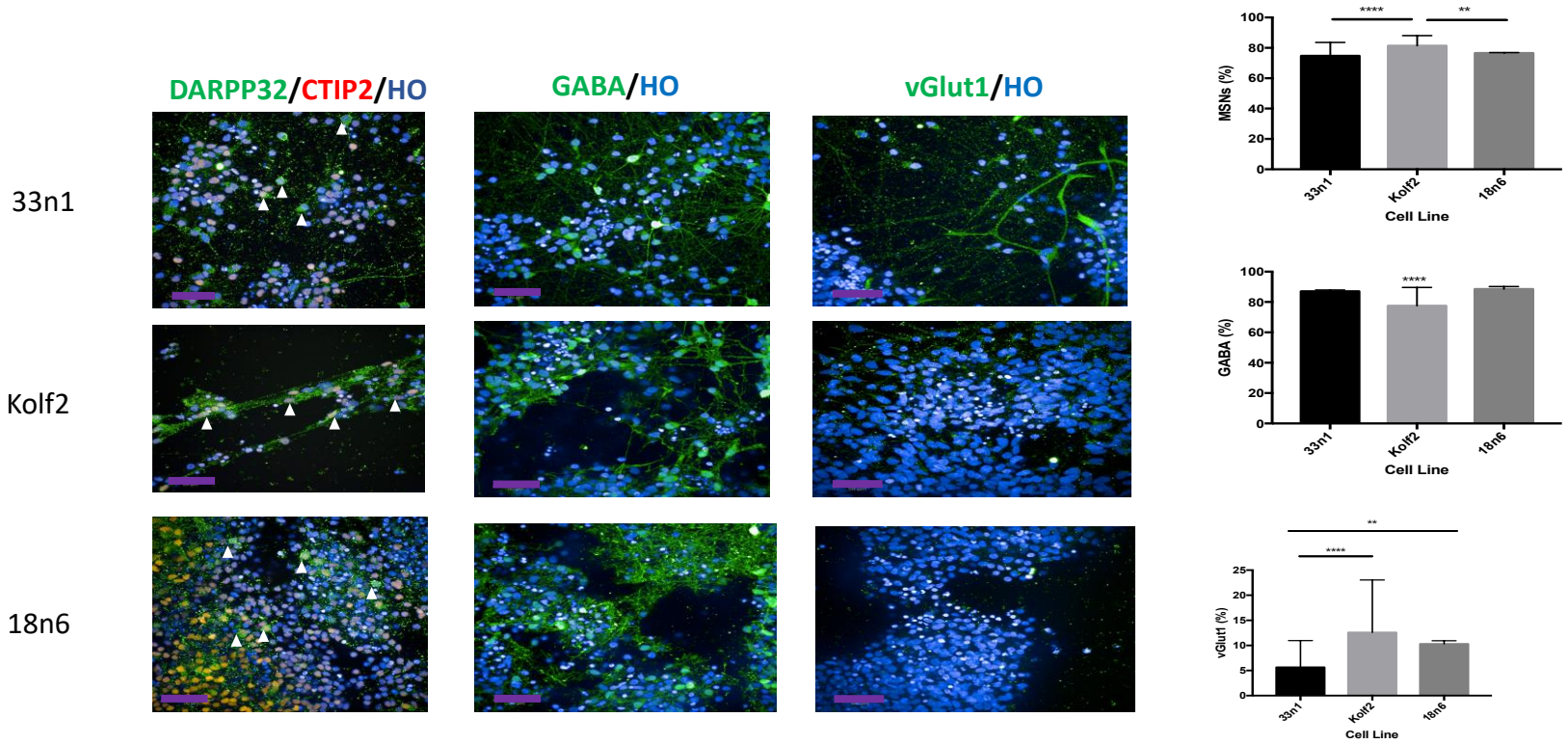

Figure 4.10. *iPSC differentiation following LIAC protocol. Left: Exemplar ICC images of MSNs as identified by co-expression of DARPP-32 and CTIP2 and GABA. Note: vGlut1 images are not represent of the entire population of cells and are presented as positive identification only (scale bar 50μm). Right: Percentage of MSNs shows variation (DF=2, F=14.05) within all cell lines however there is >20% increase in the 33n1 cell line compared to LIA protocol. The majority of all cell lines expressing GABA, albeit lower in the Kolf2 cell line (DF=2, F=59.07). Low glutamatergic (<20%) populations of cells are present within all cell lines with significantly lower observed in the 33n1 cell line (DF=2, F=21.29). Data was calculated from 3 independent differentiation and are presented as the mean with SD and one-way ANOVA with Tukey's multiple comparisons test. * p<0.05, ** p<0.01, *** p<0.001, **** p<0.0001.*

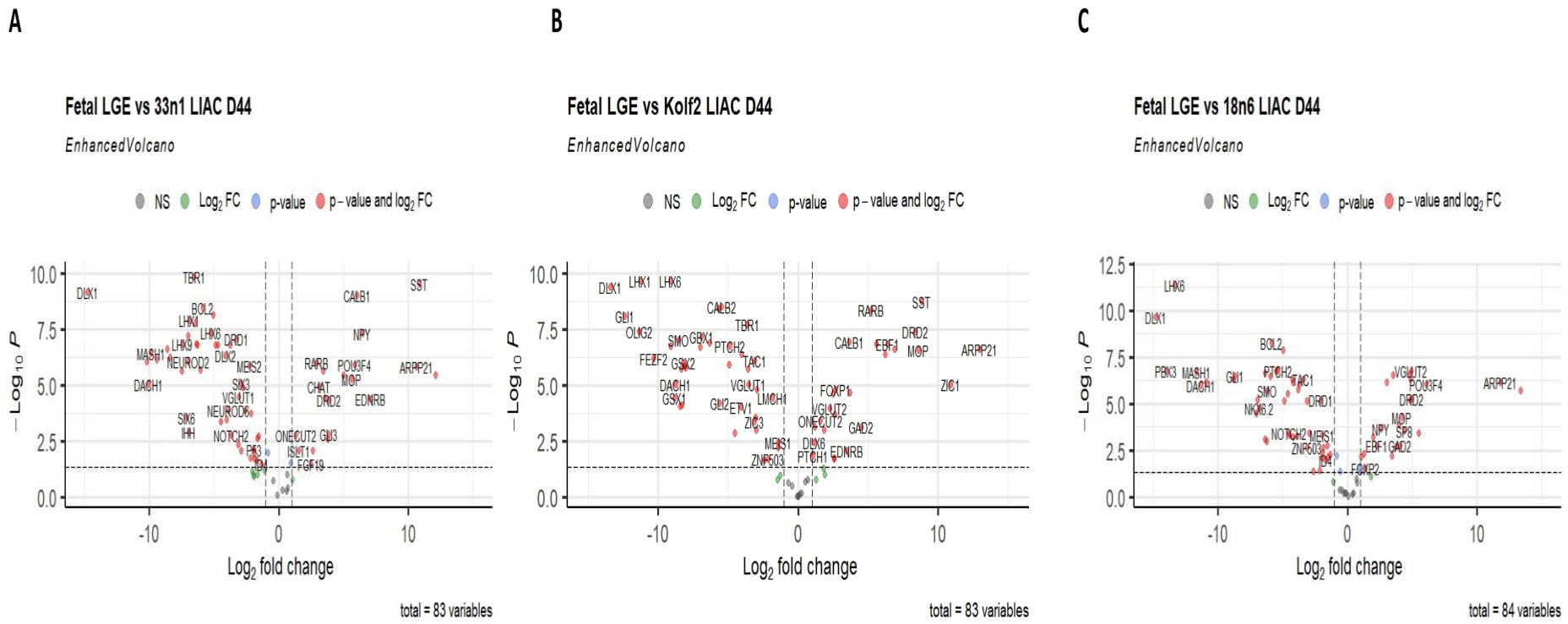

Figure 4.11. Fluidigm BioMark qPCR analysis of a panel of 83 genes of interested known to be differentially expressed during Dorso-ventral patterning of the telencephalon and enriched in the striatum and cortex. Terminal differentiation of cell lines under LIAC protocol A) 33n1 B) Kolf2 and C) 18n6 compared to average human foetal LGE. Data represents the mean of tree biological and 3 technical repeats. Volcanoplots were generated using R and Fold change and p-adjust (BH) values are presented.

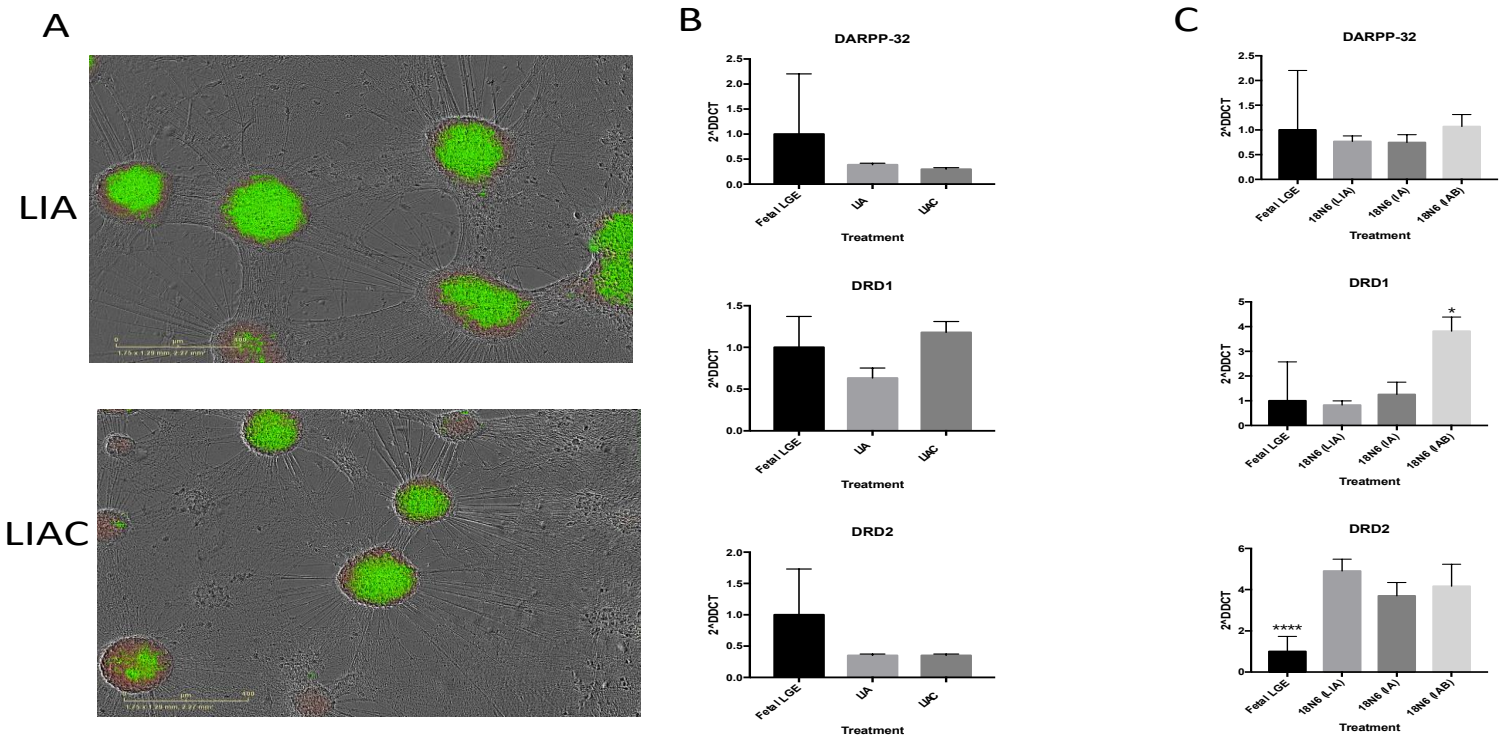

*Figure 4.12. BMP6 increases DRD1-protein and mRNA expression. A) Incucyte live cell image of isogenic (5H9) terminally differentiated neurons with BMP6 and Activin-A following LIA and LIAC patterning express DRD1 (green-antagonist) and DRD2 (Adora2a-red-agonist) neurons. B) qPCR analysis of) isogenic (5H9) terminally differentiated neurons with BMP6 and Activin-A following LIA and LIAC patterning. C) 18n6 cell line following LIA patterning were cultured for a further 6 days in either LIA, IA or IAB and terminally differentiated as previously described (Telezhkin et al., 2015). Data from isogenic control is one plate down and thus no statistical analysis. Data from 18n6 cell line was calculated from 3 independent differentiation in triplicate and are presented as the mean with SD and one-way ANOVA with Tukey's multiple comparisons test. * p<0.05, ** p<0.01, *** p<0.001, **** p<0.0001*

Chapter 5: Differential requirement of SHH and NKX2.1 in the generation of subpopulations interneurons

In chapter 4 it was shown that inhibition of the HH pathway at the level of SMO was sufficient to downregulate HH gene targets at both the mRNA and protein level. RNA sequencing suggested no off-target effects, evidenced from no DEGs within the Kolf2 and 18n6 cell lines when comparing LIA and LIAC medium. To validate this, Chapter 5 aims to generate SHH KO lines in the 33n1 cell line and to analyse, at the mRNA level, genes responsible for LGE/MSN and MGE/interneuron fate. To complement this NKX2.1 was knocked out within the 33n1 cell line. This was to investigate whether in the absence of NKX2.1, which is required for interneuron fate within the ventral telencephalon, and in the presence of SHH (endogenous), do these cells generate LGE-like progenitors and ultimately terminally differentiate into MSNs.

Abstract

The human striatum contains two predominant neuronal cell types; Medium spiny neurons (MSNs) and interneurons which comprise ~95% and 5% of striatal neurons, respectively. Whilst the lateral ganglionic eminence (LGE) is the origin of MSNs, the majority of interneurons are derived from the medial ganglionic eminence (MGE) and preoptic area (POA). Within the proliferative zones of the MGE and POA there is abundant SHH mRNA and progenitor cells express the homeodomain protein NKX2.1 which is necessary for the specification for MGE- and some POA- derived interneurons. Whilst SHH is required for the specification of many subpopulations of neurons there is no definitive evidence for its requirement in the generation of MSNs, yet differentiation protocols routinely utilise SHH proteins or HH pathway agonists.

In Chapter 4, we showed that inhibition of the HH pathway during neural patterning results in loss of NKX2.1 protein and an increase in LGE-specific transcripts in neural progenitor cells, resulting in an increased generation of MSNs upon terminal differentiation. However, although not signalling through the canonical HH pathway, SHH was still expressed in NPCs and the requirement of SHH during terminal differentiation was not addressed. To investigate this, we generated SHH and NKX2.1 knock out IPSC lines and differentiated these

following two differentiation protocols and assessed gene and protein expression at the neural progenitor and neuronal stages. Here we show that SHH and NKX2.1 are differentially required for generating subpopulations of cells, namely GABAergic neurons expressing CHAT or TH. In addition, endogenous SHH in the absence of NKX2.1 and exogenous small molecules increases both DARPP-32 and TH protein but are not believed to be of an MSN fate.

Introduction

The role of NKX2.1 in MGE development and interneuron specification has been well documented. For example, in conditionally null mice there is no identifiable globus pallidus (GP) and an enlarged striatum, which appears to extend into the area of which structures associated with the GP is found (Kimura.*et al.,* 1996; Sussel *et al.,* 1999; Ohkuno *et al.,* 2002; Butt *et al.,* 2008; Du *et al.,* 2008; Butt *et al.,* 2009). In these models parvalbumin (PV) and somatostatin (SST) containing interneurons failed to migrate tangentially to the striatum

This has been supported in a human post-mortem sample with Benign Hereditary Chorea (BHC). BHC was associated with a 7bp deletion in exon 1 of the NKX2.1 gene resulting in a premature stop codon and striatal interneuron loss (Kleiner-Fisman et al., 2005). The morphogen responsible for ventralising the telencephalon and that acts upstream of NKX2.1 expression, is the Sonic Hedgehog (SHH) protein. In SHH null embryos neuroectoderm domains lack NKX2.1 expression (Pabst *et al.,* 2000; Rallu et al., 2002), and during neurogenesis SHH is required to maintain NKX2.1 expression (Anderson et al., 2001; Xu et al., 2004; Xu et al., 2005). Perturbation of SHH-SMO signalling does not cause significant reductions in pan-GE markers, GSX2 and DLX2, both of which are enriched within the LGE and required for normal LGE development (Rallu et al., 2002; Machold et al., 2003; Xu et al., 2010). These studies suggest that during telencephalon development SHH-SMO signalling is required for normal MGE development while it is dispensable for LGE development. Nevertheless, the majority of differentiation protocols aimed at generating MSNs from either human ESCs or iPSCs have employed the use of SHH and/or small molecule agonists such as SAG or purmorphamine to ‘ventralise’ cultures (Aubry et al., 2008; Li et al., 2009; Zhang et al., 2010; Ma et al., 2012; HD iPSC consortium 2012; Carri et al., 2013; Nicoleau et al., 2012; Hunt, Pouton and Haynes 2017; Wu et al., 2018). Following initial patterning,

Aubry et al., (2015) utilised SHH in combination with DKK1 and BDNF to regionalise neuronal rosette structures and following terminal differentiation was shown to generate ~12% DARPP-32 positive neurons. Subsequently, studies have adapted this protocol with varying concentrations (10-250ng/ml), and duration (8-25 days) of SHH treatment with the aim of inducing an LGE phenotype. This has resulted in reports of varying efficiencies of MSN differentiation (5-95% DARPP-32^{+} neurons), typically requiring long periods of terminal differentiation (20-80 DIV) (Li et al., 2009; Zhang et al., 2010; Ma et al., 2012; HD iPSC consortium 2012; Carri et al., 2013; Nicoleau et al., 2012; Hunt, Pouton and Haynes 2017; Wu et al., 2018). While these studies suggest that SHH promotes MSN fate, this is in stark contrast to what we have observed in which SHH biases cells towards an MGE fate.

Despite these findings it is still possible that SHH could play a later role in MSN neurogenesis and terminal differentiation. During late gestation in the mouse DLX2^{+} expressing intermediate progenitor cells in the SVZ have been found to show a proliferative response to SHH (mediated by PTCH1) secreted from the MGE (Shikata et al., 2011). Furthermore, in SHH$^{-/-}$;Gli3$^{+/-}$ mutant mice (with normal LGE morphology) there is an increase in proliferation within the SVZ of the LGE. Thus, SHH may be involved in later stages of DLX2^{+} progenitor development. This does not however suggest a role in MSN differentiation. In fact, in the mouse striatum PTCH1 expression appears to be restricted to CHAT^{+} interneurons and astrocytes both of which interact with MSNs (Gonzalez-Reyes et al., 2012; Khan et al., 2021). Therefore, it is possible that SHH treatment could have an indirect mechanism of action on later stages of MSN development beyond progenitor cell patterning.

In our optimised patterning differentiation protocol (LIAC), SHH protein is expressed in all lines at D16. Although inter-line variability was apparent, when terminally differentiated, the major population of cells generated were MSNs. Terminally differentiated neurons did not receive continued Cyclopamine treatment and without analysis of PTCH1, CHAT and GFAP protein expression we cannot exclude HH signalling or cholinergic interneuron and astrocyte fates within the remaining population (~30%).

To gain a better understanding of the role of SHH, if any, we generated SHH$^{-/-}$ and NKX2.1$^{-/-}$ iPSC isogenic 33n1 cell lines. Regional identity was achieved using the LIA protocol and these cells were terminally differentiated and assessed for MSN fate as well as sub-type

interneuron specification. In addition, we compare the ‘default’ differentiation of these cultures in the absence of exogenous morphogens or small molecules.

Results and Discussion

Generation of SHH and NKX2.1 KO iPSC lines by CRISPR-Cas9

Generation of guide RNAs (gRNAs) were designed using Deskgen to target exon 1 of the SHH (Cas9 cut sites at 60bp and 223bp from transcriptional start site) and NKX2.1 (Cas9 cut sites at 41bp and 104bp from the transcriptional start site) genes resulting in a 146bp or 46bp deletion and frame shift mutations, respectively (Figure 5.1A-B). Following transfection of Cas9/RNPs, 33n1 clones were picked and screened by PCR as illustrated in Figure 5.1. Successful targeting of both WT alleles of the NKX2.1 gene was seen. However, targeting of the SHH gene generated additional different mutant alleles, one of the predicted deletions, Figure 5.1C_i, and a second disrupted allele comprising a complex insertion/deletion event, Figure 5.1C_{ii}. Sequencing of these samples confirmed a frame shift mutation creating a premature termination codon of the SHH (both mutated alleles) and NKX2.1 gene (Figure 5.2A-B).

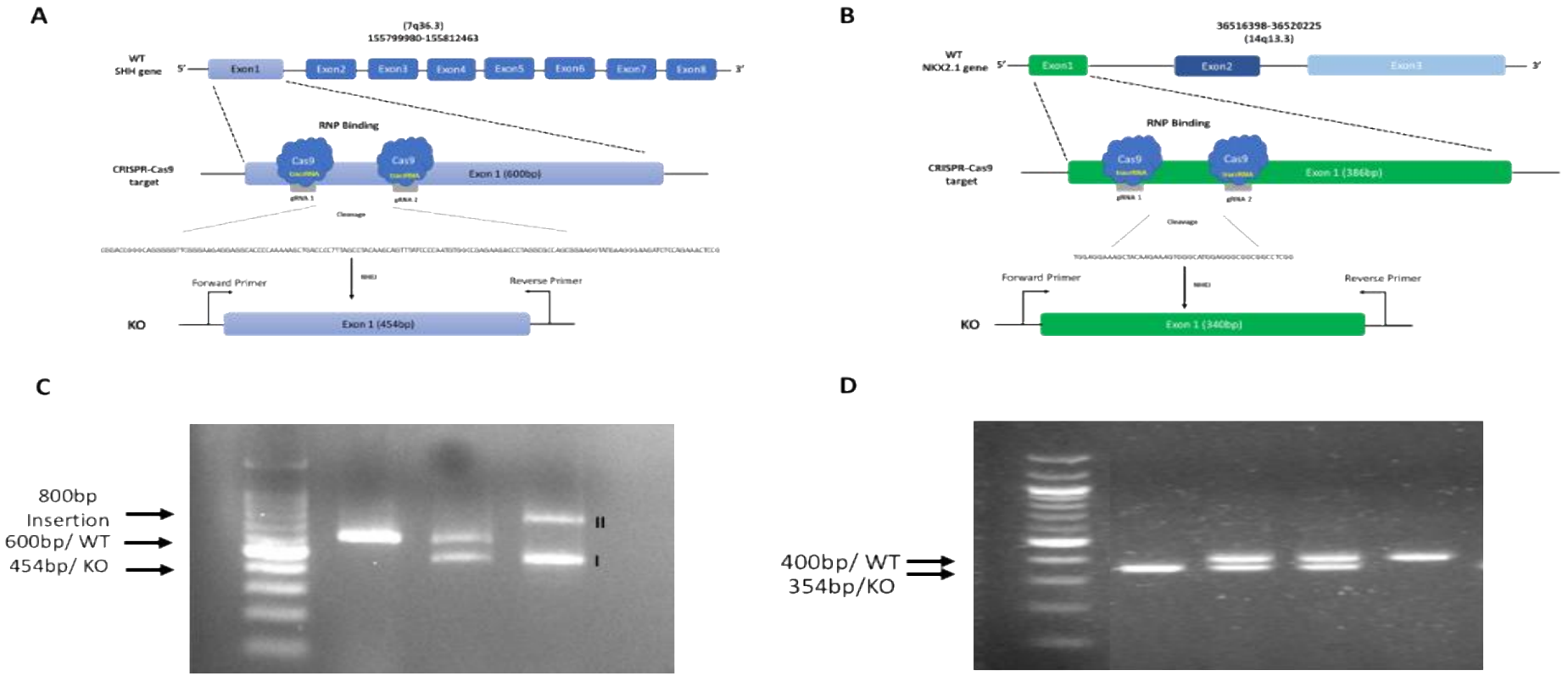

Figure 5.1: CRISPR/Cas9-edited generation of SHH and NKX2.1 knockout (KO) alleles in the 33n1 iPSC line. Schematic showing CRISPR design. Guide RNAs (gRNA1 and gRNA2) were designed to target exon 1 of SHH (600bp, A) and NKX2.1 (386bp, B). Successful Cas9 cleavage would result in a 146bp or 46bp deletion giving a mutated 454bp or 340bp exon 1 fragment of the SHH or NKX2.1. Single cell colonies were picked and screened using primers flanking exon 1.C) Exemplar SHH gel showing a 600bp WT, 454bp KO (i) and a mutated (insertions/deletions) 800bp (ii) PCR fragments (efficiency = 0.5%). D) Exemplar NKX2.1 gel showing 400bp WT and a 354bp KO PCR fragments (efficiency = 23%)

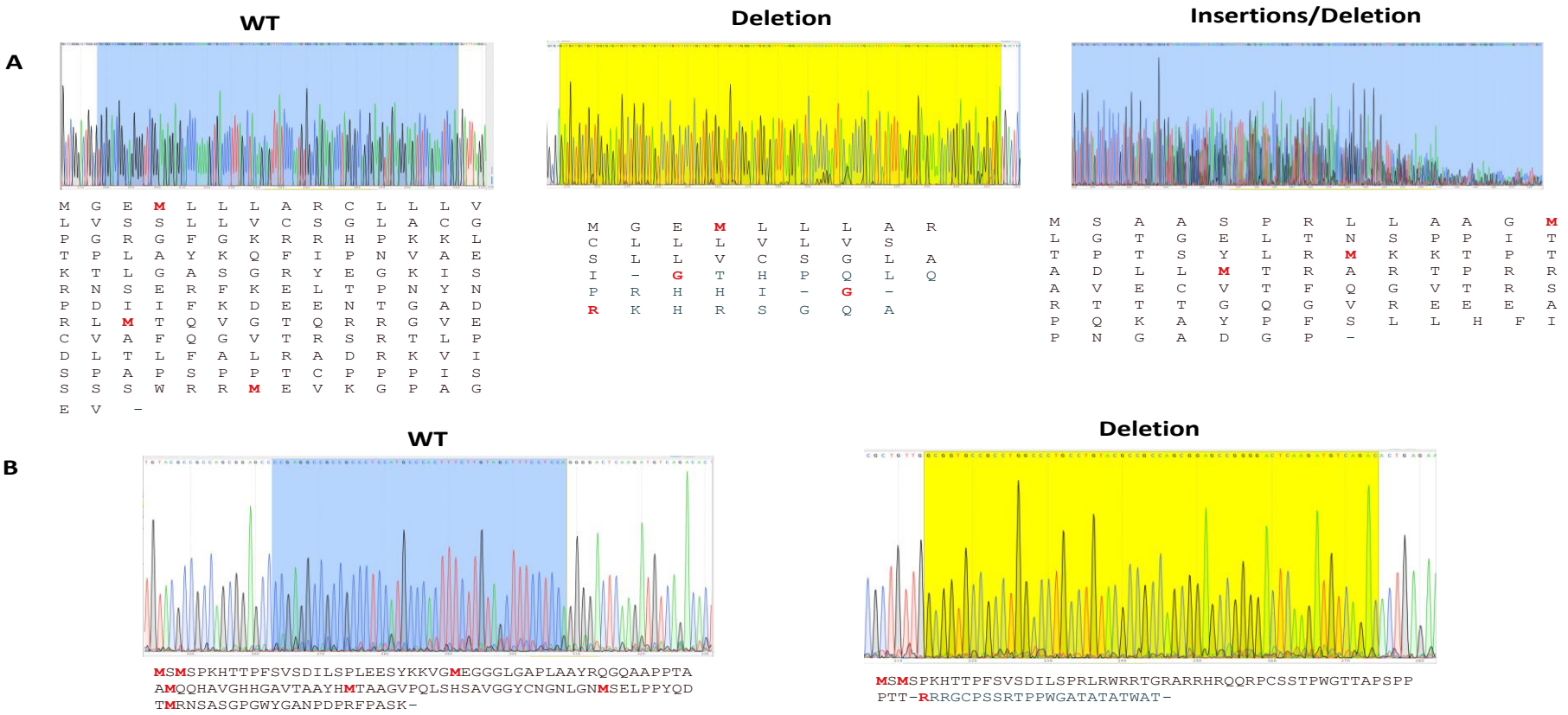

Figure 5.2. Exemplar sequencing results WT DNA sequence to be targeted (blue) of SHH (A) and NKX2.1 (B). Deletion of target DNA sequence resulting in alignment of the DNA sequence either side of WT (yellow). Insertions/Deletions of SHH WT sequence (A, blue, right) also results in premature termination.

Validation of SHH- and NKX2.1-edited iPSC-derived neural progenitors.

We have previously shown that both NKX2.1 and SHH are expressed in 33n1 NPCs following patterning at D16. Therefore, we preformed Western blot analysis to confirm the loss of SHH and NKX2.1 protein in knockout cells. Westerns of control D16 NPCs probed with the anti-SHH 5E1 antibody, to identify functional N-terminal fragments, showed an expected pattern of SHH bands, comprising predicted N-terminal cleavage products and those expected for post-translational palmitoylation (Figure 5.3; Fietz et al., 1995; Marti et al 1995; Porter et al., 1995). Importantly, none of these bands were seen in the knockout samples confirming a complete functional knockout of the SHH gene (Figure 5.3A).

Loss of SHH function was also examined by probing Westerns for NKX2.1 expression. For NKX2.1, the AB76013 antibody recommended for western analysis identified a 38kDa band in control D16 LIA NPCs, but also non-specific bands at ~32Kd. This analysis showed that control cells expressed NKX2.1, although at variable levels that appeared to correspond to different patterns of SHH N-terminal species present in individual samples. In contrast the 38kDa NKX2.1 band was not present in differentiated SHH null clones, but importantly, NKX2.1 could still be induced by treating cultures with purmorphamine, a smoothened small molecule agonist that therefore by-passes loss of SHH protein.

Western blot analysis using antibody AB76013 confirmed loss of the 38kDa band in the NKX2.1 knock out cells, but the non-specific bands still remained (Figure 5.3B). To further confirm loss of NKX2.1 a different antibody (AB227652) was used to show loss of staining by ICC. Interestingly, analysis of control clones (non-targeted subclones isolated from the CRISPR screen) revealed that one clone, G5, also did not express NKX2.1. Sequencing confirmed that the NKX2.1 gene in clone G5 did not contain any mutations in proximity to the CRISPR target site, however we cannot exclude mutation in other parts of the NKX2.1 gene. Thus, use of this control clone was excluded from further analysis.

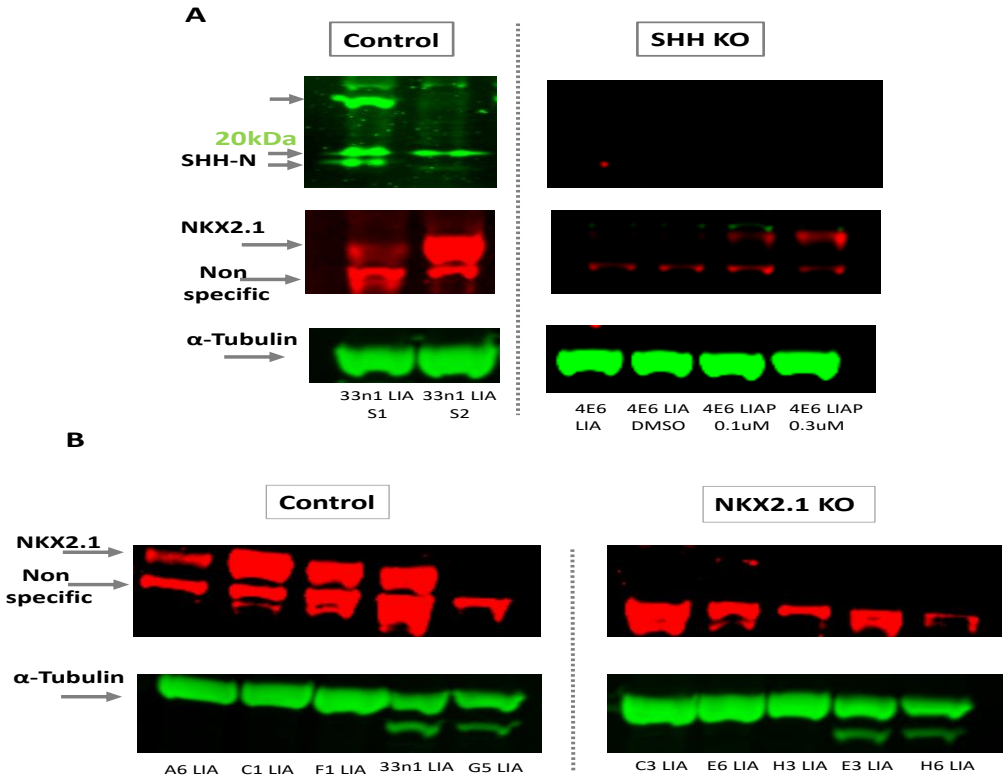

Figure 5.3: 33n1 SHH$^{-/-}$,NKX2.1$^{-/-}$and control clones were differentiated under LIA protocol to D16 to confirm KO of protein expression. A) Western blot images from 2 independent differentiation of the 33n1 parent line and one clone of the SHH KO (4E6) differentiated under LIA, LIA + DMSO (control), and addition of 2 concentrations of puramorphamine 0.1μM or 0.3μM confirm loss of SHH protein and functional HH pathway activation when an agonist is added. B) Parent line (33n1) and 4 non-targeted subclones isolated from CRISPR screen (i.e control, A6, C1, F1, G5) and 5 subclones (C3, E6, H3, E3 and H6) of NKX2.1 KO cells were differentiated using LIA protocol confirms no protein expression at expected MW 38-42kDa. Note: lower MW non-specific binding detected with this antibody.

In order to assess the downstream consequence of SHH and NKX2.1 knockout on gene expression, a panel of 89 genes were selected having been shown to be differentially expressed during development along the dorso-ventral axis of the telencephalon. Although there was an increase in both SHH (log fold change =1.8, padj=0.02) and SMO (Log fold change=1.3, padj=0.05), downstream signalling transcripts Ptch1 (Log fold change =8.8, padj=9.17 x 10^{-16}), NKX2.1 (Log fold change =4.4, padj=0.0003) and GSX1 (Log fold change =1.8, padj=0.05) were significantly downregulated in SHH knockout NPCs compared to control. In addition, a number of G-protein coupled receptors were significantly downregulated including GPR161(Log fold change =1.8, padj=7.29 x 10^{-5}) which regulates SHH signalling (Mukhopadhyay et al., 2013), and GPR153 (Log fold change =1, padj=0.02) both of which are expressed in human cortex, the latter showing a cortical layer pattern (Ehrlich et al., 2018) and are HH target genes. GPR6 (Log fold change=2.9, padj=0.02) which is enriched in striatopallidal MSNs was downregulated which may indicate bias towards generation of indirect MSNs. Further supporting this, DRD1 (Log fold change =2.7, padj=4.91 x 10^{-7}) was upregulated in SHH knockouts, as well as mRNA transcripts expressed in LGE progenitors, DLX6 (Log fold change =1.6, padj=0.007), MEIS2 (Log fold change =1.6, padj=1.49x 10^{-5}), MEIS1 (Log fold change =1, padj = 0.01), and FOXP1 (Log fold change =1.6, padj=0.001). Other LGE enriched genes such as SP8 (Log fold change = 4.2, padj=0.0002), and RARB (Log fold change =1.9, padj= 0.0003), were reduced, both of which play roles in the upregulation of DRD2 expression (Molotkova, Molotkov and Duester, 2007; Liao et al., 2008; Xu et al., 2018). Interestingly, transcripts which have critical functions in oligodendrocyte specification, OLIG2 (Log fold change =2.8, padj=3.2 x 10^{-5}), and influence oligodendrocyte progenitor cell proliferation, ACHE (Log fold change =1.7, 0.007), were both upregulated suggesting some cells may be fated to this lineage (De Angelis, Bernardo, Magnaghi, Minghetti, and Tata, 2012; Fields, Dutta, Belgrad, and Robnett, 2017; Belgrad et al., 2019; Rowitch, 2004). A gene usually suppressed by SHH, Fezf2, and is expressed at high levels in the cortex was upregulated (Log fold change =6.4, padj= 2.1 x 10^{-10}). In the forebrain Fezf2 represses a number of genes including LHX9, a negative regulator of WNT signalling (Chen et al., 2011; Peukert et al., 2011; Castelo-Branco et al., 2003; Hirabayashi et al., 2004; Israsena et al., 2004; Kuwahara et al., 2010; Munji et al., 2011), which was also downregulated in SHH knockout cells (Log fold change =1.7 , padj=2.66 x 10^{-5}). Fezf2 has also been shown to function as a transcriptional repressor during deep-layer neuronal

differentiation (Han et al., 2011; Kwan et al., 2008; Lai et al., 2008; McKenna et al., 2011 – check ref), consistent with this function, we see a significant downregulation in transcription factors that have sequential roles in the transition from intermediate progenitors to glutamatergic pyramidal neurons; TBR2 (Log fold change =2.8, padj=0.02), NEUROD6 (Log fold change =1.4, padj=0.04) and TBR1 (Log fold change =1, padj= 0.007). Differential expression of GABAergic mRNA transcripts was also observed with both CALB2 (Log fold change =1.4, padj= 0.01), and GABAR1 (Log fold change =3.8, padj=2.08 x 10^{-7}) being upregulated in SHH knockout cells, whereas NPY (Log fold change=3.4, padj=1.17 x 10^{-5}) was downregulated (Figure 5.4B).

In NKX2.1 knockout cells, a more specific change in gene expression was observed. For example, all genes assessed for HH signalling were significantly downregulated, including SHH (Log fold change =2.6, padj=0.0005) and downstream targets GLI1 (Log fold change= 2.5, padj=0.002), HHIP (Log fold change =2, padj=0.02), and PTCH2 (Log fold change = 1.5, padj= 0.03). In addition, NKX2.1 transcript (Log fold change =3, padj=0.02), was downregulated as well as its transcriptional targets LHX6 (Log fold change =6.4, padj=1.5 x 10^{-12}) and GBX1 (Log fold change =2.2, padj=0.04) (Sussel et al., 1999; Du et al., 2008; Sandberg et al., 2016). Interestingly, two transcripts which were not expressed in the mouse MGE or LGE but are strongly or moderately expressed within the POA and diagonal area, ZIC1 (Log fold change =2, padj=0.05), and ZIC3 (Log fold change =3.2, padj=0.0004), were significantly downregulated in NKX2.1 knockout cells. As SHH is enriched in this brain region, the downregulation of these may be secondary to the reduction of SHH transcripts in NKX2.1 knockout cells. ZIC1 and ZIC3 transcripts are also enriched in the olfactory bulb and in ZIC1/ZIC3 mutant mice TH^+ olfactory interneurons are significantly reduced (Inoue et al., 2007). Importantly, the GABAergic transcript NPY (Log fold change= 3.3, padj=0.006) as well as transcripts which have important roles in MSN differentiation, TAC1 (Log fold change=2.5, padj= 0.007), and EBF1 (Log fold change =2.4, padj=0.007) were significantly upregulated (Figure 5.4C).

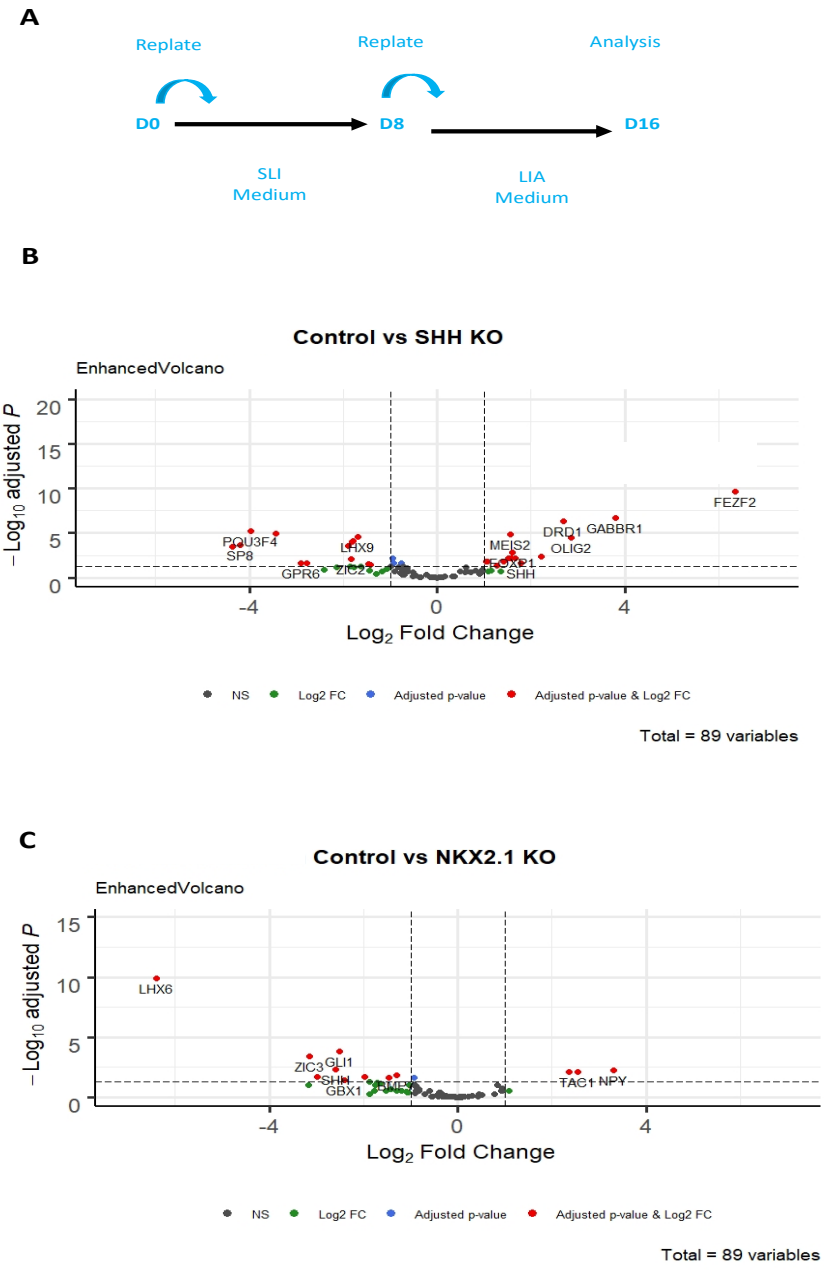

Figure 5.4. A) schematic showing the differentiation protocol followed for cell lines. Fluidigm BioMark qPCR analysis comparing B) Control cell lines and SHH knockout neural progenitor, C) Control cell lines and NKX2.1 knockout neural progenitor. Volcanoplots were generated using R and Fold change and p-adjust (BH) values are presented.

Previous differentiation protocols have suggested that the 'default' differentiation of mouse ESCs and IPSCs is to a ventral fate whereas in human PSCs it is to a dorsal fate owing to intrinsic endogenous SHH and WNT signalling respectively (Gaspard et al., 2008; Espuny-Camacho et al., 2013). However, others have reported endogenous SHH in human ESC and iPSCs (Vazin et al., 2013). In addition, in Chapter 1 and 2 we reported endogenous SHH was biasing the 33n1 cell line to a more ventral, MGE-like, cell fate. Therefore, we examined whether SHH or NKX2.1 loss of function results in a more dorsal phenotype by culturing cells in the basic medium with no additional exogenous factors.

As with use of the LIA protocol, PTCH1 (Log fold change = 5.5, padj=1.63 x 10^{-6}), and NKX2.1 (Log fold change =3.4, padj= 0.05) were both downregulated using a 'default' protocol in SHH knockout cells. In addition, FGF19 (Log fold change = 4, padj=0.002) was reduced, which functions downstream of the HH pathway in the forebrain (Miyake et al., 2005; Ishibashi and McMahon, 2002; Gimeno and Martinez, 2007) and has a known rostral-caudal expression gradient within the cortex. FGF signalling in the cortex is required for the development of GABAergic neurons, which may reflect the downregulation in NPY (Log fold change =4.7, padj=9.01 x 10^{-6}) in SHH knockout cells. In the absence of SHH and exogenous patterning cues there was an upregulation of FOXG1 (Log fold change = 1.1, padj=0.04) and NEUROD2 (Log fold change = 2.2, padj = 0.01), both of which are highly expressed in the developing cortex and have critical roles in cell cycle regulation and cortical neurogenesis, respectively (Quintana-Urzainqui et al., 2018). Two transcription factors that are enriched within the LGE, SP8 (Log fold change = 4.5, padj=0.005) and HELIOS (Log fold change = 2.7, padj=0.03) and are important in the survival of striatopalidal MSNs (Martin-Ibanez *et al.,* 2010,2012; Xu *et al.,* 2018) were downregulated in SHH KO NPCs. However, genes expressed in striatonigral MSNs such as GPR88 (Log fold change = 2, padj= 0.0004), SP9 (Log fold change = 3.8, padj=0.0009), and DRD1 (Log fold change = 2, padj=0.007) were upregulated suggesting a bias towards subpopulations of MSNs of the direct pathway. In addition, several other genes involved in MSN development were also upregulated in SHH KO NPCs including Meis1 (Log fold change = 1.6, padj=0.01), GABAR1 (Log fold change = 2, padj= 0.03), MEIS2 (Log fold change=1, padj=0.03), and FOXP1 (Log fold change = 1.4, padj=0.05). Surprisingly, GLI1 (Log fold change= 2.6, padj = 6.05 x 10^{-6}) expression was increased in SHH KO NPCs. As GLI1 is a direct target of the HH pathway this suggests 'non-canonical SHH

signalling' which can occur through crosstalk with a number of other signalling pathways including EGF, K-Ras, PKA, Notch and Wnt/β-catenin (Santoni *et al.,* 2013; Maeda *et al.,* 2006).

In NKX2.1 KO NPCs, although there was no significant downregulation in NKX2.1 transcription under 'default' differentiation conditions there was a significant reduction in its transcriptional targets LHX6 (Log fold change = 3.5, padj=0.001) and ZIC3 (Log fold change = 2.9, padj = 0.01) whose expression is enriched within the developing POA and diagonal area (Inoue *et al.,* 2007). While an increase in striatal markers MEIS2 (Log fold change = 1.3, padj=0.04), ARPP21 (Log fold change = 1.6, padj= 0.04) and FOXP2 (Log fold change = 2.2, padj = 0.01), may indicate a shift from an MGE fate to a ventral LGE fate there was also an increase in TBR1 (Log fold change = 3.1, padj = 0.03), LHX9 (Log fold change = 2.3, padj=0.04), and MEIS1 (Log fold change = 1.4, padj= 0.05) all of which are expressed at varying levels within the developing amygdala and olfactory bulb in which neurons originate from the POA, Diagonal area and LGE (Campbell *et al.,* 2009; Roy *et al.,* 2020; Toresson, Parmar & Campbell, 2000; Tole *et al.,* 2005; Garcia-Lopez *et al.,* 2008; Puelles *et al.,* 2019; Garcia-Calero *et al.,* 2020; Garcia-Calero-Calero & Puelles 2021).

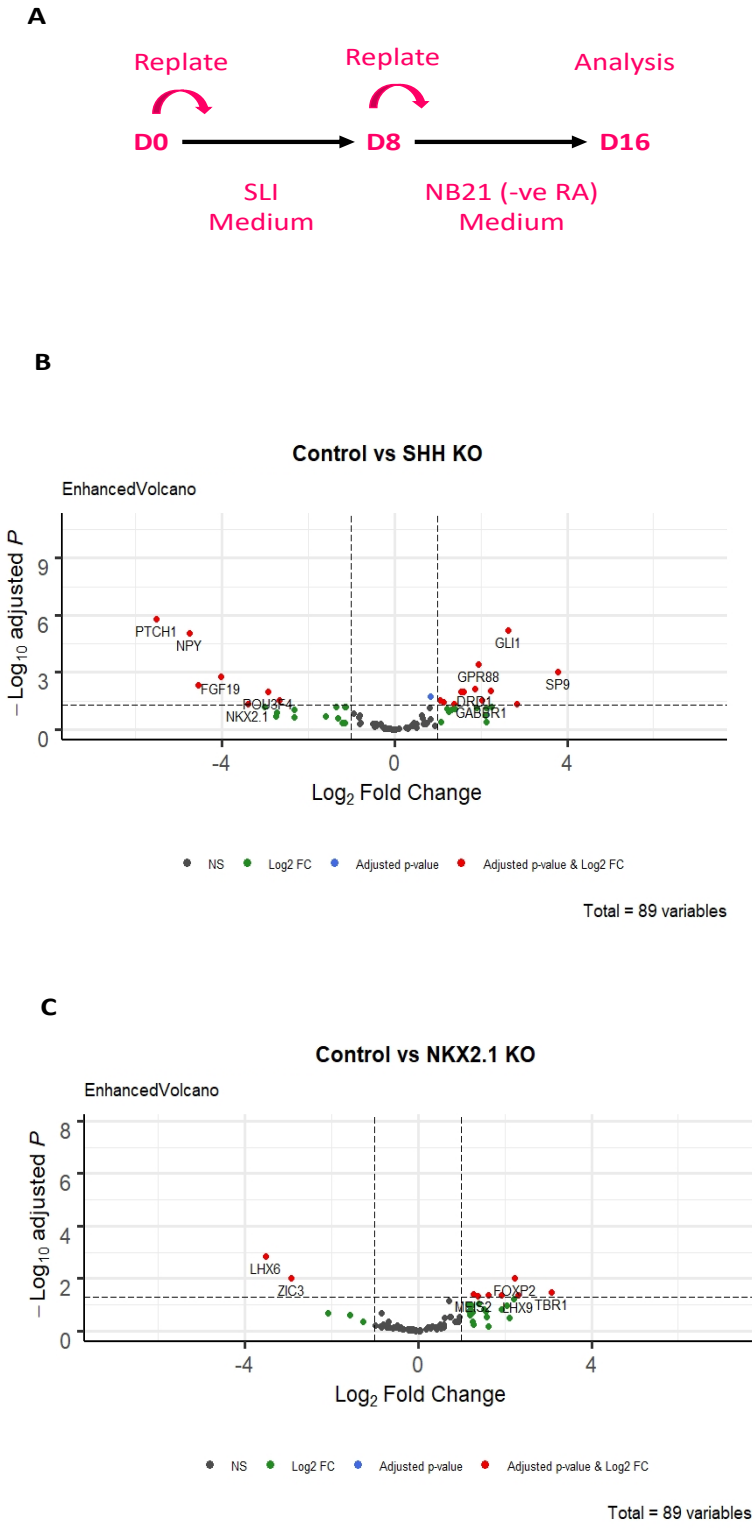

Figure 5.5. A) schematic showing differentiation protocol followed for cell lines. Fluidigm BioMark qPCR analysis comparing B) Control cell lines and SHH knockout neural progenitor, C) Control cell lines and NKX2.1 knockout neural progenitor. Volcanoplots were generated using R and Fold change and p-adjust (BH) values are presented.

SHH and NKX2.1 KO results in loss of TH$^+$ and GABA/CHAT$^+$ interneurons subtypes and MSNs following LIA protocol

Using LIA patterning, SHH $^{-/-}$cells showed a robust downregulation of HH pathway genes. Consequently, a more enriched LGE mRNA transcription profile was observed with a potential bias towards a direct pathway DRD1-MSN fate. However, resulting cells also expressed layer-specific cortical interneuron (FEZF2) and oligodendrocyte (OLIG2) lineage genes. Following 'default' differentiation, critical regulators of cortical excitatory neurons (NEUROD2, FOXG1) were also expressed. In contrast, NKX2.1 $^{-/-}$ cells showed little effect on MSN fate gene expression with the main effects seen in downregulation of HH pathway genes.

In order to investigate the consequences of differential gene expression at the neural progenitor stage on neuronal subtype specification, we terminally differentiated the SHH $^{-/-}$, NKX2.1 $^{-/-}$ and 33n1 control lines following both the LIA and 'default' patterning protocols and performed immunocytochemistry for MSN and interneuron markers.

Following differentiation using the LIA protocol ICC for co-expression of DARPP-32 and CTIP2, showed a reduction in MSNs ($F(2,307)=1271$, $p<0.0001$). This was seen in both SHH $^{-/-}$ (13.9% $\pm$ 8.2%) and NKX2.1$^{-/-}$ neurons (5.7% $\pm$ 4.3%) compared to control levels (54.5% ± 2.1%, $p<0.0001$).

Optimised dosing of SHH should be investigated as these data suggest that SHH may promote the terminal differentiation and or maturation of MSNs while during patterning (as seen in control NPCs) it downregulates LGE-enriched genes. Interestingly, in contrast to expectations from mouse studies, we did not observe an increase in MSNs in NKX2.1 $^{-/-}$ neurons. However, as seen in NKX2.1 $^{-/-}$ NPCs, SHH protein is still expressed, thus these cells may have been patterned to other cell types such as neurons generated within the POA or diagonal area, both of which provide sources of SHH within the developing telencephalon.

Previous MSN differentiation protocols have identified populations of TH$^+$ neurons (Comella-Bolla *et al.,* 2020; Cann *et al.,* 2021), and were presumed to be striatal interneurons (Huot & Parent 2007; Cossette et al., 2005). Consistent with these studies, a population of neurons (36.7% $\pm$ 13.1%) were immunoreactive for TH in control cultures. However, in SHH$^{-/-}$ and NKX2.1$^{-/-}$ neurons there was a significant reduction in TH$^+$ neurons

(10.6% ± 6.1%, 17.2% ± 9.8%, respectively, F(2,282)=127, p<0.0001). Within the mouse telencephalon two distinct embryonic domains generate TH-expressing neurons; the dLGE which generates TH^+ neurons of the OB (Yun et al., 2003) and the POA that generates TH^+ cells of the striatum and parts of the extended amygdala (Bupesh et al., 2013). As SHH is not expressed within the dLGE it is likely that the majority of control TH^+ cells are striatal and/or amygdala-like rather than OB-like. The reduction in TH^+ neurons in NKX2.1 $^{-/-}$cultures may be secondary to the reduction in SHH protein observed in NKX2.1 $^{-/-}$ NPCs or a direct consequence of NKX2.1 loss-of-function. NKX2.1 is required for cell type specification within the diencephalon, where NKX2.1 lineage cells differentiate to GABA+ve, NPY+ve and TH+ve neurons that populate the basal hypothalamus and is of this region (Phelps et al., 2003; Marin et al., 2002; Puelles & Rubenstein 2003; Yee et al., 2011).

We have seen that in 33n1 control lines at D16 ~60% cells express NKX2.1 (Figure 3.8E). In striatal interneurons NKX2.1 persists after terminal differentiation, and post-mitotic deletion of NKX2.1 in mice results in complete loss of MGE-derived striatal PV^+ and $CHAT^+$ interneurons (Bolam et al., 1984; Butt et al., 2008; Nobrega-Pereira et al., 2008). In control 33n1 cultures 48% ± 26.3% of neurons co-expressed GABA and CHAT which was reduced to 1% ± 1% and 26.5 ± 25.7% in $SHH^{-/-}$ and NKX2.1 $^{-/-}$cells, respectively (F(2,237)=107.2, p<0.0001, Figure 5.6A-B). Although there was a significant reduction in these population of cells in the NKX2.1 $^{-/-}$cultures, suggesting a striatal cholinergic phenotype, this reduction was even more profound in SHH $^{-/-}$ cells. These results are consistent with a striatal cholinergic phenotype as all cholinergic striatal interneurons are also $NKX2.1^+$ (Fragkouli et al., 2009; Magno et al., 2009; Magno et al., 2011; Flandin, Kimura & Rubenstein, 2010) and loss of NKX2.1 function from the SHH-expressing domain results in selective loss of striatal cholinergic interneurons (Kosaka et al., 1988; Obermayer et al., 2019; Bayraktar et al., 1997). It is however possible that these cells may be cortical interneurons which originate in the developing POA of which a subset also co-express CHAT and GABA (Granger *et al.,* 2020). It will be important to address the consequence of $SHH^{-/-}$ and $NKX2.1^{-/-}$ on other striatal interneuron populations in particular PV and SST when appropriate antibodies are available.

As both $SHH^{-/-}$ and $NKX2.1^{-/-}$ cultures showed a decrease in both MSN generation and interneuron specification at a protein level, we investigated whether gene expression

changes supported this observation. We selected 24 and 26 genes of interests (GOIs) known from the literature to be involved in the generation of LGE/MSN and interneuron fates respectively. Following normalisation, a heatmap was generated of the average ΔCT values, of which expression appears to be variable between $SHH^{-/-}$ and $NKX2.1^{-/-}$ clones (Figure 5.7A). As differences in LGE/MSN genes appear relatively consistent between clones, design matrixes were generated based on genotype (i.e. Control vs $SHH^{-/-}$ and Control vs $NKX2.1^{-/-}$) and the effect of SHH and NKX2.1 loss of function on overall gene expression was investigated.

Here, both SHH and NKX2.1 KO neurons downregulated HH pathway genes GLI-1, 2 and 3, GSX1, LHX6, NPY, SMO, and ZIC-1 and -3 (Figure5.7B). Consequently, there was an increase in LGE/striatal enriched genes, including ARPP21, DLX-5 and -6, DRD-1 and -2, GPR6, MEIS2, PENK1 and TAC1 (Figure 5.7C). Additionally, in NKX2.1 KO neurons there was also an increase in ADORA2A and a decrease in PTCH1 whereas in SHH KO neurons there was decrease in CHAT, NKX2.1, and SST (Figure 5.7B-C).

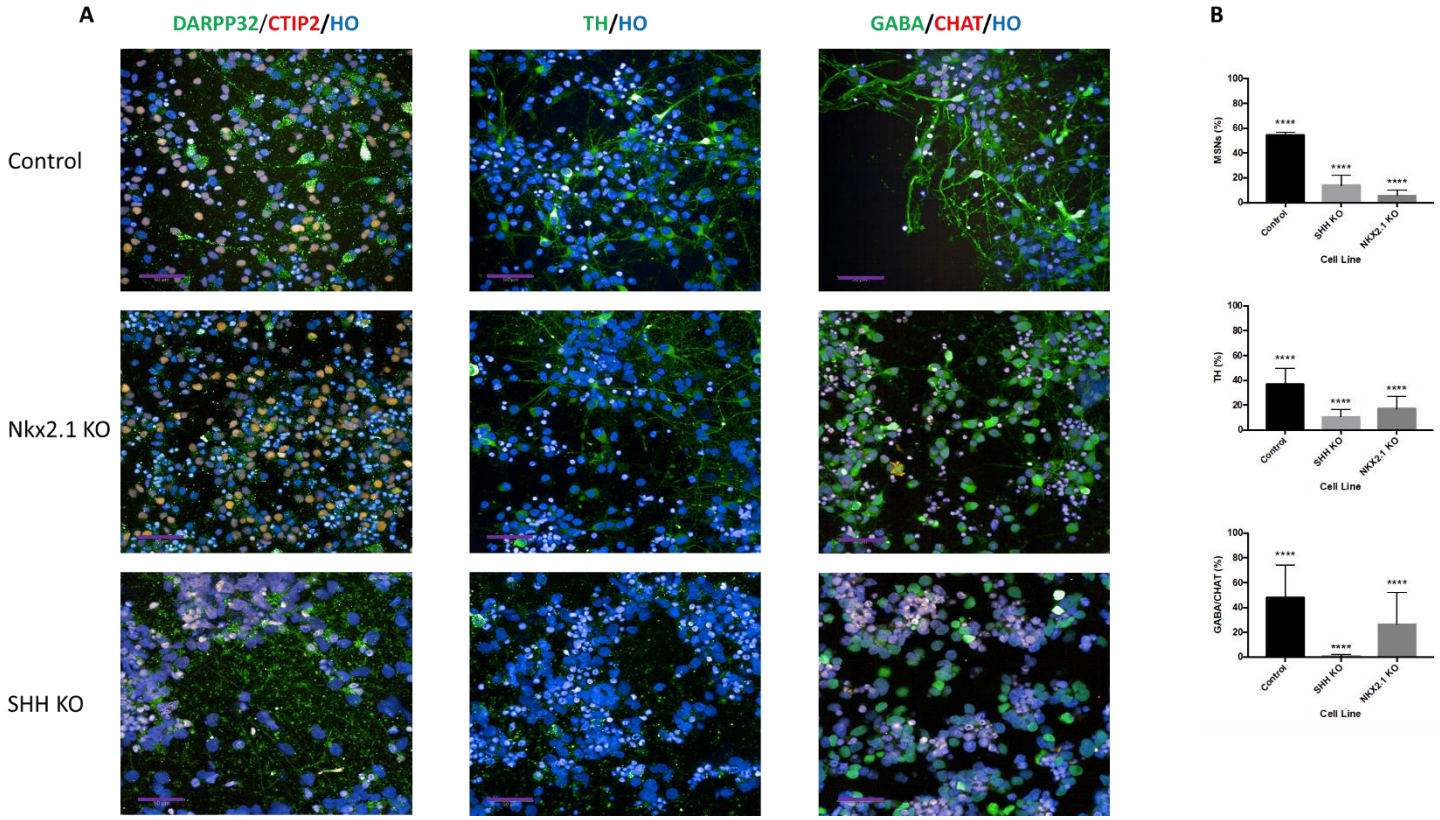

Figure 5.6: *Terminal differentiation of Control, SHH- and NKX2.1- KO cells following LIA protocol. A) Exemplar ICC images of co-expression of DARPP-32 and CTIP2 (MSNs), Tyrosine hydroxylase (TH, interneuron subclass) and CHAT/GABA (interneuron subclass (scale bar 50μm). B) Percentage of MSNs (DF=2, F=127.1) and interneuron subclasses (TH, DF=2, F=127.8; GABA/CHAT, DF=2, F=107.2) shows variation within all genotypes. Data was calculated from 3 independent differentiation and 56-149 fields of view and are presented as the mean with SD and one-way ANOVA with Tukey's multiple comparisons test. * p<0.05, ** p<0.01, *** p<0.001, **** p<0.0001.*

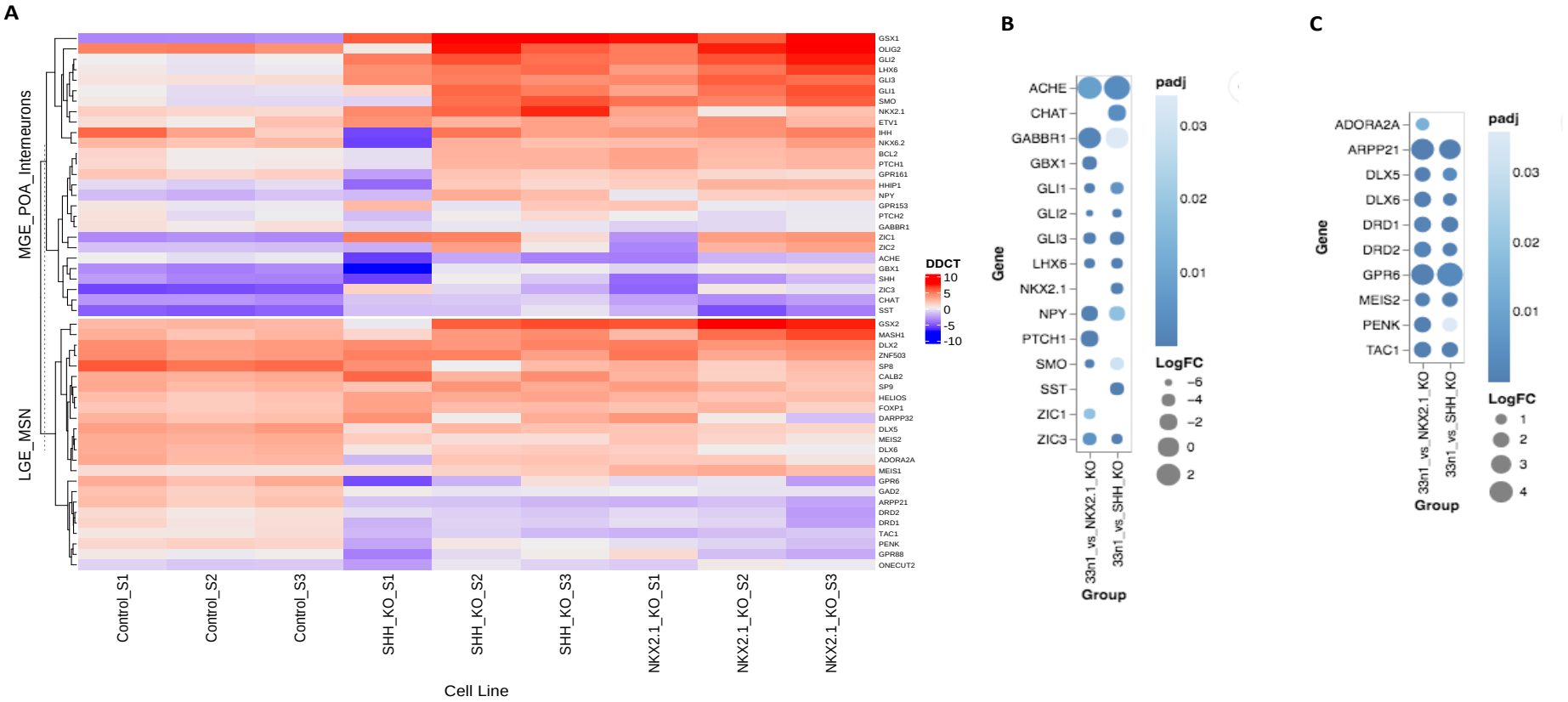

Figure 5.7: Control (33n1 parent line) SHH$^{-/-}$ and NKX2.1 $^{-/-}$ clones were differentiated under the LIA protocol and terminally differentiated for 3 weeks. A) LGE Heatmap of ΔCT values normalised to housekeeping gene and foetal expression. Dot plots were generated using R showing Log fold change and p-adjusted (BH, <0.05). Values are presented for HH signalling genes (B) and LGE/MSN genes (C).

Terminal differentiation of NKX2.1 KO cells following 'Default' patterning generated OB and or CTX neurons that express DARPP-32

Under 'default' patterning of SHH KO NPCs a robust downregulation of HH pathway genes was observed. In addition, a more enriched LGE mRNA transcript expression is achieved with potential bias towards DRD1-MSN. However, critical regulators of cortical excitatory neurons (NEUROD2, FOXG1) were also found to be expressed. In contrast, gene expression changes in NKX2.1 KO NPCs suggests that a population of cells characteristic of amygdala- and or OB- neuronal fates were generated.

In order to investigate whether default differentiation results in a pallial phenotype in the absence of endogenous SHH or NKX2.1 expression we selected a panel of genes known to be involved in LGE/MSN, cortical and neuronal subclass specification. A heatmap was generated of normalised ΔCT values across differentiation. (Figure 5.8A). No significant DEGs were observed when comparing control and SHH KO neurons. In contrast, in NKX2.1 KO neurons 8 and 1 DEGs were upregulated and downregulated, respectively.

Upregulated genes included MEIS2, ARPP21, FOXP1, DRD1, DRD2, PENK, and SP8 which have known function in MSN fate, however there was also a significant increase in VGLUT2 suggesting a glutamatergic fate (Figure 5.9B). Many of these genes are also broadly expressed within the human brain and have dual function in specification of alternative cell fates. For example, SP8 marks a specific population of OB GABAergic/non-dopaminergic populations of interneurons, and in conditional KO's there is a severe reduction in GABAergic interneuron subtypes in the OB (Waclaw et al., 2006). In addition, FOXP genes specify different neuronal populations in the mouse, such that FOXP1 co-localises with DARPP-32 and marks MSNs in the striatum but is also enriched in layers III-IV of the cerebral cortex (Precious et al., 2016; Ferland *et al.,* 2003; Hisaoka *et al.,* 2010). FOXP2 on the other hand is restricted to DARPP-32 neurons within layer VI neocortex, and with EBF1 is highly expressed in direct MSNs (Hisaoka et al., 2010; Ferland *et al.,* 2003; Lai *et al.,* 2003; Campbell *et al.,* 2009; Tinterri *et al.,* 2018). FOXP1 RNA and protein expression in the human brain, however, shows broad expression in the cortex with no regional and cell type specificity (https://www.proteinatlas.org/ENSG00000114861-FOXP1). Although there was no increase in DARPP-32 gene expression there was a significant increase in DRD1 and DRD2

in which DARPP-32 is specifically localised to neurons containing these receptors (Langley *et al.,* 1997; Gerfen *et al.,* 1990; Fink *et al.,* 1992) and some TH neurons express DRD2 in the OB (Koster *et al.,* 1999; Tillerson *et al.,* 2006). Therefore, we performed immunocytochemistry for DARPP-32 and TH to investigate whether these gene expression changes correlate at a protein level and are specific to NKX2.1 KO neurons. In this case, NKX2.1 KO neurons showed a significant increase in DARPP-32 and TH (63.8% $\pm$ 33.1%, 21.2% $\pm$ 17.2) compared to controls (23.9% $\pm$ 17.9, 3.3% $\pm$ 2.6) whereas there was no difference in expression in SHH KO neurons (23.3% $\pm$ 2.6, 1.1% $\pm$ 0.04%). Although we see DARPP-32^{+} positive cells in NKX2.1 KO neurons, these neurons clearly have a distinct morphology (Figure 5.9C) that is different from the control neurons that co-localise with CTIP2 and have previously be characterised as MSNs following LIA and LIAC protocols (Figure 3.1). DARPP-32 is also expressed in the cortex and these neurons exhibit a variety of shapes including triangular, rounded, ovalar or bipolar and are glutamatergic (Berger *et al.,* 1990). At a gene expression level, we observed and increase in VGLUT2, a marker of glutamatergic neuron. Taken together with the increase in DARPP-32 protein we hypothesis these neurons are cortical.

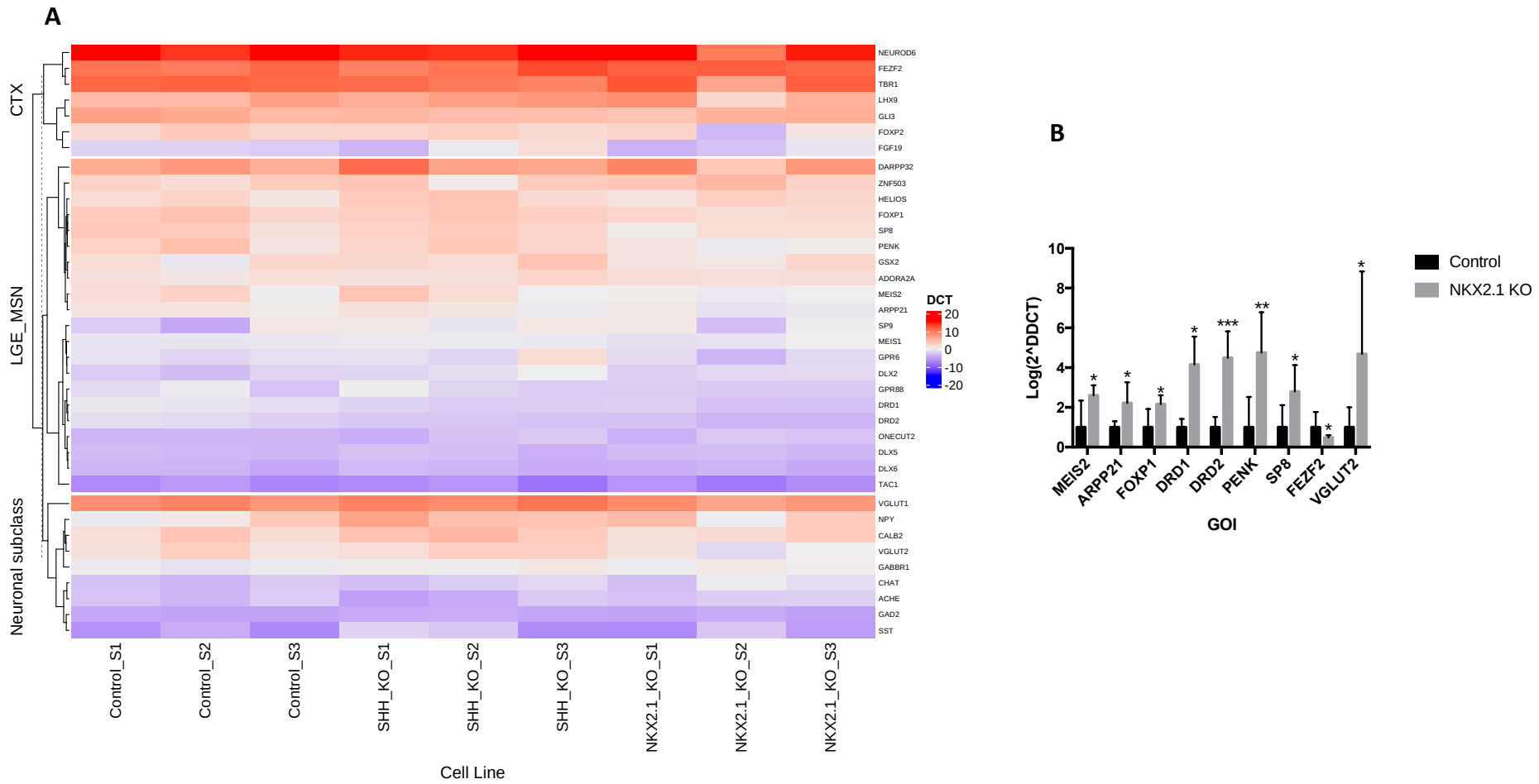

Figure 5.8: Control SHH$^{-/-}$ and NKX2.1 $^{-/-}$ clones (3 independent clones each) were differentiated under 'default' protocol and terminally differentiated for 3 weeks. A) LGE Heatmap of DCT values normalised to housekeeping gene and foetal expression. B) Bar plot of GOI with significance (BH, <0.05).

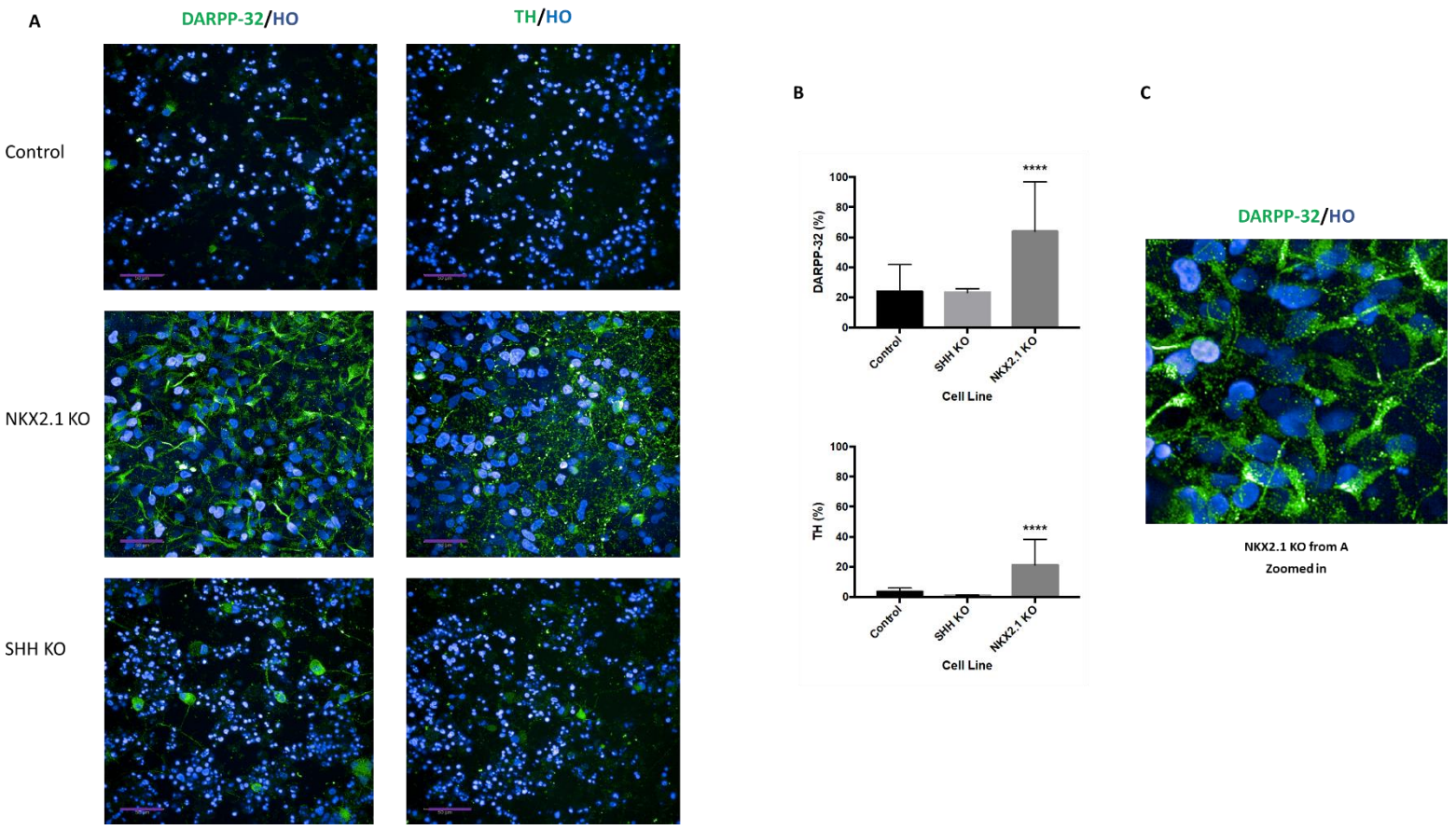

*Figure 5.9: Terminal differentiation of Control, SHH- and NKX2.1- KO cells following 'default' protocol. A) Exemplar ICC images of DARPP-32 and Tyrosine hydroxylase (TH, interneuron subclass (scale bar 50μm). B) Percentage of DARPP-32 ($F(2,507)=170.4$, $p<0.0001$) and TH ($F(2,417)=160.2$, $p<0.0001$). C) Zoomed in image from A) NKX2.1 KO. Data was calculated from 3 independent differentiation and 84-210 fields of view and are presented as the mean with SD and one-way ANOVA with Tukey's multiple comparisons test. * $p<0.05$, ** $p<0.01$, *** $p<0.001$, **** $p<0.0001$.*

Summary

We have generated SHH and NKX2.1 KO lines via CRISPR-Cas9 gene editing and successfully knocked out the proteins of interest. At a gene expression level following both LIA and 'default' protocols NPCs consistently and efficiently downregulate genes involved in HH pathway signalling and downstream effectors. However, at this stage differential expression of genes which are expressed at differing levels within the developing dorso-ventral LGE and/or POA proliferative zones of the telencephalon were also seen. Following terminal differentiation following the progenitor specification using the LIA protocol both SHH and NKX2.1 loss-of function results in a decrease in MSN generation, which is inconsistent with conditional knockout of these genes in the mouse, where removal of NKX2.1 results in an increase in the number of MSNs (Butt *et al.,* 2008; Nobrega-Pereira *et al.,* 2008) and where there is no effect of perturbing SHH-SMO signalling on LGE specification and subsequent MSN generation (Rallu *et al.,* 2002; Machold *et al.,* 2003; Xu *et al.,* 2010).

In addition, populations of TH or CHAT/GABA expressing interneurons were reduced in both SHH and NKX2.1 KO neurons. Considering the expression profile of further markers our data suggests that cells may be that of a cortical fate, however further analysis via ICC for glutamatergic and additional GABAergic markers will be required to confirm this.

Following 'default' patterning terminally differentiated NKX2.1 KO neurons generate DARPP-32^{+} neurons and are hypothesised to be that of a glutamatergic cortical fate.

Taken together, we hypothesise that SHH acts indirectly by generating differing populations of interneurons which intern support the MSNs present within the culture.

Chapter 6: Concluding remarks and Future Directions

The key findings of the studies presented in this thesis are –

1. The main source of variation in response to differentiation protocols between iPSC lines occurs during neuronal patterning of naïve neuroectodermal cells.

2. The main source of variation between lines in response to identical cues is due to endogenous SHH expression between D8-D16 of neuronal patterning.

3. Endogenous SHH expression during patterning biases cells to an MGE-like interneuron fate.

4. Inhibition of HH signaling during patterning corrects for some variation between cell lines and following terminal differentiation the percentage of MSNs is increased.

5. Knocking out SHH increases LGE-like and decreases MGE-like transcripts following patterning but failed to generate MSNs following terminal differentiation. Together, these results strongly suggest that SHH does not have a direct role in the patterning of LGE-like neural progenitor cells, however, it may act indirectly or at later stages during terminal differentiation to support the maintenance of MSNs.

6.1. Differential responses of cell lines to patterning cues occurs during neuronal patterning

We lack a comprehensive view of the molecular events regulating human iPSC neural progenitor progression to post-mitotic differentiation to an MSN-fate. A lot of time and effort is spent in different labs across the world in generating differentiation protocols which are then applied across different cell lines, generating outcomes and data of variable efficiency and meaning. To probe intrinsic developmental bias during iPSC differentiation, using multiple patterning and maturation cues, I initially sort to determine where during differentiation variation is first observed. To do this I used three control cell lines (33n1, Kolf2 and 18n6) and two differentiation protocols. Here, I have shown that intrinsic variability between lines appears early during neural progenitor specification (between D8-

D16) and can result in a differentiation bias to ventral telencephalic interneuron fates with differing efficiencies. High NKX2.1 expression, both at the mRNA and protein level, was observed within the 33n1 cell line, irrespective of the patterning cues used.

In vivo, NKX2.1 is absent from the LGE and CGE with strong expression in the MGE (Sussel *et al.,* 1999) where it has multifunctional roles during distinct temporal windows in fate determination and migration. SHH is a signalling morphogen with highest expression seen within the ventral telencephalon and acts to induce and maintain NKX2.1 (Ericson *et al.*, 1995; Dale *et al.*, 1997; Pera and Kessel, 1998; Sussel *et al.*, 1999). Therefore, my working hypothesis was that 33n1 cell line cultures possessed high endogenous SHH, which was supported by high mRNA expression of both SHH and its downstream target GLI1 within this line. Together these data suggest that endogenous SHH expression is biasing cells to an MGE-like fate during neuronal patterning.

6.2 Endogenous SHH expression is the main source of variation biasing cells to an alternative cell fate

To investigate whether SHH was the source of variability between the three cell lines and to deduce any other pathways that may be influencing cell fate, the three cell lines were studied using bulk RNA sequencing. The hypothesis that SHH was a source of variation within the 33n1 cell line was confirmed with a significant down-regulation of MGE-specific transcripts when the HH pathway was inhibited. In addition, no DEGs were identified when the HH pathway was inhibited using Cyclopamine in the Kolf2 and 18n6 cell lines suggesting that Cyclopamine had no off-target effects.

A further aim of this study was to compare the transcriptomes of differentiated iPSC cells to datasets derived from primary human fetal LGE or MGE . In order to reduce noise within these samples (i.e high expression of gene enriched within glia, oligodendrocytes etc.) initially fetal datasets were compared to each other and pathways enriched within these areas were investigated. Whilst none of the cell lines or treatments clustered with fetal LGE, this was concluded to be due to the immature state of the cell cultures. The 33n1 cell line on the other hand clustered with that of the MGE HH pathway genes (LI and LIA treatment) and non-canonical WNT pathway (LIA and LIAC treatment). The finding that non-canonical WNT signalling may play a role in human MGE development was novel and further investigation is warranted.

As Cyclopamine was sufficient to inhibit the HH pathway, the 33n1 cell line under this condition (LIAC) clustered away from that of fetal MGE and there was no detectable off-target effect within the 18n6 and Kolf2 cell lines, this protocol was investigated further following terminal differentiation. High and consistent populations of MSNs were generated (DARPP-32/CTIP2 +ve) in all three cell lines. However, inter-line variation was still detectable with possible bias towards DRD2-expressing MSNs. Preliminary results suggest a role for BMP signalling in the generation of DRD1-expressing MSNs. Further replication of this finding is needed.

Whilst this is the first in-depth investigation into endogenous differentiation bias affecting MSN subtype specification, others have recently reported differential expression of endogenous WNT and HH signalling between cell lines that affected cortical differentiation (Strano et al. 2020). This large study of 162 differentiation outcomes, using 61 iPSCs lines derived from 37 individuals revealed variable cell line bias to either a dorsal (EMX1, TBR1, NEUROG2) or ventral-like fate (NKX2.1, LHX6/8, DLX1/5) that occurred early in NPC specification (D12-D17), consistent with our observations at D16.

Although Strano *et al.*, identified HH signalling as a source of variation, some inconsistencies were seen between their results and our own. Notably, treatment of a highly ventralised line with Cyclopamine (1mM) from D7-D17 had no effect on ventral gene expression, whereas activating the canonical WNT pathway with the addition of CHIR99021 between D13-D17 resulted in >5-fold reduction in LHX8 and NKX2.1 following terminal differentiation. These differences may lie in the broader context of the differentiation protocols used, for example interaction or crosstalk between pathways regulated by Activin and LDN/IWR1 (in LIAC medium) that aimed to limit dorsal fate, compared to the use of medium that aimed to promote dorsal fate specification using a 'default' cortical differentiation protocol in the context of WNT pathway activation.

In a further study, Jerber *et al*. (2021) used population–scale single-cell RNA sequencing to analyse the efficiency and inter-line variability of neuronal differentiation, from 215 iPSC lines from the HipSci project, to generate midbrain-like dopaminergic and serotoninergic neurons, as well as with cortical neuron differentiation in cerebral organoids. Using this unparalleled data set Jerber *et al*., showed that the major sources of variation in differentiation outcomes related to differences that were intrinsic to the cell lines used.

Perhaps surprisingly, by comparing replicate cell lines derived from the same donors, they found that genetic or other donor-specific components did not account significantly for observed variability. Instead, 13% of iPSC lines expressed a single cell RNAseq expression profile that was predictive of poor neuronal differentiation potential (e.g. characterized by higher UTF1 and low TAC3 expression).

6.3. SHH is required for interneuron specification and may act indirectly during terminal differentiation to support MSNs

A purpose of this study was to confirm, genetically, with the use of CRISPR-Cas9 gene editing, the findings in chapter 4. To do this I generated SHH knockout lines from the 33n1 parent line. In addition, to investigate whether endogenous SHH expression has a role in LGE NPC specification in the absence of NKX2.1, NKX2.1 was knockout in the 33n1 parent line. Following LIA protocol differentiation gene expression patterns in the SHH knockout lines were similar to that observed with the use of Cyclopamine with the increase in LGE and decrease in MGE transcripts, whereas in NKX2.1 knockout lines only HH target genes were decreased. Following a 'default' differentiation protocol, where no additional factors are supplemented into the base medium, efficient downregulation of genes downstream of the HH pathway was also observed. It was hypothesised that following terminal differentiation SHH knockout lines, following the LIA protocol, would generate MSNs, similar to those observed with the use of Cyclopamine. However, there was a decrease in MSN population following LIA protocol in both SHH and NKX2.1 knockout lines. Conditional knockout of NKX2.1 within the mouse MGE results in an increase in MSN population in the striatum (Butt *et al.,* 2008; Nobrega-Pereira *et al.,* 2008), whereas disruption to SHH-SMO signalling has no effect on MSN generation (Rallu *et al.,* 2002; Machold *et al.,* 2003; Xu *et al.,* 2010). This is inconsistent with the in vitro findings in this study. Consistent with the requirement of NKX2.1 and SHH in specification of MGE-derived interneurons (Butt *et al.,* 2008; Xu *et al.,* 2005), I showed that knockout of these genes results in reduction of TH or CHAT/GABA expressing interneurons. Taken together, I hypothesise that SHH may act indirectly by generating differing populations of interneurons and or astrocytes which intern support the MSNs present within the culture. Further work is needed to assess other populations of cell present in these cultures. Future work will benefit from terminally differentiating SHH knockout lines following LIA protocol in the presence of SHH to elucidate whether SHH has a role following cell cycle exit.

This thesis addressed the intrinsic differences in line-to-line variations in cell signalling and differentiation and identified endogenous SHH signalling as a major contributing variable. Using this information, we were able to optimise differentiation protocols to enable more efficient generation of MSNs and importantly with reduced variability.

The rigorous analysis in this thesis demonstrates that individual protocols must be optimised for individual cell lines, considering intrinsic differences in line-to-line variations in cell signalling. This will be particularly critical in studies that aim to identify differences in gene expression and function that are disease attributes and independent of individual cell line differences.

Others have reported a delay in exit from pluripotency, neural induction, and gene expression changes consistent with delayed maturation in HD iPSC lines with large CAG repeats (HD IPSC Consortium, 2017; Conforti *et al.,* 2018; Mattis *et al.,* 2015). However, it is also possible that these phenotypes may be a result of endogenous expression of signalling morphogens. I have demonstrated that in HD109 and isogenic control lines, have a similar mRNA expression profile following patterning and terminal differentiation. However, analysis of HD60 lines, compared to their sibling controls, 33n1 lines, there was a significant difference in HH pathway genes following patterning and terminal differentiation. Interestingly, following patterning, the 33n1 line showed highest HH pathway target gene expression whereas the opposite was shown following terminal differentiation and higher mRNA expression was seen in the HD60 lines. This work illustrates the need for isogenic controls for HD lines and will enable more precise and consistent phenotypic analysis of the effect of CAG length. Without the constraints of differing biological backgrounds and endogenous expression of signalling morphogens effecting differentiation there will be increased confidence that changes in gene expression are the result of CAG length and not misinterpretation of results.

6.4 Future work

1) Further understanding of neuronal heterogeneity in iPSC-derived neural cultures and derivation of direct and in-direct pathway MSN subtypes.

Selective generation of DRD1- and DRD2- expressing MSNs

In recent years, many directed-differentiation protocols have been developed to generate a diversity of IPSC-derived neurons. Despite strong evidence for the appropriate specification of several different neuronal progenitor subtypes, relatively little attention has been paid to post-mitotic development and in *vitro* maturation protocols tailored to different neuronal subtype physiologies, functional maturation, or ageing. Typically, neural progenitors will be plated onto a poly-cationic/laminin substrates in derivatives of Neurobasal media with neurotrophins and B27 supplements. Commonly terminal differentiation and neuronal maturation proceeds over a period of months, with the emergence of increasing cell heterogeneity. Protocols that significantly accelerate and synchronise differentiation by forced cell-cycle exit and treatment with small molecules that target NOTCH, WNT and CREB pathways to promote neurogenesis have been developed (Telezhkin et al. 2016). Furthermore, media compositions have been optimised to improve physiological maturation (Bardy et al. 2015). However, these advances address pan-neuronal development and do not address aspects of subtype-specific neurogenesis and maturation. For MSNs, it is clear from studies in mice that additional developmental pathways regulate the post-mitotic diversification of MSNs to direct (Drd1-like) and indirect (Drd2-like) pathway projection neurons (Lu et al. 2016; Brady and Vaccarino 2021).

Currently no protocols have been developed that specifically generate DRD1- or DRD2-MSNs from control or HD iPSCs and cell models are limited by uncharacterised cellular heterogeneity. Consequently, phenotypes may not be specific and could compromise data interpretation, affecting insights into the basis of mHTT toxicity and applications such as drug development. The ability to differentially model Drd1 and Drd2 MSN subpopulations is important as they show different vulnerabilities to degeneration during the course of HD disease progression. *Drd2-expressing striatopallidal "indirect pathway" MSNs display higher vulnerability in HD patients* (Reiner et al. 1988; Albin et al. 1990). It is possible that other, less vulnerable cell types possess protective intrinsic factors or adaptive responses that iSPNs lack or that iSPNs possess unique vulnerability factors or neurotoxic responses, knowledge of which may point to new HD therapeutic targets. Across many neurodegenerative diseases, not just HD, the basis of enhanced or selective neuronal

vulnerability is not well understood. Thus, cell type-specific transcriptional studies across HD and HD models may provide a paradigm for future studies in other disease models.

In order to address the question of differential MSN vulnerability it is essential to gain a better understanding of MSN diversity and to not only generate high yields of MSNs but also the different subtypes that are present *in vivo.* Recently, through single cell RNA sequencing and Fluorescent In-Situ Hybridization (FISH), it has been possible to distinguish five types of MSNs in the non-human primate dorsal striatum (He et al. 2021). It was found that DRD1- and DRD2-MSNs within the striatosome are enriched in KCNT1, KHDRBS3, FAM163A, BACH2, and KCNIP1, whereas in the matrix, EPHA4, GDA, STXBP6, and SEMA3E genes were enriched. In addition, the striatosome MSNs could be further subdivided based on their expression of *PDYN* and *POU6F2* which were enriched in DRD1- and DRD2-MSN, respectively. Furthermore, the fifth identified subtype expressed both DRD1 and DRD2 (DRD1/DRD2 hybrid) accounting for ~1% of the population of MSNs, confirming observations found in the rodent striatum (Saunders et al. 2018; Märtin et al. 2019; Stanley et al. 2020). With these specific markers it would be possible to generate reporter cell lines to investigate not only selective vulnerability, i.e DRD1 verse DRD2 MSN, but also matrix verses striatosome.

In addition, looking at upstream regulators and signalling pathways may enable optimised protocols supporting the growth, survival, and maturation of these different populations. While we observed an increase in DRD1 mRNA with the addition of BMP-6 in our extended NPC culture following terminal differentiation, and functional DRD1 receptor expression with the use of a fluorescent DRD1 agonist. The mechanism of action needs to be addressed and also replicated in additional lines. It is possible that BMP-6 is acting indirectly as it has been shown in rat primary striatal cultures (Gratacòs et al. 2002). This can be investigated by firstly assessing the population of $GFAP^{+}$ astrocytes present in the cultures, and secondly by treating cultures with BMP-6 in the presence of 5-fluorodeoxyuridine, a thymidine analogue, which kills mitotically active astrocytes.

Functional profiling of DRD1- and DRD2- expressing MSNs

At a functional level, DRD1 and DRD2 MSNs have different electrophysiological profiles. Utilising bacterial artificial chromosome (BAC) transgenic mice expressing enhanced green

fluorescent protein (eGFP) under the control of promoters for the DRD1 and DRD2, a number of electrophysiological properties have been shown to be significantly different, including RMP (Gertler et al. 2008), action potential threshold (Goodliffe et al. 2018), and frequency of evoked action potentials (Ade et al. 2008; Gertler et al. 2008). Yet this has not been assessed in iPSC-derived neurons from control or HD lines. Studies typically group electrophysiological properties based on genotype and dismiss the heterogeneity of the cultures. Indeed, in many studies electrophysiological recordings of neurons derived from an MSN differentiation protocol are presumed to be from MSNs, even if DARPP32 +ve neurons represent only a minority of the neurons present, and without retrospective identification of the patched neurons. This is particularly problematic for drug screening, as phenotypes and/or selectivity and likely obscures differences between HD and controls.

2) Modelling age-associate phenotypes in iPSC-derived neurons

A fundamental limitation of iPSC reprogramming is erasure of epigenomic signatures of ageing which are present in the parent somatic cell counterparts. Global epigenetic changes include CpG DNA methylation and histone lysine and arginine tail modification (Kim et al. 2010; Papp and Plath 2013). Upon iPSC differentiation and maturation neurons exhibit foetal characteristics even after prolonged months of *in vitro* culture (Imm et al. 2021). It is well established that age-related epigenetic changes are strongly associated with physiological changes that occur with age and contribute to the onset and progression of diseases such as AD, PD and HD, where age is a major risk factor. Strikingly, life-long epigenetic change is highly predictable, to the extent that genome-wide DNA methylation profiles provide an 'epigenetic clock' that is highly predictive of a person's chronological age.

In collaboration with Katie Lunnon (Exeter university) we have profiled genome-wide DNA methylation of 33n1 iPSCs, NPCs and cortical neurons at D37 and D58. This analysis identified DNA methylation changes associated with iPSC-to-neuronal differentiation and also showed that cultures acquired a methylome equivalent to a foetal chronological age of ~100-120 days post conception (Imm et al. 2021; Steg et al. 2021). Despite often showing good levels of functional spontaneous activity (e.g., in studies by Bardy *et al*. (2015) and Telezhkin *et al*. (2016)), this study highlights the fact that iPSC derived neurons lack significant molecular (and consequently functional) maturity.

Chronological maturity and the ability to model age-associated disease mechanisms and pathology is therefore a fundamental challenge for iPSC technology. Studies using iPSC models of AD, PD and HD all show failures to recapitulate hallmark features of age-related diseases such disease-specific protein aggregation (β-amyloid, a-synuclein, mHTT respectively) (Victor et al. 2018). Typically, even after extended time in culture, additional cellular stressors are needed to elicit disease-specific phenotypes, for example, although mHTT aggregates are considered a hallmark of HD, this phenotype is only observed upon proteasome inhibition in iPSC-derived neurons (Cheng et al. 2013; Nekrasov et al. 2016). This becomes problematic in a phenotypically and epigenetically immature neuron as this does not accurately model in vivo disease processes in which dysregulation of post-translational modifications precedes that of protein aggregation (Steffan et al. 2004; Yanai et al. 2006; Chaibva et al. 2016; Arbez et al. 2017; Martin et al. 2018).

It is possible that the problem of age-associated disease modelling using iPSCs could be addressed using innovative approaches that accelerate, or promote the development of, age-associated cell and molecular phenotypes in cells in culture. However, this is a significant challenge, as to be authentic, artificially aged models would need to show a broad spectrum of phenotypes that encompass the range of epigenetic, metabolic, transcriptomic, proteomic (and other 'omic') changes that occur as an integrated consequence of ageing.

One genetic approach to model ageing has taken advantage of the mutation that induces premature-aging in Hutchinson-Gilford Progeria Syndrome (HGPS; Hutchinson 1886; Gilford and Hutchinson 1897). HGPS is a rare autosomal dominant disease caused by a mutation in the laminA gene (LMNA) resulting in constitutive production of progerin which disrupts the nuclear lamina and nuclear function. Thus, overexpression of progerin induces age-associated phenotypes including impacts of dysregulated DNA repair mechanisms, chromatin remodelling and gene expression. Transcriptome analysis of hESC-derived postmitotic neurons over-expressing progerin identified genes involved in DNA double-stranded break repair via break-induced replication (3/5 DEGs) and homologous recombination (6/46 DEGs), cell cycle (37/605 DEGs) and DNA helicase activity (6/22 dDEGs). In addition, mitochondrial defects are induced by progerin with both structural

changes (mitochondrial swelling) and an increased generation of reactive oxygen species (Miller et al. 2013).

When applied to HD- and control-iPSC derived 'Striatal' GABAergic neurons, progerin overexpression caused a significant increase in the number of differentially expressed genes in HD vs Control comparisons ($p<0.01$), with the interpretation that 'induced ageing' exacerbated disease-specific changes (Cohen-Carmon et al. 2020). Whilst it is clear that progerin induces some age-associate phenotypes and cell stress, it is less clear that changes observed reflect those relevant to natural progressive ageing. Importantly, there is no correlation between age and progerin expression levels during normal aging (McClintock et al. 2007) and progeria is not associated with accelerated DNA methylation age (Horvath 2013). In addition, LMNA gene expression is increased in late-stage AD (Méndez-López et al. 2019) and thus the use of progerin would not be physiological or provide an authentic ageing, at least for AD .

An alternative strategy to 'accelerate' age is metabolic and/or epigenetic programming. Using the concept of 'directed differentiation' where the sequential provision of developmental cues directs cell differentiation through a developmental pathway of choice, protocols may be developed to direct cells through natural stages of metabolic and epigenetic change to bring cells into an 'aged' state. One candidate approach that has been applied extensively *in vivo* to accelerate age is the treatment of animals with D-Galactose (D-Gal; reviewed in (Shwe et al. 2018)). D-Gal changes cellular metabolism by inducing a shift in energy dependency towards mitochondrial oxidative phosphorylation (MacVicar and Lane 2014) and is known to induce cellular senescence and premature ageing in mammalian cells. This may be particularly relevant to modelling age in neuronal cultures as D-Gal treatment effectively models the balance of energy dependency from glycolysis to oxidative phosphorylation (OXPHOS) to impaired OXPHOS as seen in aged neurons (Mertens et al. 2018). Hallmarks of ageing induced by D-Gal include impaired mitochondrial and lysosomal function, autophagy and impaired redox homeostasis leading to oxidative stress (Shwe et al. 2018). To date, D-Gal has only been used as a method of inducing cellular aging in immortalised cell lines and primary neuronal cultures. We have therefore established protocols for IPSC neuronal maturation (Telezhkin et al. 2016), which upon treatment with D-Gal replicate key mitochondrial, lysosomal, and redox impairments without affecting cell

viability. For example, D-Gal induced phenotypes including reduced mitotracker staining, reduced basal respiration, ATP production and spare respiratory capacity (Seahorse Bioanalyser), basal autophagy (CytoID staining), reduced lysosomal protease activity (magic red Cathepsin B – magic red staining), and elevated lysotracker staining indicative of lysosomal accumulation of unprocessed material. Impaired lysosomal function was also supported by the appearance of punctate Thioflavin T staining indicating accumulation of protein aggregates. Data from these preliminary studies are shown in Appendix 1. Although the data require further replication, they are encouraging and support the notion that directed approaches to manipulate *in vitro* culture conditions that alter cell metabolism might induce aged phenotypes following more physiological pathways. In future experiment we would test the hypothesise that D-Gal treatment would impact DNA methylation through its down regulation of the NAD+/Sirtuin pathway (Mertens et al. 2018).

References

Albin, R. L., & Greenamyre, J. T. (1992). Alternative excitotoxic hypotheses. *Neurology*, *42*(4), 733–738. https://doi.org/10.1212/wnl.42.4.733

Albin, R. L., Reiner, A., Anderson, K. D., Penney, J. B., & Young, A. B. (1990). Striatal and nigral neuron subpopulations in rigid Huntington's disease: Implications for the functional anatomy of chorea and rigidity-akinesia. *Annals of Neurology*, *27*(4), 357–365. https://doi.org/10.1002/ana.410270403

Alifragis, P., Liapi, A., & Parnavelas, J. G. (2004). Lhx6 regulates the migration of cortical interneurons from the ventral telencephalon but does not specify their GABA phenotype. *The Journal of Neuroscience : The Official Journal of the Society for Neuroscience*, *24*(24), 5643–5648. https://doi.org/10.1523/JNEUROSCI.1245-04.2004

Arber, C., Precious, S. v., Cambray, S., Risner-Janiczek, J. R., Kelly, C., Noakes, Z., Fjodorova, M., Heuer, A., Ungless, M. A., Rodríguez, T. A., Rosser, A. E., Dunnett, S. B., & Li, M. (2015). Activin a directs striatal projection neuron differentiation of human pluripotent stem cells. *Development (Cambridge)*, *142*(7), 1375–1386. https://doi.org/10.1242/DEV.117093/-/DC1

Arbez, N., Ratovitski, T., Roby, E., Chighladze, E., Stewart, J. C., Ren, M., Wang, X., Lavery, D. J., & Ross, C. A. (2017). Post-translational modifications clustering within proteolytic domains decrease mutant huntingtin toxicity. *The Journal of Biological Chemistry*, *292*(47), 19238–19254. https://doi.org/10.1074/JBC.M117.782300

Asgarian, Z., Magno, L., Ktena, N., Harris, K. D., & Kessaris, N. (2019). Hippocampal CA1 Somatostatin Interneurons Originate in the Embryonic MGE/POA. *Stem Cell Reports*, *13*(5), 793–802. https://doi.org/10.1016/J.STEMCR.2019.09.008

Aubry, L., Bugi, A., Lefort, N., Rousseau, F., Peschanski, M., & Perrier, A. L. (2008). Striatal progenitors derived from human ES cells mature into DARPP32 neurons in vitro and in quinolinic acid-lesioned rats. *Proceedings of the National Academy of Sciences of the United States of America*, *105*(43), 16707–16712. https://doi.org/10.1073/pnas.0808488105

Banghart, M. R., Neufeld, S. Q., Wong, N. C., & Sabatini, B. L. (2015). Enkephalin Disinhibits Mu Opioid Receptor-Rich Striatal Patches via Delta Opioid Receptors. *Neuron*, *88*(6), 1227–1239. https://doi.org/10.1016/J.NEURON.2015.11.010

Baydyuk, M., Nguyen, M. T., & Xu, B. (2011). Chronic deprivation of TrkB signaling leads to selective late-onset nigrostriatal dopaminergic degeneration. *Experimental Neurology*, *228*(1), 118–125. https://doi.org/10.1016/J.EXPNEUROL.2010.12.018

Baydyuk, M., Xie, Y., Tessarollo, L., & Xu, B. (2013). Midbrain-derived neurotrophins support survival of immature striatal projection neurons. *The Journal of Neuroscience : The Official Journal of the Society for Neuroscience*, *33*(8), 3363–3369. https://doi.org/10.1523/JNEUROSCI.3687-12.2013

Benn, C. L., Fox, H., & Bates, G. P. (2008). Optimisation of region-specific reference gene selection and relative gene expression analysis methods for pre-clinical trials of Huntington's disease. *Molecular Neurodegeneration*, *3*(3). https://doi.org/10.1186/1750-1326-3-17

Berger, A. J. (1990). Recent advances in respiratory neurobiology using in vitro methods. *American Journal of Physiology - Lung Cellular and Molecular Physiology*, *259*(2 3-1). https://doi.org/10.1152/ajplung.1990.259.2.l24

Bergsland, M., Werme, M., Malewicz, M., Perlmann, T., & Muhr, J. (2006). The establishment of neuronal properties is controlled by Sox4 and Sox11. *Genes & Development*, *20*(24), 3475–3486. https://doi.org/10.1101/GAD.403406

Bolam, J. P. (1984). Synapses of identified neurons in the neostriatum. *Ciba Foundation Symposium*, *107*, 30–47. https://doi.org/10.1002/9780470720882.CH3

Britto, J., Tannahill, D., & Keynes, R. (2002). A critical role for sonic hedgehog signaling in the early expansion of the developing brain. *Nature Neuroscience*, *5*(2), 103–110. https://doi.org/10.1038/NN797

Bupesh, M., Vicario, A., Abellán, A., Desfilis, E., & Medina, L. (2014). Dynamic expression of tyrosine hydroxylase mRNA and protein in neurons of the striatum and amygdala of mice, and experimental evidence of their multiple embryonic origin. *Brain Structure & Function*, *219*(3), 751–776. https://doi.org/10.1007/S00429-013-0533-7

Butt, E. (2009). cGMP-dependent protein kinase modulators. *Handbook of Experimental Pharmacology*, *191*(191), 409–421. https://doi.org/10.1007/978-3-540-68964-5_17

Castelo-Branco, G., Wagner, J., Rodriguez, F. J., Kele, J., Sousa, K., Rawal, N., Pasolli, H. A., Fuchs, E., Kitajewski, J., & Arenas, E. (2003). Differential regulation of midbrain dopaminergic neuron development by Wnt-1, Wnt-3a, and Wnt-5a. *Proceedings of the National Academy of Sciences of the United States of America*, *100*(22), 12747–12752. https://doi.org/10.1073/pnas.1534900100

Chaibva, M., Jawahery, S., Pilkington, A. W., Arndt, J. R., Sarver, O., Valentine, S., Matysiak, S., & Legleiter, J. (2016). Acetylation within the First 17 Residues of Huntingtin Exon 1 Alters Aggregation and Lipid Binding. *Biophysical Journal*, *111*(2), 349–362. https://doi.org/10.1016/J.BPJ.2016.06.018

Chen, G., Gulbranson, D. R., Hou, Z., Bolin, J. M., Probasco, M. D., Smuga-otto, K., Howden, S. E., Nicole, R., Propson, N. E., Wagner, R., Lee, G. O., Teng, J. M. C., & Thomson, J. a. (2011). Chemically defined conditions for human iPS cell derivation and culture. *Nature Methods*, *8*(5), 424–429. https://doi.org/10.1038/nmeth.1593.Chemically

Ciarochi, J. A., Calhoun, V. D., Lourens, S., Long, J. D., Johnson, H. J., Bockholt, H. J., Liu, J., Plis, S. M., Paulsen, J. S., & Turner, J. A. (2016). Patterns of Co-Occurring Gray Matter Concentration Loss across the Huntington Disease Prodrome. *Frontiers in Neurology*, *7*(SEP). https://doi.org/10.3389/FNEUR.2016.00147

Cohen-Carmon, D., Sorek, M., Lerner, V., Divya, M. S., Nissim-Rafinia, M., Yarom, Y., & Meshorer, E. (2020). Progerin-Induced Transcriptional Changes in Huntington's Disease Human Pluripotent Stem Cell-Derived Neurons. *Molecular Neurobiology*, *57*(3), 1768–1777. https://doi.org/10.1007/S12035-019-01839-8

Comella-Bolla, A., Orlandi, J. G., Miguez, A., Straccia, M., García-Bravo, M., Bombau, G., Galofré, M., Sanders, P., Carrere, J., Segovia, J. C., Blasi, J., Allen, N. D., Alberch, J., Soriano, J., & Canals, J. M. (2020). Human Pluripotent Stem Cell-Derived Neurons Are Functionally Mature In Vitro and Integrate into the Mouse Striatum Following Transplantation. *Molecular Neurobiology*, *57*(6), 2766–2798. https://doi.org/10.1007/S12035-020-01907-4

Cossette, P., Lortie, A., Vanasse, M., Saint-Hilaire, J. M., & Rouleau, G. A. (2005). Autosomal dominant juvenile myoclonic epilepsy and GABRA1. *Advances in Neurology*, *95*, 255–263. https://pubmed.ncbi.nlm.nih.gov/15508928/

Dale, J. K., Vesque, C., Lints, T. J., Sampath, T. K., Furley, A., Dodd, J., & Placzek, M. (1997). Cooperation of BMP7 and SHH in the Induction of Forebrain Ventral Midline Cells by Prechordal Mesoderm. *Cell*, *90*(2), 257–269. https://doi.org/10.1016/S0092-8674(00)80334-7

de Angelis, F., Bernardo, A., Magnaghi, V., Minghetti, L., & Tata, A. M. (2012). Muscarinic receptor subtypes as potential targets to modulate oligodendrocyte progenitor survival, proliferation, and differentiation. *Developmental Neurobiology*, *72*(5), 713–728. https://doi.org/10.1002/DNEU.20976

Dennler, S., André, J., Alexaki, I., Li, A., Magnaldo, T., ten Dijke, P., Wang, X.-J., Verrecchia, F., & Mauviel, A. (2007). Induction of Sonic Hedgehog Mediators by Transforming Growth Factor-β: Smad3-Dependent Activation of *Gli2* and *Gli1* Expression *In vitro* and *In vivo*. *Cancer Research*, *67*(14), 6981–6986. https://doi.org/10.1158/0008-5472.CAN-07-0491

DiRenzo, D. M., Chaudhary, M. A., Shi, X., Franco, S. R., Zent, J., Wang, K., Guo, L.-W., & Kent, K. C. (2016). A crosstalk between TGF-β/Smad3 and Wnt/β-catenin pathways promotes vascular smooth muscle cell proliferation. *Cellular Signalling*, *28*(5), 498–505. https://doi.org/10.1016/j.cellsig.2016.02.011

Ehrman, L. A., Mu, X., Waclaw, R. R., Yoshida, Y., Vorhees, C. v., Klein, W. H., & Campbell, K. (2013). The LIM homeobox gene Isl1 is required for the correct development of the striatonigral pathway in the mouse. *Proceedings of the National Academy of Sciences*, *110*(42), E4026–E4035. https://doi.org/10.1073/pnas.1308275110

Epping, E. A., Kim, J. I., Craufurd, D., Brashers-Krug, T. M., Anderson, K. E., McCusker, E., Luther, J., Long, J. D., & Paulsen, J. S. (2016). Longitudinal psychiatric symptoms in prodromal Huntington's disease: A decade of data. *American Journal of Psychiatry*, *173*(2), 187–192. https://doi.org/10.1176/appi.ajp.2015.14121551

Ericson, J., Muhr, J., Placzek, M., Lints, T., Jessel, T. M., & Edlund, T. (1995). Sonic hedgehog induces the differentiation of ventral forebrain neurons: A common signal for ventral

patterning within the neural tube. *Cell*, *81*(5), 747–756. https://doi.org/10.1016/0092-8674(95)90536-7

Espuny-Camacho, I., Michelsen, K. A., Gall, D., Linaro, D., Hasche, A., Bonnefont, J., Bali, C., Orduz, D., Bilheu, A., Herpoel, A., Lambert, N., Gaspard, N., Péron, S., Schiffmann, S. N., Giugliano, M., Gaillard, A., & Vanderhaeghen, P. (2013). Pyramidal neurons derived from human pluripotent stem cells integrate efficiently into mouse brain circuits in vivo. *Neuron*, *77*(3), 440–456. https://doi.org/10.1016/J.NEURON.2012.12.011

Faull, R. L. M., Waldvogel, H. J., Nicholson, L. F. B., & Synek, B. J. L. (1993). The distribution of GABAA-benzodiazepine receptors in the basal ganglia in Huntington's disease and in the quinolinic acid-lesioned rat. *Progress in Brain Research*, *99*(C), 105–123. https://doi.org/10.1016/S0079-6123(08)61341-2

Ferland, R. J., Cherry, T. J., Preware, P. O., Morrisey, E. E., & Walsh, C. A. (2003). Characterization of Foxp2 and Foxp1 mRNA and protein in the developing and mature brain. *The Journal of Comparative Neurology*, *460*(2), 266–279. https://doi.org/10.1002/CNE.10654

Ferrer, I., Goutan, E., Marín, C., Rey, M. J., & Ribalta, T. (2000). Brain-derived neurotrophic factor in Huntington disease. *Brain Research*, *866*(1–2), 257–261. http://www.ncbi.nlm.nih.gov/pubmed/10825501

Fields, R. D., Dutta, D. J., Belgrad, J., & Robnett, M. (2017). Cholinergic signaling in myelination. *Glia*, *65*(5), 687–698. https://doi.org/10.1002/GLIA.23101

Fietz, M. J., Jacinto, A., Taylor, A. M., Alexandre, C., & Ingham, P. W. (1995). Secretion of the amino-terminal fragment of the hedgehog protein is necessary and sufficient for hedgehog signalling in Drosophila. *Current Biology : CB*, *5*(6), 643–650. https://doi.org/10.1016/S0960-9822(95)00129-1

Flames, N., Pla, R., Gelman, D. M., Rubenstein, J. L. R., Puelles, L., & Marín, O. (2007). Delineation of multiple subpallial progenitor domains by the combinatorial expression of transcriptional codes. *The Journal of Neuroscience : The Official Journal of the Society for Neuroscience*, *27*(36), 9682–9695. https://doi.org/10.1523/JNEUROSCI.2750-07.2007

Flandin, P., Kimura, S., & Rubenstein, J. L. R. (2010). The progenitor zone of the ventral medial ganglionic eminence requires Nkx2-1 to generate most of the globus pallidus but few neocortical interneurons. *The Journal of Neuroscience : The Official Journal of the Society for Neuroscience*, *30*(8), 2812–2823. https://doi.org/10.1523/JNEUROSCI.4228-09.2010

Fossale, E., Seong, I. S., Coser, K. R., Shioda, T., Kohane, I. S., Wheeler, V. C., Gusella, J. F., Macdonald, M. E., & Lee, J. M. (2011). Differential effects of the Huntington's disease CAG mutation in striatum and cerebellum are quantitative not qualitative. *Human Molecular Genetics*, *20*(21), 4258–4267. https://doi.org/10.1093/HMG/DDR355

Fotaki, V., Yu, T., Zaki, P. A., Mason, J. O., & Price, D. J. (2006). Abnormal Positioning of Diencephalic Cell Types in Neocortical Tissue in the Dorsal Telencephalon of Mice Lacking Functional Gli3. *Journal of Neuroscience*, *26*(36), 9282–9292. https://doi.org/10.1523/JNEUROSCI.2673-06.2006

Fragkouli, A., van Wijk, N. v., Lopes, R., Kessaris, N., & Pachnis, V. (2009). LIM homeodomain transcription factor-dependent specification of bipotential MGE progenitors into cholinergic and GABAergic striatal interneurons. *Development*, *136*(22), 3841–3851. https://doi.org/10.1242/dev.038083

Fuccillo, M., Joyner, A. L., & Fishell, G. (2006). Morphogen to mitogen: the multiple roles of hedgehog signalling in vertebrate neural development. *Nature Reviews. Neuroscience*, *7*(10), 772–783. https://doi.org/10.1038/NRN1990

Fujiyama, F., Sohn, J., Nakano, T., Furuta, T., Nakamura, K. C., Matsuda, W., & Kaneko, T. (2011). Exclusive and common targets of neostriatofugal projections of rat striosome neurons: A single neuron-tracing study using a viral vector. *European Journal of Neuroscience*, *33*(4), 668–677. https://doi.org/10.1111/j.1460-9568.2010.07564.x

Garcia-Calero, E., Martínez-de-la-Torre, M., & Puelles, L. (2020). A radial histogenetic model of the mouse pallial amygdala. *Brain Structure & Function*, *225*(7), 1921–1956. https://doi.org/10.1007/S00429-020-02097-4

Garcia-Calero, E., & Puelles, L. (2021). Development of the mouse anterior amygdalar radial unit marked by Lhx9-expression. *Brain Structure & Function*, *226*(2), 575–600. https://doi.org/10.1007/S00429-020-02201-8

Gerfen, C. R. (1984). The neostriatal mosaic: Compartmentalization of corticostriatal input and striatonigral output systems. *Nature*, *311*(5985), 461–464. https://doi.org/10.1038/311461a0

Gerfen, C. R., Baimbridge, K. G., & Miller, J. J. (1985). The neostriatal mosaic: compartmental distribution of calcium-binding protein and parvalbumin in the basal ganglia of the rat and monkey. *Proceedings of the National Academy of Sciences of the United States of America*, *82*(24), 8780–8784. https://doi.org/10.1073/PNAS.82.24.8780

Gerfen, C. R., Engber, T. M., Mahan, L. C., Susel, Z., Chase, T. N., Monsma, F. J., & Sibley, D. R. (1990a). D1 and D2 dopamine receptor-regulated gene expression of striatonigral and striatopallidal neurons. *Science (New York, N.Y.)*, *250*(4986), 1429–1432. https://doi.org/10.1126/SCIENCE.2147780

Gerfen, C. R., Engber, T. M., Mahan, L. C., Susel, Z., Chase, T. N., Monsma, F. J., & Sibley, D. R. (1990b). D1 and D2 dopamine receptor-regulated gene expression of striatonigral and striatopallidal neurons. *Science (New York, N.Y.)*, *250*(4986), 1429–1432. https://doi.org/10.1126/SCIENCE.2147780

Gerfen, C. R., & Sawchenko, P. E. (1984). An anterograde neuroanatomical tracing method that shows the detailed morphology of neurons, their axons and terminals: Immunohistochemical localization of an axonally transported plant lectin, Phaseolus vulgaris leucoagglutinin (PHA-L). *Brain Research*, *290*(2), 219–238. https://doi.org/10.1016/0006-8993(84)90940-5

Gerfen, C. R., & Surmeier, D. J. (2011). Modulation of striatal projection systems by dopamine. *Annual Review of Neuroscience*, *34*, 441–466. https://doi.org/10.1146/annurev-neuro-061010-113641

Gharami, K., Xie, Y., An, J. J., Tonegawa, S., & Xu, B. (2008). Brain-derived neurotrophic factor over-expression in the forebrain ameliorates Huntington's disease phenotypes in mice. *Journal of Neurochemistry*, *105*(2), 369–379. https://doi.org/10.1111/J.1471-4159.2007.05137.X

Gilford, H., & Hutchinson, J. (1897). On a Condition of Mixed Premature and Immature Development. *Medico-Chirurgical Transactions*, *80*(1), 17–45. https://doi.org/10.1177/095952879708000105

Gimeno, L., & Martinez, S. (2007). Expression of chick Fgf19 and mouse Fgf15 orthologs is regulated in the developing brain by Fgf8 and Shh. *Developmental Dynamics : An Official Publication of the American Association of Anatomists*, *236*(8), 2285–2297. https://doi.org/10.1002/DVDY.21237

Goldman, P. S., & Nauta, W. J. H. (1977). Columnar distribution of cortico-cortical fibers in the frontal association, limbic, and motor cortex of the developing rhesus monkey. *Brain Research*, *122*(3), 393–413. https://doi.org/10.1016/0006-8993(77)90453-X

Gonzalez-Reyes, L. E., Verbitsky, M., Blesa, J., Jackson-Lewis, V., Paredes, D., Tillack, K., Phani, S., Kramer, E. R., Przedborski, S., & Kottmann, A. H. (2012). Sonic hedgehog maintains cellular and neurochemical homeostasis in the adult nigrostriatal circuit. *Neuron*, *75*(2), 306–319. https://doi.org/10.1016/J.NEURON.2012.05.018

Graham, N. L., Bak, T. H., & Hodges, J. R. (2003). Corticobasal degeneration as a cognitive disorder. *Movement Disorders : Official Journal of the Movement Disorder Society*, *18*(11), 1224–1232. https://doi.org/10.1002/MDS.10536

Graveland, G. A., Williams, R. S., & Difiglia, M. (1985a). A Golgi study of the human neostriatum: Neurons and afferent fibers. *Journal of Comparative Neurology*, *234*(3), 317–333. https://doi.org/10.1002/cne.902340304

Graveland, G. A., Williams, R. S., & Difiglia, M. (1985b). Evidence for degenerative and regenerative changes in neostriatal spiny neurons in Huntington's disease. *Science*, *227*(4688), 770–773. https://doi.org/10.1126/science.3155875

Graybiel, A. M., & Ragsdale, C. W. (1978). Histochemically distinct compartments in the striatum of human, monkeys, and cat demonstrated by acetylthiocholinesterase staining. *Proceedings of the National Academy of Sciences of the United States of America*, *75*(11), 5723–5726. https://doi.org/10.1073/PNAS.75.11.5723

Guth, S. I. E., & Wegner, M. (2008). Having it both ways: Sox protein function between conservation and innovation. *Cellular and Molecular Life Sciences : CMLS*, *65*(19), 3000–3018. https://doi.org/10.1007/S00018-008-8138-7

Halliday, G. M., McRitchie, D. A., Macdonald, V., Double, K. L., Trent, R. J., & McCusker, E. (1998). Regional specificity of brain atrophy in Huntington's disease. *Experimental Neurology*, *154*(2), 663–672. https://doi.org/10.1006/exnr.1998.6919

Heiman, M., Schaefer, A., Gong, S., Peterson, J. D., Day, M., Ramsey, K. E., Su?rez-Fari?as, M., Schwarz, C., Stephan, D. A., Surmeier, D. J., Greengard, P., & Heintz, N. (2008). A Translational Profiling Approach for the Molecular Characterization of CNS Cell Types. *Cell*, *135*(4), 738–748. https://doi.org/10.1016/j.cell.2008.10.028

Herkenham, M., & Pert, C. B. (1982). Light microscopic localization of brain opiate receptors: a general autoradiographic method which preserves tissue quality. *The Journal of Neuroscience : The Official Journal of the Society for Neuroscience*, *2*(8), 1129–1149. https://doi.org/10.1523/JNEUROSCI.02-08-01129.1982

Hirabayashi, T., Murayama, T., & Shimizu, T. (2004). Regulatory mechanism and physiological role of cytosolic phospholipase A2. *Biological & Pharmaceutical Bulletin*, *27*(8), 1168–1173. https://doi.org/10.1248/BPB.27.1168

Hisaoka, T., Nakamura, Y., Senba, E., & Morikawa, Y. (2010). The forkhead transcription factors, Foxp1 and Foxp2, identify different subpopulations of projection neurons in the mouse cerebral cortex. *Neuroscience*, *166*(2), 551–563. https://doi.org/10.1016/j.neuroscience.2009.12.055

Horvath, S. (2013). DNA methylation age of human tissues and cell types. *Genome Biology*, *14*(10). https://doi.org/10.1186/GB-2013-14-10-R115

Hoser, M., Potzner, M. R., Koch, J. M. C., Bösl, M. R., Wegner, M., & Sock, E. (2008). Sox12 deletion in the mouse reveals nonreciprocal redundancy with the related Sox4 and Sox11 transcription factors. *Molecular and Cellular Biology*, *28*(15), 4675–4687. https://doi.org/10.1128/MCB.00338-08

Huerta-Ocampo, I., Mena-Segovia, J., & Bolam, J. P. (2014). Convergence of cortical and thalamic input to direct and indirect pathway medium spiny neurons in the striatum. *Brain Structure & Function*, *219*(5), 1787–1800. https://doi.org/10.1007/S00429-013-0601-Z

Hunt, C. P. J., Pouton, C. W., & Haynes, J. M. (2017). Characterising the developmental profile of human embryonic stem cell-derived medium spiny neuron progenitors and assessing mature neuron function using a CRISPR-generated human DARPP-32 WT/eGFP-AMP reporter line. *Neurochemistry International*, *106*, 3–13. https://doi.org/10.1016/j.neuint.2017.01.003

Huot, P., Lévesque, M., & Parent, A. (2007). The fate of striatal dopaminergic neurons in Parkinson's disease and Huntington's chorea. *Brain*, *130*(1), 222–232. https://doi.org/10.1093/brain/awl332

Huot, P., & Parent, A. (2007). Dopaminergic neurons intrinsic to the striatum. *Journal of Neurochemistry*, *101*(6), 1441–1447. https://doi.org/10.1111/j.1471-4159.2006.04430.x

Hutchinson, J. (1886). Illustrations of Exceptional Symptoms and Examples of Rare Forms of Disease. *British Medical Journal*, *2*(1332), 61–62. https://doi.org/10.1136/BMJ.2.1332.61

Ingham, P. W., & McMahon, A. P. (2001). Hedgehog signaling in animal development: paradigms and principles. *Genes & Development*, *15*(23), 3059–3087. https://doi.org/10.1101/gad.938601

Israsena, N., Hu, M., Fu, W., Kan, L., & Kessler, J. A. (2004). The presence of FGF2 signaling determines whether beta-catenin exerts effects on proliferation or neuronal differentiation of neural stem cells. *Developmental Biology*, *268*(1), 220–231. https://doi.org/10.1016/J.YDBIO.2003.12.024

Kedaigle, A. J., Fraenkel, E., Atwal, R. S., Wu, M., Gusella, J. F., MacDonald, M. E., Kaye, J. A., Finkbeiner, S., Mattis, V. B., Tom, C. M., Svendsen, C., King, A. R., Chen, Y., Stocksdale, J. T., Lim, R. G., Casale, M., Wang, P. H., Thompson, L. M., Akimov, S. S., … Ross, C. A. (2020). Bioenergetic deficits in Huntington's disease iPSC-derived neural cells and rescue with glycolytic metabolites. *Human Molecular Genetics*, *29*(11), 1757–1771. https://doi.org/10.1093/HMG/DDY430

Kim, J. I., Long, J. D., Mills, J. A., Downing, N., Williams, J. K., & Paulsen, J. S. (2015). Performance of the 12-item WHODAS 2.0 in prodromal Huntington disease. *European Journal of Human Genetics*, *23*(11), 1584–1587. https://doi.org/10.1038/ejhg.2015.11

Kim, S., Kim, D., Cho, S. W., Kim, J., & Kim, J. S. (2014). Highly efficient RNA-guided genome editing in human cells via delivery of purified Cas9 ribonucleoproteins. *Genome Research*, *24*(6), 1012–1019. https://doi.org/10.1101/GR.171322.113

Kleiner-Fisman, G., Calingasan, N. Y., Putt, M., Chen, J., Beal, M. F., & Lang, A. E. (2005). Alterations of striatal neurons in benign hereditary chorea. *Movement Disorders : Official Journal of the Movement Disorder Society*, *20*(10), 1353–1357. https://doi.org/10.1002/MDS.20577

Kuschel, S., Rüther, U., & Theil, T. (2003). A disrupted balance between Bmp/Wnt and Fgf signaling underlies the ventralization of the Gli3 mutant telencephalon. *Developmental Biology*, *260*(2), 484–495. https://doi.org/10.1016/S0012-1606(03)00252-5

Langley, K., & Grant, N. J. (1997). Are exocytosis mechanisms neurotransmitter specific? *Neurochemistry International*, *31*(6), 739–757. https://doi.org/10.1016/S0197-0186(97)00040-5

le Cann, K., Foerster, A., Rösseler, C., Erickson, A., Hautvast, P., Giesselmann, S., Pensold, D., Kurth, I., Rothermel, M., Mattis, V. B., Zimmer-Bensch, G., von Hörsten, S., Denecke, B., Clarner, T., Meents, J., & Lampert, A. (2021). The difficulty to model Huntington's disease in vitro using striatal medium spiny neurons differentiated from human induced pluripotent stem cells. *Scientific Reports*, *11*(1). https://doi.org/10.1038/S41598-021-85656-X

Lee, S. J., Lodder, B., Chen, Y., Patriarchi, T., Tian, L., & Sabatini, B. L. (2021). Cell-type-specific asynchronous modulation of PKA by dopamine in learning. *Nature*, *590*(7846), 451–456. https://doi.org/10.1038/s41586-020-03050-5

Li, W., Wei, W., Zhu, S., Zhu, J., Shi, Y., Lin, T., Hao, E., Hayek, A., Deng, H., & Ding, S. (2009). Generation of Rat and Human Induced Pluripotent Stem Cells by Combining Genetic Reprogramming and Chemical Inhibitors. *Cell Stem Cell*, *4*(1), 16–19. https://doi.org/10.1016/j.stem.2008.11.014

Liao, W.-L., Tsai, H.-C., Wang, H.-F., Chang, J., Lu, K.-M., Wu, H.-L., Lee, Y.-C., Tsai, T.-F., Takahashi, H., Wagner, M., Ghyselinck, N. B., Chambon, P., & Liu, F.-C. (n.d.). *Modular patterning of structure and function of the striatum by retinoid receptor signaling*. Retrieved September 29, 2017, from http://www.pnas.org/content/105/18/6765.full.pdf

Lim, R. G., Salazar, L. L., Wilton, D. K., King, A. R., Stocksdale, J. T., Sharifabad, D., Lau, A. L., Stevens, B., Reidling, J. C., Winokur, S. T., Casale, M. S., Thompson, L. M., Pardo, M., D?az-Barriga, A. G. G., Straccia, M., Sanders, P., Alberch, J., Canals, J. M., Kaye, J. A., … Svendsen, C. N. (2017). Developmental alterations in Huntington's disease neural cells and pharmacological rescue in cells and mice. *Nature Neuroscience*, *20*(5), 648–660. https://doi.org/10.1038/nn.4532

Lin, T., & Wu, S. (2015). Reprogramming with Small Molecules instead of Exogenous Transcription Factors. *Stem Cells International*, *2015*, 794632. https://doi.org/10.1155/2015/794632

Liodis, P., Denaxa, M., Grigoriou, M., Akufo-Addo, C., Yanagawa, Y., & Pachnis, V. (2007). Lhx6 activity is required for the normal migration and specification of cortical interneuron subtypes. *The Journal of Neuroscience : The Official Journal of the Society for Neuroscience*, *27*(12), 3078–3089. https://doi.org/10.1523/JNEUROSCI.3055-06.2007

Lobo, M. K., Karsten, S. L., Gray, M., Geschwind, D. H., & Yang, X. W. (2006). FACS-array profiling of striatal projection neuron subtypes in juvenile and adult mouse brains. *Nature Neuroscience*, *9*(3), 443–452. https://doi.org/10.1038/nn1654

Ma, L., Hu, B., Liu, Y., Vermilyea, S. C., Liu, H., Gao, L., Sun, Y., Zhang, X., & Zhang, S.-C. (2012). Human embryonic stem cell-derived GABA neurons correct locomotion deficits in quinolinic acid-lesioned mice. *Cell Stem Cell*, *10*(4), 455–464. https://doi.org/10.1016/j.stem.2012.01.021

Machold, K. P., & Smolen, J. S. (2003). Adalimumab - a new TNF-alpha antibody for treatment of inflammatory joint disease. *Expert Opinion on Biological Therapy*, *3*(2), 351–360. https://doi.org/10.1517/14712598.3.2.351

MacVicar, T. D. B., & Lane, J. D. (2014). Impaired OMA1-dependent cleavage of OPA1 and reduced DRP1 fission activity combine to prevent mitophagy in cells that are dependent on oxidative phosphorylation. *Journal of Cell Science*, *127*(Pt 10), 2313–2325. https://doi.org/10.1242/JCS.144337

Maeda, O., Kondo, M., Fujita, T., Usami, N., Fukui, T., Shimokata, K., Ando, T., Goto, H., & Sekido, Y. (2006). Enhancement of GLI1-transcriptional activity by beta-catenin in human cancer cells. *Oncology Reports*, *16*(1), 91–96. http://www.ncbi.nlm.nih.gov/pubmed/16786128

Magno, L., Catanzariti, V., Nitsch, R., Krude, H., & Naumann, T. (2009). Ongoing expression of Nkx2.1 in the postnatal mouse forebrain: Potential for understanding NKX2.1 haploinsufficiency in humans? *Brain Research*, *1304*, 164–186. https://doi.org/10.1016/j.brainres.2009.09.050

Magno, L., Kretz, O., Bert, B., Ersözlü, S., Vogt, J., Fink, H., Kimura, S., Vogt, A., Monyer, H., Nitsch, R., & Naumann, T. (2011). The integrity of cholinergic basal forebrain neurons depends on expression of Nkx2-1. *European Journal of Neuroscience*, *34*(11), 1767–1782. https://doi.org/10.1111/j.1460-9568.2011.07890.x

Marti, E., Bumcrot, D. A., Takada, R., & McMahon, A. P. (1995). Requirement of 19K form of Sonic hedgehog for induction of distinct ventral cell types in CNS explants. *Nature*, *375*(6529), 322–325. https://doi.org/10.1038/375322A0

Martín-Ibáñez, R., Crespo, E., Esgleas, M., Urban, N., Wang, B., Waclaw, R., Georgopoulos, K., Martínez, S., Campbell, K., Vicario-Abejón, C., Alberch, J., Chan, S., Kastner, P., Rubenstein, J. L., & Canals, J. M. (2012). Helios transcription factor expression depends on Gsx2 and Dlx1&2 function in developing striatal matrix neurons. *Stem Cells and Development*, *21*(12), 2239–2251. https://doi.org/10.1089/SCD.2011.0607

Martín-Ibáñez, R., Crespo, E., Urbán, N., Sergent-Tanguy, S., Herranz, C., Jaumot, M., Valiente, M., Long, J. E., Pineda, J. R., Andreu, C., Rubenstein, J. L. R., Marín, Ó., Georgopoulos, K., Mengod, G., Fariñas, I., Bachs, O., Alberch, J., & Canals, J. M. (2010). Ikaros-1 couples cell cycle arrest of late striatal precursors with neurogenesis of enkephalinergic neurons. *The Journal of Comparative Neurology*, *518*(3), 329–351. https://doi.org/10.1002/CNE.22215

McClintock, D., Ratner, D., Lokuge, M., Owens, D. M., Gordon, L. B., Collins, F. S., & Djabali, K. (2007). The mutant form of lamin A that causes Hutchinson-Gilford progeria is a biomarker of cellular aging in human skin. *PloS One*, *2*(12). https://doi.org/10.1371/JOURNAL.PONE.0001269

McCubrey, J. A., Rakus, D., Gizak, A., Steelman, L. S., Abrams, S. L., Lertpiriyapong, K., Fitzgerald, T. L., Yang, L. v., Montalto, G., Cervello, M., Libra, M., Nicoletti, F., Scalisi, A., Torino, F., Fenga, C., Neri, L. M., Marmiroli, S., Cocco, L., & Martelli, A. M. (2016). Effects of mutations in Wnt/β-catenin, hedgehog, Notch and PI3K pathways on GSK-3 activity—Diverse effects on cell growth, metabolism and cancer. *Biochimica et Biophysica Acta (BBA) - Molecular Cell Research*, *1863*(12), 2942–2976. https://doi.org/10.1016/J.BBAMCR.2016.09.004

McGlinn, E., Richman, J. M., Metzis, V., Town, L., Butterfield, N. C., Wainwright, B. J., & Wicking, C. (2008). Expression of the NET family member Zfp503 is regulated by hedgehog and BMP signaling in the limb. *Developmental Dynamics : An Official Publication of the American Association of Anatomists*, *237*(4), 1172–1182. https://doi.org/10.1002/DVDY.21508

Mendez-Lopez, M., Arias, J. L., Bontempi, B., & Wolff, M. (2013). Reduced cytochrome oxidase activity in the retrosplenial cortex after lesions to the anterior thalamic nuclei. *Behavioural Brain Research*, *250*, 264–273. https://doi.org/10.1016/J.BBR.2013.04.052

Miller, C., & Nolan, J. (2013). Towards evidence based emergency medicine: best BETs from the Manchester Royal Infirmary. BET 1: the use of adrenaline and long-term survival in cardiopulmonary resuscitation following cardiac arrest. *Emergency Medicine Journal : EMJ*, *30*(3), 249–250. https://doi.org/10.1136/EMERMED-2013-202363.2

Miyake, A., Nakayama, Y., Konishi, M., & Itoh, N. (2005). Fgf19 regulated by Hh signaling is required for zebrafish forebrain development. *Developmental Biology*, *288*(1), 259–275. https://doi.org/10.1016/j.ydbio.2005.09.042

Mizuno, Y., Ikebe, S. ichirou, Hattori, N., Nakagawa-Hattori, Y., Mochizuki, H., Tanaka, M., & Ozawa, T. (1995). Role of mitochondria in the etiology and pathogenesis of Parkinson's disease. *Biochimica et Biophysica Acta*, *1271*(1), 265–274. https://doi.org/10.1016/0925-4439(95)00038-6

Molero, A. E., Gokhan, S., Gonzalez, S., Feig, J. L., Alexandre, L. C., & Mehler, M. F. (2009). Impairment of developmental stem cell-mediated striatal neurogenesis and pluripotency genes in a knock-in model of Huntington's disease. *Proceedings of the National Academy of Sciences of the United States of America*, *106*(51), 21900–21905. https://doi.org/10.1073/pnas.0912171106

Molotkova, N., Molotkov, A., & Duester, G. (2007). Role of retinoic acid during forebrain development begins late when Raldh3 generates retinoic acid in the ventral subventricular zone. *Developmental Biology*, *303*(2), 601–610. https://doi.org/10.1016/J.YDBIO.2006.11.035

Moreno-Blas, D., Gorostieta-Salas, E., Pommer-Alba, A., Muciño-Hernández, G., Gerónimo-Olvera, C., Maciel-Barón, L. A., Konigsberg, M., Massieu, L., & Castro-Obregón, S. (2019). Cortical neurons develop a senescence-like phenotype promoted by dysfunctional autophagy. *Aging*, *11*(16), 6175–6198. https://doi.org/10.18632/AGING.102181

Morris, S.-A. L., & Huang, S. (2016). Crosstalk of the Wnt/β-catenin pathway with other pathways in cancer cells. *Genes & Diseases*, *3*(1), 41–47. https://doi.org/10.1016/J.GENDIS.2015.12.003

Munji, R. N., Choe, Y., Li, G., Siegenthaler, J. A., & Pleasure, S. J. (2011). Wnt signaling regulates neuronal differentiation of cortical intermediate progenitors. *The Journal of Neuroscience : The Official Journal of the Society for Neuroscience*, *31*(5), 1676–1687. https://doi.org/10.1523/JNEUROSCI.5404-10.2011

Nekrasov, E. D., Vigont, V. A., Klyushnikov, S. A., Lebedeva, O. S., Vassina, E. M., Bogomazova, A. N., Chestkov, I. v., Semashko, T. A., Kiseleva, E., Suldina, L. A., Bobrovsky, P. A., Zimina, O. A., Ryazantseva, M. A., Skopin, A. Y., Illarioshkin, S. N., Kaznacheyeva, E. v., Lagarkova, M. A., & Kiselev, S. L. (2016). Manifestation of Huntington's disease pathology in human induced pluripotent stem cell-derived neurons. *Molecular Neurodegeneration*, *11*(1). https://doi.org/10.1186/S13024-016-0092-5

Neves, J., Vachkov, I., & Giraldez, F. (2013). Sox2 regulation of hair cell development: Incoherence makes sense. *Hearing Research*, *297*, 20–29. https://doi.org/10.1016/j.heares.2012.11.003

Nicoleau, C., Varela, C., Bonnefond, C., Maury, Y., Bugi, A., Aubry, L., Viegas, P., Bourgois-Rocha, F., Peschanski, M., & Perrier, A. L. (2013). Embryonic stem cells neural differentiation qualifies the role of Wnt/β-Catenin signals in human telencephalic specification and regionalization. *STEM CELLS*, *31*(9), 1763–1774. https://doi.org/10.1002/stem.1462

Niewiadomski, P., Kong, J. H., Ahrends, R., Ma, Y., Humke, E. W., Khan, S., Teruel, M. N., Novitch, B. G., & Rohatgi, R. (2014). Gli Protein Activity Is Controlled by Multisite Phosphorylation in Vertebrate Hedgehog Signaling. *Cell Reports*, *6*(1), 168–181. https://doi.org/10.1016/J.CELREP.2013.12.003

Niewiadomski, P., Zhujiang, A., Youssef, M., & Waschek, J. A. (2013). Interaction of PACAP with Sonic hedgehog reveals complex regulation of the Hedgehog pathway by PKA. *Cellular Signalling*, *25*(11), 2222–2230. https://doi.org/10.1016/j.cellsig.2013.07.012

Nóbrega-Pereira, S., Kessaris, N., Du, T., Kimura, S., Anderson, S. A., & Marín, O. (2008). Postmitotic Nkx2-1 controls the migration of telencephalic interneurons by direct repression of guidance receptors. *Neuron*, *59*(5), 733–745. https://doi.org/10.1016/J.NEURON.2008.07.024

Obermayer, J., Luchicchi, A., Heistek, T. S., de Kloet, S. F., Terra, H., Bruinsma, B., Mnie-Filali, O., Kortleven, C., Galakhova, A. A., Khalil, A. J., Kroon, T., Jonker, A. J., de Haan, R., van den Berg, W. D. J., Goriounova, N. A., de Kock, C. P. J., Pattij, T., & Mansvelder, H. D. (2019). Prefrontal cortical ChAT-VIP interneurons provide local excitation by cholinergic synaptic transmission and control attention. *Nature Communications*, *10*(1). https://doi.org/10.1038/S41467-019-13244-9

Ohkubo, Y., Chiang, C., & Rubenstein, J. L. R. (2002). Coordinate regulation and synergistic actions of BMP4, SHH and FGF8 in the rostral prosencephalon regulate morphogenesis of the telencephalic and optic vesicles. *Neuroscience*, *111*(1), 1–17. https://doi.org/10.1016/S0306-4522(01)00616-9

Pabst, O., Rummelies, J., Winter, B., & Arnold, H. H. (2003). Targeted disruption of the homeobox gene Nkx2.9 reveals a role in development of the spinal accessory nerve. *Development*, *130*(6), 1193–1202. https://doi.org/10.1242/dev.00346

Paina, S., Garzotto, D., DeMarchis, S., Marino, M., Moiana, A., Conti, L., Cattaneo, E., Perera, M., Corte, G., Calautti, E., & Merlo, G. R. (2011). Wnt5a is a transcriptional target of Dlx homeogenes and promotes differentiation of interneuron progenitors in vitro and in vivo. *The Journal of Neuroscience : The Official Journal of the Society for Neuroscience*, *31*(7), 2675–2687. https://doi.org/10.1523/JNEUROSCI.3110-10.2011

Papp, B., & Plath, K. (2013). Epigenetics of reprogramming to induced pluripotency. *Cell*, *152*(6), 1324–1343. https://doi.org/10.1016/J.CELL.2013.02.043

Paulsen, J. S., Langbehn, D. R., Stout, J. C., Aylward, E., Ross, C. A., Nance, M., Guttman, M., Johnson, S., MacDonald, M., Beglinger, L. J., Duff, K., Kayson, E., Biglan, K., Shoulson, I., Oakes, D., & Hayden, M. (2008). Detection of Huntington's disease decades before diagnosis: The Predict-HD study. *Journal of Neurology, Neurosurgery and Psychiatry*, *79*(8), 874–880. https://doi.org/10.1136/jnnp.2007.128728

Pera, E. M., & Kessel, M. (1998). Demarcation of ventral territories by the homeobox gene NKX2.1 during early chick development. *Development Genes and Evolution*, *208*(3), 168–171. http://www.ncbi.nlm.nih.gov/pubmed/9601992

Pert, C. B., Kuhar, M. J., & Snyder, S. H. (1976). Opiate receptor: Autoradiographic localization in rat brain. *Proceedings of the National Academy of Sciences of the United States of America*, *73*(10), 3729–3733. https://doi.org/10.1073/pnas.73.10.3729

Pert, C. B., & Snyder, S. H. (1976). Opiate receptor binding-enhancement by opiate administration in vivo. *Biochemical Pharmacology*, *25*(7), 847–853. https://doi.org/10.1016/0006-2952(76)90157-X

Peukert, D., Weber, S., Lumsden, A., & Scholpp, S. (2011). Lhx2 and Lhx9 determine neuronal differentiation and compartition in the caudal forebrain by regulating Wnt signaling. *PLoS Biology*, *9*(12). https://doi.org/10.1371/JOURNAL.PBIO.1001218

Phelps, C. J., Romero, M. I., & Hurley, D. L. (2003). Growth hormone-releasing hormone-producing and dopaminergic neurones in the mouse arcuate nucleus are independently regulated populations. *Journal of Neuroendocrinology*, *15*(3), 280–288. https://doi.org/10.1046/J.1365-2826.2003.01009.X

Popolo, M., McCarthy, D. M., & Bhide, P. G. (2004). Influence of dopamine on precursor cell proliferation and differentiation in the embryonic mouse telencephalon. *Developmental Neuroscience*, *26*(2–4), 229–244. https://doi.org/10.1159/000082140

Precious, S. v., Kelly, C. M., Reddington, A. E., Vinh, N. N., Stickland, R. C., Pekarik, V., Scherf, C., Jeyasingham, R., Glasbey, J., Holeiter, M., Jones, L., Taylor, M. v., & Rosser, A. E. (2016). FoxP1 marks medium spiny neurons from precursors to maturity and is required for their differentiation. In *Experimental Neurology* (Vol. 282, pp. 9–18). https://doi.org/10.1016/j.expneurol.2016.05.002

Puelles, L. (2019). Survey of Midbrain, Diencephalon, and Hypothalamus Neuroanatomic Terms Whose Prosomeric Definition Conflicts With Columnar Tradition. *Frontiers in Neuroanatomy*, *13*. https://doi.org/10.3389/FNANA.2019.00020

Puelles, L., & Rubenstein, J. L. R. (2003). Forebrain gene expression domains and the evolving prosomeric model. *Trends in Neurosciences*, *26*(9), 469–476. https://doi.org/10.1016/S0166-2236(03)00234-0

Rallu, M., Corbin, J. G., & Fishell, G. (2002). Parsing the prosencephalon. *Nature Reviews Neuroscience*, *3*(12), 943–951. https://doi.org/10.1038/nrn989

Rallu, M., Machold, R., Gaiano, N., Corbin, J. G., McMahon, A. P., & Fishell, G. (2002). Dorsoventral patterning is established in the telencephalon of mutants lacking both Gli3 and hedgehog signaling. *Development*, *129*(21), 4963–4974. https://doi.org/10.1242/dev.129.21.4963

Reiner, A., Albin, R. L., Anderson, K. D., D'Amato, C. J., Penney, J. B., & Young, A. B. (1988). Differential loss of striatal projection neurons in Huntington disease. *Proceedings of the National Academy of Sciences of the United States of America*, *85*(15), 5733–5737. https://doi.org/10.1073/PNAS.85.15.5733

Rosas, H. D., Liu, A. K., Hersch, S., Glessner, M., Ferrante, R. J., Salat, D. H., van der Kouwe, A., Jenkins, B. G., Dale, A. M., & Fischl, B. (2002). Regional and progressive thinning of the cortical ribbon in Huntington's disease. *Neurology*, *58*(5), 695–701. https://doi.org/10.1212/WNL.58.5.695

Rowitch, D. H. (2004). Glial specification in the vertebrate neural tube. *Nature Reviews. Neuroscience*, *5*(5), 409–419. https://doi.org/10.1038/NRN1389

Roy, A. L., Sierra, F., Howcroft, K., Singer, D. S., Sharpless, N., Hodes, R. J., Wilder, E. L., & Anderson, J. M. (2020). A Blueprint for Characterizing Senescence. *Cell*, *183*(5), 1143–1146. https://doi.org/10.1016/J.CELL.2020.10.032

Santoni, M., Burattini, L., Nabissi, M., Beatrice Morelli, M., Berardi, R., Santoni, G., & Cascinu, S. (2013). Essential Role of Gli Proteins in Glioblastoma Multiforme. *Current Protein & Peptide Science*, *14*(2), 133–140. https://doi.org/10.2174/1389203711314020005

Sap, K. A., Guler, A. T., Bezstarosti, K., Bury, A. E., Juenemann, K., Demmers, J. A. A., & Reits, E. A. (2019). Global Proteome and Ubiquitinome Changes in the Soluble and Insoluble Fractions of Q175 Huntington Mice Brains. *Molecular & Cellular Proteomics : MCP*, *18*(9), 1705–1720. https://doi.org/10.1074/MCP.RA119.001486

Shikata, Y., Okada, T., Hashimoto, M., Ellis, T., Matsumaru, D., Shiroishi, T., Ogawa, M., Wainwright, B., & Motoyama, J. (2011). Ptch1-mediated dosage-dependent action of Shh signaling regulates neural progenitor development at late gestational stages. *Developmental Biology*, *349*(2), 147–159. https://doi.org/10.1016/J.YDBIO.2010.10.014

Smith-Geater, C., Hernandez, S. J., Lim, R. G., Adam, M., Wu, J., Stocksdale, J. T., Wassie, B. T., Gold, M. P., Wang, K. Q., Miramontes, R., Kopan, L., Orellana, I., Joy, S., Kemp, P. J., Allen, N. D., Fraenkel, E., & Thompson, L. M. (2020). Aberrant Development Corrected in Adult-Onset Huntington's Disease iPSC-Derived Neuronal Cultures via WNT Signaling Modulation. *Stem Cell Reports*, *14*(3), 406–419. https://doi.org/10.1016/J.STEMCR.2020.01.015

Song, L., Li, Z.-Y., Liu, W.-P., & Zhao, M.-R. (2015). Crosstalk between Wnt/β-catenin and Hedgehog/Gli signaling pathways in colon cancer and implications for therapy. *Cancer Biology & Therapy*, *16*(1), 1. https://doi.org/10.4161/15384047.2014.972215

Stanslowsky, N., Reinhardt, P., Glass, H., Kalmbach, N., Naujock, M., Hensel, N., Lübben, V., Pal, A., Venneri, A., Lupo, F., de Franceschi, L., Claus, P., Sterneckert, J., Storch, A., Hermann, A., & Wegner, F. (2016). Neuronal dysfunction in iPSC-derived medium spiny neurons from

chorea-acanthocytosis patients is reversed by Src kinase inhibition and F-actin stabilization. *Journal of Neuroscience*, *36*(47), 12027–12043. https://doi.org/10.1523/JNEUROSCI.0456-16.2016

Straccia, M., Barriga, G. G. D., Sanders, P., Bombau, G., Carrere, J., Mairal, P. B., Vinh, N. N., Yung, S., Kelly, C. M., Svendsen, C. N., Kemp, P. J., Arjomand, J., Schoenfeld, R. C., Alberch, J., Allen, N. D., Rosser, A. E., & Canals, J. M. (2015). Quantitative high-throughput gene expression profiling of human striatal development to screen stem cell-derived medium spiny neurons. *Molecular Therapy - Methods and Clinical Development*. https://doi.org/10.1038/mtm.2015.30

Strano, A., Tuck, E., Stubbs, V. E., & Livesey, F. J. (2020). Variable Outcomes in Neural Differentiation of Human PSCs Arise from Intrinsic Differences in Developmental Signaling Pathways. *Cell Reports*, *31*(10). https://doi.org/10.1016/J.CELREP.2020.107732

Sussel, L., Marin, O., Kimura, S., & Rubenstein, J. L. (1999). Loss of Nkx2.1 homeobox gene function results in a ventral to dorsal molecular respecification within the basal telencephalon: evidence for a transformation of the pallidum into the striatum. *Development*, *126*(15).

Szlachcic, W. J., Wiatr, K., Trzeciak, M., Figlerowicz, M., & Figiel, M. (2017). Corrigendum: The Generation of Mouse and Human Huntington Disease iPS Cells Suitable for In vitro Studies on Huntingtin Function. *Frontiers in Molecular Neuroscience*, *10*, 312. https://doi.org/10.3389/fnmol.2017.00312

Telezhkin, V., Schnell, C., Yarova, P., Yung, S., Cope, E., Hughes, A., Thompson, B. A., Sanders, P., Geater, C., Hancock, J. M., Joy, S., Badder, L., Connor-Robson, N., Comella, A., Straccia, M., Bombau, G., Brown, J. T., Canals, J. M., Randall, A. D., … Kemp, P. J. (2016a). Forced cell cycle exit and modulation of GABA $_{A}$, CREB, and GSK3β signaling promote functional maturation of induced pluripotent stem cell-derived neurons. *American Journal of Physiology - Cell Physiology*, *310*(7), C520–C541. https://doi.org/10.1152/ajpcell.00166.2015

Telezhkin, V., Schnell, C., Yarova, P., Yung, S., Cope, E., Hughes, A., Thompson, B. A., Sanders, P., Geater, C., Hancock, J. M., Joy, S., Badder, L., Connor-Robson, N., Comella, A., Straccia, M., Bombau, G., Brown, J. T., Canals, J. M., Randall, A. D., … Kemp, P. J. (2016b). Forced cell cycle exit and modulation of GABAA, CREB, and GSK3β signaling promote functional maturation of induced pluripotent stem cell-derived neurons. *American Journal of Physiology. Cell Physiology*, *310*(7), C520–C541. https://doi.org/10.1152/AJPCELL.00166.2015

The HD iPSC Consortium, The Hd Ipsc, C., & Phenotypes, S. C. (2012). Induced Pluripotent Stem Cells from Patients with Huntington's Disease Show CAG-Repeat-Expansion-Associated Phenotypes. *Cell Stem Cell*, *11*(2), 264–278. https://doi.org/10.1016/j.stem.2012.04.027

Thu, Y. M., & Richmond, A. (2010). NF-κB inducing kinase: A key regulator in the immune system and in cancer. *Cytokine and Growth Factor Reviews*, *21*(4), 213–226. https://doi.org/10.1016/j.cytogfr.2010.06.002

Tillerson, J. L., Caudle, W. M., Parent, J. M., Gong, C., Schallert, T., & Miller, G. W. (2006). Olfactory discrimination deficits in mice lacking the dopamine transporter or the D2 dopamine receptor. *Behavioural Brain Research*, *172*(1), 97–105. https://doi.org/10.1016/J.BBR.2006.04.025

Tinterri, A., Menardy, F., Diana, M. A., Lokmane, L., Keita, M., Coulpier, F., Lemoine, S., Mailhes, C., Mathieu, B., Merchan-Sala, P., Campbell, K., Gyory, I., Grosschedl, R., Popa, D., & Garel, S. (2018). Active intermixing of indirect and direct neurons builds the striatal mosaic. *Nature Communications*, *9*(1). https://doi.org/10.1038/S41467-018-07171-4

Tole, S., Remedios, R., Saha, B., & Stoykova, A. (2005). Selective requirement of Pax6, but not Emx2, in the specification and development of several nuclei of the amygdaloid complex. *Journal of Neuroscience*, *25*(10), 2753–2760. https://doi.org/10.1523/JNEUROSCI.3014-04.2005

Toresson, H., Parmar, M., & Campbell, K. (2000). Expression of Meis and Pbx genes and their protein products in the developing telencephalon: implications for regional differentiation. *Mechanisms of Development*, *94*(1–2), 183–187. https://doi.org/10.1016/S0925-4773(00)00324-5

Tuson, M., He, M., & Anderson, K. v. (2011). Protein kinase A acts at the basal body of the primary cilium to prevent Gli2 activation and ventralization of the mouse neural tube. *Development (Cambridge, England)*, *138*(22), 4921–4930. https://doi.org/10.1242/DEV.070805

Uday Bhanu, M., Mandraju, R. K., Bhaskar, C., & Kondapi, A. K. (2010). Cultured cerebellar granule neurons as an in vitro aging model: topoisomerase IIβ as an additional biomarker in DNA repair and aging. *Toxicology in Vitro : An International Journal Published in Association with BIBRA*, *24*(7), 1935–1945. https://doi.org/10.1016/J.TIV.2010.08.003

Vazin, T., Ashton, R. S., Conway, A., Rode, N. A., Lee, S. M., Bravo, V., Healy, K. E., Kane, R. S., & Schaffer, D. v. (2014). The effect of multivalent Sonic hedgehog on differentiation of human embryonic stem cells into dopaminergic and GABAergic neurons. *Biomaterials*, *35*(3), 941–948. https://doi.org/10.1016/J.BIOMATERIALS.2013.10.025

Ventimiglia, R., Jones, B. E., & Møller, A. (1995). A quantitative method for morphometric analysis in neuronal cell culture: unbiased estimation of neuron area and number of branch points. *Journal of Neuroscience Methods*, *57*(1), 63–66. https://doi.org/10.1016/0165-0270(94)00126-2

Ventimiglia, R., Mather, P. E., Jones, B. E., & Lindsay, R. M. (1995). The NeurotroDhins BDNF, NT-3 and NT-4/5 Promote Survival and Morphological and Biochemical Differentiation of Striatal Neurons In Vitro. *European Journal of Neuroscience*, *7*(2), 213–222. https://doi.org/10.1111/j.1460-9568.1995.tb01057.x

Victor, M. B., Richner, M., Olsen, H. E., Lee, S. W., Monteys, A. M., Ma, C., Huh, C. J., Zhang, B., Davidson, B. L., Yang, X. W., & Yoo, A. S. (2018). Striatal neurons directly converted from

Huntington's disease patient fibroblasts recapitulate age-associated disease phenotypes. *Nature Neuroscience*, *21*(3), 341–352. https://doi.org/10.1038/S41593-018-0075-7

Vonsattel, J. P., Myers, R. H., Stevens, T. J., Ferrante, R. J., Bird, E. D., & Richardson, E. P. (1985). Neuropathological classification of huntington's disease. *Journal of Neuropathology and Experimental Neurology*, *44*(6), 559–577. https://doi.org/10.1097/00005072-198511000-00003

Waclaw, R. R., Allen, Z. J., Bell, S. M., Erdélyi, F., Szabó, G., Potter, S. S., & Campbell, K. (2006). The zinc finger transcription factor Sp8 regulates the generation and diversity of olfactory bulb interneurons. *Neuron*, *49*(4), 503–516. https://doi.org/10.1016/J.NEURON.2006.01.018

Wang, B., Fallon, J. F., & Beachy, P. A. (2000). Hedgehog-regulated processing of Gli3 produces an anterior/posterior repressor gradient in the developing vertebrate limb. *Cell*, *100*(4), 423–434. https://doi.org/10.1016/S0092-8674(00)80678-9

Watabe-Uchida, M., Zhu, L., Ogawa, S. K., Vamanrao, A., & Uchida, N. (2012). Whole-brain mapping of direct inputs to midbrain dopamine neurons. *Neuron*, *74*(5), 858–873. https://doi.org/10.1016/J.NEURON.2012.03.017

Wechsler-Reya, R. J., & Scott, M. P. (1999). Control of neuronal precursor proliferation in the cerebellum by Sonic Hedgehog. *Neuron*, *22*(1), 103–114. https://doi.org/10.1016/S0896-6273(00)80682-0

Wilczyński, J. R. (2006). Immunological analogy between allograft rejection, recurrent abortion and pre-eclampsia - the same basic mechanism? *Human Immunology*, *67*(7), 492–511. https://doi.org/10.1016/J.HUMIMM.2006.04.007

Wonders, C. P., Taylor, L., Welagen, J., Mbata, I. C., Xiang, J. Z., & Anderson, S. A. (2008). A spatial bias for the origins of interneuron subgroups within the medial ganglionic eminence. *Developmental Biology*, *314*(1), 127–136. https://doi.org/10.1016/J.YDBIO.2007.11.018

Wu, M., Huang, Y., Chen, T., Wang, W., Yang, S., Ye, Z., & Xi, X. (2019). LncRNA MEG3 inhibits the progression of prostate cancer by modulating miR-9-5p/QKI-5 axis. *Journal of Cellular and Molecular Medicine*, *23*(1), 29–38. https://doi.org/10.1111/JCMM.13658

Xu, J. (2005). Preparation, culture, and immortalization of mouse embryonic fibroblasts. *Current Protocols in Molecular Biology*, *Chapter 28*. https://doi.org/10.1002/0471142727.MB2801S70

Xu, K., Bastia, E., & Schwarzschild, M. (2005). Therapeutic potential of adenosine A(2A) receptor antagonists in Parkinson's disease. *Pharmacology & Therapeutics*, *105*(3), 267–310. https://doi.org/10.1016/J.PHARMTHERA.2004.10.007

Xu, L., & Massagué, J. (2004). Nucleocytoplasmic shuttling of signal transducers. *Nature Reviews Molecular Cell Biology*, *5*(3), 209–219. https://doi.org/10.1038/nrm1331

Xu, Q. (2005). Sonic hedgehog maintains the identity of cortical interneuron progenitors in the ventral telencephalon. *Development*, *132*(22), 4987–4998. https://doi.org/10.1242/dev.02090

Xu, W. (2004). Interleukin-20. *International Immunopharmacology*, *4*(5), 627–633. https://doi.org/10.1016/j.intimp.2004.01.006

Yanai, A., Huang, K., Kang, R., Singaraja, R. R., Arstikaitis, P., Gan, L., Orban, P. C., Mullard, A., Cowan, C. M., Raymond, L. A., Drisdel, R. C., Green, W. N., Ravikumar, B., Rubinsztein, D. C., El-Husseini, A., & Hayden, M. R. (2006). Palmitoylation of huntingtin by HIP14 is essential for its trafficking and function. *Nature Neuroscience*, *9*(6), 824–831. https://doi.org/10.1038/NN1702

Yu, W., Wang, Y., McDonnell, K., Stephen, D., & Bai, C. B. (2009). Patterning of ventral telencephalon requires positive function of Gli transcription factors. *Developmental Biology*, *334*(1), 264–275. https://doi.org/10.1016/J.YDBIO.2009.07.026

Yuan, J., Xing, H., Li, Y., Song, Y., Zhang, N., Xie, M., Liu, J., Xu, Y., Shen, Y., Wang, B., Zhang, L., & Yang, M. (2021). EPB41 suppresses the Wnt/β-catenin signaling in non-small cell lung cancer by sponging ALDOC. *Cancer Letters*, *499*, 255–264. https://doi.org/10.1016/J.CANLET.2020.11.024

Yun, C. C. (2003). Concerted roles of SGK1 and the Na+/H+ exchanger regulatory factor 2 (NHERF2) in regulation of NHE3. *Cellular Physiology and Biochemistry : International Journal of Experimental Cellular Physiology, Biochemistry, and Pharmacology*, *13*(1), 29–40. https://doi.org/10.1159/000070247

Zhang, N., An, M. C., Montoro, D., & Ellerby, L. M. (2010). Characterization of Human Huntington's Disease Cell Model from Induced Pluripotent Stem Cells. *PLoS Currents*, *2*, RRN1193. https://doi.org/10.1371/currents.RRN1193

Zuccato, C., Ciammola, A., Rigamonti, D., Leavitt, B. R., Goffredo, D., Conti, L., MacDonald, M. E., Friedlander, R. M., Silani, V., Hayden, M. R., Timmusk, T., Sipione, S., & Cattaneo, E. (2001). Loss of Huntingtin-Mediated BDNF Gene Transcription in Huntington's Disease. *Science*, *293*(5529), 493–498. https://doi.org/10.1126/science.1059581

Zuccato, C., Tartari, M., Crotti, A., Goffredo, D., Valenza, M., Conti, L., Cataudella, T., Leavitt, B. R., Hayden, M. R., Timmusk, T., Rigamonti, D., & Cattaneo, E. (2003). Huntingtin interacts with REST/NRSF to modulate the transcription of NRSE-controlled neuronal genes. *Nature Genetics*, *35*(1), 76–83. https://doi.org/10.1038/ng1219

Zuccato, C., Valenza, M., & Cattaneo, E. (2010). Molecular Mechanisms and Potential Therapeutical Targets in Huntington's Disease. *Physiological Reviews*, *90*(3), 905–981. https://doi.org/10.1152/physrev.00041.2009

Appendix

A

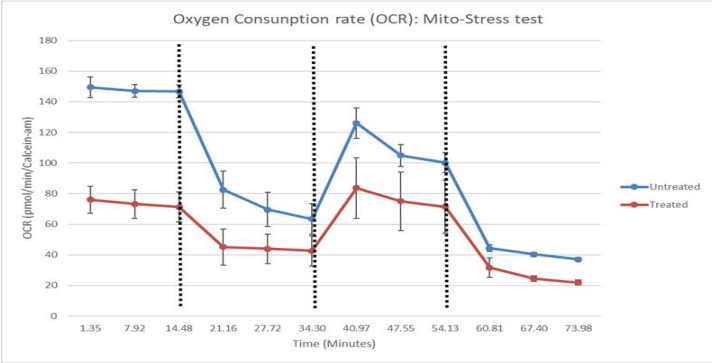

B

Parameters (pmol/min)	Untreated (+/-S.D.)	Treated (+/- S.D.)	Multiple T-test
. Basal Respiration	110.1 ± 5.315	51.34 ± 14.051	t(4) = 6.773, p=0.002
ATP production	77.54 ± 23.677	29.26 ± 13.164	t(4) = 3.087, p=0.04
Maximal respiration	67.98 ± 12.378	53.12 ± 36.241	t(4) = 0.6721, p=0.538
Spare respiratory capacity	42.11 ± 12.309	-1.77 ± 44.795	t(4) = 1.636, p=0.177
Non-mitochondrial oxygen consumption	36.98 ± 2.16	21.86 ± 2.96	t(4) = 7.149, p=0.002

C

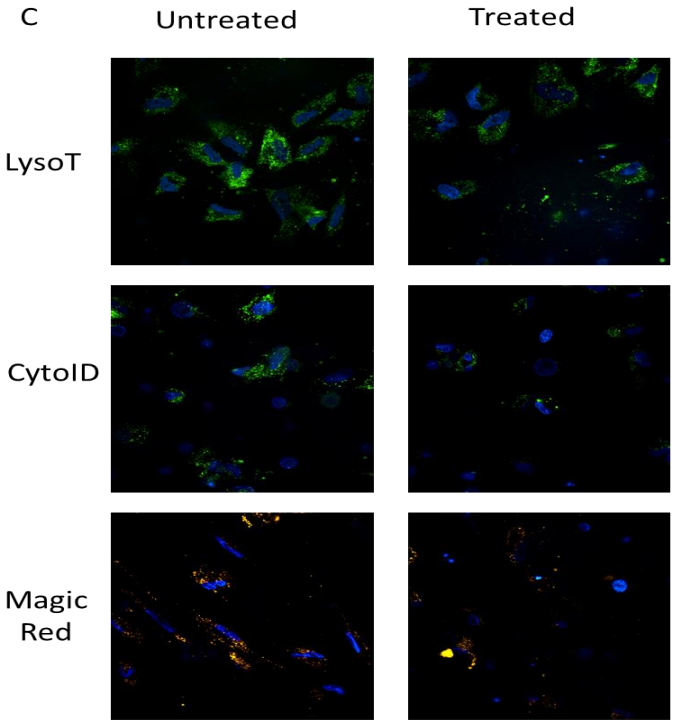

D

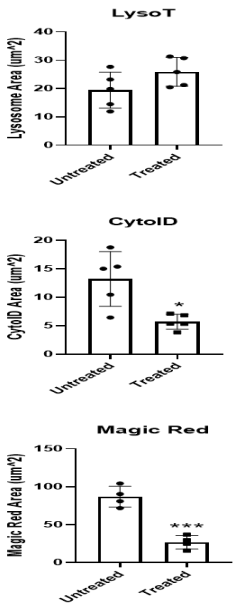

7.1: Mito Stress Test in treated and untreated neurons. A) Oxygen consumption rate in treated and untreated cells. B) Calculated values for respiratory parameters and Multiple T-test. C) Exemplar live cell immunohistochemistry images D) calculated lysotracker, CytoID and Magic Red values. ** p<0.05, ** p<0.01, *** p<0.001, **** p<0.0001*

Brief description of protocol

Control HPSIO114i-Kolf_2-C1 (Kolf2), IPSC lines were differentiated using SLI medium for dual SMAD and WNT inhibition to day 8, to generate naïve neural progenitors. Day8 cultures were split and cultured in Basic media (BM) to allow 'default' cortical patterning for a further 8 days. Following this media was change to NF for 4 days. Terminal differentiation was carried out as described in Telezhkin et al., 2015. Once neurons were functionally 'mature' as assessed via MEA, media Astro-D medium which consisted of: astrocyte conditioned (34D6) ADF/PSG and Neurobasal A (1:1) supplemented with 2% Neurobrew-21 (With Vit A), with and without D-Galactose (Sigma,10 mg/ml).
Analysis of cultures was carried out 1 week following treatment.

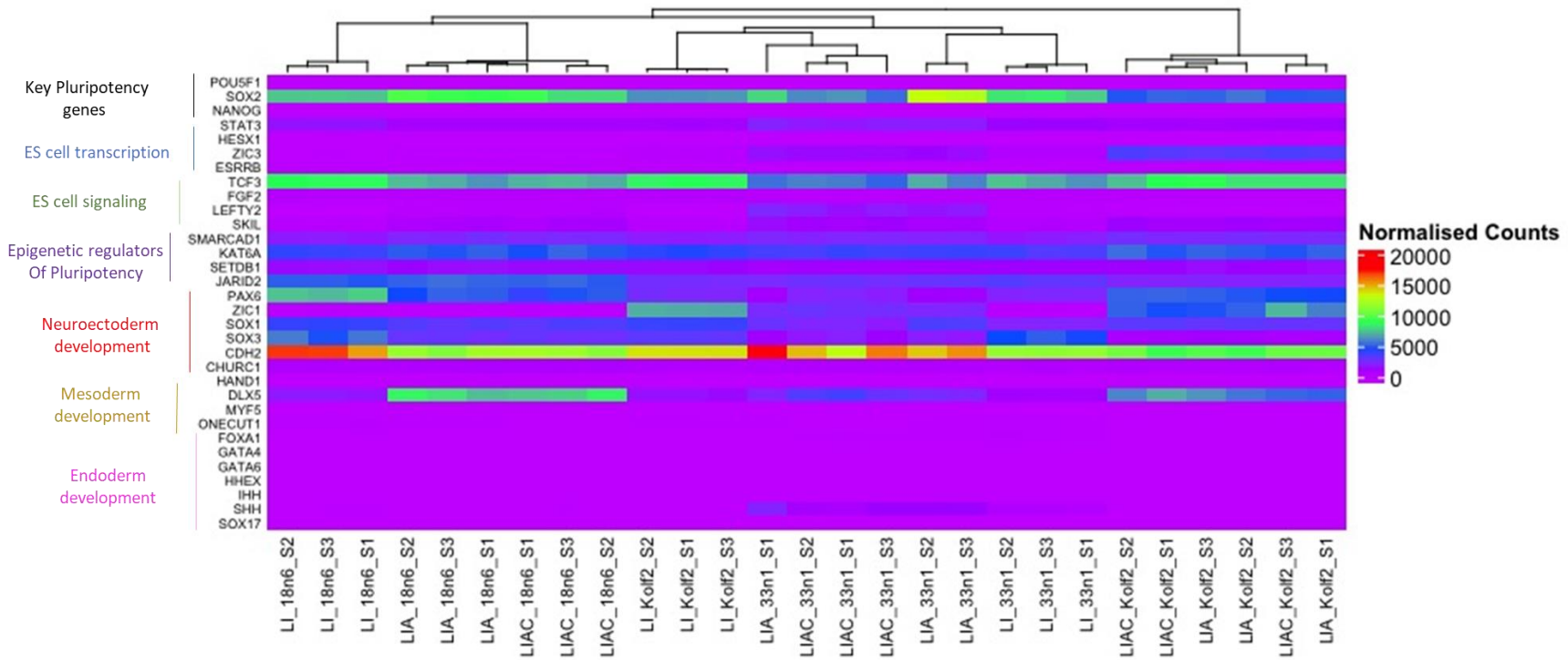

Figure 7.2. RNA sequencing data shows core pluripotency, mesoderm and endoderm genes show null counts across all samples and treatments.